Progress in Polymer Science 34 (2009) 125–155

Contents lists available at ScienceDirect

Progress in Polymer Science

journal homepage: www.elsevier.com/locate/ppolysci

Nano-biocomposites: Biodegradable polyester/nanoclay systems

Perrine Bordes, Eric Pollet, Luc Avérous*

LIPHT-ECPM, UMR 7165, Université de Strasbourg, 25 rue Becquerel, 67087 Strasbourg Cedex 2, France

ARTICLE INFO

Article history:
Received 1 June 2008
Received in revised form 27 October 2008
Accepted 28 October 2008
Available online 14 November 2008

Keywords:
Biopolyesters
Nano-biocomposites
Clay
Biodegradable

ABSTRACT

In the recent years, bio-based products have raised great interest since sustainable development policies tend to expand with the decreasing reserve of fossil fuel and the growing concern for the environment. Consequently, biopolymers, i.e., biodegradable polymers, have been the topic of many researches. They can be mainly classified as agro-polymers (starch, protein, etc.) and biodegradable polyesters (polyhydroxyalkanoates, poly(lactic acid), etc.). These latter, also called biopolyesters, can be synthesized from fossil resources but main productions are obtained from renewable resources. Unfortunately for certain applications, biopolyesters cannot be fully competitive with conventional thermoplastics since some of their properties are too weak. Therefore, to extend their applications, these biopolymers have been formulated and associated with nano-sized fillers, which could bring a large range of improved properties (stiffness, permeability, crystallinity, thermal stability). The resulting 'nano-biocomposites' have been the subject of many recent publications. This review is dedicated to this novel class of materials based on clays, which are nowadays the main nanofillers used in nanocomposites systems. This review highlights the main researches and developments in biopolyester/nanoclay systems during the last decade.

Contents

* Corresponding author. Tel.: +33 3 90 242 707; fax: +33 3 90 242 716.
E-mail address: AverousL@ecpm.u-strasbg.fr (L. Avérous).

0079-6700/$ – see front matter © 2008 Elsevier Ltd. All rights reserved.
doi:10.1016/j.progpolymsci.2008.10.002

1. Introduction

In recent years biopolymers, i.e., biodegradable polymers, have attracted more and more interest due to increasing environmental concern and decreasing fossil resources. This evolution motivates academic and industrial research to develop novel materials labelled as "environmentally-friendly", i.e., materials produced from alternative resources, with lower energy consumption, biodegradable and non-toxic to the environment. Since biopolymers are biodegradable and the main productions are obtained from renewable resources such as agro-resources, they represent an interesting alternative route to common non-degradable polymers for short-life range applications (packaging, agriculture, etc.). Nevertheless, until now, most biopolymers are costly compared to conventional thermoplastic and they are sometimes too weak for practical use. Therefore, it appears necessary to improve these biopolymers to make them fully competitive with common thermoplastics.

Nanocomposites are novel materials with drastically improved properties due to the incorporation of small amounts (less than 10 wt%) of nano-sized fillers into a polymer matrix. Nanofillers can be classified according to their morphology, such as particles that are (i) layered (e.g., clays), (ii) spherical (e.g., silica) or (iii) acicular (e.g., whiskers, carbon nanotubes). Their specific geometrical dimensions, and thus aspect ratios, partly affect the final materials properties. Layered silicate clays offer high surface area, more than 700 m^2/g, i.e., a huge interface with the polymer (matrix), which governs the material properties. The final behavior can be considerably improved by the strong and extensive polymer–nanofiller interactions, as well as, good particle dispersion.

Nano-biocomposites are obtained by adding nanofillers to biopolymers, resulting in very promising materials since they show improved properties with preservation of the material biodegradability, without eco-toxicity. Such materials are mainly destined to biomedical applications and different short-term applications, e.g., packaging, agriculture or hygiene devices. They thus represent a strong and emerging answer for improved and eco-friendly materials. Although few articles were published on this topic during the last century, but numerous publications have already appeared since that time.

This review reports on an aspect of the state of the art in wide field of nano-biocomposites materials, namely to nano-biocomposites based on biopolyester/clay systems. Layered silicates are widely used in nanocomposites systems and biopolyesters are currently the most promising biopolymers for wide range of important applications. The first part describes several biopolymers, focusing on the origins and characteristics of the principal biopolyesters. In the second part, the structure and properties of nano-biocomposites based on biopolyester/clays systems are reported in detail.

2. Biodegradable polymers classification

A vast number of biodegradable polymers (biopolymers) are chemically synthesized or biosynthesized during the growth cycles of all organisms. Some micro-organisms and enzymes capable of degrading them have been identified [1–4]. Fig. 1 proposes a classification with four different categories, depending on the synthesis [5]:

(a) polymers from biomass such as the agro-polymers from agro-resources, e.g., starch, cellulose,
(b) polymers obtained by microbial production, e.g., the polyhydroxyalkanoates,
(c) polymers chemically synthesized using monomers obtained from agro-resources, e.g., poly(lactic acid),
(d) polymers whose monomers and polymers are both obtained by chemical synthesis from fossil resources.

Of these, only categories (a)–(c) are obtained from renewable resources. We can sort these different biodegradable polymers into two main families, the agro-polymers (category a) and the biodegradable polyesters (categories b–d), also called biopolyesters.

3. Biodegradable polyesters

Table 1 and Fig. 2 show the chemical structures, trade names and main properties of commercially available biopolyesters.

3.1. Polyesters based on agro-resources

3.1.1. Poly(lactic acid)

Lactic acid is a chiral molecule existing as two stereoisomers, L- and D-lactic acid which can be produced in different ways, i.e., biologically or chemically synthesized [6].

In the first case, lactic acid is obtained by fermentation of carbohydrates from lactic bacteria, belonging mainly to the genus *Lactobacillus*, or fungi [7,8]. This fermentative pro-

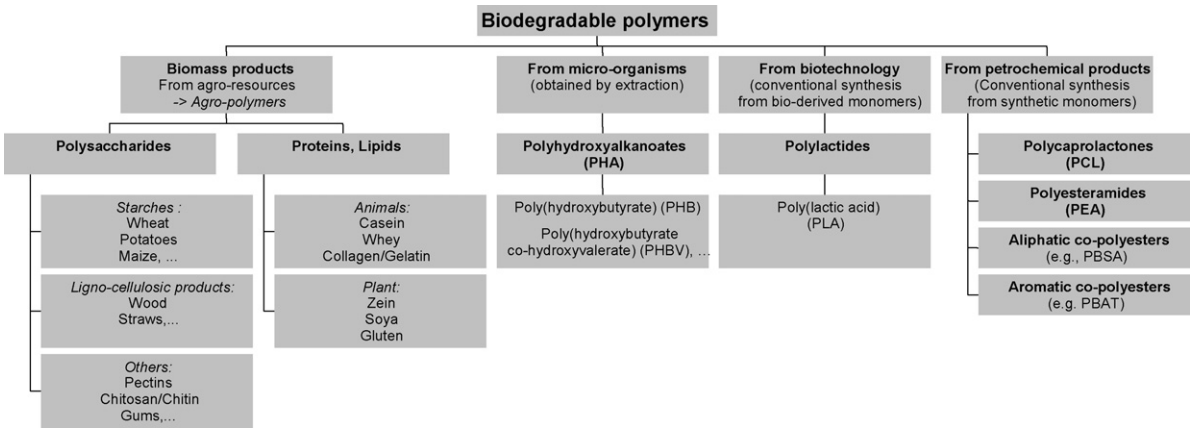

Fig. 1. Classification of the biodegradable polymers. Reproduced with permission from Averous [190] copyright (2004) of Marcel Dekker, Inc.

cess requires a bacterial strain but also sources of carbon (carbohydrates), nitrogen (yeast extract, peptides, etc.) and mineral elements to allow the growth of bacteria and the production of lactic acid. The lactic acid as-formed exists almost exclusively as L-lactic acid and leads to poly(L-lactic acid) PLLA with low molecular weight by polycondensation reaction. However, Moon et al. [9,10] have proposed an alternative solution to obtain higher molecular weight PLLA by the polycondensation route.

In contrast, the chemical process could lead to various ratio of L- and D-lactic acid. Indeed, the chemical reactions leading to the formation of the cyclic dimer, the lactide, as an intermediate step to the production of PLA, could lead to macromolecular chains with L- and D-lactic acid monomers. This mechanism of ring-opening polymerization ROP from the lactide explains the formation of two enantiomers. This ROP route has the advantage of reaching high molecular weight polymers [1,7,11,12] and allows control of the PLA final properties by adjusting the proportions and the sequencing of L- and D-lactic acid units.

At present, due to its availability on the market and its low price [13–16], PLA has one of the highest potentials among biopolyesters, particularly for packaging [14,16] and medical applications. For instance, Cargill has developed processes that use corn and other feedstock to produce different PLA grades (NatureWorks®) [15,17]. For this company, the actual production is estimated to 50–60 ktons per year although the production capacity is given at 140 ktons (http://www.natureworksllc.com). However, presently, it is the highest and worldwide production of biodegradable polyester. Its price was around 2€/kg in 2006, but nowadays the cost has slightly increased. Different companies such as Mitsui Chemicals (Japan), Mitsubishi (Japan), Biomer (Germany), Shimadzu (Japan), Galactic-Total (Belgium), Toyota (Japan), Purac (Netherlands), Treofan (Netherlands) or Dainippon Ink Chemicals (Japan) produce smaller PLAs outputs with different D/L ratios. Commercially available, we can find 100% PLLA which present a high crystallinity C-PLA and copolymers of PLLA and poly(D,L-lactic acid) PDLLA which are rather amorphous A-PLA [17–19]. PLA can show crystalline polymorphism [20] which can lead

Table 1
Physical data of some commercial biopolyesters. Reproduced with permission from Averous [190] copyright (2004) of Marcel Dekker, Inc.

	PLA Dow–Cargill (NatureWorks)	PHBV Monsanto (Biopol D400G – HV = 7 mol%)	PCL Solvay (CAPA 680)	PEA Bayer (BAK 1095)	PBSA Showa (Bionolle 3000)	PBAT Eastman (Eastar bio 14766)
Density	1.25	1.25	1.11	1.07	1.23	1.21
Melting point (°C)[a]	152	153	65	112	114	110–115
Glass transition (°C)[a]	58	5	−61	−29	−45	−30
Crystallinity[b] (in %)	0–1	51	67	33	41	20–35
Modulus (MPa) (NFT 51-035)	2050	900	190	262	249	52
Elongation at break (%) (NFT 51-035)	9	15	>500	420	>500	>500
Tensile stress at break or max. (MPa) (NFT 51-035)	–	–	14	17	19	9
Biodegradation[c] (mineralization in %)	100	100	100	100	90	100
Water permeability WVTR at 25 °C ($g/m^2/day$)	172	21	177	680	330	550
Surface tension (γ) (mN/m)	50	–	51	59	56	53
γ_d (dispersive component)	37	–	41	37	43	43
γ_p (polar component)	13	–	11	22	14	11

[a] Measured by DSC.
[b] Determined on granules, before processing.
[c] After 60 days in controlled composting according to ASTM 5336.

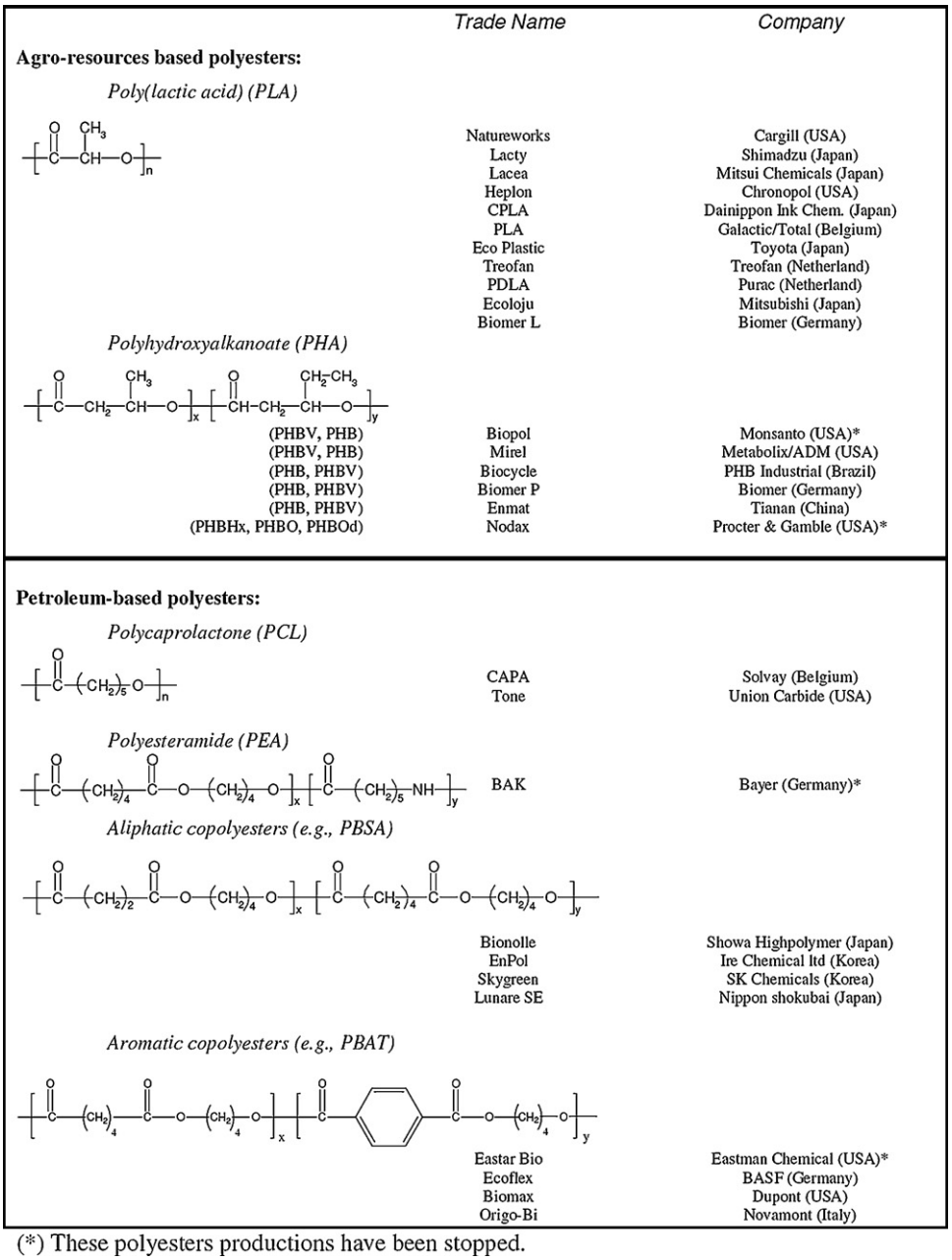

Fig. 2. Structure, trade names and suppliers of main biodegradable polyesters commercially available. Reproduced with permission from Averous [190] copyright (2004) of Marcel Dekker, Inc.

to different melting peaks [21] with a main endotherm at 152 °C for the PDLLA (see Table 1). Furthermore, PLA can be plasticized using oligomeric lactic acid *o*-LA [21], citrate ester [22] or low molecular weight polyethylene glycol PEG [21,23–25]. The effect of plasticization increases the chain mobility and then favors PLA organization and crystallization. After plasticization, we obtain a crystallinity ranging between 20% and 30%. PLA presents a medium water and oxygen permeability level [16,26] comparable to polystyrene [27]. These different properties associated with its tunability and its availability favor its actual developments in different packaging applications (trays, cups, bottles, films, etc.) [14,16,17]. McCarthy et al. [28] showed that A-PLA presents a soil degradation rate much slower compared to polybutylene succinate/adipate PBSA. PLA is presumed to be biodegradable although the role of hydrolysis vs. enzymatic depolymerization in this process remains open to debate [29]. Regarding biodegradation in compost, adequate conditions are only found in industrial units with a high temperature (above 50 °C) and a high relative humidity RH% to promote chain hydrolysis. According to Tuominen et al. [30],

PLA biodegradation does not exhibit any eco-toxicological effect.

3.1.2. Polyhydroxyalkanoates

Polyhydroxyalkanoates PHAs are naturally produced by micro-organisms from various carbon substrates as a carbon or energy reserve. A wide variety of prokaryotic organisms [31,32] accumulate PHA from 30% to 80% of their cellular dry weight. Biotechnological studies revealed that polyhydroxybutyrate homopolymer PHB is produced under balanced growth conditions when the cells become limited for an essential nutrient but are exposed to an excess of carbon [33]. Depending on the carbon substrates and the metabolism of the micro-organism, different monomers, and thus (co)polymers, could be obtained [34]. Although PHB is the main polymer of the polyhydroxyalkanoates family, different poly(hydroxybutyrate-*co*-hydroxyalkanoates) copolyesters exist such as poly(hydroxybutyrate-*co*-hydroxyvalerate) PHBV (see Fig. 2), or poly(hydroxybutyrate-*co*-hydroxyhexanoate) PHBHx, poly(hydroxybutyrate-*co*-hydroxyoctanoate) PHBO and poly(hydroxybutyrate-*co*-hydroxyoctadecanoate) PHBOd. With progress in biotechnologies, it is possible for recombinant bacteria [32], but also plants [32,35,36] to produce such polymers. However, the recovery process, i.e., the extraction and purification steps, is decisive to obtain a highly pure PHA and often explains why such polymers are still expensive. Pure synthetic PHA can be produced by the ROP from butyrolactone and other lactones [37–42]. Thus, according to the synthesis route, we obtain different structures, isotactic with random stereosequences for the bacterial copolyesters and with partially stereoregular block for the synthetic copolyesters. Recently, Monsanto has developed genetic modification of plants to make them produce small quantities of PHB [35,43,44].

PHB is a highly crystalline polyester (above 50%) with a high melting point, T_m = 173–180 °C, compared to the other biodegradable polyesters. Glass transition temperature T_g is around 5 °C. The homopolymer shows a narrow window for the processing conditions. To ease the transformation, PHB can be plasticized with citrate ester, but the PHBV copolymer is more adapted for the process. A large range of bacterial copolymer grades had been industrially produced by Monsanto under the Biopol® trade mark, with HV contents reaching 20%. The production was stopped at the end of 1999. Metabolix bought Biopol® assets in 2001. Presently, Telles™, a joint venture between Metabolix and Archer Daniels Midlands Company (ADM), has marketed the Mirel™ product as a new bio-based biodegradable plastic from corn sugar. ADM has begun to build the first plant in Clinton, Iowa (US) which will be able to produce 50,000 tons of resin per year. The startup is scheduled for late 2008 (http://www.metabolix.com).

Different small companies currently produce bacterial PHA, e.g., PHB Industrial (Brazil) produces PHB and PHBV (HV = 12%) 45% crystalline, from sugar cane molasses [45]. The Biocycle® production is planned to be 4000 tons/year in 2008 and then, to be extended to 14,000 tons/year [46]. In 2004, Procter & Gamble (US) and Kaneka Corporation (Japan) announced a joint development agreement for the completion of R&D leading to the commercialization of Nodax, a large range of polyhydroxybutyrate-*co*-hydroxyalkanoates (PHBHx, PHBO, PHBOd) [47]. Although the industrial production was planned for 2006 with a target price around 2€/kg, the production was stopped [48].

The production of PHAs is intended to replace synthetic non-degradable polymers for a wide range of applications [48]: packaging, agriculture but also medicine [34,49] since PHAs are biocompatible. Fig. 2 and Table 1 give the chemical structure and the properties of some PHBV, respectively. Material properties can be tailored by varying the HV content. An increase of the HV content induces an increase of the impact strength and a decrease of the melting temperature and glass transition [50], the crystallinity [51], the water permeability [51] and the tensile strength [52].

Besides, PHBV properties can evolve when plasticization occurs, e.g., with citrate ester (triacetin) [52,53]. The polyhydroxyalkanoates, like the PLAs, are sensitive to the processing conditions. Under extrusion, we obtain a rapid diminution of the viscosity and the molecular weight due to macromolecular chain cleavage by increasing the shear level, the temperature and/or the residential time [54]. Regarding the biodegradable behavior, the kinetic of enzymatic degradation is variable according to the crystallinity, the structure [45,55] and then, to the processing history [56]. Bacterial copolyesters biodegrade faster than homopolymers [57] and synthetic copolyesters [58].

3.2. Petroleum-based polyesters

A large number of biodegradable polyesters are based on petroleum resources, obtained chemically from synthetic monomers [11–15,17,18]. According to the chemical structures (see Fig. 2), we can distinguish (see Table 1) polycaprolactones, polyesteramides, aliphatic or aromatic copolyesters. All these polyesters are soft at room temperature.

3.2.1. Polycaprolactone

Poly(ε-caprolactone) PCL is usually obtained by ROP of ε-caprolactone in the presence of metal alkoxides (aluminium isopropoxide, tin octoate, etc.) [11,12,58]. PCL is widely used as a PVC solid plasticizer or for polyurethane applications, as polyols, but it finds also some applications based on its biodegradable character in domains such as biomedicine (e.g., drugs controlled release) and environment (e.g., soft compostable packaging). Different commercial grades are produced by Solvay (CAPA®),[1] by Union Carbide (Tone®) and by Daicel (Celgreen®). Fig. 2 and Table 1 give, respectively, the chemical structure and the properties of this polyester. PCL shows a very low T_g (−61 °C) and a low melting point (65 °C), which could be a handicap in some applications. Therefore, PCL is generally blended [29,59–61] or modified (e.g., copolymerization, crosslinking [62]). Tokiwa and Suzuki [63] have discussed the hydrolysis of PCL and biodegradation by fungi. They have shown that PCL can be easily enzymatically degraded. According to Bastioli [29], the biodegradability can be clearly claimed but the homopolymer hydrolysis rate is

[1] Solvay has recently sold this activity to Perstorp (Sweden).

very low. The presence of starch can significantly increase the biodegradation rate of PCL [59].

3.2.2. Biodegradable aliphatic polyesters

A large number of aliphatic copolyesters are biodegradable copolymers based on petroleum resources. They are obtained by the combination of diols such as 1,2-ethanediol, 1,3-propanediol or 1,4-butadenediol, and dicarboxylic acids like adipic, sebacic or succinic acid. Showa Highpolymer (Japan) has developed a large range of polybutylene succinate PBS obtained by polycondensation of 1,4-butanediol and succinic acid. Polybutylene succinate/adipate PBSA, presented in Fig. 2, is obtained by addition of adipic acid. These copolymers are commercialized under the Bionolle® trademark [17]. Table 1 shows the properties of such biopolyester. Ire Chemical (Korea) commercializes exactly the same kind of copolyesters under EnPol® trademark. Skygreen®, a product from SK Chemicals (Korea) is obtained by polycondensation of 1,2-ethanediol, 1,4-butadenediol with succinic and adipic acids [64]. Nippon Shokubai (Japan) also commercializes an aliphatic copolyester under Lunare SE® trademark. These copolyesters properties depend on the structure [65], i.e., the combination of diols and diacids used. These products biodegradability depends also on the structure. The addition of adipic acid, which decreases the crystallinity [66] tends to increase the compost biodegradation rate [67]. According to Ratto et al. [68], the biodegradation results demonstrate that although PBSA is inherently biodegradable, the addition of starch filler significantly improves the rate of degradation. Blending PBSA with non-degradable polymers such as poly(vinyl acetate) PVAc or linear low density poly(ethylene) LLDPE leads to immiscible systems whereas PBSA presents very good miscibility with poly(epichlorohydrin) PECH [69–71].

3.2.3. Aromatic copolyesters

Compared to totally aliphatic copolyesters, aromatic copolyesters are often based on terephthalic acid. Fig. 2 and Table 1 show, respectively, the chemical structure and the properties of such products (e.g., Eastar Bio® from Eastman). Besides, BASF and DuPont commercialize aromatic copolyesters under Ecoflex® [17] and Biomax® trademarks, respectively. Biomax® shows a high terephthalic acid content which modifies some properties such as the melting temperature (200 °C). But, according to Muller et al. [65], an increase of terephthalic acid content tends to decrease the degradation rate. Ecoflex® biodegradation has been analysed by Witt et al. [72]. They concluded that there is no indication for an environmental risk (eco-toxicity) when aliphatic–aromatic copolyesters of the Ecoflex®-type are introduced into composting processes.

3.2.4. Polyesteramide

Polyesteramide was industrially obtained from the statistical copolycondensation of polyamide (PA 6 or PA 6-6) monomers and adipic acid [17,73]. Bayer had developed different commercial grades under BAK® trademark but their productions stopped in 2001. Fig. 2 and Table 1 show, respectively, the chemical structure and the properties of this poly(butylene adipate-*co*-amino caproate). Table 1 shows that this polyester presents the highest polar component, and then presents good compatibility with other polar products, e.g., starchy compounds. Besides, it has the highest water permeability (see Table 1). Currently, the environmental impact of this copolymer is open to discussion. Fritz [74] had shown that, after composting, this biodegradable polyester presented a negative ecotoxicological impact but more recently, Bruns et al. [75] have infirmed these results. These authors discussed Fritz's experiments and more precisely the composting methods used.

4. Biopolyester/clay nano-biocomposites

Before discussing about the different nano-biocomposites based on the polyesters described above, it is necessary to consider some general information about the clays specific properties, as well as the different and possible elaboration routes of such materials.

4.1. Generalities

4.1.1. Clays

The clays most commonly used in the field of nanocomposites belong to the family of 2:1 layered silicates, also called 2:1 phyllosilicates (montmorillonite, saponite). Their structure consists of layers made up of two tetrahedrally coordinated silicon atoms fused to an edge-shared octahedral sheet of either aluminium or magnesium hydroxide (see Fig. 3). Each layered sheet is about 1 nm thick and its length varies from tens of nanometers to more than one micron, depending on the layered silicate. Layer stacking leads to a regular Van der Waals gap between the platelets called the interlayer or the gallery. Isomorphic substitution may occur inside the sheet since Al^{3+} can be replaced by Mg^{2+} or Fe^{2+}, and Mg^{2+} by Li^{+}. Globally negatively charged platelets are counterbalanced by alkali and alkali earth cations (Na^{+}, Ca^{2+}, etc.) located in the galleries, which increases the clay hydrophilic character. Most polymers, and particularly the biopolyesters are considered to be organophilic compounds. Thus, to obtain better affinity between the filler and the matrix, and eventually to improve final properties, the inorganic cations located inside the galleries (Na^{+}, Ca^{2+}, etc.) are generally exchanged by ammonium or phosphonium cations bearing at least one long alkyl chain, and possibly other substituted groups. The resulting clays are called organomodified layered silicates OMLS and, in the case of montmorillonite MMT, are abbreviated OMMT. By modifying the layered silicate, it is possible to compatibilize the matrix and the filler, which will affect the material nanostructure, and consequently the properties of the nanocomposites. Tables 2 and 3 present the characteristics of the main 2:1 layered silicates and commercial clays.

4.1.2. Elaboration routes

An important key factor in the nanocomposites preparation is the elaboration protocol. Nowadays, three main

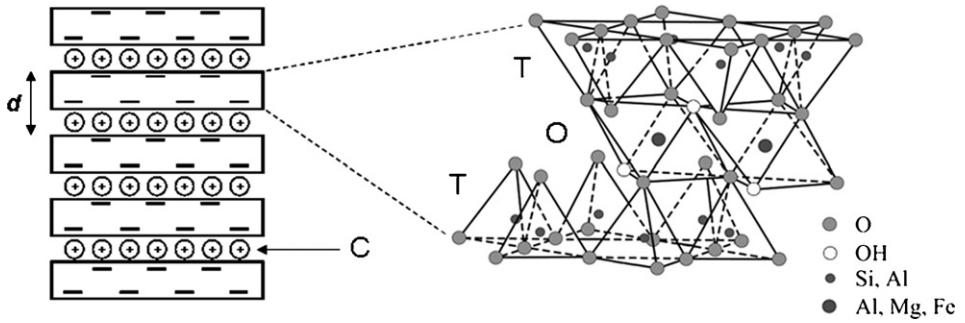

Fig. 3. 2:1 layered silicate structure (T, tetrahedral sheet; O, octahedral sheet; C, intercalated cations; *d*, interlayer distance). Reproduced with permission from Lagaly [191] copyright (1993) of Marcel Dekker.

Table 2
Structural characteristics of principal 2:1 layered silicates. Adapted and reproduced with permission from Sinha Ray et al. and Utracki et al. [192,193] copyright (2003) of Elsevier Science Ltd. and copyright (2007) of John Wiley & Sons, Ltd.

Phyllosilicates	Octahedra occupancy	Interlayer cations	CEC (meq/100 g)	Aspect ratio
Smectites				
Hectorite	Mg (3/3)	Na^+, Ca^{2+}, Mg^{2+}	120	200–300
Montmorillonite	Al (2/3)	Na^+, Ca^{2+}, Mg^{2+}	110	100–150
Saponite	Mg (3/3)	Na^+, Ca^{2+}, Mg^{2+}	86.6	50–60

methods are applied: (i) the solvent intercalation route which consists in swelling the layered silicates in a polymer solvent to promote the macromolecules diffusion in the clay interlayer spacing, (ii) the in-situ intercalation method for which the layered silicates are swollen in the monomer or monomer solution before polymerization, and (iii) the melt intercalation process which is based on polymer processing in the molten state such as extrusion. Obviously, the latter method is highly preferred in the context of sustainable development since it avoids the use of organic solvents, which are not eco-friendly and then alter the life cycle analysis LCA.

4.1.3. Nanocomposites structures

Finally, different structures of nanocomposites could be obtained:

(i) a microcomposite when the clay layers are still stacked and the polymer is not intercalated within the (O)MMT's layers due to poor polymer-clay affinity, the material thus presents phase separation;
(ii) an intercalated nanocomposite for which the polymer is partially intercalated between the silicate layers; these latter are still stacked but the interlayer spacing has increased;

Table 3
Commercial (O)MMT and their characteristics.

Commercial clays Supplier/trade name/designation		Clay type	Organomodifier type	Modifier concentration (meq/100 g)	Δw[a] (%)	*d*-spacing (Å)
Southern Clay Products (USA)						
Cloisite®Na	CNa	MMT	–	–	7	11.7
Cloisite®15A	C15A	MMT	$N^+(Me)_2(tallow)_2$	125	43	31.5
Cloisite®20A	C20A	MMT	$N^+(Me)_2(tallow)_2$	95	38	24.2
Cloisite®25A	C25A	MMT	$N^+(Me)_2(C_8)(tallow)$	95	34	18.6
Cloisite®93A	C93A	MMT	$NH^+(Me)(tallow)_2$	90	37.5	23.6
Cloisite®30B	C30B	MMT	$N^+(Me)(EtOH)_2(tallow)$	90	30	18.5
Süd-Chemie (Germany)						
Nanofil®804	N804	MMT	$N^+(Me)(EtOH)_2(tallow)$		21	18
Laviosa Chimica Mineraria (Italy)						
Dellite® LVF	LVF	MMT	–	105	4–6	9.8
Dellite® 43B	D43B	MMT	$N^+(Me)_2(CH_2\text{-}\phi)(tallow)$	95	32–35	18.6
CBC Co. (Japan)						
Somasif	MEE	SFM	$N^+(Me)(EtOH)_2(coco\ alkyl)$	120	28	
	MAE	SFM	$N^+(Me)_2(tallow)_2$	120	41	

Tallow: ~65% C_{18}; ~30% C_{16}; ~5% C_{14}.
[a] %Weight loss on ignition.

(iii) eventually, an exfoliated nanocomposite showing individual and well-dispersed clay platelets into the matrix; in this case, the layered structure does not exist anymore.

4.2. Polyesters matrices based on agro-resources

4.2.1. Poly(lactic acid)-based nano-biocomposites

PLA is a very promising material since it has good mechanical properties, thermal plasticity and biocompatibility. However, some of its properties, like flexural properties, gas permeability and heat distortion temperature, are too low for widespread applications. Therefore, many attempts were carried out to reach exfoliation state in corresponding nano-biocomposites. Various organoclays with different organomodifiers were selected and several elaboration routes were tested (see Table 4).

Ogata et al. [76] first attempted to prepare PLA-based nanocomposites by the solvent intercalation method. Unfortunately, the layered silicates were not individually well dispersed but rather formed tactoids consisting of several stacked silicate monolayers. Consequently, although the Young's modulus increased with the clay content, the increments were small compared to conventional nanocomposites. Later, Chang et al. [77,78] examined the influence of the layered silicates aspect ratio (montmorillonite, fluorinated synthetic mica), of the organomodifier ($N^+(Me)_2(C_8)$(tallow)-C25A-, hexadecylamine-C_{16}-, dodecyltrimethyl ammonium bromide-DTA) and of the clay content on the nanofiller dispersion into a PLA matrix. It was shown by X-ray diffraction XRD and transmission electron microscopy TEM that intercalated structures were obtained, leading to some improvements in mechanical and barrier properties with only small amount of fillers. Compared to neat PLA, the ultimate strength increased by about 65%, 47% and 131% in the case of PLA with 2 wt% of C25A, 4 wt% of C_{16}-MMT and C_{16}-mica, respectively. However, it appeared that the mechanical enhancement was limited to a small range of clay content (up to 4–6 wt% depending on the organomodifier). Above these clay contents, properties decreased due to layered silicates agglomeration. Considering O_2 permeability, a decrease of more than a half is observed at 10 wt% of OMMT. The initial degradation temperatures decreased linearly with an increasing OMMT amount reaching a maximum shift of 49 and 41 °C in the case of 8 wt% of C_{16}-MMT and C25A, respectively. In the case of C_{16}-mica at the same clay loading, the decrease was only of 16 °C. It was also shown that DTA-MMT presents a particular thermal behavior since the initial degradation temperature was not affected by the clay content [78].

Finally, Krikorian and Pochan [79] successfully prepared exfoliated materials with randomly distributed clay platelets via solvent intercalation in the presence of C30B. Since C30B bears a long alkyl chain and hydroxyl groups, the interactions between OH functions from the clay organomodifier and C=O moieties of the PLA backbone favored exfoliation. Therefore, the mechanical properties were improved, e.g., the storage modulus increased by 61% with 15 wt% of C30B. A complete study of the crystallization behavior of such materials was also conducted [80,81],

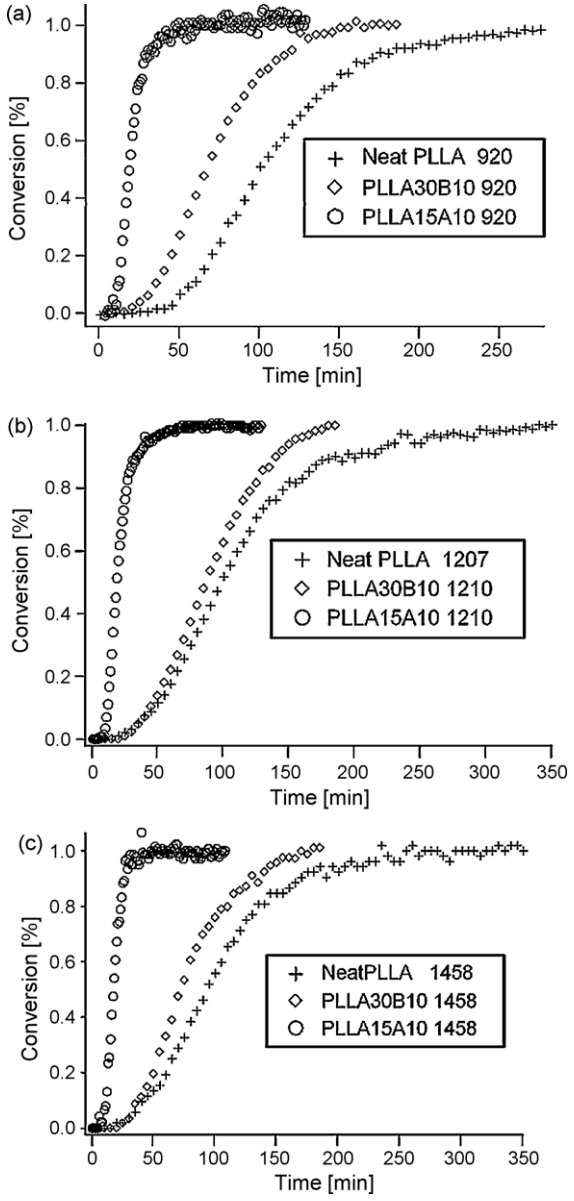

Fig. 4. FT-IR normalized peak intensities at (a) 920, (b) 1210, and (c) 1458 cm^{-1} as a function of crystallization time for neat PLLA, PLLA with 10% of C15A and PLLA with 10% of C30B. Reproduced with permission from Krikorian and Pochan [81] copyright (2005) of the American Chemical Society.

focusing on the role of intercalated or exfoliated layered silicates on the nucleation, the growth, and thus, the overall crystallinity. They demonstrated that addition of highly miscible clay leads to low spherulite nucleation, low bulk crystallization, and as a result, much lower extent of crystallinity compared to neat polymer. Moreover, from FTIR analyses, they described the mechanisms of crystallization and explained how the highly miscible clay hinders the crystal nuclei formation (see Fig. 4) [81].

Exfoliated structure of PLA-based nanocomposites was also obtained by Wu and Wu [82] using a solution mixing process. They increased the interactions between the

Table 4
Structure of the studied PLA/clay nano-biocomposites.

Process	System	Structure	Reference
Solvent intercalation	MMT-$N^+(Me)_2(C_{18})_2$/chloroform	Tactoids	[76]
	SFM-$NH_3^+(C_{16})$/dimethylacetamide MMT-$NH_3^+(C_{16})$/dimethylacetamide MMT-$N^+(Me)_3(C_{12})$/dimethylacetamide MMT-$N^+(Me)_2(C_8)$(tallow)/dimethylacetamide	Intercalated	[77,78]
	MMT-$N^+(Me)(EtOH)_2$(tallow)/dichloromethane	Exfoliated	[79]
	MMT-$N^+(Me)_3(C_{16})$ + chitosan/methylene chloride	Exfoliated	[82]
In-situ intercalation	MMT-$N^+(Me)_2(C_8)$(tallow)/triethylaluminium	Intercalated	[108,113]
	MMT-$N^+(Me)_2(C_8)$(tallow)/tin octoate	Intercalated	[113]
	MMT-$N^+(Me)(EtOH)_2$(tallow)/triethylaluminium	Exfoliated	[108,113]
	MMT-$N^+(Me)(EtOH)_2$(tallow)/tin octoate	Exfoliated	[113]
	MMT-$N^+(Me)(EtOH)_2$(tallow)/α-ω-diOH o-PEG/tin octoate	Exfoliated	[108]
Melt intercalation	MMT-$NH_3^+(C_{18})$	Intercalated-flocculated Intercalated	[88,92–94] [84,112]
	MMT-$NH_3^+(C_{18})$/o-PCL	Intercalated-flocculated	[88]
	MMT-$NH_3^+(C_{18})$/o-PEG	Intercalated	[112]
	MMT-$NH_3^+(C_{18})$/diglycerine tetraacetate	Intercalated	[112]
	MMT-$NH^+(EtOH)_2(C_{18})$ MMT-$NH^+(EtOH)_2(C_{18})$/o-PEG MMT-$NH^+(EtOH)_2(C_{18})$/diglycerine tetraacetate	Intercalated	[112]
	MMT-$N^+(Me)_3(C_{18})$	Intercalated	[86,89,92,94,97]
	MMT-$N^+(Me)_2(C_{18})_2$	Intercalated-flocculated Intercalated (tactoids of 5–7 layers)	[94,95] [96,97]
	MMT-$N^+(Me)_2(C_{18})_2$/PCL	Intercalated	[105]
	MMT-$N^+(Me)_2(C_{18})_2$/o-PEG	Intercalated	[111]
	MMT-$N^+(Me)_2(C_{18})_2$/PEG	Intercalated	[111]
	MMT-$N^+(Me)_2(CH_2\text{-}\phi)(C_{18})$/o-PEG	Intercalated	[111]
	MMT-$N^+(Me)_2(CH_2\text{-}\phi)(C_{18})$/PEG	Intercalated	[111]
	MMT-$N^+(Me)_2(C_8)$(tallow)	Intercalated	[107]
	MMT-$N^+(Me)_2(C_8)$(tallow)/PBS	Intercalated	[102,103]
	MMT-$N^+(Me)_2(C_8)$(tallow)/o-PEG	Intercalated	[106,107,109,110]
	GPS-g-MMT-$N^+(Me)_2(C_8)$(tallow)/PBS	Exfoliated or Intercalated/exfoliated	[102,103]
	MMT-$N^+(Me)_2$(tallow)$_2$	Intercalated	[98]
	MMT-$N^+(Me)_2$(tallow)$_2$/o-PEG	Intercalated	[106,109,110]
	MMT-$N^+(Me)(ButOH)_2(C_{18})$	Flocculated (tactoids of 1–3 layers)	[96,97]
	MMT-$N^+(Me)(EtOH)_2$(tallow)	Intercalated	[98]
	MMT-$N^+(Me)(EtOH)_2$(tallow)/o-PEG	Intercalated	[106,109,110]
	MMT-$P^+(But)_3(C_{16})$	Intercalated	[85]
	Smectite-$P^+(But)_3(C_8)$	Not intercalated	[85]
	Smectite-$P^+(But)_3(C_{12})$	Intercalated	[85]
	Smectite-$P^+(But)_3(C_{16})$	Intercalated and low ordered	[85]
	Smectite-$P^+(Me)(\phi)_3$	Not intercalated	[85]
	Mica-$P^+(But)_3(C_{16})$	Intercalated and well ordered	[85]
	SFM-$N^+(Me)(EtOH)_2$(coco alkyl)	Intercalated/exfoliated Intercalated-flocculated	[87] [90,92,94]
	SFM-$N^+(Me)_2$(tallow)$_2$	Intercalated	[84]
	SAP-$P^+(But)_3(C_{16})$	Exfoliated	[92,94]
Masterbatch	MMT-$N^+(Me)_2(EtOH)_2$/PLLA/triethylaluminium + PDLLA MMT-$N^+(Me)_2(EtOH)_2$/PLLA/o-PEG/triethylaluminium + PDLLA	Intercalated/exfoliated	[108]
	MMT-$N^+(Me)_2(C_8)$(tallow)/PLLA + PDLLA	N.D.	[104]

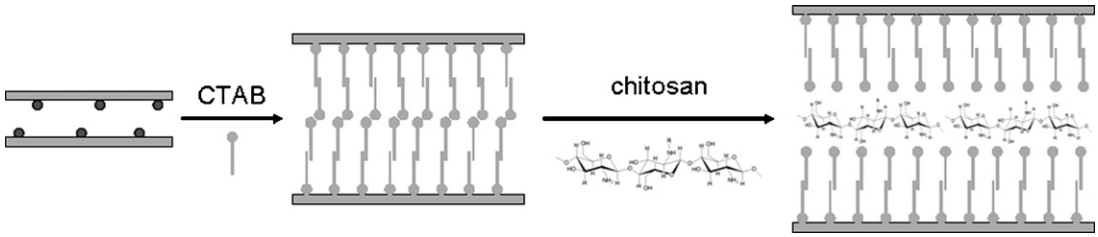

Fig. 5. Schematic drawing of montmorillonite organomodification by CTAB and chitosan. Reproduced with permission from Wu and Wu [82] copyright (2006) of Elsevier Science Ltd.

filler and the matrix by treating the montmorillonite with *n*-hexadecyl trimethylammonium bromide (CTAB) cations and then modified it with chitosan, a biodegradable and biocompatible polymer (see Fig. 5).

The elaboration of PLA/clay nano-biocomposites by melt intercalation is also widely described in the literature [83–98], leading to various materials structures. Okamoto and his group at Toyota Technological Institute (Nagoya, Japan) tested a lot of PLA-based systems differing from the OMLS in the aspect ratio of the inorganic platelets, the nature of the organomodifier, and the clay content [85–95]. Depending on these parameters, intercalated, intercalated-and-flocculated, nearly exfoliated, or the coexistence of intercalated and exfoliated states were obtained. They even proposed an interpretation of the nanocomposites structure related to the aspect ratio and the organomodifier chain lengths [85]. Regarding the aspect ratio, it was demonstrated that the smaller the silicate layers size, the lower the physical jamming, restricting the conformation of organomodifier alkyl chains, and thus, the lower the coherency of the organoclay (see Fig. 6). Due to a nicely stacked structure of organomodified mica, the polymer chains can hardly penetrate up to the core of the silicate layers, contrary to smaller size of silicate layers such as smectite and MMT (see Fig. 6). The effect of organomodifiers organization in the interlayer space was also examined considering an interdigitated layer structure of the surfactants [99].

Flocculated structures were further studied by Nam et al. [96,97] using bis(4-hydroxy butyl) methyl

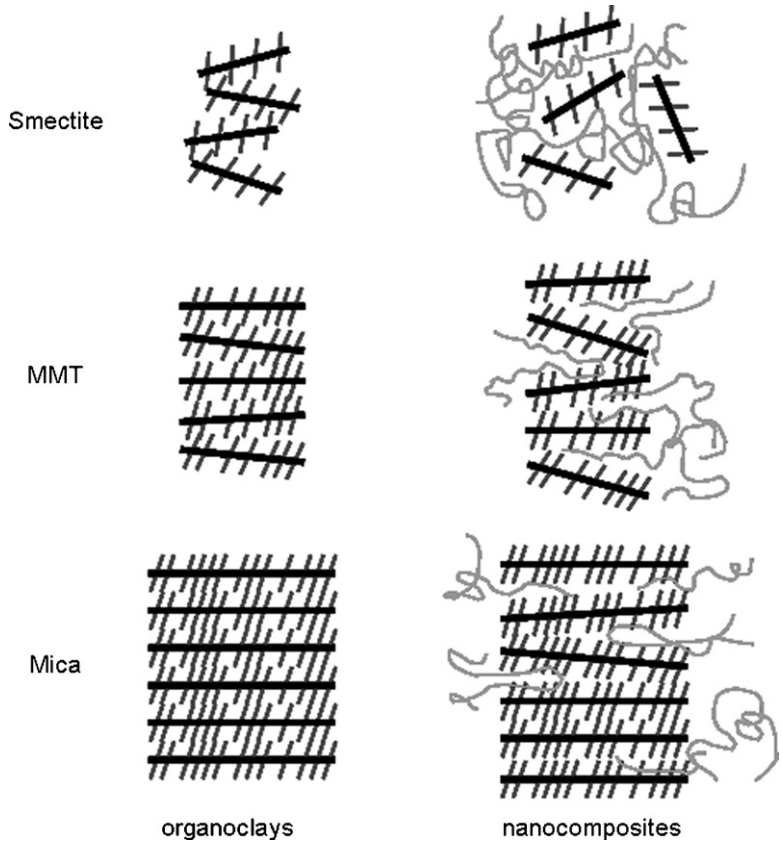

Fig. 6. Structure of organoclays and the corresponding nanocomposites depending on the type of layered silicates. Reproduced with permission from Maiti et al. [85] copyright (2002) of the American Chemical Society.

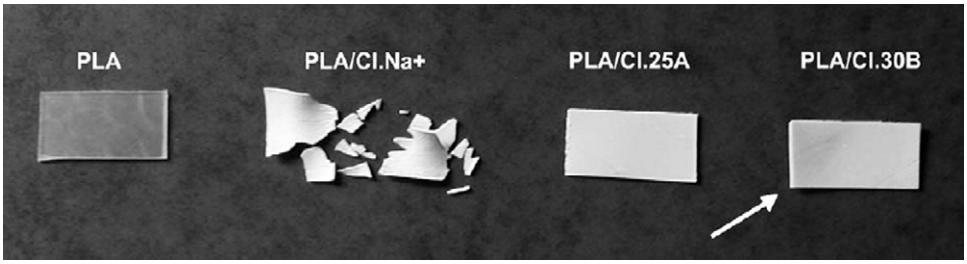

Fig. 7. Visual aspect of PLA matrix, microcomposite based on CNa and nanocomposites based on C25A and C30B, respectively, after five and a half months of hydrolysis (the white arrow points the curvature of the sample). Reproduced with permission from Paul et al. [98] copyright (2005) of Elsevier Science Ltd.

octadecyl ammonium modified montmorillonite (MMT-$N^+(Me)(ButOH)_2(C_{18})$). From polarized optical microscopy POM, TEM and particularly FT-IR, they showed that the formation of such nanocomposite structures could be due to hydrogen bonding among the hydroxyl groups of the surfactant, those of platelets edges and those of both ends of the PLA chains.

As a consequence of the nanostructure, and despite of the fact that incomplete exfoliation was obtained by melt intercalation, all these nano-biocomposites exhibited dramatic enhancements of various materials properties. These improvements included mechanical and flexural properties, heat distortion temperature, and O_2 gas permeability. However, it has to be noticed that the increments strongly depend on the structure of the nanocomposites. A particular study of the crystallization behavior of the well-ordered intercalated PLA/octadecylammonium OMMT (MMT-$NH_3^+(C_{18})$) nanocomposite revealed a spherulite size decrease and an overall crystallization rate enhancement compared to neat PLA [100]. This was attributed to the clay nucleating effect. Furthermore, since the compostability is controlled by the crystallinity, the molecular weight and the (OM)LS dispersion, it was enhanced by the incorporation of layered silicates [92,101]. Paul et al. [98] studied the hydrolytic degradation in such materials and concluded that the more hydrophilic the filler, the more pronounced the degradation. This was expressed by increasing opacity and shape modification before fragmentation (see Fig. 7).

Eventually, the addition of the most appropriate OMLS could also enhance the properties of polymers blends as described by Chen et al. [102,103] who used a specific organoclay to compatibilize an immiscible PLLA/PBS blend. They introduced epoxy groups to C25A by treating the clay with (glycidoxypropyl)trimethoxy silane (GPS) to produce a twice-functionalized organoclay TFC (see Fig. 8). Reacting with epoxy groups located on the clay surface, the biopolyesters tend to delaminate the platelets (see Fig. 9). However, since TFC was highly compatible with PLLA rather than PBS, at small TFC content, the clays are located almost exclusively in the PLLA phase and are fully exfoliated. At higher TFC content, the clay layers were dispersed in both PBS and PLLA phases with intercalated/exfoliated coexisting morphology. The domains size of the dispersed PBS phase decreased sharply since the platelets hinders the PBS domains coalescence. The addition of TFC to the PLLA/PBS blend not only improved the tensile modulus but also the elongation at break, while the incorporation of C25A to the same polymer blend increased the tensile modulus but at the cost of the elongation at break. The thermal stability of these materials, in terms of onset temperature and activation energy of degradation was also enhanced [103].

Therefore, by a judicious choice of the OMLS, it is possible to tune the material properties [92]. Furthermore, the process could also play a key role in the final nano-biocomposites structure and properties. For example, Lewitus et al. [104] prepared nano-biocomposites

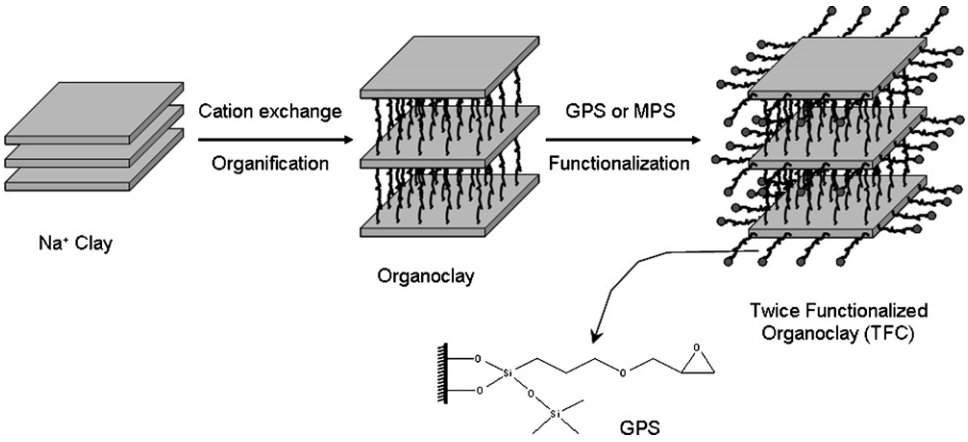

Fig. 8. Schematic drawing of the twice-functionalized organoclay (TFC) preparation. Reproduced with permission from Chen and Yoon [182] copyright (2005) of the Society of Chemical Industry.

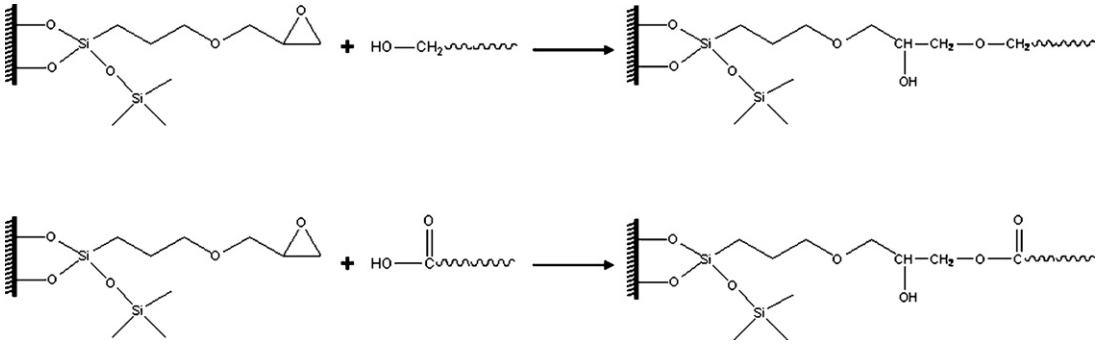

Fig. 9. Reaction between the epoxy groups in TFC and the functional end-groups of the polyesters Reproduced with permission from Chen and Yoon [103] copyright (2005) of Elsevier Science Ltd.

from PLLA-based masterbatches which were dispersed into different matrices (PLLA, PDLLA, PBAT). Compared to neat PLLA, the corresponding nano-biocomposites demonstrated enhanced film properties, showing a potential extend to film applications as, e.g., compostable packaging. The most significant improvements were obtained when the PLLA-nanoclays masterbatches were dispersed into the same PLLA matrix. In this case, the incorporation of 5 wt% of clay increased the tensile modulus and the elongation at break of PLLA by 36% and 48%, respectively, while the tensile strength did not change significantly. Authors attributed this toughening effect to molecular interactions between nanoclays and PLA but also to a high degree of exfoliation. Unfortunately, without complementary characterizations of these systems, these results could not be confirmed. Regarding the thermal properties, it was proved that clays acted as nucleating agent since the cold crystallization temperature was decreased by 15 °C.

The melt intercalation process allows incorporation of additives such as compatibilizers and plasticizers. The addition of oligo-PCL [88] (o-PCL) or PCL [105] to PLA-clay systems had not a beneficial effect on the interlayer spacing. However, the o-PCL, used as compatibilizer, induced a flocculated state due to hydroxylated edge–edge interactions of layered silicates leading to great enhancement of mechanical properties. Hasook et al. [105] also obtained reinforced materials properties when adding 5 wt% of PCL with short chain length (<40,000).

Some authors were also interested in developing plasticized PLA-based nanocomposites to reduce the brittleness and to improve the flowability during the process. Thus, PLA plasticized with PEG [106–111] or diglycerine tetraacetate [112] was melt compounded with different organoclays leading to intercalated structures. Paul et al. [106] and Pluta et al. [109] showed that there is a real competition between PEG and PLA for the intercalation into the clay interlayer. Tanoue et al. [111] also studied the structure of such materials using PEG with different molecular weight. With a certain type of organoclay, i.e., dimethyl distearyl ammonium modified MMT (MMT-$N^+(Me)_2(C_{18})_2$), these authors demonstrated that the interlayer distance depends on the PEG chain length. Besides, they pointed out that addition of PEG affects the dispersion of clay in the PLA matrix resulting in more aggregated structures. Mechanical properties can be improved [111,112] and crystallization enhanced [107,112] by selecting the right organoclay, plasticizer nature, content and chain length. Nevertheless, Pluta et al. [110] demonstrated that although the dispersed nanoclays can slow down the phase separation, particularly in the case of better PLA-clay affinity (i.e., C20A and C30B), PEG can diffuse toward the surface. Therefore, Paul et al. [108] settled a protocol consisting in the in-situ polymerization of lactide from end-hydroxylated PEG in presence of C30B with tin octoate ($Sn(Oct)_2$) as an activator/initiator. This polymerization method, called the "coordination-insertion" method, leads to PLA chains grafted onto the clay surface via the hydroxylated ammonium organomodifier and to PLA-b-PEG-b-PLA triblock copolymer intercalated into the clay gallery. The plasticizing effect is ensured by the PEG sequence of the triblock without phase separation. More generally, this mechanism allows complete exfoliation by ROP of lactide after adequate activation [113]. In the particular case of activation reaction with triethylaluminium ($AlEt_3$) [108], the polymerization is initiated by the hydroxyl groups of the OMMT organomodifier (see Fig. 10). The as-obtained PLA/OMMT nanocomposites presented enhanced thermal properties since the temperature corresponding to 50% of weight loss is shifted by ~30 °C towards higher temperature. The crystallinity was also affected since the mobility of the resulting grafted chains was restricted while T_g and T_m were not influenced by the clay [108].

Recent publications reported works on more applicative researches since they deal with PLA-based nanocomposites for preparation of porous ceramic materials [114] or for scaffolds as supports for tissue regeneration [115,116]. Foams were also elaborated from PLA/OMMT nanocomposites with the aim of obtaining high cell density and a controlled morphology varying from microcellular to nanocellular structures [117].

To conclude, the literature shows many publications on PLA-based nano-biocomposites, wherein several answers and strategies are proposed to improve the material properties since PLA is commercially and largely available.

4.2.2. Polyhydroxyalkanoates-based nano-biocomposites

Some drawbacks of PHAs, such as brittleness and poor thermal stability restrict their developments and uses. Therefore, nano-biocomposites appear as a possi-

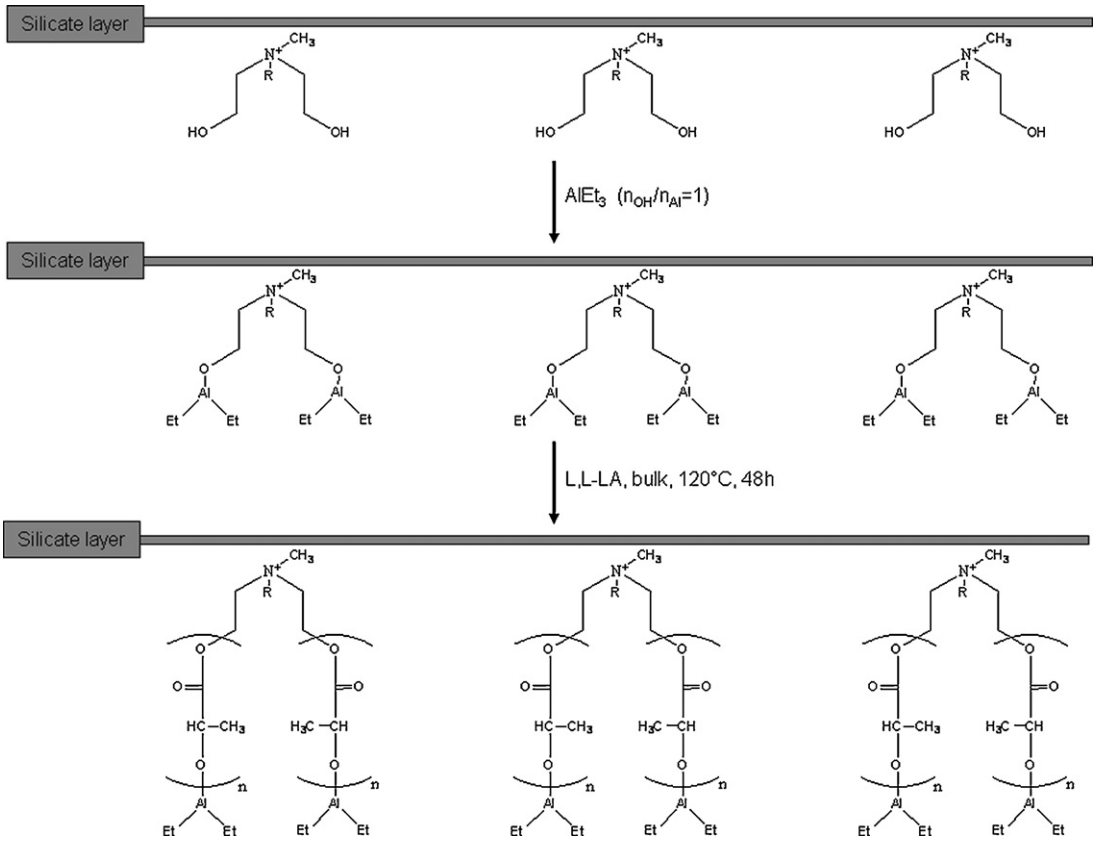

Fig. 10. Schematic representation of the L,L-lactide polymerization performed in-situ from C30B using triethylaluminium ($AlEt_3$) as initiator precursor (R stands for tallow chain). Reproduced with permission from Paul et al. [108] copyright (2005) of Wiley-VCH.

ble answer to overcome these problems and to improve different properties as, e.g., permeability. The studied PHA-based nano-biocomposites are summarized in Table 5 and described below.

First, Maiti et al. [118] prepared PHB-based nanocomposites by melt extrusion. PHB was then reinforced using organomodified fluoromicas or montmorillonite containing 2 wt% and up to 4 wt% of clay, respectively. MEE and MAE fluoromicas (see Table 3) as well as OMMT modified with octadecylammonium (MMT-$NH_3^+(C_{18})$) were selected. XRD and TEM revealed well-ordered intercalated nanocomposites with decreasing *d*-spacing with clay content increases. Dynamic mechanical analyses revealed a better reinforcing effect of fluoromica compared to montmorillonite. The storage modulus *E′* increased with clay content reaching an increment of 35% with 3.6 wt% of MMT-C_{18}, +33% and +40% with 2 wt% of MAE and MEE, respectively. These authors explained this behavior by an enhanced degradation in presence of OMMT, due to the presence of Al Lewis acid sites in the inorganic layers which catalyze the ester linkages hydrolysis. This phenomenon does not occur in the case of fluoromica since they are based on magnesium. Nevertheless, recently, Hablot et al. [119] reported that PHB enhanced degradation can also be caused by decomposition products of clay organomodifiers which have a catalyzing effect on the thermal or thermo-mechanical degradation. Eventually, the biodegradation studies also highlighted the difference between montmorillonite and fluoromicas since the initial degradation rate of PHB with MMT-$NH_3^+(C_{18})$ was higher than with fluo-

Table 5
Structure of the studied PHA/clay nano-biocomposites.

PHA	Process	System	Structure	Reference
PHB	Solvent intercalation	MMT-$N^+(Me)_2(C_8)$(tallow)/chloroform	Intercalated	[120]
	Melt intercalation	MMT-$NH_3^+(C_{18})$	Intercalated	[84,118]
		MMT-$N^+(Me)(EtOH)_2$(tallow)/MA-g-PHB	Intercalated, well delaminated	[126]
		SFM-$N^+(Me)(EtOH)_2$(coco alkyl)	Intercalated	[84,118]
		SFM-$N^+(Me)_2$(tallow)$_2$	Intercalated	[84,118]
PHBV	Solvent intercalation	MMT-$N^+(Me)_3(C_{16})$/chloroform	Intercalated	[122–124]
	Melt intercalation	MMT-$N^+(Me)(EtOH)_2$(tallow)	Intercalated, nanodispersion	[121]

romicas [118]. In this case, the degradation rates have been considerably reduced and even suppressed with MEE.

A similar study on PHB-based nanocomposites was carried out by Lim et al. [120]. Nevertheless, they used solvent intercalation route to obtain PHB/C25A with 3, 6 and 9 wt% of clay content. XRD data led to the conclusion of intercalated structures, the interlayer distance reaching 35 Å, but no dependence on clay content was observed. These results were confirmed by FTIR analyses showing that two distinct different phases coexisted. These structural observations were completed by the thermal stability investigation. TGA results indicated an increase of the onset temperature of weight loss and a decrease of the degradation rate with 3 wt% of C25A. This was attributed to the nanoscale OMMT layers dispersion decreasing the diffusion of volatile decomposition products. At higher clay contents (>6 wt%), although the onset of thermal degradation did not increase because of the organomodifier's thermal sensitivity, the nanocomposites degradation rates decreased due to restricted thermal motion of the polymer chains in the OMMT interlayer.

Scientists were also interested in the development of PHBV-based nanocomposites since the PHBV presents better properties than PHB and better processability. In 2003, Choi et al. [121] described the microstructure as well as the thermal and mechanical properties of PHBV/C30B nanocomposites with low clay content. These materials were prepared by melt intercalation using a Brabender mixer. XRD and TEM clearly confirmed that intercalated nanostructures were obtained. Such structures were formed thanks to the strong hydrogen bond interactions between PHBV and the hydroxyl groups of the C30B organomodifier. They demonstrated that the nanodispersed organoclay acted as a nucleating agent, increasing the temperature and rate of PHBV crystallization. Moreover, the DSC thermograms revealed that the crystallite size was reduced in the presence of nanodispersed layers since the PHBV melting temperature are shifted to lower temperatures. Nanocomposites thermal stabilities were also studied. Thermogravimetric analyses revealed that the temperature corresponding to 3% of weight loss increased with C30B content (+10 °C with 3 wt% of filler). They explained these trends by the nanodispersion of the silicate layers into the matrix and thus concluded that the well-dispersed and layered structure accounts for an efficient barrier to the permeation of oxygen and combustion gas. Eventually, the mechanical properties showed that clays can also act as an effective reinforcing agent since the Young's modulus significantly increases from 480 to more than 790 MPa due to strong hydrogen bonding between PHBV and C30B.

Wang et al. [122] and Zhang and co-workers [123,124] have investigated the structure and the properties of PHBV/OMMT nanocomposites. They synthesized PHBV with 3 and 6.6 mol% of HV units as well as organomodified MMT via cationic exchange in an aqueous solution with hexadecyl-trimethylammonium bromide (MMT-$N^+(Me)_3(C_{16})$). Nanocomposites were prepared by the solution intercalation method, adding 1, 3, 5 or 10 wt% OMMT to a chloroform solution of PHBV and then exposing the resulting dispersions to an ultra-sonication treatment. These conditions led to intercalated structures, as shown by XRD, but clay aggregation occurred when increasing the clay content to 10 wt%.

A detailed study of the PHBV/OMMT crystallization behavior was achieved. It was shown that OMMT acted as a nucleating agent in the PHBV matrix, which increased the nucleation and the overall crystallization rate, leading to more perfect PHBV crystals [123]. With increasing amount of OMMT, the predominant crystallization mechanism of PHBV was shifted from the growth of crystals to the formation of crystalline nuclei. The nucleation effect of the organophilic clay decreased with the clay content increase. Wang et al. [122] postulated that the nanoscaled OMMT layers affect the crystallization in two opposite ways. On one hand, a small part of OMMT can increase the crystalline nuclei thus causing a more rapid crystallization rate. On the other hand, owing to the interaction of OMMT layers with PHBV chains, most of the OMMT layers restrict the motion of the PHBV chains. Therefore, the crystallization rate increased whereas the relative degree of crystallinity decreased with increasing amount of clay in the PHBV/OMMT nanocomposites. Furthermore, the PHBV processing behavior could be improved with OMMT-based nanocomposites since the processing temperature range enlarged by lowering melting temperature with the increasing clay content. The tensile properties of the corresponding materials were improved by incorporation of 3 wt% of clay [124]. Above this clay content, aggregation of clay occurred and tensile strength and strain at break decrease. Dynamic mechanical analysis, through the study of the modulus and the T_α relaxation temperature (see Fig. 11), revealed that the interface was maximized because of the nanometer size, which restricts segmental motion near the organic-inorganic interface. Thus, it confirmed that intercalated nanocomposites were formed. Eventually, the biodegradability of these nanocomposites systems in soil suspension decreased with increasing OMMT. This was related to the interactions between PHBV and OMMT, but also to water permeability, the degree of crystallinity, and the anti-microbial property of OMMT.

Eventually, Misra et al. developed a novel solvent-free method to prepare PHB functionalized by maleic anhydride (MA-g-PHB) [125]. The functionalization was successfully achieved by free radical grafting of maleic anhydride using a peroxide initiator by reactive extrusion processing. Then, they have mixed MA-g-PHB with C30B to make the organomodifier hydroxyl functions react with the MA [126]. Although, the *d*-spacing was comparable to PHB/C30B prepared by melt blending, the decrease in intensity of XRD signals and TEM images showed that more delaminated platelets were obtained.

To conclude, most of the articles reported the preparation of PHA-based nanocomposite by solvent intercalation, and whatever the elaboration route, full exfoliation state was neither obtained nor clearly demonstrated.

4.3. Petroleum-based polyesters

4.3.1. Polycaprolactone-based nano-biocomposites

PCL-based nanocomposite was the first studied nano-biocomposite. In the early 1990s, Giannelis' group from

Table 6
Structure of the studied PCL/clay nano-biocomposites.

Process	System	Structure	Reference
Solvent intercalation	MMT-$N^+(Me)_2(C_{18})_2$/chloroform	Slightly intercalated	[164]
Melt intercalation	MMT-$N^+(Me)_2(C_{18})_2$	Intercalated	[140]
	MMT-$N^+(Me)_2(C_8)$(tallow)	Intercalated	[135,145,159]
	MMT-$NH_3^+(C_{11}COOH)$	Microcomposite	[135]
	MMT-$N^+(Me)(EtOH)_2$(tallow)	Intercalated/exfoliated	[135,145,159]
		Exfoliated	[148,149]
	Smectite-$P^+(But)_3(C_8)$/o-PCL	Intercalated	[158]
	Smectite-$P^+(But)_3(C_{12})$-/o-PCL	Intercalated	[158]
	Smectite-$P^+(But)_3(C_{16})$/o-PCL	Intercalated	[158]
	Smectite-$P^+(Me)(\phi)_3$/o-PCL	Intercalated	[158]
	SFM-$P^+(But)_3(C_{16})$/o-PCL	Intercalated	[158]
	Hectorite-$P^+(But)_3(C_{16})$/o-PCL	Intercalated, almost exfoliated	[158]
Masterbatch	MMT-Na-g-PCL + PCL	Intercalated	[150]
	MMT-$N^+(Me)_2(C_8)$(tallow)-g-PCL + PCL	Intercalated	[150]
	MMT-$N^+(Me)(EtOH)_2$(tallow)-g-PCL + PCL	Intercalated	[150]
	MMT/dibutylamine terminated o-CL + PCL	Intercalated (low o-CL chain length) Intercalated/exfoliated (high o-CL chain length)	[151]
In-situ intercalation	Fluorohectorite-Cr^{3+}	Intercalated	[128]
	MMT-$NH_3^+(C_{18})$	Intercalated	[140]
	MMT-$NH_3^+(C_{11}COOH)$	Exfoliated	[127,129,132–134]
		Intercalated	[127,129,132–135,140]
	MMT-$N^+(Me)_2(C_{18})_2$	Microcomposite	[127,140]
	MMT-$N^+(Me)_3(C_{16})$	Intercalated	[131]
	MMT-$N^+(Me)_2(C_8)$(tallow)	Microcomposite	[140]
	MMT-$N^+(Me)(EtOH)_2$(tallow)	Exfoliated	[140]
	MMT/water	Slightly intercalated	[130]
	MMT-Na/tin octoate	Intercalated	[135,140]
	MMT-Na/dibutyltin dimethoxide	Intercalated	[140]
	MMT-$NH_3^+(C_{18})$/tin octoate or dibutyltin dimethoxide	Intercalated	[135,140]
	MMT-$NH_3^+(C_{11}COOH)$/tin octoate or dibutyltin dimethoxide	Intercalated	[135,140]
	MMT-$N^+(Me)_2(C_{18})_2$/tin octoate or dibutyltin dimethoxide	Intercalated	[135,140]
	MMT-$N^+(Et)_2(CH_2CHOHCH_3)(C_{18})$/tin octoate	Exfoliated or Intercalated/exfoliated	[136]
	MMT-$N^+(Me)_2(C_8)$(tallow)/tin octoate	Intercalated	[135,140,141]
	MMT-$N^+(Me)_2(C_8)$(tallow)/dibutyltin dimethoxide	Intercalated	[135–137,140,159]
	MMT-$N^+(Me)(EtOH)_2$(tallow)/tin octoate	Exfoliated	[135,137,140,142,159]
	MMT-$N^+(Me)(EtOH)_2$(tallow)/dibutyltin dimethoxide	Exfoliated	[135,140,141]
	MMT-$[N^+(Me)_2(EtOH)(C_{16})]_x[N^+(Me)_3(C_{16})]_y$/Tin (II) or Tin (IV) or Al(III) alkoxide	Exfoliated or Intercalated/exfoliated	[138,139]
	MMT-$[N^+(Me)_2(EtOH)(C_{16})]_x[N^+(Me)_3(C_{16})]_y$/triethylaluminium/toluene	Exfoliated	[143]
	SAP-$N^+(Me)_3(C_{16})$/dibutyltin dimethoxide	Intercalated	[162,163]
	SAP-$N^+(Me)_2(EtOH)(C_{16})$/dibutyltin dimethoxide		
	SAP-$N^+(Me)(EtOH)_2(C_{16})$/dibutyltin dimethoxide		
	SAP-$P^+(Me)_3(C_{16})$/dibutyltin dimethoxide		
	LAP-$N^+(Me)_3(C_{16})$/dibutyltin dimethoxide		
	LAP-$N^+(Me)_2(EtOH)(C_{16})$/dibutyltin dimethoxide		
	LAP-$N^+(Me)(EtOH)_2(C_{16})$/dibutyltin dimethoxide		
	LAP-$P^+(Me)_3(C_{16})$/dibutyltin dimethoxide		
	SAP-$P^+(Me)_3(C_{14})$/dibutyltin dimethoxyde	Intercalated	[163]
	SAP-$P^+(Me)_3(C_{12})$/dibutyltin dimethoxyde		

Cornell University (Ithaca, New York, USA) started to work on the elaboration of PCL-based nanocomposite by intercalative polymerization [127–129]. Their work was motivated by previous studies involving polymerization of ε-caprolactam in the presence of layered silicates, which suggested that lactone ROP can be catalyzed by layered silicates. Then, they decided to investigate the intercalation and polymerization of ε-caprolactone within the gallery of layered silicates. The very first PCL-based nanocomposite prepared was based on fluorohectorite, a mica-type layered silicate [128] (see Table 6). The ROP of ε-caprolactone (ε-CL) was activated by the surface of the Cr^{3+}-exchanged fluorohectorite. Indeed, the type of interlayer cations (e.g., Cr^{3+}, Cu^{2+}, Co^{2+}, Na^+) is impor-

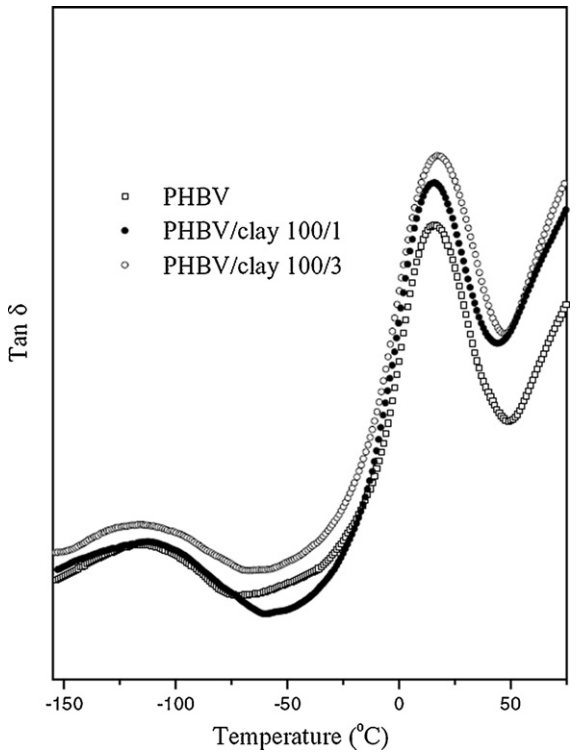

Fig. 11. Tan δ of neat PHBV and PHBV/clay nanocomposites with respectively 1 and 3 wt% of MMT-$N^+(Me)_3(C_{16})$. Reproduced with permission from Chen et al. [124] copyright (2002) of Kluwer Academic Publishers.

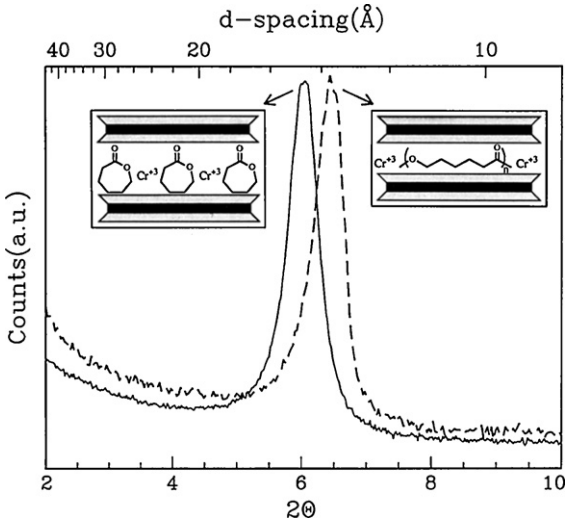

Fig. 12. XRD patterns of PCL nanocomposite before (solid lines) and after (dashed lines) polymerization. Reproduced with permission from Messersmith and Giannelis [128] copyright (1993) of the American Chemical Society.

tant in achieving polymerization since it proceeds through cleavage of the acyl-oxygen bond catalyzed by the interlayer Cr^{3+} ions which present a more acidic character than mono- and divalent cations. The polymer–clay chemical interactions at the interface was proved to be strong and the intercalation of the polymer irreversible. However, authors could also observe the decrease of *d*-spacing after polymerization. They attributed this phenomenon to a change in the intercalated molecules organization from the monomer to the polymer (see Fig. 12). Similar results were also obtained later by Kiersnowski et al. [130] who prepared the PCL-based composites by in-situ polymerization catalyzed by water. Afterwards, Messersmith and Giannelis [127] attempted to prepare PCL-based nanocomposites by in-situ polymerization thermally activated and initiated by organic acid. This one constituted the OMMT organomodifier, namely the protonated form of 12-aminododecanoic acid ($NH_3^+(C_{11}COOH)$), which was thus present on the clay surface and initiated the ROP by a nucleophilic attack on the ε-caprolactone carbonyl. The resulting PCL was therefore ionically bound to the silicate layers through the protonated amine chain end. XRD results suggested that individual silicate layers were dispersed in the matrix. On the contrary, OMMT layers organomodified with a less polar ammonium (dimethyl dioctadecyl-$N^+(Me)_2(C_{18})_2$- [127] or hexadecyltrimethyl-$N^+(Me)_3(C_{16})$- [131] ammonium) showed no dispersion in CL or PCL. Subsequently, the interactions occurring at the interface of a PCL/OMMT exfoliated nanocomposite were investigated [132,133] and the crystallinity, the permeability and the rheological behavior were examined [127,129,132,134]. Both, the crystallinity and the crystallite size decreased because of the dispersed silicate layers that represent physical barriers, and hinder PCL crystal growth. The dispersion of high aspect ratio platelets also reduced the water permeability, nearly by an order of magnitude at 4.8 vol% silicate [127]. Tortora et al. [134] who examined the water and dichloromethane permeability, assumed that the diffusion path of the polar water molecules is slowed down compared to dichloromethane vapor, not only because of the physical barrier of the clay layers, but also because of the hydrophilic character of the platelets. Eventually, the linear viscoelastic behavior of the nanocomposites with various OMMT contents was examined. A "pseudo solid-like" behavior was clearly seen at silicate loading greater than 3 wt% suggesting that domains were formed wherein some long-range order was preserved and the silicate layers were oriented in some direction. Furthermore, the non-terminal effect was more pronounced with increasing clay content. These long-range order and domain structures were hence likely to become better defined when the mean distance between the layers becomes less than the lateral dimensions of the silicate layers and thus forcing some preferential orientation between the layers.

Dubois' group (Mons, Belgium) has worked on PCL nanocomposites. They were interested in the in-situ ROP of ε-CL and in the melt intercalation route. They demonstrated that the formation of PCL-based nanocomposites depends not only on the ammonium cation and related functionality, but also on the elaboration route. Contrary to Messersmith and Giannelis [127,128], PCL-based nanocomposites were prepared by in-situ ROP according to a "coordination-insertion" mechanism [135–141] (see Fig. 13), as for PLA [108,113]. This reaction consists in swelling the OMMT organomodified by alkylammo-

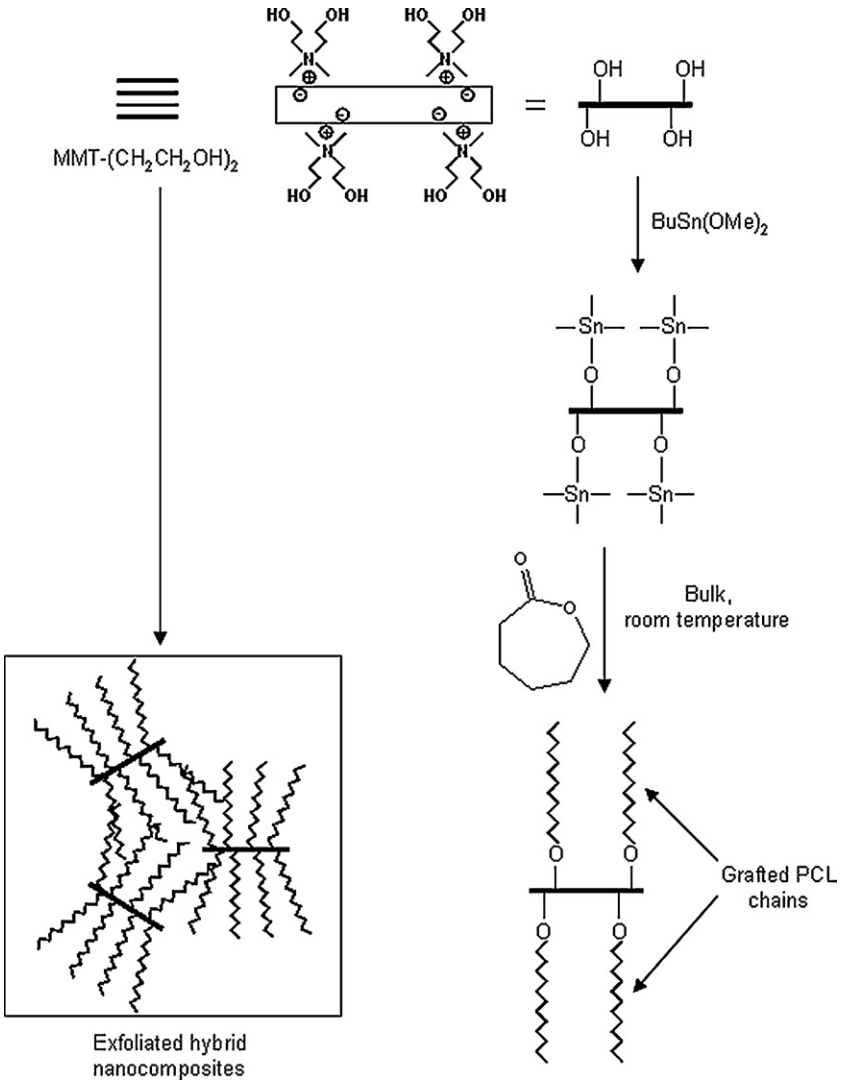

Fig. 13. Scheme of the ε-CL in-situ ring-opening polymerization from the C30B organoclay according to the "coordination-insertion" mechanism. Reproduced with permission from Lepoittevin et al. [137] copyright (2002) of the American Chemical Society.

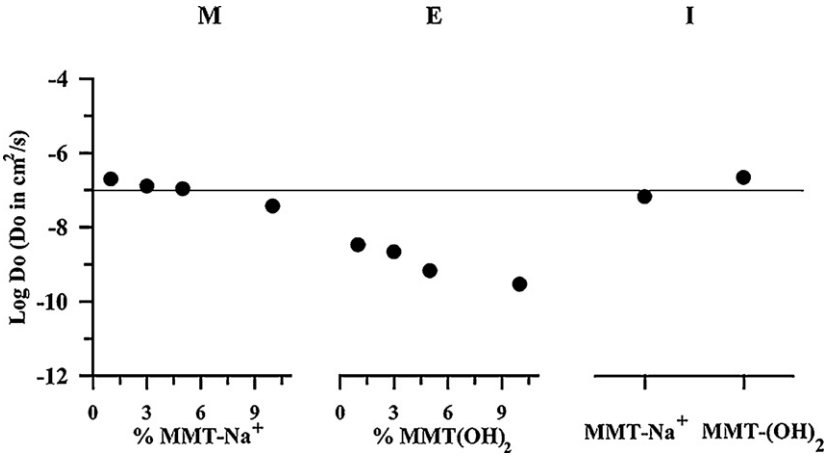

Fig. 14. log D_0 (D_0 in cm^2/s) to water vapor, as function of clay content for the PCL microcomposite (*M*), the exfoliated PCL nanocomposites (*E*) and the 3 wt% intercalated PCL nanocomposites (*I*). Reproduced with permission from Gorrasi et al. [142] copyright (2003) of Elsevier Science Ltd.

nium bearing hydroxyl groups (MMT-$N^+(Me)_2(EtOH)(C_{16})$ or MMT-$N^+(Me)(EtOH)_2$(tallow)) and then adding an initiator/activator such as tin(II) octoate ($Sn(Oct)_2$), dibutyltin-(IV) dimethoxide ($Bu_2Sn(OMe)_2$) or triethylaluminium ($AlEt_3$). The ammonium is thus activated and can yield surface grafted PCL chains. Every hydroxyl function generates a PCL chain. Consequently, the higher the hydroxyl groups content, the lower the PCL average molar masses. It is worth noting that, in the presence of tin(IV) catalysts, since they are more efficient towards ε-CL ROP, the preparation took place in milder conditions compared to $Sn(Oct)_2$ [135]. Moreover, in all cases, the nanocomposites exhibited a continuous decrease of molar masses with clay concentration. This can be explained by OH functions, which can act both as co-initiator and chain transfer agent. This in-situ polymerization process led to well-exfoliated PCL-based nanocomposites with 3 wt% of clay while with higher content (10 wt%) partially exfoliated/partially intercalated structures were observed. Further morphological observations were carried out by scanning probe microscopy (SPM), while surface analysis was examined by X-ray photoelectron spectroscopy (XPS) and Fourier transform infrared spectroscopy in the reflection absorption mode (FT-IRAS) [141]. Taking into account the structure, the thermal stability increased and the water permeability decreased (see Fig. 14) since the well-dispersed fillers with high aspect ratio acted as barriers to oxygen and volatile degradation products [135,142]. In contrast, nanocomposites filled with non-hydroxyl functional clays exhibited only intercalated structures [136,137,140].

Since ε-CL polymerization is initiated by OH groups, polymer chains lengths can be predetermined and controlled by the clay loading. Thus, the clay content is limited to a certain range of concentrations to prevent from obtaining too short PCL chain lengths. Nevertheless, this can be modulated by tuning the number of OH groups, e.g., by modifying the clay surface by a mixture of non-functional alkylammonium and monohydroxylated ammonium cations [138,139,143]. Thus, using this interesting in-situ intercalative process, the inorganic content, the quantitative surface grafting, the number of polyester chains per clay surface as well as the polymer chain length and molecular weight distribution are well controlled [139]. Viville et al. [143] also studied the morphology of PCL grafted chains on the silicate layer surface depending on the OH content. They showed that the grafting density drastically increased as the proportion of OH-substituted alkylammonium cations used to organomodify the clay increased. Since separate polymer islands were formed in the low OH systems (see Fig. 15), they assumed that a phase separation process occurred between the ammonium ions induced by the polymerization reaction. Homogeneous coverage and subsequent thickening only take place from 50% OH content. When this situation was achieved, adjacent platelets become fully independent of each other, which greatly favored exfoliation.

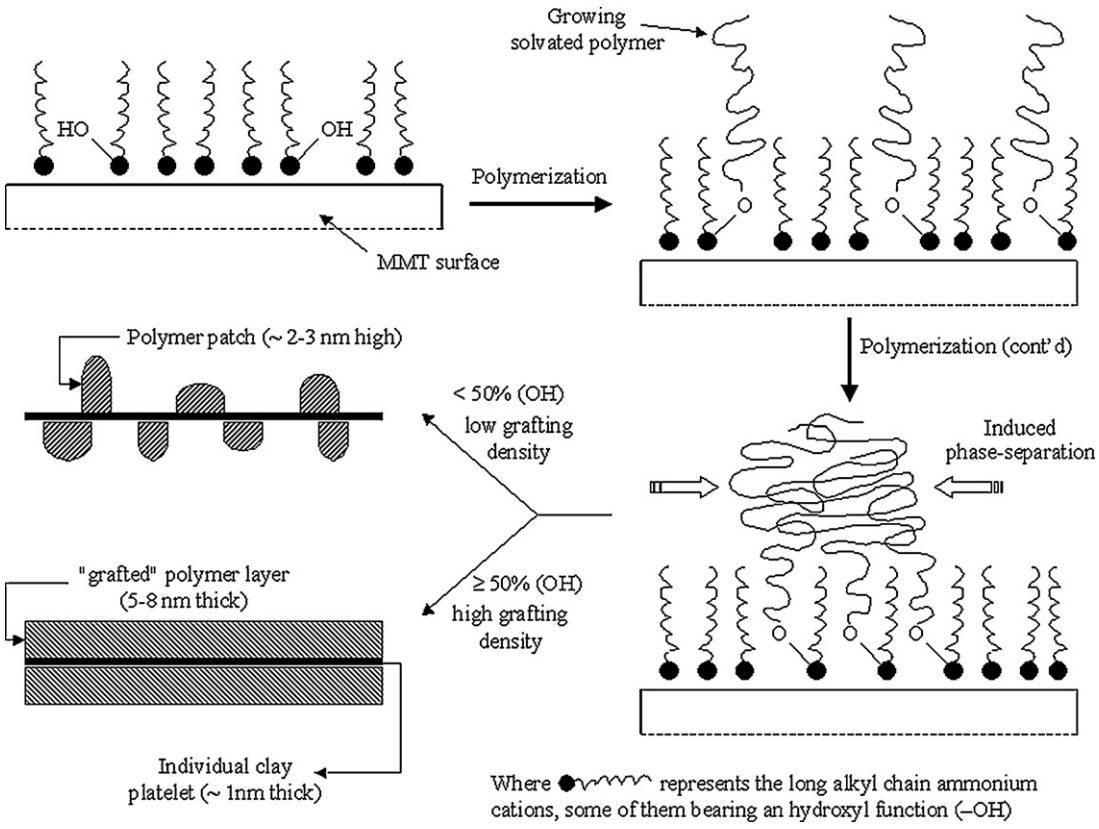

Fig. 15. Polymer surface grafting onto individual clay platelets and concomitant phase separation. Reproduced with permission from Viville et al. [143] copyright (2004) of the American Chemical Society.

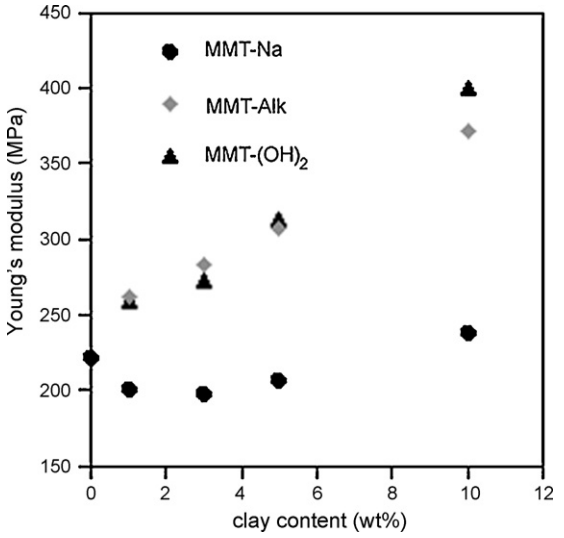

Fig. 16. Dependence of Young's modulus on the clay content for PCL modified by CNa, C25A and C30B. Reproduced with permission from Lepoittevin et al. [145] copyright (2002) of Elsevier Science Ltd.

The "coordination-insertion" mechanism, i.e., in-situ intercalation catalyzed by initiators, was compared to the thermally activated in-situ intercalation with various OMMT [140]. Messersmith and Giannelis' results [127] stating that large catalytic surface of montmorillonite can contribute to polymerization of ε-CL were confirmed. Exchanged cations bearing protic functions like NH_3^+, OH, COOH significantly favored the polymerization and lead to similar structures to those obtained by the "coordination-insertion" mechanism. Nevertheless, the PCL molecular weights remained low and the polydispersity index at high conversion reached values higher than 2, confirming that the in-situ intercalation in presence of OH groups and initiators provides better polymerization control.

Eventually, the melt intercalation route led to intercalated or intercalated/exfoliated structures when PCL was associated with OMMT bearing quaternized octadecylamine (MMT-$NH_3^+(C_{18})$), di(hydrogenated tallow) dimethyl ammonium (MMT-$N^+(Me)_2(tallow)_2$), dimethyl 2-ethylhexyl(hydrogenated tallow) (C25A), or methyl bis(2-hydroxyethyl) (hydrogenated tallow) (C30B) [135,144,145]. On the contrary, MMT-Na and MMT organomodified with ammonium bearing 12-aminododecanoic acid (MMT-$NH_3^+(C_{11}COOH)$) formed microcomposites since no change of interlayer gap was observed whereas the in-situ intercalation showed exfoliation in the case of MMT-$NH_3^+(C_{11}COOH)$ [127,135,140]. Therefore, contrary to the in-situ intercalative process, complete exfoliation was not reached by the melt intercalation route, whatever the OMMT considered (see Table 6). However, the tensile and thermal properties were improved. For instance, the modulus increased from 210 MPa for unfilled PCL to 280 MPa or 400 MPa with 3 wt% of MMT-$NH_3^+(C_{18})$, MMT-$N^+(Me)_2(tallow)_2$ or C25A, and 10 wt% of C30B, respectively, attesting for an almost two-fold increase of the PCL rigidity in the latter case (see Fig. 16) [144,145]. Chen and Evans [146] demonstrated on similar systems that the elastic modulus trends with clay volume fraction may be interpreted using well-established theory for conventional composites, namely the Hashin–Shtrikman bounds. At OMMT content higher than 5 wt%, the elongation at break dropped off due to clay aggregation [144,145].

Dynamic mechanical measurements also revealed that with 1 wt% clay, nanocomposites materials exhibited a pseudo solid-like behavior [145]. However, Kwak and Oh [147] demonstrated that PCL chains can diffuse further into the silicate gallery due to additionally subjecting the samples to heat during the analyses and finally, extended exfoliation are achieved. The 50% weight loss temperature is shifted by 60 °C towards higher temperature on the addition of 1 wt% of clay, whereas the temperature shift is only 30 °C at 10 wt%. Thus, PCL nanocomposites combine high stiffness, good ductility and improved thermal stability at low clay content (<5 wt%).

Only Di et al. [148] reached exfoliated state in the case of PCL/C30B systems prepared by direct melt intercalation with 2–5 wt% of clay. Obviously, they reported great enhancements of mechanical and thermal properties as well as a pseudo solid-like rheological behavior caused by the strong interactions between the organoclay layers and PCL, and by the good dispersion of exfoliated organoclay platelets. Moreover, the isothermal crystallization behavior [149] revealed that the well-dispersed organoclay platelets act as nucleating agents, but also affected the crystals quality by the restricted chains mobility.

Since the direct melt intercalation suffers a lack of efficiency towards clay dispersion, an elaboration route combining in-situ ε-CL polymerization and material redispersion by melt intercalation was settled. This masterbatch process [150], or equivalent [151], yielded intercalated/exfoliated structures that are rather difficult to reach by direct melt blending. This process also turned out to be a good way to compatibilize and thus to reinforce other thermoplastics like conventional polymers (SAN [131,152], PVC [150], PC [153], PP, PE, PS and ABS [154],) or biopolymers (PBS, PBAT [155]). Conversely, PCL was blended by a reactive process with thermoplastic-clay systems [156,157] to improve the properties of the final material.

A remarkable study on the nanocomposite preparation of oligo-PCL/OMMT by simply mechanical mixing was reported by Maiti [158]. Different types of clays having different aspect ratios (hectorite, mica, smectite) organomodified with various phosphonium cations were selected to investigate their influence on miscibility with oligo-PCL (o-PCL). The alkyl phosphonium cations were *n*-octyltri-*n*-butylphosphonium ($P^+(But)_3(C_8)$), *n*-dodecyltri-*n*-butylphosphonium (($P^+(But)_3(C_{12})$), *n*-hexadecyltri-*n*-butylphosphonium ($P^+(But)_3(C_{16})$) and methyltriphenylphosphonium ($P^+(Me)(\phi)_3$). Immiscible, intercalated, and exfoliated nanostructures were observed in o-PCL nanocomposites, depending on the nature of the organic modifier as well as the aspect ratio (see Table 6). Fig. 17 sums up their interpretation according to experimental results but also to thermodynamic considerations. According to Maiti, when o-PCL is immiscible with a certain organic modifier, it cannot intercalate into the

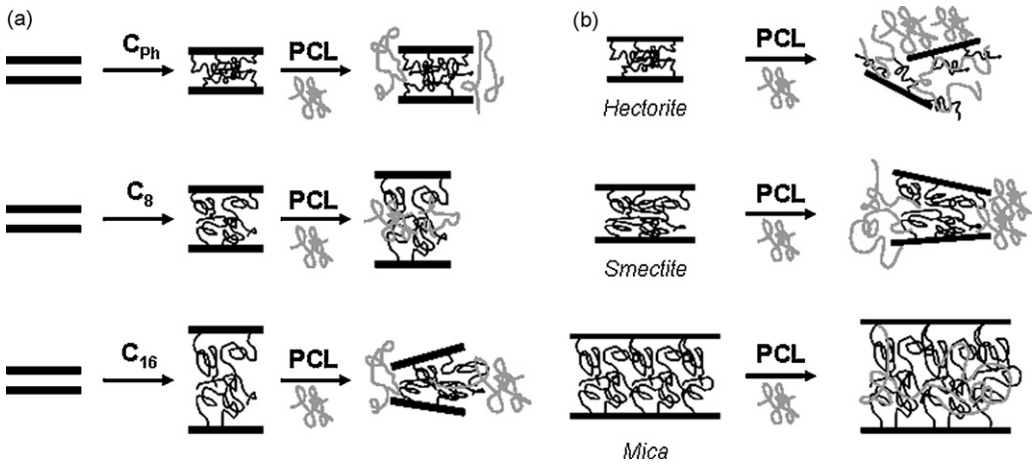

Fig. 17. Schematic representation of PCL oligomers nanocomposites depending (a) on the nature of the organomodifier and (b) on the clay aspect ratio. Reproduced with permission from Maiti [158] copyright (2003) of the American Chemical Society.

silicate gallery, while, for a short chain miscible modifier, o-PCL intercalates and, in the case of a long chain modifier, the modifier orients itself away from the silicate surface and is solubilized into the o-PCL phase, resulting in the collapse of the silicate gallery (see Fig. 17a).

Considering the effect of the aspect ratio with a given organomodifier, when the aspect ratio is low, combined with a high CEC, the organic modifier is favored to diffuse out the gallery and to interact with o-PCL leading to exfoliated structure. For higher aspect ratio, i.e., for larger lateral dimensions of the silicate layers, the organic modifier hardly access outside the gallery, and thus, the o-PCL must intercalate (see Fig. 17b).

Other works attempted to better understand the mechanism of intercalation/exfoliation process either by melt intercalation or in-situ ε-CL polymerization by molecular dynamics simulations [159–161]. Very recently, solid-state NMR has emerged as a tool to characterize clay/polymer nanocomposites in complement to data from classical methods (XRD, TEM) since it is a powerful technique for probing the molecular structure, conformation, and dynamics of species at interfaces. Therefore, solid-state NMR was used in PCL-based nanocomposites to investigate how the surfactant conformation and mobility are changed by the polymer adsorption and how the polymer motion is perturbed after intercalation in the nanocomposites [159,162,163]. Finally, Calberg et al. [159] validated this characterization method to determine the structure of PCL-based nanocomposites since they demonstrated that there was a correlation between variations in the proton relaxation times T1(H) and the quality of clay dispersion.

To conclude, PCL-based nanocomposites have been widely studied and several well-controlled routes have been settled to reach exfoliated state. To be precise, the solvent intercalation route is not one of those since no satisfactory results were obtained regarding the structure [164] (see Table 6). Excepting this, elaboration of such materials turned out to be very useful not only for PCL properties enhancement, but also for other thermoplastics ones.

4.3.2. Biodegradable aliphatic copolyester-based nano-biocomposites

4.3.2.1. Polybutylene succinate. PBS presents many interesting properties, including biodegradability, melt processability, and thermal and chemical resistance, but low gas barrier properties and softness still limit its use. Therefore, particular attention has been paid to the elaboration of PBS-based nano-biocomposites (see Table 7) to overcome these issues and to improve the material properties.

Sinha Ray et al. [165] first reported structure and properties of PBS/clay nanocomposites (PBSCN) obtained by melt intercalation. Other studies [166–168] investigated the effect of the organoclay type on the composites structures and properties. High molecular weight PBS (HMWPBS) were synthesized by a coupling reaction with a chain extender, namely the hexamethylene diisocyanate (OCN-C_6H_{12}-NCO), resulting in urethane moities (see Fig. 18) and terminal hydroxyl groups. Different OMMT were tested such as octadecylammonium and octadecyltrimethylammonium modified montmorillonite (MMT-$NH_3^+(C_{18})$ and MMT-$N^+(Me)_3(C_{18})$, respectively) and hexadecyltributylphosphonium modified saponite (SAP-$P^+(But)_3(C_{16})$). Intercalated and extended flocculated nanocomposites were obtained with the PBS/MMT-$NH_3^+(C_{18})$ systems. For MMT-$N^+(Me)_3(C_{18})$-based materials, nanocomposites showed an intercalated and flocculated structure, whereas the coexistence of the stacked intercalated and delaminated structure was observed in PBS/SAP-$P^+(But)_3(C_{16})$ nanocomposite. According to the authors, the flocculation occurred due to urethane moieties of PBS that make hydrogen bonds with the silicate hydroxyl edge groups leading to very strong interactions between matrix and silicate layers [167,168] (see Fig. 19).

These structures were confirmed, by mechanical, rheological and barrier properties. For instance, G' determined by DMA presented significant enhancements with increasing clay loading, particularly with MMT-$NH_3^+(C_{18})$ and MMT-$N^+(Me)_3(C_{18})$ since increments reached more than 200% [166]. Furthermore, since they noticed that properties of PBS/MMT-$NH_3^+(C_{18})$ and PBS/MMT-$N^+(Me)_3(C_{18})$

Table 7
Structure of the studied PBS/clay nano-biocomposites.

Process	System	Structure	Reference
Solvent intercalation	MMT-($C_5H_5N^+$)(C_{16})	Intercalated	[172]
	MMT-$N^+(Me)_3(C_{16})$	Intercalated	[172]
Melt intercalation	MMT-$NH_3^+(C_{18})$	Intercalated and flocculated	[165]
		Highly intercalated and homogeneous dispersion	[169]
	MMT-$NH_3^+(C_{18})$/HMWPBS	Intercalated and flocculated	[167]
	MMT-$NH_3^+(C_{12})$	Highly intercalated and homogeneous dispersion	[169]
	MMT-$NH_3^+(C_{11}COOH)$	Microcomposite	[169]
	MMT-$NH^+(EtOH)_2(C_{12})$	Highly intercalated and homogeneous dispersion	[169]
	MMT-$NH^+(EtOH)_2(CH_2CHOHCH_3)$	Microcomposite	[169]
	MMT-$N^+(Me)_2(C_8)$(tallow)	Intercalated	[170,171]
	GPS-g-MMT-$N^+(Me)_2(C_8)$(tallow)	Intercalated/exfoliated	[170,171]
	MMT-$N^+(Me)(EtOH)_2$(tallow)	Intercalated and flocculated	[155]
	MMT-$N^+(Me)(EtOH)_2$(tallow)/dibutyltin dilaurate	Intercalated/exfoliated	
	Or titanium butoxide	Intercalated	
	Or antimony oxide	Intercalated	
	SAP-$P^+(But)_3(C_{16})$/HMWPBS	Stacked intercalated and delaminated	[167]
Masterbatch	MMT-$NH_3^+(C_{18})$/HMWPBS + HMWPBS	Intercalated and flocculated	[166]
	MMT-$N^+(Me)_3(C_{18})$/HMWPBS + HMWPBS	Intercalated and flocculated	[166,168]
	MMT-$N^+(Me)(EtOH)_2$(tallow)-g-PCL/dibutyltin dilaurate or titanium butoxide or antimony oxide + PBS	Intercalated	[155]
	SAP-$P^+(But)_3(C_{16})$/HMWPBS + HMWPBS	Stacked intercalated and delaminated	[166]

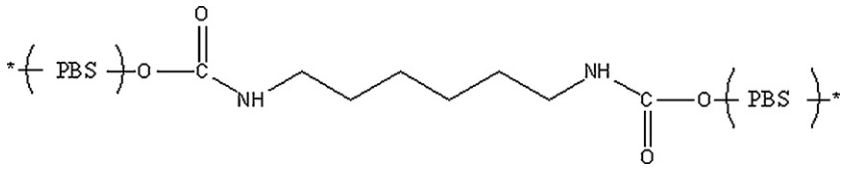

Fig. 18. HMWPBS obtained by chain extension using hexamethylene diisocyanate. Redrawn with permission from Sinha Ray et al. [167] copyright (2003) of the American Chemical Society.

suddenly increased beyond a certain clay content, they concluded to the existence of a percolation threshold value (3.3 wt% for MMT-$NH_3^+(C_{18})$) [167], and less than 3.6 wt% for MMT-$N^+(Me)_3(C_{18})$ [168]). Above this clay content, dispersed and flocculated silicate layers form a network and contribute to reinforce considerably the matrix. This structure affected the tensile properties and the rheological behavior of the PBS. Indeed, with the increasing clay content, it was shown that the tensile modulus increased while the tensile strength decreased [168]. Besides, rheologi-

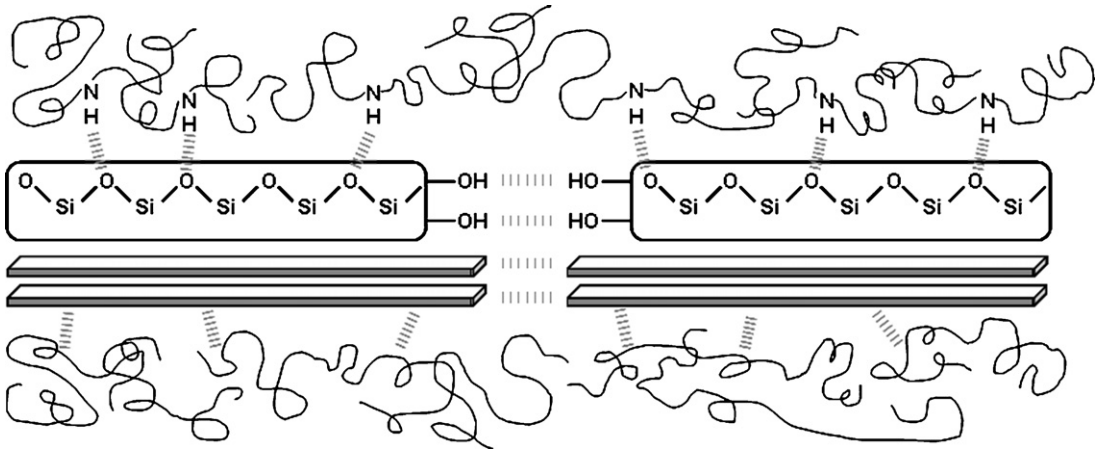

Fig. 19. Formation of hydrogen bonds between PBS and clay, leading to flocculation of the dispersed silicate layers. Reproduced with permission from Sinha Ray et al. [167] copyright (2003) of the American Chemical Society.

cal measurements revealed pseudo solid-like behavior of PBSCNs at high clay content, suggesting a prevented relaxation due to the high geometric constraints or physical jamming of the stacked silicate layers. This PBSCN structure was also confirmed by the lower slope values and the higher absolute values of the dynamic moduli [167]. Barrier properties were also consistent with flocculated and percolated structures since the O_2 permeability decreased of 52% with 3.6 wt% of MMT-$NH_3^+(C_{18})$ [166], i.e., above the percolation threshold. Eventually, on the basis of the biodegradation tests realized in compost and SEC data, authors concluded that the PBS fragmentation was significantly improved generating higher surface area for further micro-organisms attack [167].

Someya et al. [169] tested different OMMT to determine the effect of variations in hydrophobicity and polar/steric interactions. Five OMMT organomodified with primary amines (dodecylamine-MMT-$NH_3^+(C_{12})$-, octadecylamine-MMT-$NH_3^+(C_{18})$-, 12-aminolauric acid-MMT-$NH_3^+(C_{11}$COOH)) or tertiary amines (*N*-lauryldiethanolamine-MMT-$NH^+(EtOH)_2(C_{12})$-, and 1-[*N*,*N*-bis(2-hydroxyethyl)amino]-2-propanol-MMT-$NH^+(EtOH)_2(CH_2CHOHCH_3)$) were prepared and added to PBS by melt intercalation at contents from 1 to 10 wt%, and then the samples were injection molded. Highly intercalated structures and homogeneous clay dispersion were observed with MMT-$NH_3^+(C_{12})$, MMT-$NH_3^+(C_{18})$, and MMT-$NH^+(EtOH)_2(C_{12})$. On the contrary, some clusters or agglomerated particles were observed with MMT-$NH_3^+(C_{11}$COOH), MMT-$NH^+(EtOH)_2(CH_2CHOHCH_3)$, and unmodified MMT. The authors showed that the d-spacing enlargement determined by XRD was well correlated with the clay dispersion improvement and with the increase of tensile and flexural moduli and the decrease of tensile strength. Dynamic viscoelastic measurements were also consistent with structural results since PBS/MMT-$NH^+(EtOH)_2(C_{12})$ nanocomposite had higher storage modulus and glass-transition temperature. This indicated that intercalation of PBS within the OMMT layers affected the molecular motion.

Another group achieved to improve PBS properties using compatibilization approach. Chen et al. [170] proposed to graft epoxy groups onto C25A with (glycidoxypropyl)trimethoxy silane (GPS) leading to twice-functionalized organoclay (TFC, i.e., GPS-g-C25A), as already done for PLA [102]. Tethering PBS molecules to the epoxy groups on the surface of TFC was attempted through melt compounding. Higher exfoliation degrees and better properties were reached in PBS/TFC nanocomposites compared to those of PBS/C25A due to the increased PBS–TFC interfacial interactions. XRD results showed that *d*-spacing values were comparable when 10 wt% of C25A or TFC were added, but the difference of peak intensity attested that partial disruption of parallel stacking of TFC had occurred. The intercalation/exfoliation coexistence in the PBS/TFC systems has also been demonstrated by TEM images, whereas intercalated clay tactoids have been observed with C25A. The mechanical properties are increased up to 10 wt% of filler. Dynamic mechanical analyses also showed that E' was higher than that for neat PBS and increases with the clay content. Furthermore, a weak shoulder appearing at $\sim$50 °C in the tan δ profile was attributed to the relaxation of PBS segments confined within the clay layers, in agreement with the structure deduced from morphological characterizations. Eventually, the study of the non-isothermal crystallization behavior showed out that well-dispersed TFC layers enhanced the nucleation and crystallization rate of the PBS matrix [171].

C30B was also used for the preparation of 3 wt% filled PBS-based nanocomposites by melt intercalation [155]. Since the *d*-spacing increased, intercalated structure was obtained resulting in PBS rigidity improvement (+25% Young's modulus). Furthermore, authors also tested metal-based catalysts (dibutyltin dilaurate $Sn(Bu)_2(Lau)_2$, titanium(IV) butoxide $Ti(OBu)_4$ and antimony(III) oxide Sb_2O_3) to promote transesterification between the ester moiety of the PBS and the organomodifier OH groups to graft PBS chains onto the organoclay surface. $Sn(Bu)_2(Lau)_2$ appeared to be the most appropriate catalyst since XRD and TEM clearly showed higher levels of clay exfoliation. Extraction process followed by TGA showed that grafting reaction had occurred. Consequently, material stiffness improved considerably by a Young's modulus increase of +60% compared to neat PBS.

Shih et al. [172] investigated different organoclays functionalized by ammonium salts such as cetylpyridinium chloride ($(C_5H_5N^+)(C_{16})$) and cetyltrimethylammonium bromide ($N^+(Me)_3(C_{16})$), which were mixed with PBS by solvent intercalation at 1, 3 and 5 wt%. The enhancement of E' and E'' showed that the stiffness and toughness of PBS were simultaneously improved (see Fig. 20). Weak shoulders on tan δ peaks at 5 wt% of clay were observed corresponding to the relaxation of PBS segments confined within the clay platelets, suggesting an intercalated structure and inhomogeneous dispersion due to clay aggregation, as mentioned by Chen et al. [170]. However, PBS/MMT-$N^+(Me)_3(C_{16})$ nanocomposites exhibited higher storage and loss moduli than PBS/MMT-$(C_5H_5N^+)(C_{16})$ systems. Thus, aliphatic chain in $N^+(Me)_3(C_{16})$, compared to the aromatic group in cetylpyridinium, may interact more favorably with the aliphatic PBS because of their similar structures. Morphological characterizations were consistent with mechanical properties namely intercalated structures were obtained and better extent of *d*-spacing was observed with MMT-$N^+(Me)_3(C_{16})$. Furthermore, TEM confirmed the coexistence of intercalated and exfoliated structures with 3 wt% of MMT-$N^+(Me)_3(C_{16})$ nanocomposite, whereas aggregation was obtained with 5 wt% OMMT.

4.3.2.2. Polybutylene succinate-co-adipate. Sinha Ray et al. [173–176] also reported PBSA-based nanocomposites studies. First, they have investigated various types of organoclays from Southern Clay Products (C15A, C93A and C30B) which present different polarity [174] (see Table 8). XRD and TEM have shown that the polymer–clay compatibility plays a key role in attaining high *d*-spacing and high quality of dispersion. Finally, C30B appeared the most suitable nanofiller for PBSA-based nanocomposites prepared by melt intercalation. Highly disordered and exfoliated platelets coexist with a few stacked intercalated layers due to interactions between C=O groups (PBSA backbone) and OH functions (C30B). Nevertheless, the dispersion quality

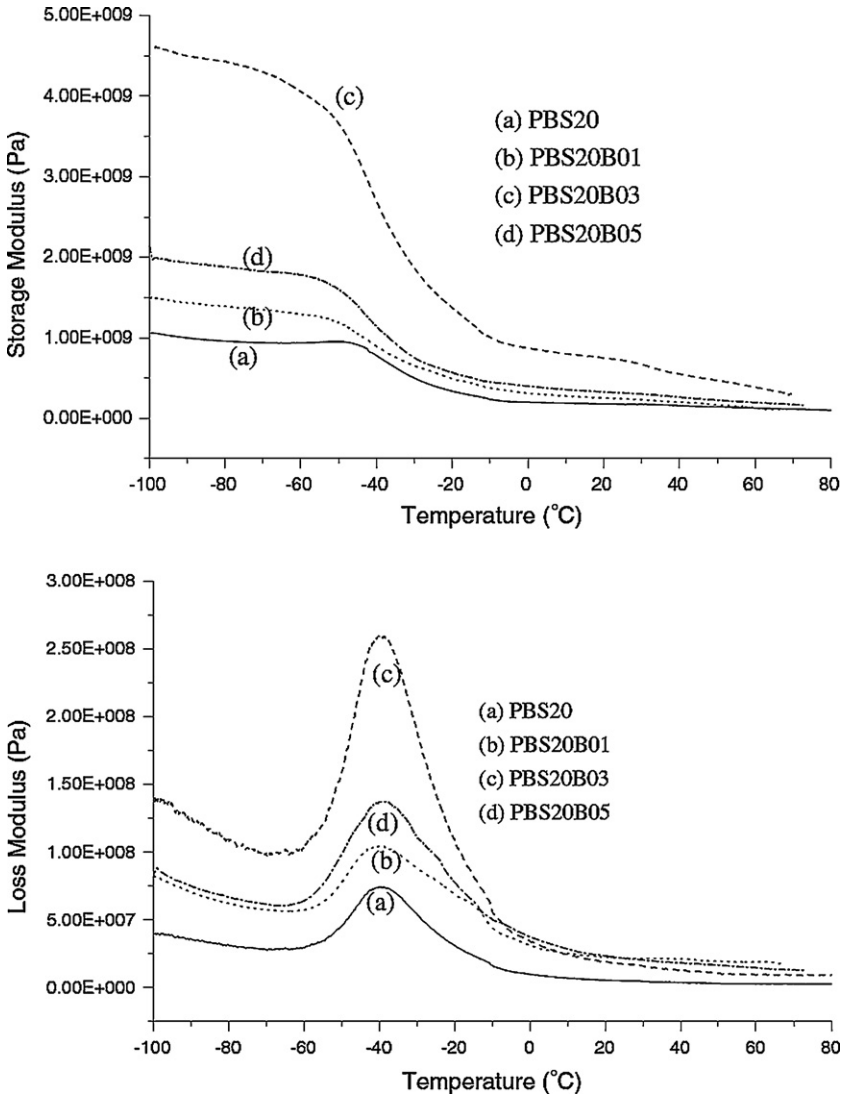

Fig. 20. Temperature dependence of the storage and loss moduli for neat PBS (a) and PBS composites (b–d) with respectively 1, 3 and 5 wt% of MMT-($C_5H_5N^+$)(C_{16}). Reproduced with permission from Shih et al. [172] copyright (2007) of Springer Science.

Table 8
Structure of the studied PBSA/clay nano-biocomposites.

Process	System	Structure	Reference
Solvent intercalation	MMT-$N^+(Me)_2(C_8)$(tallow)/chloroform	Intercalated	[177,178]
	MMT-$N^+(Me)_2(C_8)$(tallow)/poly(epichlorohydrin)/methylene chloride	Intercalated	[180,181]
Melt intercalation	MMT-$N^+(Me)(EtOH)_2$(tallow)	Exfoliated (high clay content)	[64]
		Intercalated (low clay content)	[173,174]
		Intercalated/exfoliated	
	MMT-$N^+(Me)_2(C_8)$(tallow)	Intercalated	[179]
	MMT-$NH^+(Me)$(tallow)$_2$	Intercalated	[174]
	MMT-$N^+(Me)_2(C_8)$(tallow)	Intercalated	[174]
	GPS-g-MMT-$N^+(Me)_2(C_8)$(tallow)	Intercalated	[182]
	MPS-g-MMT-$N^+(Me)_2(C_8)$(tallow)		
	SFM-$N^+(Me)(EtOH)_2$(coco alkyl)	Intercalated/exfoliated	[176,183]

was lowered with increasing clay content [173]. Consequently, thermal and mechanical properties were affected by the clay induced structure according to the nature and content of organoclay. First, although the PBSA crystal structure was not altered by the incorporation of clay, the crystallinity systematically decreased with the increasing dispersion degree of silicate layers into PBSA matrix. In the case of strong polymer–clay interactions, the mobility and flexibility of the polymer chains are hindered, limiting their ability to fold and participate to the crystallization growth front. A significant increase in E' was observed due to the intercalation of chains within the silicate layers and this increase was more important with higher C30B content [173]. Furthermore, it was also shown a substantial increase for E'' suggesting the presence of strong internal friction between homogeneously dispersed intercalated silicate particles. Tensile properties were also examined: the tensile modulus and elongation at break increased in presence of organoclay, but the improvement was strongly dependent on the degree of dispersion and on the C30B content. These improvements were only due to the structure formation since crystallinity decrease on addition of clays. The rheological properties also pointed out a gradual change of behavior from liquid-like to solid-like with the increasing polymer-OMMT affinity. These results were mainly attributed to the extent of dispersion and distribution of the clay lamellae that form, beyond a threshold concentration (3 wt% in the case of C30B), three dimensional percolating networks rendering the system highly elastic. Eventually, better thermal stability was obtained for PBSA/C30B, but this enhancement was limited to low clay content since a decrease was observed above 9 wt%, probably due to the excess of organic modifier containing OH groups on the clay surface, which undergoes Hofmann degradation at around 200 °C.

Lee et al. [64] also tested C30B dispersion in Skygreen® at various clay contents ranging from 1 to 30 wt% by melt intercalation. The highest content values are unusual for nanocomposites since high content promotes aggregation. Nevertheless, in this case, exfoliated states were achieved above 15 wt% whereas intercalation was obtained with lower clay contents. The authors attributed this phenomenon to the combination of high shear rate reached during melt intercalation and the polymer-OMMT affinity. As seen before [96,97,121], strong interactions or miscibility exist between the polymer and the C30B, due to strong hydrogen bonding between the carboxyl group from the biodegradable polyester and the OH group from C30B. These results were confirmed by TEM since the nanocomposites showed ordered intercalated structures with expanded layer gap and good dispersion at 10 wt%. Tensile properties enhancements were consistent with the structural results. The nanocomposite biodegradability decreased with increasing organoclay amount. This behavior was explained by the difficulty for micro-organisms to reach the bulk matrix due to the presence of dispersed clay layers with large aspect ratio that make the diffusion path more tortuous.

C25A was also tested as a nanofiller to improve Skygreen® properties [177–180]. Regardless of the elaboration route, solvent [177,178] or melt intercalation [179], or the organoclay content studied (<15 wt%), intercalated structures were observed. Even for Skygreen® blended with polyepichlorohydrin (PECH), no larger d-spacing was obtained [180,181], although the interlayer gap of PECH/OMMT nanocomposites can attain high values (>55 Å). Moreover, TEM observations but also the decrease and the broadening of d_{001} peak intensity with the decreasing clay content supposed that structures were much more inhomogeneous at low clay content showing exfoliated platelets at 3 wt% of C25A [179]. Rheological measurements showed that shear–thinning behavior and solid-like properties at low frequency region were enhanced by the addition of organoclay. These characterization techniques also led to definition of a critical volume fraction. Beyond that threshold, the tactoids and individual layers are prevented from relaxing completely when subjected to shear, due to physical jamming or percolation, leading to the solid-like behavior observed in both intercalated and exfoliated nanocomposites. Creep and recovery tests were found consistent with these conclusions. Although the tensile modulus dramatically increases with the clay content, the elongation at break decreases and the onset temperature of thermal decomposition drop beyond a certain clay loading [178]. The collapse of mechanical and thermal properties is attributed to the OMMT aggregation. However, regarding the thermal stability in the presence of C25A, with or without PECH, the decomposition phenomenon in terms of onset temperature and degradation rate is not fully understood. In this case, the decomposition rate increased with the increasing clay content, while the onset degradation temperature was improved [178]. Authors then supposed that, in a first step, the clay acts as a heat barrier and leads to the char formation after thermal decomposition. However, in a second step, the tactoids domain could hold accumulated heat, which could be a source, in conjunction with the heat flow supplied by the external heat source, to accelerate the decomposition process.

C25A was further modified by Chen and Yoon [182], based on the protocol established for PLLA-based [102] and PBS-based nanocomposites [170]. The C25A was functionalized by grafting epoxy group at the surface using silane coupling agent. In this case, they tested (glycidyloxypropyl)trimethoxy silane (GPS) and (methacryloyloxypropyl)trimethoxy silane (MPS) as coupling agents. According to the authors, the silane compounds are located mainly on the edge of the silicate layers where the concentration of the silanol groups is higher than on the plain surface. The preparation of the resulting twice-functionalized clay (TFC, i.e., GPS-g-C25A or MPS-g-C25A) is shown in Figs. 6 and 7. From XRD and TEM, it was concluded that both the reaction between the PBSA end-groups and the GPS-g-C25A epoxy groups, and the polar interaction between the ester groups in MPS-g-C25A and PBSA, should have enhanced the compatibility. A larger increase of d-spacing and better clay layers dispersion were observed with 2 wt% of GPS-g-C25A or MPS-g-C25A, compared to same C25A loading. The macroscopic properties were improved too. The storage modulus of PBSA/TFC was much higher than that of PBSA/C25A, especially in the low-frequency region, and non-terminal behavior was observed

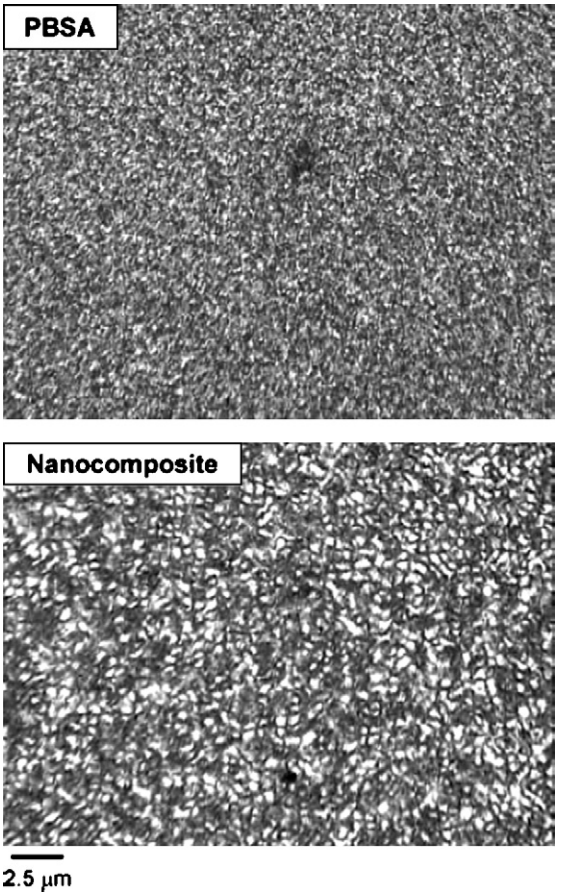

Fig. 21. Polarized optical microscopy images of PBSA and its nanocomposite with 6 wt% of SFM-N_+(Me)$(EtOH)_2$(coco alkyl) recorded at 70 °C during non-isothermal crystallization from their melts (150 °C) at a cooling rate of 10 °C min^{-1}. Reproduced with permission from Sinha Ray and Bousmina [183] copyright (2006) of Wiley-VCH.

at the terminal zone as a result of the enhanced PBSA–TFC interactions. Tensile modulus and strength at break were greatly improved with GPS-g-C25A and MPS-g-C25A due to the increased interfacial interaction.

A study of PBSA/synthetic fluorinated mica nanocomposites was carried out by Sinha Ray et al. [176,183]. Organomodified SFM (OSFM, Somasif from CO-OP Chemicals Ltd.) was melt mixed with Bionolle®. The resulting nanocomposites showed that some intercalated stacked and disordered and/or exfoliated silicate layers coexist. The thermo-mechanical properties were improved over the temperature range investigated, and particularly above the T_g since E' increased by more than 100% compared to neat PBSA. Considering the crystallization behavior [183], the non-isothermal crystallization kinetics of the nanocomposite and its higher activation energy calculated from model were in agreement with prior results [173]. Namely, the incorporation of OSFM slows the nucleation mechanism and PBSA crystal growth as a result of the full dispersion of silicate layers into the matrix, which act as obstacles (see Fig. 21). The homogeneous dispersion was shown to increase the cold crystallization temperature of the nanocomposite. Three prominent melting endotherms of PBSA resulting from the melting–recrystallization process were shifted towards lower temperature and decreased in intensity due to the clay dispersion that restricted the motions of polymer chains. Besides, the thermal stability of PBSA was moderately increased in the presence of OSFM under both nitrogen and air atmospheres overall thermal degradation temperature range. In the early stage of the decomposition, although the surfactant, and thus the nanocomposite, seemed to be more prone to degrade in thermo-oxidative conditions than pyrolytic conditions, the main degradation temperature and char formation were increased in air compared to nitrogen. According to authors, the different types of char formation mechanisms under oxidative environment actually slow the oxygen diffusion, thus hindering the oxidation procedure under thermo-oxidative conditions. Consequently, the flame retardance property of the nanocomposite was improved. To conclude, the activation energy of the nanocomposite thermal degradation calculated from the Kissinger model was slightly higher than that of neat PBSA, in agreement with previous results [174,178]. Classical and original processes were investigated as means to reach an exfoliated state and improved aliphatic copolyester-based nano-biocomposites properties, with more-or-less success (see Table 8). Furthermore, whatever the systems considered, the properties were well correlated to the materials structures.

4.3.3. Aromatic copolyester-based nano-biocomposites

PBAT is flexible and has a higher elongation at break than most biodegradable polyesters, such as PLA and PBS, and therefore is more suitable for food packaging and agricultural films. Only few articles report studies of PBAT/clay nano-biocomposites (see Table 9).

Recently, Someya et al. [184] have prepared OMMT which have been proved to be the more efficient with PBS [169], i.e., MMT-$NH_3^+(C_{12})$, MMT-$NH_3^+(C_{18})$, MMT-$NH^+(EtOH)_2(C_{12})$. They investigated the morphology and the properties of PBAT/clay nanocomposites prepared by melt intercalation containing 3–10 wt% OMMT. Intercalation occurred in the case of MMT-$NH_3^+(C_{12})$ and MMT-$NH^+(EtOH)_2(C_{12})$ and exfoliation, in addition to some intercalation, occurred with MMT-$NH_3^+(C_{18})$, which was also more finely dispersed in the matrix. Authors demonstrated that the mechanical properties were related to the structure as well as the crystallinity of the nanocomposites, leading globally to higher properties for PBAT/MMT-$NH_3^+(C_{18})$. Furthermore, they showed that the clay reinforcing effect is really effective above T_g, because of restricted polymer chains motions. Biodegradability was evaluated by the aerobic tests both in the soil and the aqueous medium containing activated sludge [185]. Compared to neat PBAT, the microcomposite based on unmodified montmorillonite exhibited a higher weight loss than PBAT/MMT-$NH_3^+(C_{18})$ nanocomposites.

Chivrac et al. [186,187] have expanded this work, testing various organoclays such as C20A, D43B and N804. The results relating to the structure and properties were compared to neat PBAT and the PBAT/MMT-Na, i.e., with non-modified montmorillonite. They also compared elaboration processes, i.e., solvent or melt intercalation. This study revealed that higher intercalation degrees were

Table 9
Structure of the studied PBAT/clay nano-biocomposites.

Process	System	Structure	Reference
Solvent intercalation	MMT-$N^+(Me)_2(tallow)_2$/chloroform MMT-$N^+(Me)_2(CH_2$-$\phi)$(tallow)/chloroform	Intercalated	[186]
Melt intercalation	MMT-$NH_3^+(C_{12})$	Intercalated	[184]
	MMT-$NH_3^+(C_{18})$	Intercalated/exfoliated	[184]
	MMT-$NH^+(EtOH)_2(C_{12})$	Intercalated	[184]
	MMT-$N^+(Me)_2(tallow)_2$	Intercalated	[186]
	MMT-$N^+(Me)_2(CH_2$-$\phi)$(tallow)	Intercalated	[186]
	MMT-$N^+(Me)(EtOH)_2$(tallow)	Intercalated	[155]
Masterbatch	MMT-$N^+(Me)(EtOH)_2$(tallow)-g-PCL + PBAT	Intercalated	[155]

obtained by solvent intercalation, C20A and D43B presenting better affinity with PBAT. No impact of the clay has been noticed on the T_g and T_m, whereas the crystallinity was affected by increasing clay content. Thus, they investigated the influence of the clay on the PBAT crystallization [187]. Kinetics models were applied and it was concluded that addition of a small amount of MMT enhances the PBAT nucleation mechanism, but also hinders crystallite growth. These two antagonist phenomena lead to different crystallization behavior depending on the clay dispersion. Furthermore, tensile tests have shown that the stiffness increases continuously with clay content. This was attributed to the existence of strong interactions between PBAT and nanofillers, particularly with C20A, since the crystallinity decreases with increasing clay content. Nevertheless, decreases of the strain at yield and at break have been observed due to more aggregated structures at higher clay contents (see Fig. 22). The onset degradation temperatures have been examined by TGA. The highest improvements were observed for nano-biocomposites filled with 3 wt% of MMT-Na. However, a decrease of the onset degradation temperatures is observed for higher clay contents, both with melt and solvent intercalations. This phenomenon is similar to the one described before by Lim et al. [178], i.e., clays act as heat barrier and lead to char formation after thermal decomposition, but unfortunately, tactoids can accumulate heat which could be used to accelerate the decomposition reaction.

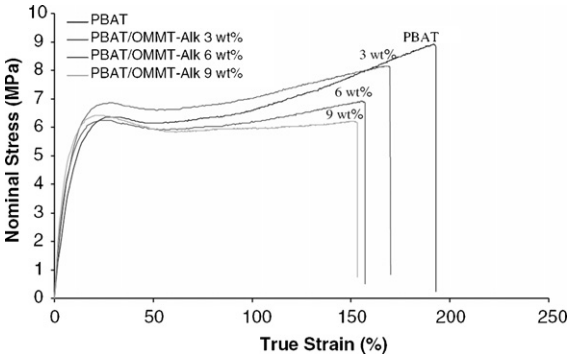

Fig. 22. Typical tensile curves obtained for neat PBAT and PBAT nanocomposites with 3, 6 and 9 wt% of C20A. Reproduced with permission from Chivrac et al. [186] copyright (2006) of Springer Science.

To conclude, a large range of OMMT has been tested, leading to different PBAT-based nanocomposites structures. These studies thus highlighted the relationship between the materials structures and their properties.

4.3.4. Polyesteramide-based nano-biocomposites

Because, the polyesteramide presents high water permeability (see Table 1), it appears necessary to improve this property, particularly if such materials are aimed at packaging applications.

Krook et al. [188,189] studied the barrier and mechanical properties of biodegradable melt-mixed polyesteramide/octadecylamine-treated montmorillonite (MMT-$NH_3^+(C_{18})$) containing 5 or 13 wt% of clay processed in different conditions (temperature, extruder screw speed). An increase of *d*-spacing was observed, suggesting that intercalated structures were reached upon extrusion. A decrease in XRD peak intensity with increasing screw speed was observed, which implied that higher shear rates promoted delamination. TEM observations indicated that clay stacks were delaminated into smaller aggregates, containing generally one to three clay sheets. They also showed the presence of shear-induced voids almost exclusively located between the clay layers, which was confirmed by density measurements. These voids limited the improvement in barrier properties. The oxygen and water vapor transmission rates decreased with increasing clay content. According to the authors, the presence of voids prevents gas diffusion through the film. The low barrier properties improvement was due to the non-uniformly dispersed clay particles. However, the large improvement in stiffness and strength with filler content indicated that the mechanical properties were unaffected by the voids.

Authors have also highlighted that the void content was reduced by compression molding after extrusion. This treatment led to higher crystallinity. This behavior induces lower gas transmission rates and higher mechanical properties (stiffness, yield point at higher stress levels).

These results were completed with a series of injection-molded samples [189]. XRD and TEM showed that these samples contained clay stacks. However, TEM also revealed that clay layers were largely delaminated and oriented "unidirectionally" over several microns. The transport and mechanical properties were greatly improved. This was attributed to a combined effect of a lower void content, higher crystallinity and greater degree of orientation.

To conclude, since packaging applications are considered for these materials, characterizations were focused on mechanical and barrier properties. The elaboration process was optimized to ensure good dispersion of clay and to avoid defects. Further properties were tested like optical transparency, weld strength, hot tack and transport properties [188].

5. Conclusion

This review presents the state of the art in biopolyester/clay nano-biocomposites. It has been clearly demonstrated that different parameters such as elaboration route, polymer/clay affinity and clay content can affect the structure and the nano-biocomposites properties. These latter can consequently be tuned as desired by controlling the parameters previously mentioned. It has to be noted that the higher reinforcing effect is generally limited to small clay amounts (<5 wt%) and is reached for exfoliated states, which are not so trivial to obtain. Indeed, although the more convenient clays to obtain delaminated platelets into biopolyesters appear to be those matching the matrix polarity, i.e., clay with organomodifier bearing at least one hydroxyl group, structure also depends on the elaboration process. Considering PLA and PCL matrices, nano-biocomposites with highly exfoliated clays can be obtained thanks to a well controlled in-situ polymerization process, whereas the melt and/or solvent intercalation methods lead to more aggregated structures. Thus, for some biopolyester matrices like PHA, aliphatic or aromatic polyesters, exfoliated states were not reported or clearly demonstrated. Eventually, temperature sensitivity of some biopolyesters can also prevent good clay delamination and properties enhancement.

In the case of good delamination and dispersion of clays, the mechanical reinforcement, thermal stability, biodegradability and barrier properties were generally improved. Rheological measurements also revealed that nano-biocomposites could present a more-or-less pronounced pseudo solid-like behavior indicating restricted motions of the biopolymer chains.

Finally, nano-biocomposites present concurrent improvement in various material properties at very low filler content, using conventional plastic processing in the elaboration. Nano-biocomposites usefulness is no longer in question, and more and more reports are focussed on application aspects in the environment, packaging, agriculture devices, biomedical fields, etc. Moreover, since industry is concerned with sustainable developments, the production cost of biopolymers goes on decreasing, which will allow strong developments of biopolymers-based materials, such as the nano-biocomposites. Therefore, these materials will be technically and financially competitive towards synthetic polymer-based nanocomposites, opening a new dimension for the plastic industry.

Future research will address some actual issues such as the difficulty to exfoliate the clay with some biopolyester matrixes (e.g., PHA). Further work should furnish valuable insight into new methods of nano-biocomposites designed to establish new approaches to tailor novel nano-architectures.

References

[1] Kaplan DL, Mayer JM, Ball D, McCassie J, Allen AL, Stenhouse P. Fundamentals of biodegradable polymers. In: Ching C, Kaplan DL, Thomas EL, editors. Biodegradable polymers and packaging. Lancaster: Technomic Pub. Co.; 1993. p. 1–42.

[2] Kaplan DL. Biopolymers from renewable resources. Berlin: Springer Verlag; 1998.

[3] Chandra R, Rustgi R. Biodegradable polymers. Prog Polym Sci 1998;23:1273–335.

[4] Steinbuchel A. Biopolymers, general aspects and special applications. Weinheim, Germany: Wiley-VCH; 2003.

[5] Averous L, Boquillon N. Biocomposites based on plasticized starch: thermal and mechanical behaviors. Carbohydr Polym 2004;56:111–22.

[6] Averous L. Polylactic acid: synthesis, properties and applications. In: Belgacem N, Gandini A, editors. Monomers, oligomers, polymers and composites from renewable resources. Oxford: Elsevier Limited Publication; 2008. p. 433–50.

[7] Garlotta D. A literature review of poly(lactic acid). J Polym Environ 2001;9:63–84.

[8] Wee Y-J, Kim J-N, Ryu H-W. Biotechnological production of lactic acid and its recent applications. Food Technol Biotech 2006;44:163–72.

[9] Moon SI, Lee CW, Miyamoto M, Kimura Y. Melt polycondensation of L-lactic acid with Sn(II) catalysts activated by various proton acids: a direct manufacturing route to high molecular weight poly(L-lactic acid). J Polym Sci Polym Chem 2000;38:1673–9.

[10] Moon S-I, Lee C-W, Taniguchi I, Miyamoto M, Kimura Y. Melt/solid polycondensation of L-lactic acid: an alternative route to poly(L-lactic acid) with high molecular weight. Polymer 2001;42:5059–62.

[11] Okada M. Chemical syntheses of biodegradable polymers. Prog Polym Sci 2002;27:87–133.

[12] Albertsson A-C, Varma IK. Aliphatic polyesters: synthesis, properties and applications. Adv Polym Sci 2002;157:1–40.

[13] Vert M, Schwarch G, Coudane J. Present and future of PLA polymers. J Macromol Sci A 1995;32:787–96.

[14] Sinclair RG. The case for polylactic acid as a commodity packaging plastic. J Macromol Sci A 1996;33:585–97.

[15] Lunt J. Large-scale production, properties and commercial applications of polylactic acid polymers. Polym Degrad Stabil 1998;59:145–52.

[16] Auras R, Harte B, Selke S. An overview of polylactides as packaging materials. Macromol Biosci 2004;4:835–64.

[17] Steinbuchel A, Doi Y. Polyesters III—applications and commercial products. Weinheim, Germany: Wiley-VCH; 2002.

[18] Bigg DM. Effect of copolymer ratio on the crystallinity and properties of polylactic acid copolymers. In: Proceedings of the 54th annual technical conference of the society of plastics engineers, vol. 2. Boca Raton (FL), USA: Published by CRC Press; 1996. p. 2028–39.

[19] Perego G, Cella GD, Bastioli C. Effect of molecular weight and crystallinity on poly(lactic acid) mechanical properties. J Appl Polym Sci 1996;59:37–43.

[20] Cartier L, Okihara T, Ikada Y, Tsuji H, Puiggali J, Lotz B. Epitaxial crystallization and crystalline polymorphism of polylactides. Polymer 2000;41:8909–19.

[21] Martin O, Averous L. Poly(lactic acid): plasticization and properties of biodegradable multiphase systems. Polymer 2001;42:6209–19.

[22] Labrecque LV, Kumar RA, Dave V, Gross RA, McCarthy SP. Citrate esters as plasticizers for poly(lactic acid). J Appl Polym Sci 1997;66:1507–13.

[23] Jacobsen S, Fritz HG. Plasticizing polylactide—the effect of different plasticizers on the mechanical properties. Polym Eng Sci 1999;39:1303–10.

[24] Kranz H, Ubrich N, Maincent P, Bodmeier R. Physicomechanical properties of biodegradable poly(D,L-lactide) and poly(D,L-lactide-co-glycolide) films in the dry and wet states. J Pharm Sci US 2000;89:1558–66.

[25] Ljungberg N, Andersson T, Wesslen B. Film extrusion and film weldability of poly(lactic acid) plasticized with triacetine and tributyl citrate. J Appl Polym Sci 2003;88:3239–47.

[26] Van Tuil R, Fowler P, Lawther M, Weber CJ. Properties of biobased packaging materials. In: Biobased packaging materials for the food industry—status and perspectives. Frederiksberg, Denmark: KVL; 2000. p. 8–33.

[27] Lehermeier HJ, Dorgan JR, Way JD. Gas permeation properties of poly(lactic acid). J Membr Sci 2001;190:243–51.

[28] McCarthy SP, Ranganthan A, Ma W. Advances in properties and biodegradabilility of co-continuous, immiscible, biodegradable, polymer blends. Macromol Symp 1999;144:63–72.
[29] Bastioli C. Biodegradable materials—present situation and future perspectives. Macromol Symp 1998;135:193–204.
[30] Tuominen J, Kylma J, Kapanen A, Venelampi O, Itävaara M, Seppälä J. Biodegradation of lactic acid based polymers under controlled composting conditions and evaluation of the ecotoxicological impact. Biomacromolecules 2002;3:445–55.
[31] De Koning GJM. Prospects of bacterial poly[(*R*)-3-hydroxyalkanoates]. PhD Thesis. Eindhoven: Eindhoven University of Technology; 1993.
[32] Madison LL, Huisman GW. Metabolic engineering of poly(3-hydroxyalkanoates): from DNA to plastic. Microbiol Mol Biol Rev 1999;63:21–53.
[33] Doi Y. Microbial polyesters. New York: John Wiley & Sons, Inc.; 1990.
[34] Zinn M, Witholt B, Egli T. Occurrence, synthesis and medical application of bacterial polyhydroxyalkanoate. Adv Drug Deliv Rev 2001;53:5–21.
[35] Valentin HE, Broyles DL, Casagrande LA, Colburn SM, Creely WL, DeLaquil PA, et al. PHA production, from bacteria to plants. Int J Biol Macromol 1999;25:303–6.
[36] Poirier Y. Polyhydroxyalkanoate synthesis in plants as a tool for biotechnology and basic studies of lipid metabolism. Prog Lipid Res 2002;41:131–55.
[37] Hori Y, Suzuki M, Yamaguchi A, Nishishita T. Ring-opening polymerization of optically active β-butyrolactone using distannoxane catalysts: synthesis of high-molecular-weight poly(3-hydroxybutyrate). Macromolecules 1993;26:5533–4.
[38] Hori Y, Takahashi Y, Yamaguchi A, Nishishita T. Ring-opening copolymerization of optically active β-butyrolactone with several lactones catalyzed by distannoxane complexes: synthesis of new biodegradable polyesters. Macromolecules 1993;26:4388–90.
[39] Hori Y, Hagiwara T. Ring-opening polymerisation of β-butyrolactone catalysed by distannoxane complexes: study of the mechanism. Int J Biol Macromol 1996;25:235–47.
[40] Kobayashi T, Yamaguchi A, Hagiwara T, Hori Y. Synthesis of poly(3-hydroxyalkanoate)s by ring-opening copolymerization of (*R*)-β-butyrolactone with other four-membered lactones using a distannoxane complex as a catalyst. Polymer 1995;36:4707–10.
[41] Nobes GAR, Kazlauskas RJ, Marchessault RH. Lipase-catalyzed ring-opening polymerization of lactones: a novel route to poly(hydroxyalkanoate)s. Macromolecules 1996;29:4829–33.
[42] Juzwa M, Jedlinski Z. Novel synthesis of poly(3-hydroxybutyrate). Macromolecules 2006;39:4627–30.
[43] Asrar J, Mitsky TA, Shah DT. Polyhydroxyalkanoates of narrow molecular weight distribution prepared in transgenic plants. Patent US6091002 assigned to Monsanto Company, St Louis, MO; 2000.
[44] Asrar J, Mitsky TA, Shah DT. Polyhydroxyalkanoates of narrow molecular weight distribution prepared in transgenic plants. Patent US6228623 assigned to Monsanto Company, St Louis, MO; 2001.
[45] El-Hadi A, Schnabel R, Straube E, Müller G, Henning S. Correlation between degree of crystallinity, morphology, glass temperature, mechanical properties and biodegradation of poly(3-hydroxyalkanoate) PHAs and their blends. Polym Test 2002;21:665–74.
[46] Velho L, Velho P. Innovation in resource-based technology clusters: investigating the lateral migration thesis—the development of a sugar-based plastic in Brazil. Report of the Centre for Poverty, Employment and Growth. Published by the Human Science Research Council, Pretoria (South Africa). http://www.hsrc.ac.za/research/output/outputDocuments/4221_Velho_DevelopmentofsugarbasedplasticinBrazil.pdf; 2006.
[47] Noda I, Green PR, Satkowski MM, Schechtman LA. Preparation and properties of a novel class of polyhydroxyalkanoate copolymers. Biomacromolecules 2005;6:580–6.
[48] Philip S, Keshavarz T, Roy I. Polyhydroxyalkanoates: biodegradable polymers with a range of applications. J Chem Technol Biotechnol 2007;82:233–47.
[49] Williams SF, Martin DP, Horowitz DM, Peoples OP. PHA applications: addressing the price performance issue. I. Tissue engineering. Int J Biol Macromol 1999;25:111–21.
[50] Amass W, Amass A, Tighe B. A review of biodegradable polymers: uses, current developments in the synthesis and characterization of biodegradable polyesters, blends of biodegradable polymers and recent advances in biodegradation studies. Polym Int 1998;47:89–144.
[51] Shogren R. Water vapor permeability of biodegradable polymers. J Environ Polym Degrad 1997;5:91–5.
[52] Kotnis MA, O'Brien GS, Willett JL. Processing and mechanical properties of biodegradable poly(hydroxybutyrate-co-valerate)-starch compositions. J Environ Polym Degrad 1995;3:97–105.
[53] Shogren RL. Poly(ethylene oxide)-coated granular starch-poly(hydroxybutyrate-co-hydroxyvalerate) composite materials. J Environ Polym Degrad 1995;3:75–80.
[54] Ramkumar DHS, Bhattacharya M. Steady shear and dynamic properties of biodegradable polyesters. Polym Eng Sci 1998;38:1426–35.
[55] Karlsson S, Albertsson A-C. Biodegradable polymers and environmental interaction. Polym Eng Sci 1998;38:1251–3.
[56] Parikh M, Gross RA, McCarthy SP. The influence of injection molding conditions on biodegradable polymers. J Inject Molding Technol 1998;2:30.
[57] Rosa DS, Calil MR, Guedes CGF, Rodrigues TC. Biodegradability of thermally aged PHB, PHB-V, and PCL in soil compostage. J Polym Environ 2004;12:239–45.
[58] Chiellini E, Solaro R. Biodegradable polymeric materials. Adv Mater 1996;8:305–13.
[59] Bastioli C, Cerutti A, Guanella I, Romano GC, Tosin M. Physical state and biodegradation behavior of starch–polycaprolactone systems. J Environ Polym Degrad 1995;3:81–95.
[60] Bastioli C. Properties and applications of Mater-Bi starch-based materials. Polym Degrad Stabil 1998;59:263–72.
[61] Averous L, Moro L, Dole P, Fringant C. Properties of thermoplastic blends: starch–polycaprolactone. Polymer 2000;41:4157–67.
[62] Koenig MF, Huang SJ. Evaluation of crosslinked poly(caprolactone) as a biodegradable, hydrophobic coating. Polym Degrad Stabil 1994;45:139–44.
[63] Tokiwa Y, Suzuki T. Hydrolysis of polyesters by lipases. Nature 1977;270:76–8.
[64] Lee S-R, Park H-M, Lim H, Kang T, Li X, Cho W-J, et al. Microstructure, tensile properties, and biodegradability of aliphatic polyester/clay nanocomposites. Polymer 2002;43:2495–500.
[65] Muller R-J, Witt U, Rantze E, Deckwer W-D. Architecture of biodegradable copolyesters containing aromatic constituents. Polym Degrad Stabil 1998;59:203–8.
[66] Yokota Y, Marechal H. Processability of biodegradable poly(butylene) succinate and its derivates. A case study. In: Biopolymer Conference, Würzburg (Germany). 1999.
[67] Fujimaki T. Processability and properties of aliphatic polyesters, 'Bionolle', synthesized by polycondensation reaction. Polym Degrad Stabil 1998;59:209–14.
[68] Ratto JA, Stenhouse PJ, Auerbach M, Mitchell J, Farrell R. Processing, performance and biodegradability of a thermoplastic aliphatic polyester/starch system. Polymer 1999;40:6777–88.
[69] Kim J, Shin TK, Choi HJ, Jhon MS. Miscibility of biodegradable synthetic aliphatic polyester and poly(epichlorohydrin) blends. Polymer 1999;40:6873–6.
[70] Kim J, Kim JH, Shin TK, Choi HJ, Jhon MS. Miscibility and rheological characteristics of biodegradable aliphatic polyester and linear low density polyethylene blends. Eur Polym J 2001;37:2131–9.
[71] Kim J, Lim ST, Choi HJ, Jhon MS. Rheological and mechanical characterization of biodegradable aliphatic polyester and poly(epichlorohydrin) blends. Macromol Chem Phys 2001;202:2634–40.
[72] Witt U, Einig T, Yamamoto M, Kleeberg I, Deckwer W-D, Muller R-J. Biodegradation of aliphatic–aromatic copolyesters: evaluation of the final biodegradability and ecotoxicological impact of degradation intermediates. Chemosphere 2001;44:289–99.
[73] Grigat E, Koch R, Timmermann R. BAK 1095 and BAK 2195: completely biodegradable synthetic thermoplastics. Polym Degrad Stabil 1998;59:223–6.
[74] Fritz J. Ecotoxicity of biogenic materials during and after their biodegradation. PhD Thesis. Vienna, Austria: University of Agriculture; 1999.
[75] Bruns C, Gottschall R, De Wilde B. Ecotoxicological trials with BAK 1095 according to DIN V 54900. Orbit J 2001;1:1–10.
[76] Ogata N, Jimenez G, Kawai H, Ogihara T. Structure and thermal/mechanical properties of poly(L-lactide)-clay blend. J Polym Sci Polym Phys 1997;35:389–96.
[77] Chang J-H, An YU, Cho D, Giannelis EP. Poly(lactic acid) nanocomposites: comparison of their properties with montmorillonite and synthetic mica (II). Polymer 2003;44:3715–20.
[78] Chang J-H, An YU, Sur GS. Poly(lactic acid) nanocomposites with various organoclays. I. Thermomechanical properties, morphology, and gas permeability. J Polym Sci Polym Phys 2003;41:94–103.
[79] Krikorian V, Pochan DJ. Poly(L-lactic acid)/layered silicate nanocomposite: fabrication, characterization and properties. Chem Mater 2003;15:4317–24.

[80] Krikorian V, Pochan DJ. Unusual crystallization behavior of organoclay reinforced poly(L-lactic acid) nanocomposites. Macromolecules 2004;37:6480–91.
[81] Krikorian V, Pochan DJ. Crystallization behavior of poly(L-lactic acid) nanocomposites: nucleation and growth probed by infrared spectroscopy. Macromolecules 2005;38:6520–7.
[82] Wu T-M, Wu C-Y. Biodegradable poly(lactic acid)/chitosan-modified montmorillonite nanocomposites: preparation and characterization. Polym Degrad Stabil 2006;91:2198–204.
[83] Pluta M, Galeski A, Alexandre M, Paul M-A, Dubois P. Polylactide/montmorillonite nanocomposites and microcomposites prepared by melt blending: structure and some physical properties. J Appl Polym Sci 2002;86:1497–506.
[84] Maiti P, Giannelis EP, Batt CA. Biodegradable polyester/layered silicate nanocomposites. Mater Res Soc Symp Proc 2002;740:141–5.
[85] Maiti P, Yamada K, Okamoto M, Ueda K, Okamoto K. New polylactide/layered silicate nanocomposites: role of organoclays. Chem Mater 2002;14:4654–61.
[86] Sinha Ray S, Yamada K, Okamoto M, Ueda K. Polylactide-layered silicate nanocomposite: a novel biodegradable material. Nano Lett 2002;2:1093–6.
[87] Sinha Ray S, Yamada K, Ogami A, Okamoto M, Ueda K. New polylactide/layered silicate nanocomposite: nanoscale control over multiple properties. Macromol Rapid Commun 2002;23:943–7.
[88] Sinha Ray S, Maiti P, Okamoto M, Yamada K, Ueda K. New polylactide/layered silicate nanocomposites. 1. Preparation, characterization and properties. Macromolecules 2002;35:3104–10.
[89] Sinha Ray S, Yamada K, Okamoto M, Ueda K. New polylactide-layered silicate nanocomposites. 2. Concurrent improvements of material properties, biodegradability and melt rheology. Polymer 2003;44:857–66.
[90] Sinha Ray S, Yamada K, Okamoto M, Ogami A, Ueda K. New polylactide/layered silicate nanocomposites. 3. High-performance biodegradable materials. Chem Mater 2003;15:1456–65.
[91] Sinha Ray S, Yamada K, Okamoto M, Ogami A, Ueda K. New polylactide/layered silicate nanocomposites. 4. Structure, properties and biodegradability. Compos Interfaces 2003;10:435–50.
[92] Sinha Ray S, Yamada K, Okamoto M, Fujimoto Y, Ogami A, Ueda K. New polylactide/layered silicate nanocomposites. 5. Designing of materials with desired properties. Polymer 2003;44:6633–46.
[93] Sinha Ray S, Okamoto M. New polylactide/layered silicate nanocomposites. 6. Melt rheology and foam processing. Macromol Mater Eng 2003;288:936–44.
[94] Sinha Ray S, Okamoto M. Biodegradable polylactide and its nanocomposites: opening a new dimension for plastics and composites. Macromol Rapid Commun 2003;24:815–40.
[95] Sinha Ray S, Yamada K, Okamoto M, Ueda K. Biodegradable polylactide/montmorillonite nanocomposites. J Nanosci Nanotechnol 2003;3:503–10.
[96] Nam PH, Fujimori A, Masuko T. Flocculation characteristics of organo-modified clay particles in poly(L-lactide)/montmorillonite hybrid systems. e-Polymers 2004, no. 005.
[97] Nam PH, Fujimori A, Masuko T. The dispersion behavior of clay particles in poly(L-lactide)/organo-modified montmorillonite hybrid systems. J Appl Polym Sci 2004;93:2711–20.
[98] Paul M-A, Delcourt C, Alexandre M, Degée P, Monteverde F, Dubois P. Polylactide/montmorillonite nanocomposites: study of the hydrolytic degradation. Polym Degrad Stabil 2005;87:535–42.
[99] Yoshida O, Okamoto M. Direct melt intercalation of polylactide chains into nano-galleries: interlayer expansion and nanocomposite structure. Macromol Rapid Commun 2006;27:751–7.
[100] Nam JY, Sinha Ray S, Okamoto M. Crystallization behavior and morphology of biodegradable polylactide/layered silicate nanocomposite. Macromolecules 2003;36:7126–31.
[101] Sinha Ray S, Yamada K, Okamoto M, Ueda K. Control of biodegradability of polylactide via nanocomposite technology. Macromol Mater Eng 2003;288:203–8.
[102] Chen G-X, Kim H-S, Kim E-S, Yoon J-S. Compatibilization-like effect of reactive organoclay on the poly(L-lactide)/poly(butylene succinate) blends. Polymer 2005;46:11829–36.
[103] Chen G-X, Yoon J-S. Thermal stability of poly(L-lactide)/poly (butylene succinate)/clay nanocomposites. Polym Degrad Stabil 2005;88:206–12.
[104] Lewitus D, McCarthy S, Ophir A, Kenig S. The effect of nanoclays on the properties of PLLA-modified polymers Part 1: mechanical and thermal properties. J Polym Environ 2006;14:171–7.
[105] Hasook A, Tanoue S, Lemoto Y, Unryu T. Characterization and mechanical properties of poly(lactic acid)/poly(ε-caprolactone)/organoclay nanocomposites prepared by melt compounding. Polym Eng Sci 2006;46:1001–7.
[106] Paul M-A, Alexandre M, Degée P, Henrist C, Rulmont A, Dubois P. New nanocomposite materials based on plasticized poly(L-lactide) and organo-modified montmorillonites: thermal and morphological study. Polymer 2003;44:443–50.
[107] Pluta M. Morphology and properties of polylactide modified by thermal treatment, filling with layered silicates and plasticization. Polymer 2004;45:8239–51.
[108] Paul M-A, Delcourt C, Alexandre M, Degée P, Monteverde F, Rulmont A, et al. (Plasticized) polylactide/(organo-)clay nanocomposites by in situ intercalative polymerization. Macromol Chem Phys 2005;206:484–98.
[109] Pluta M, Paul M-A, Alexandre M, Dubois P. Plasticized polylactide/clay nanocomposites. I. The role of filler content and its surface organo-modification on the physico-chemical properties. J Polym Sci Polym Phys 2006;44:299–311.
[110] Pluta M, Paul M-A, Alexandre M, Dubois P. Plasticized polylactide/clay nanocomposites. II. The effect of aging on structure and properties in relation to the filler content and the nature of its organo-modification. J Polym Sci Polym Phys 2006;44:312–25.
[111] Tanoue S, Hasook A, Iemoto Y, Unryu T. Preparation of poly(lactic acid)/poly(ethylene glycol)/organoclay nanocomposites by melt compounding. Polym Compos 2006;27:256–63.
[112] Shibata M, Someya Y, Orihara M, Miyoshi M. Thermal and mechanical properties of plasticized poly(L-lactide) nanocomposites with organo-modified montmorillonites. J Appl Polym Sci 2006;99:2594–602.
[113] Paul M-A, Alexandre M, Degée P, Calberg C, Jerome R, Dubois P. Exfoliated polylactide/clay nanocomposites by in-situ coordination-insertion polymerization. Macromol Rapid Commun 2003;24:561–6.
[114] Sinha Ray S, Okamoto K, Yamada K, Okamoto M. Novel porous ceramic material via burning of polylactide/layered silicate nanocomposite. Nano Lett 2002;2:423–5.
[115] Lee JH, Park TG, Park HS, Lee DS, Lee YK, Yoon SC, et al. Thermal and mechanical characteristics of poly(L-lactic acid) nanocomposite scaffold. Biomaterials 2003;24:2773–8.
[116] Lee YH, Lee JH, An I-G, Kim C, Lee DS, Lee YK, et al. Electrospun dual-porosity structure and biodegradation morphology of Montmorillonite reinforced PLLA nanocomposite scaffolds. Biomaterials 2005;26:3165–72.
[117] Ema Y, Ikeya M, Okamoto M. Foam processing and cellular structure of polylactide-based nanocomposites. Polymer 2006;47:5350–9.
[118] Maiti P, Batt CA, Giannelis EP. Renewable plastics: synthesis and properties of PHB nanocomposites. Polym Mater Sci Eng 2003;88:58–9.
[119] Hablot E, Bordes P, Pollet E, Avérous L. Thermal and thermo-mechanical degradation of PHB-based multiphase systems. Polym Degrad Stabil 2008;93:413–21.
[120] Lim ST, Hyun YH, Lee CH, Choi HJ. Preparation and characterization of microbial biodegradable poly(3-hydroxybutyrate)/organoclay nanocomposite. J Mater Sci Lett 2003;22:299–302.
[121] Choi WM, Kim TW, Park OO, Chang YK, Lee JW. Preparation and characterization of poly(hydroxybutyrate-co-hydroxyvalerate)-organoclay nanocomposites. J Appl Polym Sci 2003;90:525–9.
[122] Wang S, Song C, Chen G, Guo T, Liu J, Zhang B, et al. Characteristics and biodegradation properties of poly(3-hydroxybutyrate-co-3-hydroxyvalerate)/organophilic montmorillonite (PHBV/OMMT) nanocomposite. Polym Degrad Stabil 2005;87:69–76.
[123] Chen GX, Hao GJ, Guo TY, Song MD, Zhang BH. Crystallization kinetics of poly(3-hydroxybutyrate-co-3-hydroxyvalerate)/clay nanocomposites. J Appl Polym Sci 2004;93:655–61.
[124] Chen GX, Hao GJ, Guo TY, Song MD, Zhang BH. Structure and mechanical properties of poly(3-hydroxybutyrate-co-3-hydroxyvalerate) (PHBV)/clay nanocomposites. J Mater Sci Lett 2002;21:1587–9.
[125] Misra M, Desai SM, Mohanty AK, Drzal LT. Novel solvent-free method for functionalization of polyhydroxyalkanoates: synthesis and characterizations. In: Proceedings of the 62nd annual technical conference of the society of plastics engineers, vol.2. Boca Raton (FL), USA: CRC Press; 2004. p. 2442–6.
[126] Drzal LT, Misra M, Mohanty AK. Sustainable biodegradable green nanocomposites from bacterial bioplastic for automotive applications. In: Proceedings of the US EPA 2004 STAR progress review workshop – nanotechnology and the environment II. Washington, DC (USA): Published by US Environmental Protection Agency. Report number EPA/600/R-05/089;

2005. p 23–5. http://es.epa.gov/ncer/nano/publications/8-18-04/fnanoproc_092005.pdf.
[127] Messersmith PB, Giannelis EP. Synthesis and barrier properties of polycaprolactone-layered silicate nanocomposites. J Polym Sci Polym Chem 1995;33:1047–57.
[128] Messersmith PB, Giannelis EP. Polymer-layered silicate nanocomposites: in situ intercalative polymerization of ε-caprolactone in layered silicates. Chem Mater 1993;5:1064–6.
[129] Krishnamoorti R, Giannelis EP. Rheology of end-tethered polymer layered silicate nanocomposites. Macromolecules 1997;30:4097–102.
[130] Kiersnowski A, Dabrowski P, Budde H, Kressler J, Piglowski J. Synthesis and structure of poly(ε-caprolactone)/synthetic montmorillonite nano-intercalates. Eur Polym J 2004;40:2591–8.
[131] Kiersnowski A, Piglowski J. Polymer-layered silicate nanocomposites based on poly(ε-caprolactone). Eur Polym J 2004;40:1199–207.
[132] Pucciariello R, Villani V, Belviso S, Gorrasi G, Tortora M, Vittoria V. Phase behavior of modified montmorillonite-poly(ε-caprolactone) nanocomposites. J Polym Sci Polym Phys 2004;42:1321–32.
[133] Pucciariello R, Villani V, Langerame F, Gorrasi G, Vittoria V. Interfacial effects in organophilic montmorillonite-poly(ε-caprolactone) nanocomposites. J Polym Sci Polym Phys 2004;42:3907–19.
[134] Tortora M, Vittoria V, Galli G, Ritrovati S, Chiellini E. Transport properties of modified montmorillonite-poly(ε-caprolactone) nanocomposites. Macromol Mater Eng 2002;287:243–9.
[135] Pantoustier N, Lepoittevin B, Alexandre M, Kubies D, Calberg C, Jerome R, et al. Biodegradable polyester layered silicate nanocomposites based on poly(ε-caprolactone). Polym Eng Sci 2002;42:1928–37.
[136] Kubies D, Pantoustier N, Dubois P, Rulmont A, Jerome R. Controlled ring-opening polymerization of ε-caprolactone in the presence of layered silicates and formation of nanocomposites. Macromolecules 2002;35:3318–20.
[137] Lepoittevin B, Pantoustier N, Devalckenaere M, Alexandre M, Kubies D, Calberg C, et al. Poly(ε-caprolactone)/clay nanocomposites by in-situ intercalative polymerization catalyzed by dibutyltin dimethoxide. Macromolecules 2002;35:8385–90.
[138] Lepoittevin B, Pantoustier N, Alexandre M, Calberg C, Jerome R, Dubois P. Polyester layered silicate nanohybrids by controlled grafting polymerization. J Mater Chem 2002;12:3528–32.
[139] Lepoittevin B, Pantoustier N, Alexandre M, Calberg C, Jerome R, Dubois P. Layered silicate/polyester nanohybrids by controlled ring-opening polymerization. Macromol Symp 2002;183:95–102.
[140] Pantoustier N, Alexandre M, Degée P, Kubies D, Jerome R, Henrist C, et al. Intercalative polymerization of cyclic esters in layered silicates: thermal vs catalytic activation. Compos Interfaces 2003;10:423–33.
[141] Viville P, Lazzaroni R, Pollet E, Alexandre M, Dubois P, Borcia G, et al. Surface characterization of poly(ε-caprolactone)-based nanocomposites. Langmuir 2003;19:9425–33.
[142] Gorrasi G, Tortora M, Vittoria V, Pollet E, Lepoittevin B, Alexandre M, et al. Vapor barrier properties of polycaprolactone montmorillonite nanocomposites: effect of clay dispersion. Polymer 2003;44:2271–9.
[143] Viville P, Lazzaroni R, Pollet E, Alexandre M, Dubois P. Controlled polymer grafting on single clay nanoplatelets. J Am Chem Soc 2004;126:9007–12.
[144] Pantoustier N, Alexandre M, Degée P, Calberg C, Jerome R, Henrist C, et al. Poly(ε-caprolactone) layered silicate nanocomposites: effect of clay surface modifiers on the melt intercalation process. e-Polymers 2001, no. 009.
[145] Lepoittevin B, Devalckenaere M, Pantoustier N, Alexandre M, Kubies D, Calberg C, et al. Poly(ε-caprolactone)/clay nanocomposites prepared by melt intercalation: mechanical, thermal and rheological properties. Polymer 2002;43:4017–23.
[146] Chen B, Evans JRG. Poly(ε-caprolactone)-clay nanocomposites: structure and mechanical properties. Macromolecules 2006;39:747–54.
[147] Kwak S-Y, Oh KS. Effect of thermal history on structural changes in melt-intercalated poly(ε-caprolactone)/organoclay nanocomposites investigated by dynamic viscoelastic relaxation measurements. Macromol Mater Eng 2003;288:503–8.
[148] Di Y, Iannace S, Di MaioE, Nicolais L. Nanocomposites by melt intercalation based on polycaprolactone and organoclay. J Polym Sci Polym Phys 2003;41:670–8.
[149] Di Maio E, Iannace S, Sorrentino L, Nicolais L. Isothermal crystallization in PCL/clay nanocomposites investigated with thermal and rheometric methods. Polymer 2004;45:8893–900.
[150] Lepoittevin B, Pantoustier N, Devalckenaere M, Alexandre M, Calberg C, Jerome R, et al. Polymer/layered silicate nanocomposites by combined intercalative polymerization and melt intercalation: a masterbatch process. Polymer 2003;44:2033–40.
[151] Shibata M, Teramoto N, Someya Y, Tsukao R. Nanocomposites based on poly(ε-caprolactone) and the montmorillonite treated with dibutylamine-terminated e-caprolactone oligomer. J Appl Polym Sci 2007;104:3112–9.
[152] Kim SW, Jo WH, Lee MS, Ko MB, Jho JY. Preparation of clay-dispersed poly(styrene-co-acrylonitrile) nanocomposites using poly(ε-caprolactone) as a compatibilizer. Polymer 2001;42:9837–42.
[153] Gonzalez I, Eguiazabal JI, Nazabal J. New clay-reinforced nanocomposites based on a polycarbonate/polycaprolactone blend. Polym Eng Sci 2006;46:864–73.
[154] Zheng X, Wilkie CA. Nanocomposites based on poly(ε-caprolactone) (PCL)/clay hybrid: polystyrene, high impact polystyrene, ABS, polypropylene and polyethylene. Polym Degrad Stabil 2003;82:441–50.
[155] Pollet E, Delcourt C, Alexandre M, Dubois P. Transesterification catalysts to improve clay exfoliation in synthetic biodegradable polyester nanocomposites. Eur Polym J 2006;42:1330–41.
[156] Kalambur SB, Rizvi SS. Starch-based nanocomposites by reactive extrusion processing. Polym Int 2004;53:1413–6.
[157] Yoshioka M, Takabe K, Sugiyama J, Nishio Y. Newly developed nanocomposites from cellulose acetate/layered silicate/poly(ε-caprolactone): synthesis and morphological characterization. J Wood Sci 2006;52:121–7.
[158] Maiti P. Influence of miscibility on viscoelasticity, structure, and intercalation of oligo-poly(caprolactone)/layered silicate nanocomposites. Langmuir 2003;19:5502–10.
[159] Calberg C, Jerome R, Grandjean J. Solid-state NMR study of poly(ε-caprolactone)/clay nanocomposites. Langmuir 2004;20:2039–41.
[160] Gardebien F, Gaudel-Siri A, Bredas J-L, Lazzaroni R. Molecular dynamics simulations of intercalated poly(ε-caprolactone)-montmorillonite clay nanocomposites. J Phys Chem B 2004;108:10678–86.
[161] Gardebien F, Bredas J-L, Lazzaroni R. Molecular dynamics simulations of nanocomposites based on poly(ε-caprolactone) grafted on montmorillonite clay. J Phys Chem B 2005;109:12287–96.
[162] Hrobarikova J, Robert J-L, Calberg C, Jerome R, Grandjean J. Solid-state NMR study of intercalated species in poly(ε-caprolactone)/clay nanocomposites. Langmuir 2004;20:9828–33.
[163] Urbanczyk L, Hrobarikova J, Calberg C, Jerome R, Grandjean J. Motional heterogeneity of intercalated species in modified clays and poly(ε-caprolactone)/clay nanocomposites. Langmuir 2006;22:4818–24.
[164] Jimenez G, Ogata N, Kawai H, Ogihara T. Structure and thermal/mechanical properties of poly(ε-caprolactone)-clay blend. J Appl Polym Sci 1997;64:2211–20.
[165] Sinha Ray S, Okamoto K, Maiti P, Okamoto M. New poly(butylene succinate)/layered silicate nanocomposites: Preparation and mechanical properties. J Nanosci Nanotechnol 2002;2:171–6.
[166] Okamoto K, Ray SS, Okamoto M. New poly(butylene succinate)/layered silicate nanocomposites. II. Effect of organically modified layered silicates on structure, properties, melt rheology, and biodegradability. J Polym Sci Polym Phys 2003;41:3160–72.
[167] Sinha Ray S, Okamoto K, Okamoto M. Structure-property relationship in biodegradable poly(butylene succinate)/layered silicate nanocomposites. Macromolecules 2003;36:2355–67.
[168] Sinha Ray S, Okamoto K, Okamoto M. Structure and properties of nanocomposites based on poly(butylene succinate) and organically modified montmorillonite. J Appl Polym Sci 2006;102:777–85.
[169] Someya Y, Nakazato T, Teramoto N, Shibata M. Thermal and mechanical properties of poly(butylene succinate) nanocomposites with various organo-modified montmorillonites. J Appl Polym Sci 2004;91:1463–75.
[170] Chen G-X, Kim E-S, Yoon J-S. Poly(butylene succinate)/twice functionalized organoclay nanocomposites: Preparation, characterization, and properties. J Appl Polym Sci 2005;98:1727–32.
[171] Chen G-X, Yoon J-S. Non-isothermal crystallization kinetics of poly(butylene succinate) composites with a twice functionalized organoclay. J Polym Sci Polym Phys 2005;43:817–26.
[172] Shih YF, Wang TY, Jeng RJ, Wu JY, Teng CC. Biodegradable nanocomposites based on poly(butylene succinate)/organoclay. J Polym Environ 2007;15:151–8.
[173] Sinha Ray S, Bousmina M, Okamoto K. Structure and properties of nanocomposites based on poly(butylene succinate-co-adipate)

and organically modified montmorillonite. Macromol Mater Eng 2005;290:759–68.
[174] Sinha Ray S, Bousmina M. Poly(butylene sucinate-co-adipate)/montmorillonite nanocomposites: effect of organic modifier miscibility on structure, properties, and viscoelasticity. Polymer 2005;46:12430–9.
[175] Sinha Ray S, Bandyopadhyay J, Bousmina M. Effect of organoclay on the morphology and properties of poly(propylene)/poly[(butylene succinate)-co-adipate] blends. Macromol Mater Eng 2007;292: 729–47.
[176] Sinha Ray S, Bandyopadhyay J, Bousmina M. Thermal and thermomechanical properties of poly[(butylene succinate)-co-adipate] nanocomposite. Polym Degrad Stabil 2007;92:802–12.
[177] Lee CH, Lim ST, Hyun YH, Choi HJ, Jhon MS. Fabrication and viscoelastic properties of biodegradable polymer/organophilic clay nanocomposites. J Mater Sci Lett 2003;22:53–5.
[178] Lim ST, Hyun YH, Choi HJ, Jhon MS. Synthetic biodegradable aliphatic polyester/montmorillonite nanocomposites. Chem Mater 2002;14:1839–44.
[179] Lim ST, Lee CH, Choi HJ, Jhon MS. Solid-like transition of melt-intercalated biodegradable polymer/clay nanocomposites. J Polym Sci Polym Phys 2003;41:2052–61.
[180] Lim ST, Lee CH, Kim HB, Choi HJ, Jhon MS. Polymer/organoclay nanocomposites with biodegradable aliphatic polyester and its blends: preparation and characterization. e-Polymers 2004, no. 026.
[181] Lee CH, Kim HB, Lim ST, Choi HJ, Jhon MS. Biodegradable aliphatic polyester-poly(epichlorohydrin) blend/organoclay nanocomposites: synthesis and rheological characterization. J Mater Sci 2005;40:3981–5.
[182] Chen G, Yoon J-S. Nanocomposites of poly[(butylene succinate)-co-(butylene adipate)](PBSA) and twice-functionalized organoclay. Polym Int 2005;54:939–45.
[183] Sinha Ray S, Bousmina M. Crystallization behavior of poly[(butylene succinate)-co-adipate] nanocomposite. Macromol Chem Phys 2006;207:1207–19.
[184] Someya Y, Sugahara Y, Shibata M. Nanocomposites based on poly(butylene adipate-co-terephthalate) and montmorillonite. J Appl Polym Sci 2005;95:386–92.
[185] Someya Y, Kondo N, Teramoto N, Shibata M. Studies of biodegradation of poly (butylene adipate-co-butylene terephtharate)/layered silicate nanocomposites. Polym Prepr Jpn 2005;54:5362.
[186] Chivrac F, Kadlecova Z, Pollet E, Averous L. Aromatic copolyester-based nano-biocomposites: elaboration, structural characterization and properties. J Polym Environ 2006;14:393–401.
[187] Chivrac F, Pollet E, Averous L. Nonisothermal crystallization behavior of poly(butylene adipate-co-terephthalate)/clay nano-biocomposites. J Polym Sci Polym Phys 2007;45:1503–10.
[188] Krook M, Albertsson A-C, Gedde UW, Hedenqvist MS. Barrier and mechanical properties of montmorillonite/polyesteramide nanocomposites. Polym Eng Sci 2002;42:1238–46.
[189] Krook M, Morgan G, Hedenqvist MS. Barrier and mechanical properties of injection molded montmorillonite/polyesteramide nanocomposites. Polym Eng Sci 2005;45:135–41.
[190] Averous L. Biodegradable multiphase systems based on plasticized starch: a review. J Macromol Sci Polym Rev 2004;C44:231–74.
[191] Lagaly G. From clay mineral crystals to colloidal clay mineral dispersions. In: Dobias B, editor. Coagulation and flocculation—theory and applications. New York: Dekker; 1993. p. 427.
[192] Sinha Ray S, Okamoto M. Polymer/layered silicate nanocomposites: a review from preparation to processing. Prog Polym Sci 2003;28:1539–641.
[193] Utracki LA, Sepehr M, Boccaleri E. Synthetic, layered nanoparticles for polymeric nanocomposites (PNCs). Polym Adv Technol 2007;18:1–37.

Progress in Polymer Science 34 (2009) 156–193

Contents lists available at ScienceDirect

Progress in Polymer Science

journal homepage: www.elsevier.com/locate/ppolysci

Developments and new applications of UV-induced surface graft polymerizations

Jianping Deng[a,b], Lifu Wang[a,b], Lianying Liu[a,b], Wantai Yang[a,b,*]

[a] State Key Laboratory of Chemical Resource Engineering, Beijing University of Chemical Technology, Beijing 100029, China
[b] College of Materials Science and Engineering, Beijing University of Chemical Technology, Beijing 100029, China

ARTICLE INFO

Article history:
Received 28 November 2007
Received in revised form 25 May 2008
Accepted 16 June 2008
Available online 17 October 2008

Keywords:
UV light
Polymer surface
Graft polymerization
Modification
Functionalization

ABSTRACT

As one of the major techniques developed to achieve surface modification of polymeric materials, UV-induced surface graft polymerization has been widely applied as a simple, useful and versatile approach to improve the surface properties of polymers. This review surveys the recent advances in UV light induced surface graft polymerizations, predominantly focusing on: (1) various initiating methods, controlled/living grafting, self-initiated grafting (grafting without the addition of photoinitiators), graft polymerizations with monomer pairs able to form charge transfer (CT) complexes, grafting in liquid, vapor and bulk phase, and the substrates used for grafting; (2) the topography of grafted surface layers, including granular structure, crosslinked structure, and well-defined structure; and (3) the application of techniques to prepare functionalized polymer surfaces with designed performances, e.g., to obtain polymer materials suitable for biomedical applications, membranes or microfluidics.

Contents

Abbreviations: AA, acrylic; ADPMA, *N*-(4-aminodiphenylmethane) acrylamide; AEMA, 2-aminoethyl methacrylate hydrochloride (AEMA); AFM, atomic force microscopy; AG, allyl glucoside; $AgNO_3$, silver nitrate; AIBN, 2,2′-azo-bis-isobutyronitrile; AQ, anthraquinone; AQS, anthraquinone-2-sulfonate sodium; ATR-IR, attenuated total reflection infrared; BOPP, biaxially oriented polypropylene; BP, benzophenone; BPO, benzoyl peroxide; BTC, (4-benzoyl benzyl) trimethylammonium chloride; CAN, ceric ammonium nitrate; CdS, cadmium sulfide; CO_2, carbon dioxide; COC, cylic olefin copolymers; COP, cycloolefin polymer; CP, conversion percentage; CPP, casting polypropylene; CT, charge transfer CT; DEAAm, *N*,*N*′-diethylacrylamide; DEAEA, (diethylamino)ethyl acrylate; DMAMS, (dimethylamino)methyl styrene; DMF, *N*,*N*-dimethylformamide; DVB, 1,2-divinylbenzene; DVE-3, triethylene glycol divinyl ether; EPDM, terpolymer ethylene/propylene/5-ethylidene-2-norbornene; ePTFE, expanded poly(tetrafluoroethylene); $FeCl_3$, ferric chloride; FE-SEM, Field-emission scanning electron microscopy; FT-IR, Fourier Transform Infrared; *g*, graft; GE, grafting efficiency; GMA, glycidyl methacrylate; GOD, glucose oxidase; gVCD, grafting chemical vapor deposition; HDPE, high density polyethylene; HEA, 2-hydroxyethyl acrylate; HEMA, 2-hydroxyethyl methacrylate; HVV, *N*-hexyl-*N*′-(4-vinylbenzyl)-4,4′-bipyridinium bromide chloride; ISC, intersystem crossing; ITX, isopropylthioxanthone; $K_2S_2O_8$, potassium persulphaste; LDPE, low density polyethylene; MAH, maleic anhydride; MBAA, *N*,*N*-methylene bisacrylamide; MePEGA, methoxy poly(ethylene glycol) acrylate; MIP, molecular imprinted polymer; MPC, 2-methacryloyloxyethyl phosphorylcholine; NVP, *N*-vinyl pyrrolidone; O_2, oxygen; O_3, ozone; OM, optical microscopy; *p*, *para*-; PAA, polyacrylic acid; PAN, polyacrylonitrile; PANI, polyaniline; PDA, 1,4-phenylenediamine; PDMS, poly(dimethylsiloxane); PE, polyethylene; PEG, poly(ethylene glycol); PES, poly(ether sulfone); PET, poly(ethylene terephthalate); pH, power of hydrogen; PHBV, poly(3-hydroxybutyrate-*co*-3-hydroxyvalerate); PLA, poly(L-lactide); PMAA, poly(methacrylic acid); PMMA, poly(methyl methacrylate); PNIPAAm, poly(*N*-isopropylacrylamide); PP, polypropylene; PP-*g*-PAA/PANI, polyprolylene-*graft*-polyacrylic acid/polyaniline; PPY, polypyrrole; PS, polystyrene; SAM, self-assembled-monolayer; SEM, scanning electron microscopy; SFM, scanning force microscopy; TEMPTA, trimethylopropane triacrylate; THF, tetrahydrogen furan; THO, theophylline; UV, ultraviolet; UV–vis, ultraviolet visable; VAC, vinyl acetate; VQAS, vinyl quarternary ammonium salt; XAN, xanthone.

* Corresponding author at: Beijing University of Chemical Technology, P.O. Box 37#, China. Tel.: +86 10 6443 2262; fax: +86 10 6441 6338.
E-mail address: yangwt@mail.buct.edu.cn (W. Yang).

0079-6700/$ – see front matter © 2008 Elsevier Ltd. All rights reserved.
doi:10.1016/j.progpolymsci.2008.06.002

1. Introduction

The surface of a solid is important to the material performance in at least two respects: first, the microstructure and properties of surfaces are usually different from those in the bulk; second, among all parts of a material, the outmost surface is most prone to both physical and chemical interactions with its environment. To achieve materials with desired surface properties for specific applications, chemically tailoring the surface of solids has many advantages, including (1) improvement of the surface properties of a material without affecting its bulk properties; (2) elimination of the need to redesign the bulk material to achieve a target surface performance; and (3) reduction in cost since all necessary chemistry is confined to the surface.

Most polymeric materials have pristine surfaces with low surface energies, and are hydrophobic rather than hydrophilic. This situation leads to two major problems: the first is that the hydrophobic surfaces are difficult to bond with polar surfaces, often necessary in fields requiring high adhesion, such as coatings, adhesives, paints, printing inks, etc. [1,2]; the second involves some special uses of polymers such as separation membranes, biosensors and microfluidics. When used as biomaterials, hydrophobic surfaces generally adsorb proteins, resulting in so-called "bio-fouling" (deposition and growth of microorganisms on surfaces) [3–5]. Thus, the control of chemistry at polymer surfaces has become increasingly important for at least the major number of applications. Among all possible methods, polymer surface modification has gathered much attention, and has been used to introduce surface functionalities onto substrates to enhance numerous properties such as adhesiveness, wettability, biocompatibility, antifouling, etc. [6–10].

To date, a number of effective technologies have been developed to improve the surface properties of polymers, including either physical deposition of surface-active compounds [11], covalent immobilization of polymer chains onto a substrate surface by coupling reactions ("grafting-to" techniques) [12], or planting graft polymer chains on the substrate surface via plasma or glow discharge [13–16], corona discharge [17–19], and grafting initiated by γ-ray [20–22] ("grafting-from" techniques). Physical deposition of surface compounds on the substrates usually results in noncovalently bound coatings, which are potentially unstable and readily removed from the substrate. For the grafting-to methods, limitations such as incomplete surface coverage, difficulty in uniform diffusion of the polymer

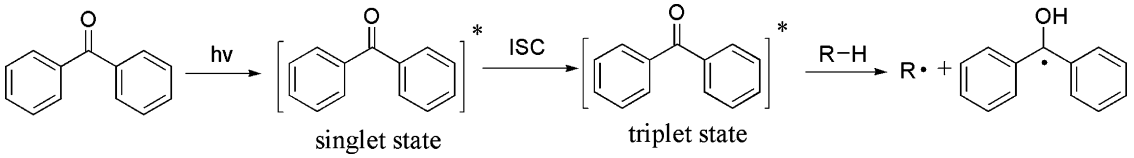

Scheme 1. Photografting polymerization initiated by BP (Ref. [55]).

chains to the substrate, and irregular distribution of the target reactive sites are addressed by the steric repulsion of the polymer chains [23]. Most of the grafting-from methods mentioned above would substantially deteriorate the bulk properties of the materials and/or the modification effects would remain only for a short period. Compared with other modification methods, surface graft polymerizations induced by UV irradiation exhibit some advantages, e.g., fast reaction rate, low cost of processing, simple equipment, easy industrialization, and maybe the most important, the distribution of grafted chains is limited to a shallow region near the surface. Surface photografting polymerization thus offers the unique ability to tune and manipulate surface properties without damaging the bulk material. The pioneering work on photografting polymerization initiated by UV light was published in the 1950s by Oster and Shibata [24]. At that time, only a few scientists realized the importance of it. Until the 1980s, most investigations related to surface graft polymerizations were focused on initiation by high energy irradiation [25–31]. Investigations into surface photografting have grown rapidly in the last several decades and numerous papers have been published. In the history of surface photografting, liquid phase systems [32] and vapor phase systems [33,34] were predominantly employed in the initial stage; continuous operation system [35–37] and bulk surface photografting technology [38–40] based on the earlier work were developed later. The realization of control/living grafting was another significant advance [41].

Despite the rapid progress in this promising research field, only a few review papers have been published to address the surface photografting polymerizations and the related applications. Up to now, the review papers found include the reviews written by Rånby around 1998 [42–44], and several others containing only a section involving photografting [45–48]. In view of the significance of the technique and the rapidly extending applications, it is therefore reasonable to summarize the latest advances in this focal research area. This review is thus expected to inspire the interests from both material scientists and industrialists.

This article first reviews the various techniques to perform surface photografting polymerization from the perspectives of initiating method (different photoinitiators), effective controlling on the grafting (controlled/living grafting), self-initiated grafting (without the addition of photoinitiator), grafting systems containing a charge transfer (CT) complex, grafting in liquid, vapor and bulk, and grafting on different substrates (Section 2); thereafter the typical topographies of the grafted surfaces are discussed, including granular, crosslinked and well-defined structures (Section 3); finally, the performances and applications of the grafted surfaces are summarized, therein the wettability, adhesivity/autoadhesivity,

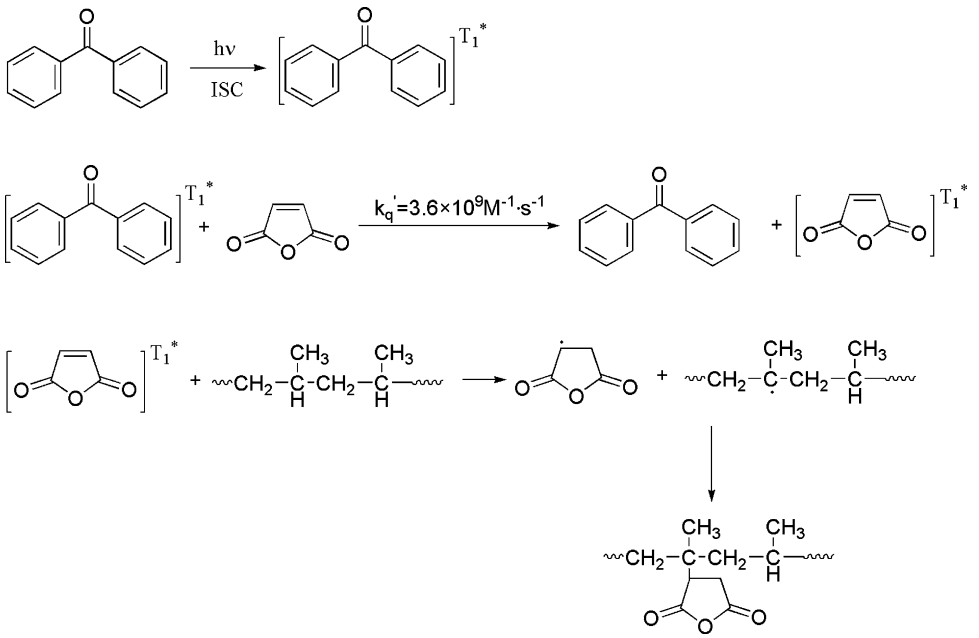

Scheme 2. Excitation of MAH through the energy-transfer process and the initiation of the grafting process (Ref. [55]).

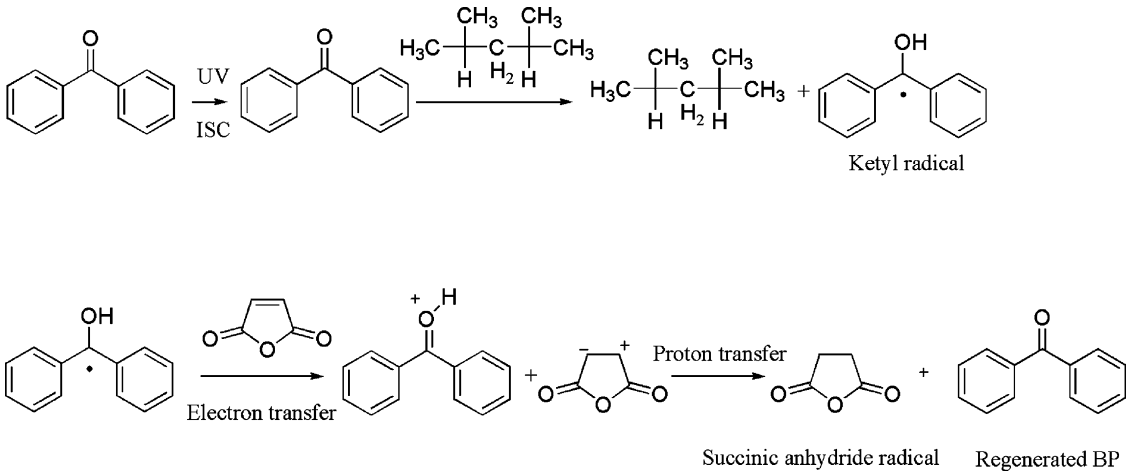

Scheme 3. Process of regenerating of BP from a ketal radical through electron and proton transfer (Ref. [55]).

and environment-responsiveness of the grafted surfaces are primarily introduced, followed by the demonstration of surface photografting for lamination, for chemical tailored microfluidic devices and functional membranes, even for some biomedical-related applications (Section 4).

2. Surface photografting polymerization

2.1. Techniques in initiation

UV light is extensively used to carry out surface graft polymerization, often in the presence of a photoinitiator or photosensitizer. Compared with Norrish type I photoinitiators [49–51], Norrish type II photoinitiators were more frequently used, predominantly because the latter results in higher grafting efficiency, while the former leads to higher polymerization yield and higher polymerization rate, but lower grafting efficiency [52,53]. Among the existing Norrish type II photoinitiators, probably the most widely selected have been benzophenone (BP) [54,55] and its derivatives [56–58], shown to effectively initiate or co-initiate a number of radical-induced surface photografting polymerizations. In principle, when UV irradiated, BP or BP-based molecules are excited to a singlet state and then jump to a triplet state by intersystem crossing (ISC; Scheme 1). Investigations have demonstrated that BP and its derivatives in a triplet state undergo hydrogen-abstracting reactions from substrates, consequently providing surface radicals ($R^{\bullet}$) capable of initiating surface graft polymerization. The resulting benzopinacol radicals ($BP–OH^{\bullet}$) are relatively less reactive and not prone to free radical polymerization, but tend to participate in termination by coupling reaction.

Deng and Yang [58] compared the initiating efficiency of BP and several other frequently used photoinitiators, including isopropylthioxanthone (ITX), xanthone (XAN), anthraquinone (AQ), benzoyl peroxide (BPO), 2,2′-azo-bis-isobutyronitrile (AIBN), etc. When vinyl acetate (VAC) was used as the monomer, the graft polymerization with BP as photoinitiator showed the highest grafting efficiency, whereas AQ, BPO and AIBN could not initiate the graft polymerization of VAC. In addition to BP, Geuskens et al. [59] used anthraquinone-2-sulfonate sodium (AQS) and (4-benzoyl benzyl) trimethylammonium chloride (BTC) as photoinitiator to accomplish surface graft polymerization of acrylamide in aqueous solution. They first adsorbed the photoinitiator on the surface of substrate, and then irradiated the substrate with UV light. With this method, the homopolymer of acrylamide as a by-product could not be avoided. In comparison, AQS was more suited because it has a higher adsorption coefficient. Hong and coworkers investigated the performance of a blend of photoinitiators including BP and ITX [60] and found that the addition of a small amount of ITX markedly enhanced both graft yield and surface polarity of the substrate, which should be ascribed to the so-called "photosensitization effect" [61–64] in which a reactant, e.g., BP in this case, unable to absorb UV light in appreciable quantities is activated by a different substance. In this case, ITX acting as a photosensitizer absorbs the light and then carries the resulting energy to BP molecules. In more detail, ITX may also act as a photosensitizer and transfer electrons or energy to BP by forming the excited-state complex (exciplex), thereby improving the efficiency of the photoinitiator to produce more active species. In the work by Woo et al. [65], a combination of two photoinitiators, BP and 4,4′-bis(diethylamino)-benzophenone was used. When used as co-photoinitiator with BP, ferric chloride ($FeCl_3$) could remarkably enhance the grafting due to the "synergistic effect" between Fe^{3+} and BP [66]; in other words, the presence of Fe^{3+} enhanced the initiating effects of BP.

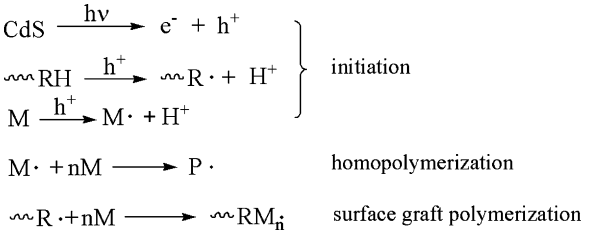

Scheme 4. Photografting polymerization initiated by CdS (Ref. [69]).

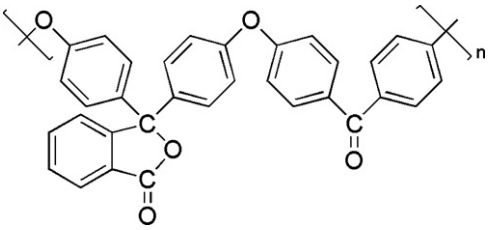

Scheme 5. Structure of cardo polyetherketone.

The detailed initiating mechanism for a given photoinitiator may be, depend on factors such as the monomer type or other conditions, an effect well exemplified by BP/maleic anhydride (MAH) photografting system [55]. According to the investigations by Moore and coworkers [55], efficient photografting of MAH may be performed smoothly, even though in many cases MAH could not readily undergo polymerization initiated by free radicals. The occurrence of photografting polymerization of MAH could be ascribed to the following two possible mechanisms, which may co-

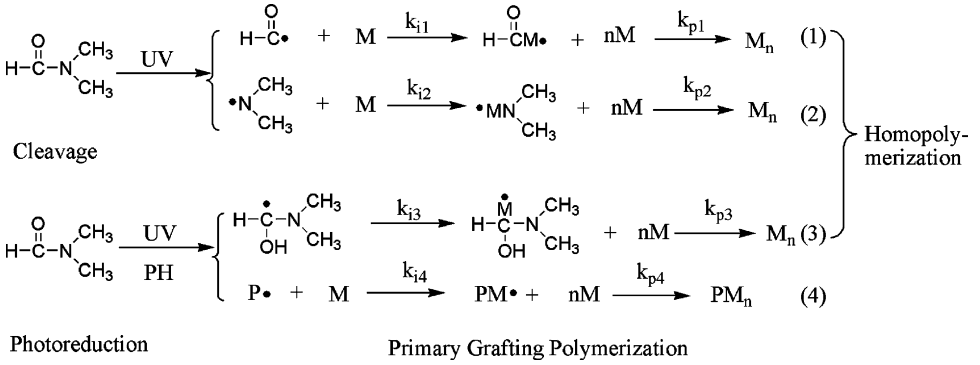

Scheme 6. Photografting polymerization initiated by DMF (Ref. [80]).

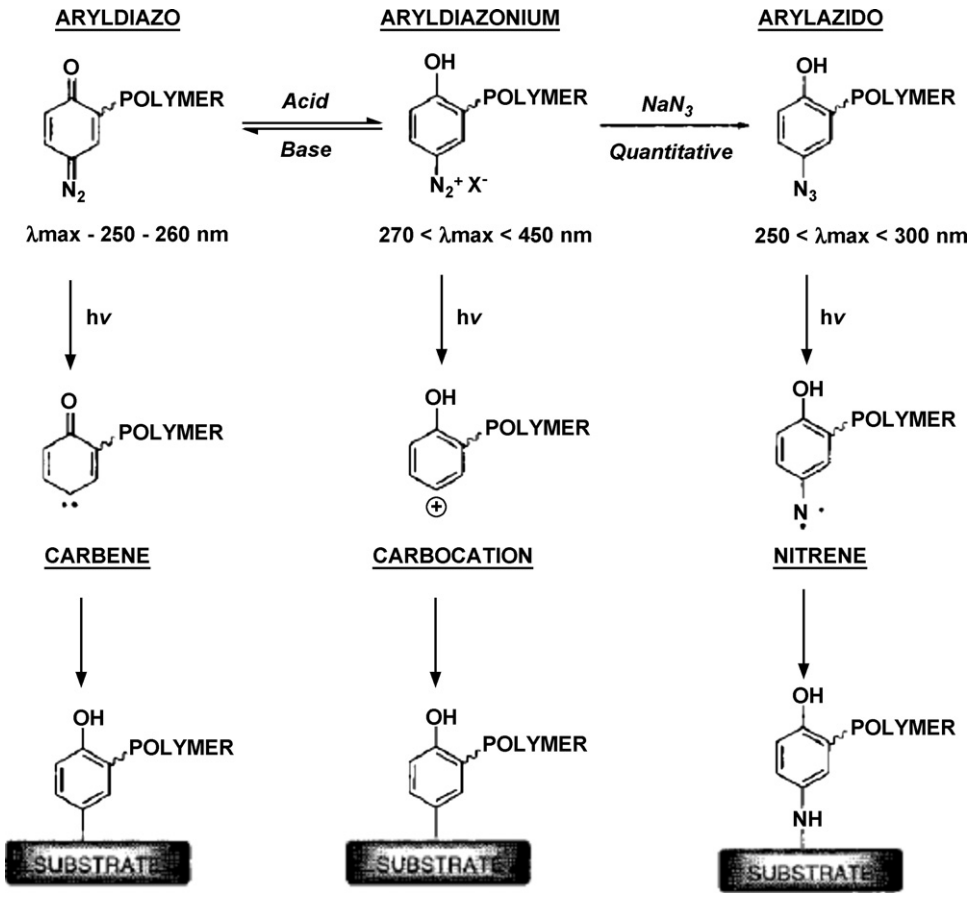

Scheme 7. Schematic representation of the photochemical processes involved in the surface modification of polymer substrate (Ref. [94]).

exist (Schemes 2 and 3): (1) via the formation of excited triplet state of MAH sensitized by BP; (2) via the electron transfer process, followed by the proton transfer between MAH and semibenzopinacol radicals. In the latter case, BP concentration is expected to decrease more slowly than in the photolysis process that does not involve MAH, as observed in the experiment (Scheme 3).

Apart from the common photoinitiators, other new compounds are also utilized to initiate surface photografting polymerization. EI-Wakil reported a method for photografting where BPO was used to initiate the graft polymerization of *N*-(4-aminodiphenylmethane) acrylamide (ADPMA) onto natural rubber under UV irradiation [67]; in the work of Zhou and Liu [68], BPO was used to carry out the photografting. Semiconductor-based photocatalysts, e.g., cadmium sulfide (CdS), worked well as an initiator to induce vinyl monomers' grafting on substrate [69]. The possible initiation mechanism is proposed below (Scheme 4).

Upon UV irradiation, CdS generates an electron (e^-) in the conduction band and a positive hole (h^+) in the valence band (Eq. (1)); the positive hole transfers the charge to a substrate molecule (R–H) producing a free radical ($R^\bullet$) and a proton (H^+) (Eq. (2)); the free radicals can initiate both the graft polymerization and homopolymerization of the monomer (M) (Eqs. (3) and (4)); both grafted polymer and homopolymer were formed through the coupling reactions (Eqs. 5–7).

Some ketones and aldehydes undergo hydrogen abstraction from the substrate material upon UV irradiation, which can be utilized to carry out surface photografting polymerization. The initiating efficiency of several ketones and aldehydes were compared experimentally by Yang and Rånby [70]. The unique characteristics of high triplet state energy, strong UV absorption, stable molecular structure and low initiating reactivity of the ketyl free radicals derived from ketones make them applicable to surface photografting polymerization. When mixed with water or ethanol as the solvent mixture and irradiated by UV light, aliphatic ketones (butanone, pentan-3-one, pentane-2-one, and heptane-3-one) could effectively initiate the graft polymerization of methacrylic acid onto HDPE [71,72]. Acetone is another ketone designedly used as photoinitiator [73]. Additionally, when the substrate contains photo-sensitive ketone moieties [74], e.g., cardo polyetherketone [75] (Scheme 5), in situ graft polymerization took place on the substrate upon UV irradiation in the absence of additional photoinitiator (cardo, from the Latin *loop*, was introduced to refer to side-chain cyclic aromatic groups that lie perpendicular to a planar aromatic backbone).

Eosin moieties immobilized on the substrate surface are capable of initiating photografting polymerization of vinyl monomers. When UV irradiated in the presence of a reducing agent and oxygen, the eosin moiety would undergo redox reaction and generate free radicals, which initiate polymerization [76]. The uses of titanium (III)-potassium persulphaste ($K_2S_2O_8$) redox initiator system [77] and ceric ammonium nitrate (CAN) [78] to initiate photografting were also reported. Cationic photoinitiators can initiate graft polymerizations, as investigated by Kumar and coworkers [79]. Even a common solvent, *N*,*N*-dimethylformamide (DMF) could initiate the surface photografting polymerization of methyl methacrylate on LDPE films [80]. The proposed mechanism is presented below (Scheme 6).

Surface photografting polymerizations are generally conducted with UV light in a full range of wavelength, but it was demonstrated that UV light below 300 nm (the far UV light) played a predominant role in initiating grafting [81,82]. In some cases, UV light of certain wavelengths was employed as the irradiation source. For example, when poly(ether sulfone) ultrafiltration membrane was used as the substrate, if photografting polymerization of *N*-vinyl-2-pyrrolidinone was carried out under UV light but without filtering out 254 nm wavelength light, the resulting grafted membrane showed a severe loss of protein rejection [83]. Therefore, benzene or an aromatic polyester film should be used as light filters. In addition, the efficiency of 172 nm UV monochromatic light to initiate graft polymerization was evaluated by Zhu and Kelley [84]. In the research of Ziani-Cherif et al. [85], even visible-light was used to induce surface grafting polymerization.

For some substrates containing carbonyl or ester groups, photografting polymerization can proceed smoothly even without any photoinitiator. For example, after UV irradiated with a high pressure mercury lamp, PET films immersed in a 10 wt.% aqueous solution of acrylamide containing an appropriate quantity of periodate ($NaIO_4$), gave a highly hydrophilic surface [86]; the concentration of $NaIO_4$ was an important factor for the occurrence of graft polymerization [86,87].

Azido photochemistry was frequently used to introduce functional groups onto substrate surfaces. It is also one of the so-called "grafting to" techniques through which surface modification and/or functionalization can be efficiently realized [88–91]. The basic idea is to introduce organic functional groups onto the surface via highly reactive intermediates (Scheme 7). The typical procedures were demonstrated clearly by the groups of Roger and coworkers [92], Knaus et al. [93], Matsuda and coworkers [94,95] and Chen et al. [96].

2.2. Controlled/living grafting

The conventional photografting methods may not lead to well-controlled graft polymerization. If no special strategy is taken, the graft polymerizations are usually accompanied by the homopolymerization of monomers, branching and/or crosslinking of the grafted chains [58,97], and even degradation of the substrate [98]. The high level of formation of homopolymers and crosslinking of the substrate is inconsistent with the intent of surface modification through grafting polymerization. Still, the formation of homopolymer or the over crosslinking of the substrate is sometimes detrimental to subsequent applications. To circumvent these shortcomings, "living" or controlled grafting polymerization concept was developed by Yang and Rånby [41]. Living polymerization is one type of polymerizations in which chain transfer and chain termination are absent. Nearly all living/controlled polymerization systems have active and inactive (dormant) species, which are in a dynamic equilibrium. Therefore, such polymerizations are controllable [99]. Similarly, living grafting polymeriza-

tions make it possible to effectively control the length, composition, and the distribution of the grafted chains on the surfaces of interest, which in turn enables to realize precisely functionalized surfaces. Among the reported "grafting from" methods to achieve controlled surface grafting, atom-transfer radical polymerization (ATRP) may be the most efficient and especially well-suited for surface modification [100–102]. By this technique combined with Langmuir–Blodgett, Ejaz et al. realized the precise control of molecular weight, molecular weight distribution, and surface density of graft chains [103]. Therefore, the realization of living/controlled surface grafting polymerization is of great significance for future practical applications.

In the work of Yang and Rånby [41], the strategy to achieve living graft polymerization consists of two steps: the first is to covalently attach dormant end groups on the surface of the substrate by photografting monomer solutions containing BP, which introduces graft chains end-capped with semibenzopinacol groups onto LDPE; the second step is to perform living radical graft polymerization of monomers by re-activating the dormant end groups by either heating or UV irradiation to form surface free radicals. Of the two steps, the first is crucial, controlling the nature and the efficiency of the subsequent graft polymerization. The above procedures are presented in Scheme 8.

The above practice on living radical graft polymerization possesses unique advantages over solution and bulk graft polymerizations. The growing radicals covalently rooted on the substrate surface are not readily terminated by bimolecular coupling due to the existence of the substrate to which the chains are bonded, the low concentration of living growing chains and the low mobility of the active species. Thereby, the above grafting polymerization features living characteristics, and the surface photografting is "controllable". Various experiments have confirmed the feasibility of this idea [104]. It was experimentally demonstrated that grafting density and grafted polymer chain length can be controlled by choosing the reaction conditions in the first step and in the subsequent step independently. In the second step, a linear relationship was observed between the graft polymerization rate and the monomer concentration. Bowman and coworkers [105] investigated the effects of principal factors further, including monomer type, solvent, etc. It was found that the graft polymerization rate of acrylic acid increases linearly with increasing surface initiator concentration, and the formation rate of the surface initiator follows a decreasing order dependant on solvent: benzene > chloroform > hexane > methanol > cyclohexane > dimethyl sulfoxide. The main reasons were attributed to

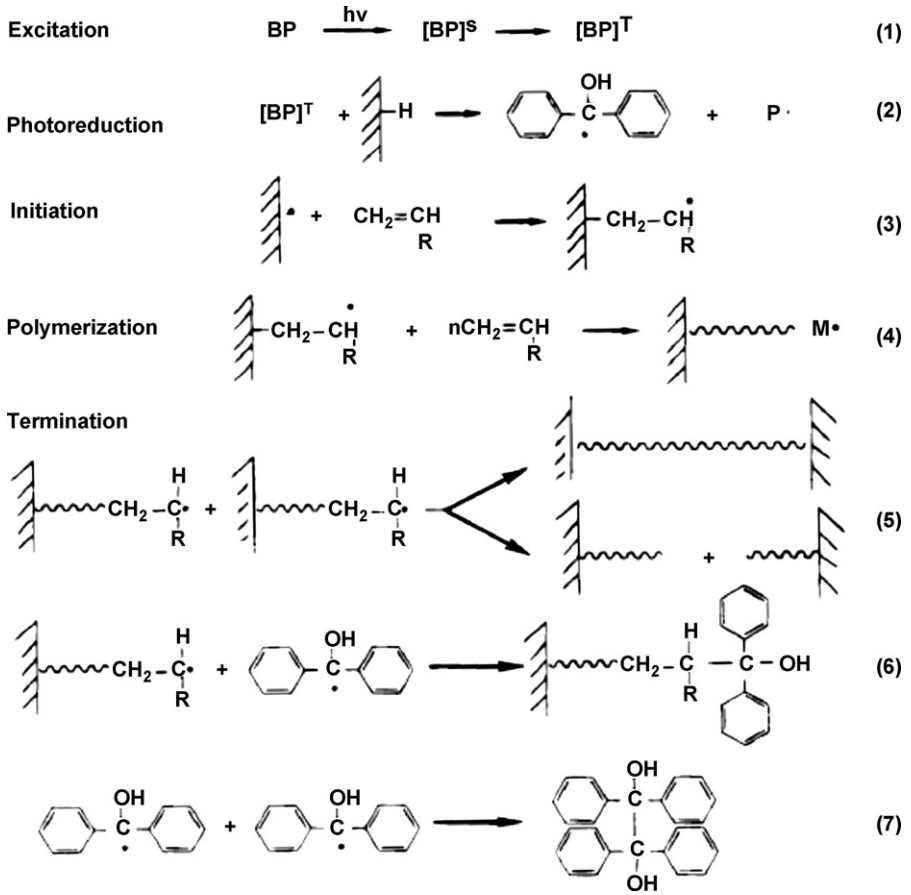

Scheme 8. The mechanism of living grafting polymerization developed by Yang and Rånby (Ref. [41]).

the relative ability to abstract hydrogen from the solvent and the wettability of the substrate by the solvent.

Another effective route to realize living/controlled surface photografting was through the utilization of "photo-iniferters", as reported by Matsuda et al. [106–108]. The first work about iniferter, an abbreviation of *initiator*, *transfer* agent, and *terminator*, was reported by Otsu and Yoshida [109]. The relevant mechanism of living/controlled surface photografting is illustrated in Scheme 9 [106].

Photolysis of the iniferter by UV irradiation yields a pair of radicals: the reactive one can initiate monomers to produce a polymer end radical; the less reactive one cannot initiate the polymerization of monomers, but prefers to terminate the growing polymer chains, forming dithiocarbamyl end-capped chain which can be dissociated again to form a radical pair by UV radiation. In this way, living/controlled polymerization can be realized. When the iniferter is chemically bonded to substrates, living graft polymerization can be accomplished, as reported [106].

Since controlled/living graft polymerization proceeds only with UV irradiation and on the UV irradiated regions, controlled grafting can be realized and applied to various fields, such as regionally precise modification, photopatternable grafting [110–113], grafting with controlled densities at spatial locations [114], and microfluidic devices [115]. Moreover, for substrates containing "iniferter" segments, controlled/living graft polymerization is also feasible [116,117].

Although the detailed procedures varied with the two different methods introduced above, the underlying concept is the same as illustrated in Schemes 7 and 8. Both methods consist of two steps: the first is to introduce a specific structure onto the substrate's surface; the second is to reactivate and dissociate the specific structure again under heating or UV radiation, yielding two radicals. One is active enough to initiate the polymerization, and the other one is less reactive and only participates in the coupling reaction. The two methods introduced above enable relatively fine control over the graft polymerization, whereby a large number of practical applications could be realized.

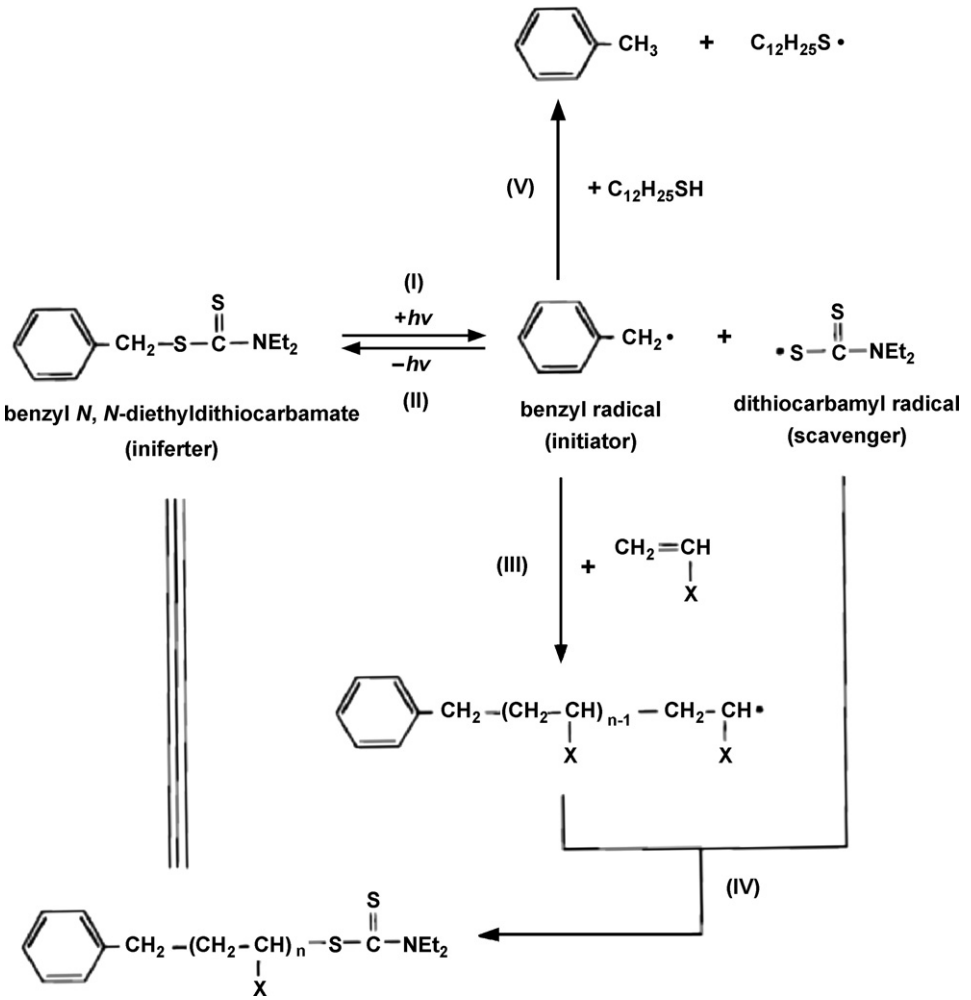

Scheme 9. Living grafting polymerization via iniferter (Ref. [106]).

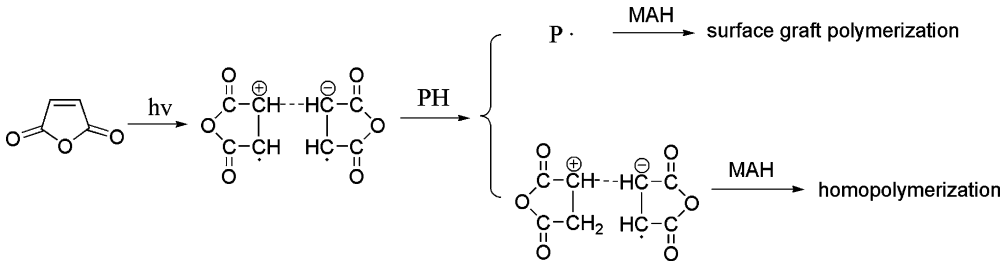

Scheme 10. Schematic representation of the self-initiated grafting polymerization and crosslinking reaction of MAH (Ref. [118]).

2.3. Self-initiated grafting

Most photografting polymerizations require the addition of photoinitiators, just as discussed in Section 2.1. However, some special monomers demonstrated unique self-initiating abilities, i.e., undergoing photografting polymerization without any photoinitiator. Maleic anhydride (MAH) is one of such monomers [118]. With LDPE as the substrate and after UV irradiation, the conversion percentage (CP) and grafting efficiency (GE: defined as the mass of the grafted polymer divided by the total weight of the polymer produced) of MAH can reach nearly 80 and 70%, respectively, even though no photoinitiator was presented. It was further found that the far UV light (200–300 nm) played a decisive role in the photografting polymerization of MAH. Moreover, crosslinking reaction of the substrate LDPE was found to occur simultaneously during the graft polymerization, and the gel content was about 45%. The proposed mechanism is schematically represented in Scheme 10 [118].

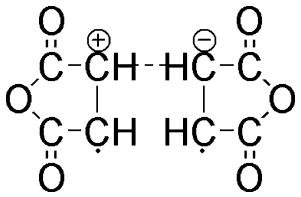

Scheme 11. Excimer formed by MAH upon being irradiated by UV light.

When irradiated with UV light, MAH molecules produce excimers first (compound **1**, •MAH-MAH• in Scheme 11); the excimers could abstract hydrogen from the backbones of LDPE and form surface free radicals which could consequently initiate graft polymerization and homopolymerization of MAH and crosslinking reaction of the substrate. Due to this unique characteristic of self-initiation, MAH could function as a photoinitiator for other monomers. For example, it was capable of initiating the graft polymerization of acrylic acid, as shown in [118]. The grafting efficiency was as high as about 55%, despite that it seemed to be lower compared with that using BP as the photoinitiator.

In addition to MAH, other monomers such as styrene [119,120] (the relevant mechanism is shown in Scheme 12), and even acrylic acid, methacrylic acid, glycidyl acrylate,

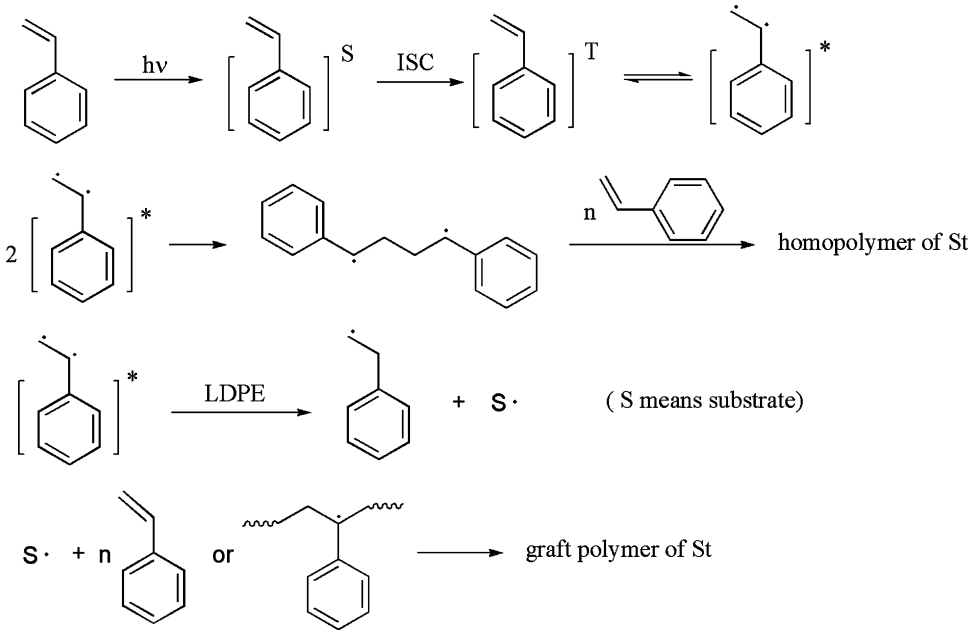

Scheme 12. Self-initiated grafting polymerization of styrene (Ref. [119]).

2-hydroxyethyl acrylate, and 2-hydroxyethyl methacrylate [121] somewhat exhibited this feature. Some monomer pairs, especially those electron acceptor–donor monomer pairs also possessed this feature, which will be discussed below in more details. It should be pointed out that these special monomers and monomer pairs are significant for the development of initiator-free photografting and photocuring systems.

2.4. Grafting of electron donor–acceptor monomer pairs

The finding that charge transfer (CT) complexes could photopolymerize in the absence of photoinitiator [122–124] stimulated the use of CT complexes as monomer pairs to perform surface photografting polymerizations. The advantage of using CT complexes as monomer for photografting is twofold: (1) it is useful for developing photoinitiator-free photografting systems and (2) it considerably widens the range of monomers.

When initiated by free radical, MAH generally polymerizes with much difficulty; however, it undergoes photografting polymerization more easily [55]. Furthermore, UV-induced graft polymerizations became much easier when MAH was used as a comonomer together with VAC, compared with the homopolymerizations of these two monomers alone [125–129]. For example, MAH and VAC binary monomers could be grafted onto substrates with two different methods: (1) MAH, VAC and the photoinitiator were first dissolved in a solvent, and then the solution was coated on the substrate and subjected to UV irradiation and (2) BP was first coated to the substrate and subjected to UV irradiation and thereafter, the irradiated setup was immersed in monomer solution to conduct a thermally grafting polymerization. It was found that the ratio of two monomers and the total monomer concentration had large influence on the graft polymerization. The graft copolymerization of the monomer pairs can be completed at a much higher speed, in comparison with the corresponding graft homopolymerization of the two individual monomers. CT complexes formed between MAH and VAC played crucial roles in the grafting copolymerization and the relevant kinetics were investigated systemically [128,129]. The results showed that the content of MAH in the grafted chains increased with increasing concentration of MAH in the monomer feed ratio; this phenomenon could be amplified by either increasing the total monomer concentration of MAH and VAC or the reaction temperature. In addition, the maximum graft copolymerization rate did not appear in the system with [VAC]/[MAH] = 1:1, but in the system with a bit more VAC. These findings should be assigned to the unique self-initiating performance of MAH, as discussed in Section 2.3. More importantly, both free monomer molecules and the CT complexes formed by MAH and VAC took part in the graft polymerization. The mechanism of grafting copolymerization of MAH/VAC system is presented in detail in Ref. [126].

Other CT complexes, MAH/*n*-butyl vinyl ether [130–132], MAH/styrene [133,134], and MAH/*N*-vinylpyrrolidone [135] were also examined for the surface photografting polymerization. Garnett et al. investigated the photografting system containing MAH and triethylene glycol divinyl ether (DVE-3), which can form CT complex [136]. They found that the grafting degree in the absence of solvent was very high; addition of solvent lowered the grafting yield progressively; some solvents may have taken part in grafting because they could form a CT complex with MAH. The related mechanism is presented in Scheme 13.

Ng et al. [137] investigated the photografting polymerizations with styrene as an electron donor and vinyl monomers as electron acceptor. Photografting polymerization smoothly took place without photoinitiator, and different vinyl monomers performed differently. The crucial conclusion made in this research was that styrene is able to form CT complex with certain monomers, which can initiate grafting polymerization under UV irradiation without any photoinitiator. These results may be helpful for solving the problems existing in photografting and photocuring systems, that is, how to exclude the residual photoinitiators in these systems after UV irradiation. Undoubtedly, developing novel photografting and photocuring systems free of photoinitiator offers great potential for solving these problems. Furthermore, since the combination of monomers with different properties can be selected, grafting with CT complex systems seems to be an emerging field for polymer surface design and modification.

2.5. Combinatorial techniques in grafting

Most surface photografting polymerizations are carried out through the "one-step" or simultaneous method, i.e., grafting proceeds in the presence of monomer and photoinitiator under UV irradiation [138,139], or by the "two-step" method here designated as combinatorial techniques, i.e., first introducing dormant groups on substrates under UV light, and then grafting polymerization is initiated by heating or irradiation [41,104,105,139]. In fact, pretreatment of the substrate with UV irradiation, O_3, or plasma can yield peroxide groups in substrate, which are capable of initiating the subsequent surface grafting/photografting polymerizations [140–143].

Martínez et al. [143] grafted MAH onto PE substrate by first irradiation of the substrate with UV light to produce hydroperoxide groups on the substrate (preirradiation step) and then grafting MAH by heating the peroxide groups to produce radicals (grafting step). The detailed processes are illustrated in Scheme 14.

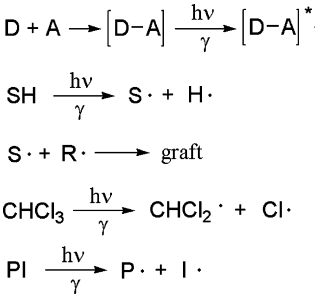

Scheme 13. Mechanism of CT grafting process proposed by JL Garnett et al. (Ref. [136]). D, donor; A, acceptor; SH, substrate; PI, photoinitiator.

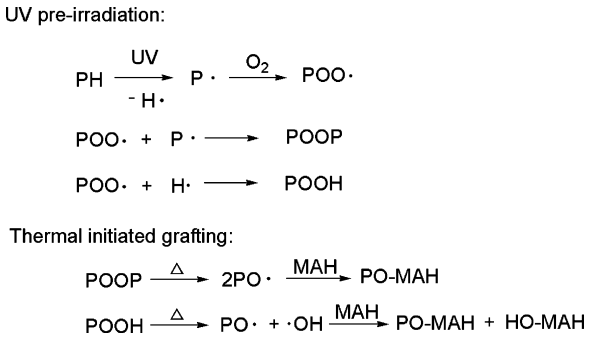

Scheme 14. Peroxidation mechanism of polymers and the grafting reaction (Ref. [143]).

Khan et al. achieved the graft polymerization of methacrylic acid and acrylic acid onto jute fiber and methyl methacrylate onto lignocellulose fiber [144] by UV preirradiation method in the presence of photoinitiator 1-hydroxycyclohexyl-phenylketone [145]. Adopting the same strategy, Khan et al. investigated the physical and mechanical properties of jute yarn grafted with 1,6-hexanediol diacrylate [146]. Lacoste and coworkers [147] used anthracene as a sensitizer for the production of singlet oxygen under 365 nm irradiation to functionalize substrates (terpolymer ethylene/propylene/5-ethylidene-2-norbornene: EPDM) with –OOH groups (EPDM–OOH). Grafting on the prepared EPDM–OOH was performed by UV irradiation in the presence of monomers in three different ways. In the first case, the EPDM–OOH film was irradiated in the vapor of monomer in the absence of O_2; the second one involved dipping the EPDM–OOH film in aqueous solution of monomer at 100 °C for different times; in the third one, EPDM–OOH film was UV irradiated in methanol solution of monomer. With a similar strategy, Guan et al. [148] functionalized the surface of polyurethane membrane by a combination of photooxidation and UV irradiation grafting method.

Pretreatment by plasma technology is also able to introduce peroxide groups onto organic surfaces, which form free radicals under subsequent UV irradiation. Initiated by these radicals, surface graft polymerization can be accomplished successfully [149–158]. Although plasma can be used as a precursor to other surface modification techniques, plasma generation generally requires a vacuum to empty the chamber of latent gases, and this will elicit complications for continuous operation in a large scale industrial situation.

2.6. Grafting in liquid, vapor, bulk and the derivative methods

Surface photografting polymerization can be conducted in liquid phase [159], and the used solvents could have large influence on the grafting effects. Wang and Brown [160] discovered that for (meth)acrylic acid, aliphatic solvents, such as chloroform, cyclohexane are favorable for the graft polymerization; polar solvents such as ethanol does not benefit the graft polymerization; for aromatic solvent, such as toluene, rather acts as a screening agent for UV light and thus is not a useful solvent. Different solvents also result in different surface topography of the grafted substrate [160]. It was also reported that solvents could directly affect the wettability of the grafted substrates. For PE grafted with poly(methacrylic acid), the wettability of the PE-*g*-PMAA prepared in dichloromethane, petroleum ether, cyclohexane, and chloroform, exhibited only a small decrease in the contact angle of water. If 30% acetone/water is used as the solvent, the water absorbance of the grafted PE film was about twice as that of the PE film grafted in the other solvents. It was assumed that for the solvents other than acetone/water, the grafted layer was partially buried below the surface layer due to the low affinity of the grafted chains to the solvent [161].

Kubota and coworkers [162–166] investigated the effects of mixed solvent consisting of water and organic solvent by scanning electron microscopy (SEM) and attenuated total reflection infrared (ATR-IR) spectroscopy, and found that the distribution of the grafted chains in the substrate was largely influenced by the type of the organic solvent chosen. The monomer solution could be introduced to the substrate using either “dip” or “immersion” techniques, and then the setup was UV irradiated. Both the two methods were effective for realizing the graft polymerization [167]. The continuous method was reported to be conveniently put into practical applications [168].

Photografting in the vapor phase is another method frequently used to conduct surface graft polymerization [169,170]. It is solvent-free and highly efficient [171–173], causing less homopolymerization and easy purification of the grafted substrates [173]. Regarding grafting polymerization in vapor phase, Gleason and coworkers [174] explored a new method, i.e., grafting chemical vapor deposition (gCVD), to achieve solvent-free surface photoinitiated polymerization. At low temperatures, gCVD was successfully used to coat Nylon fabric and poly(methyl methacrylate) (PMMA) thin films with antimicrobial polymers of (dimethylamino)methyl styrene (DMAMS) and (diethylamino)ethyl acrylate (DEAEA), respectively. This novel process, as an all-dry technique, is applicable to the grafting polymerization of monomers that lack solubility in desirable solvents. The low temperature merit also makes it an ideal method for grafting on fragile polymeric substrates. Together with the other CVD techniques such as hot-filament CVD [175] and initiated CVD [176], gCVD is expected to find wide applications due to their environment-friendliness.

Yang and Rånby [38,39] made extensive efforts to investigate the surface photografting polymerization with bulk surface photografting process, which means the photoinitiators were dissolved in monomers without the assistant of any solvent upon UV-induced grafting. In the extended investigations, Deng et al. [177] found that the affinity of the solvent with the substrate, the absorption of UV light by the solvent, and the reactivity and initiating ability of the solvent are the key factors affecting the grafting yield and the distribution of the grafted chains in the substrate. In this research [177], a sandwiched setup consisting of two covering substrates and an inner reaction solution was employed, as presented in Fig. 1. BP-containing PE films were prepared in advance and the monomer VAC was

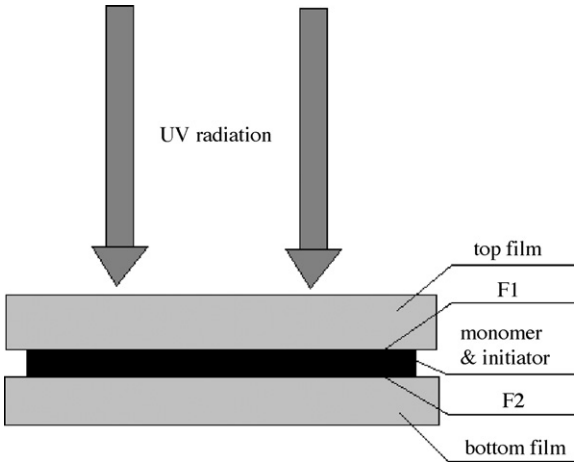

Fig. 1. Cross section of grafting polymerization (Ref. [177]).

placed between the two films. The effects of solvent on grafting polymerization of VAC are schematically shown in Fig. 2.

When *n*-hexane and chloroform is used as the solvent of BP, they permeate into PE films rapidly carrying BP molecules. When VAC is added, it cannot penetrate PE films as deeply as BP, consequently leading to weak contact of VAC and BP (Fig. 2a). For acetone, methanol, THF, dioxane, ethyl acetate and benzene, their affinity with PE film is nearly the same as that of VAC, so VAC molecules are able to contact with BP molecules effectively and efficiently, resulting in smooth grafting polymerization of VAC in the grafting step (Fig. 2b). For the third class of solvent

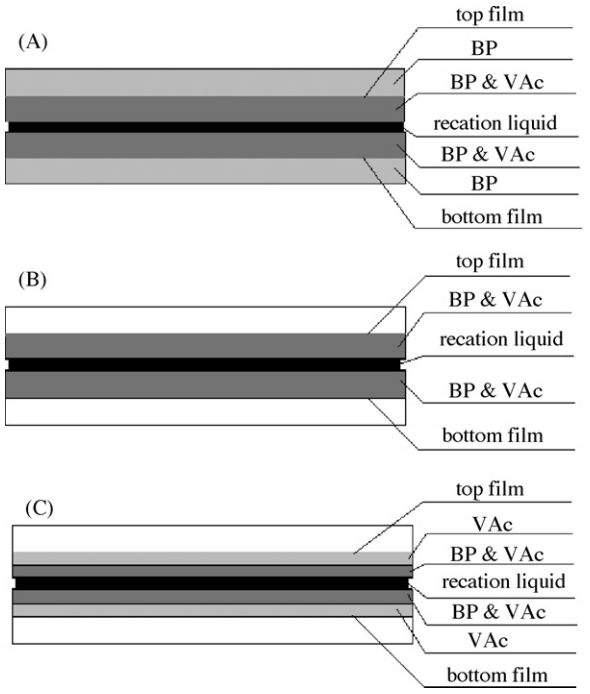

Fig. 2. Effects of affinity of the solvents with PE films on grafting polymerization (Ref. [177]).

including DMF, its affinity with PE film is the lowest. When deposited between the two films, DMF remains principal on the inner surfaces of the films (F1 and F2 in Fig. 1). When VAC was deposited, VAC carries BP along to the deeper layers of the film, improving contact (Fig. 2c). Thus graft polymerization of VAC proceeds more smoothly than that in the system using the first class solvents but less smoothly than those using the second class of solvents introduced above. These results are useful for selecting suitable solvents for surface photografting polymerizations.

With a method derived from the sandwiched setup, Deng et al. studied the graft polymerization of MAH onto LDPE film in a melt phase [178]. In this research, MAH solution was coated onto the substrate LDPE film; thereafter the solvent was evaporated and the PE film containing a layer of dry MAH was subjected to UV irradiation at a temperature above the melting point of MAH (52 °C). Using this method, MAH was grafted on PE films readily, even though MAH generally undergoes free radical polymerization with much difficulty.

2.7. Substrates

Conventionally, surface photografting polymerizations were achieved using polymeric materials as the substrate, predominantly synthetic PP and PE films. However, it has been evidently proved that surface modification is also feasible for the substrates other than PP and PE films. The substrates can be synthetic polymers like polypyrrole [179], poly(3-hydroxybutyrate-*co*-3-hydroxyvalerate) (PHBV) [180], substrates of rubber film or sheet [181–184], PE [185] and PET fibers [186], or natural polymers including jute yarn [187,188] and jute fiber [189], cellulose fiber [190–193] and sisal fiber [194]. Inorganic substrates can also be employed, such as silica [195] and gold electrodes coated with an alkanethiol monolayer [196]. All these investigations demonstrated that surface photografting polymerization is widely applicable and offers modified surface matching the needs of the end uses.

Deng and Yang et al. [39,40,53] compared the grafting performances of different polymeric substrates. These substrates were reported to show different behaviors,

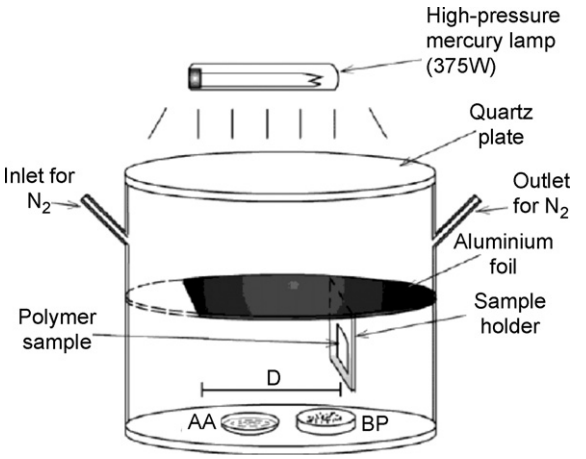

Fig. 3. The apparatus for photografting polymerization (Ref. [198]).

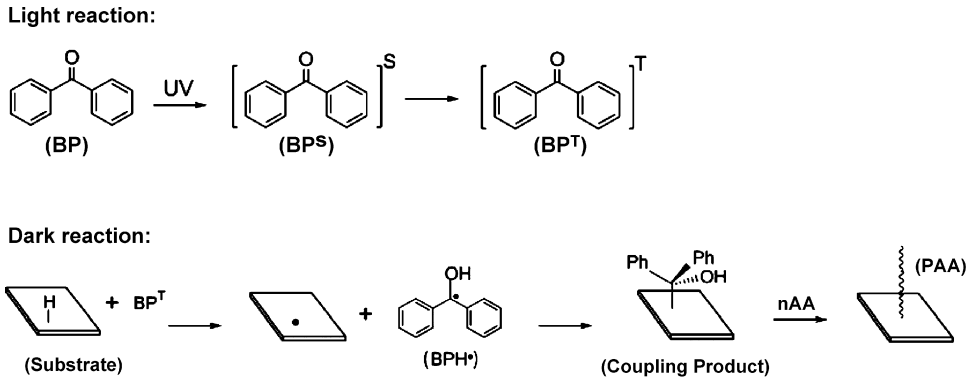

Scheme 15. Mechanism of photografting reaction (Ref. [198]).

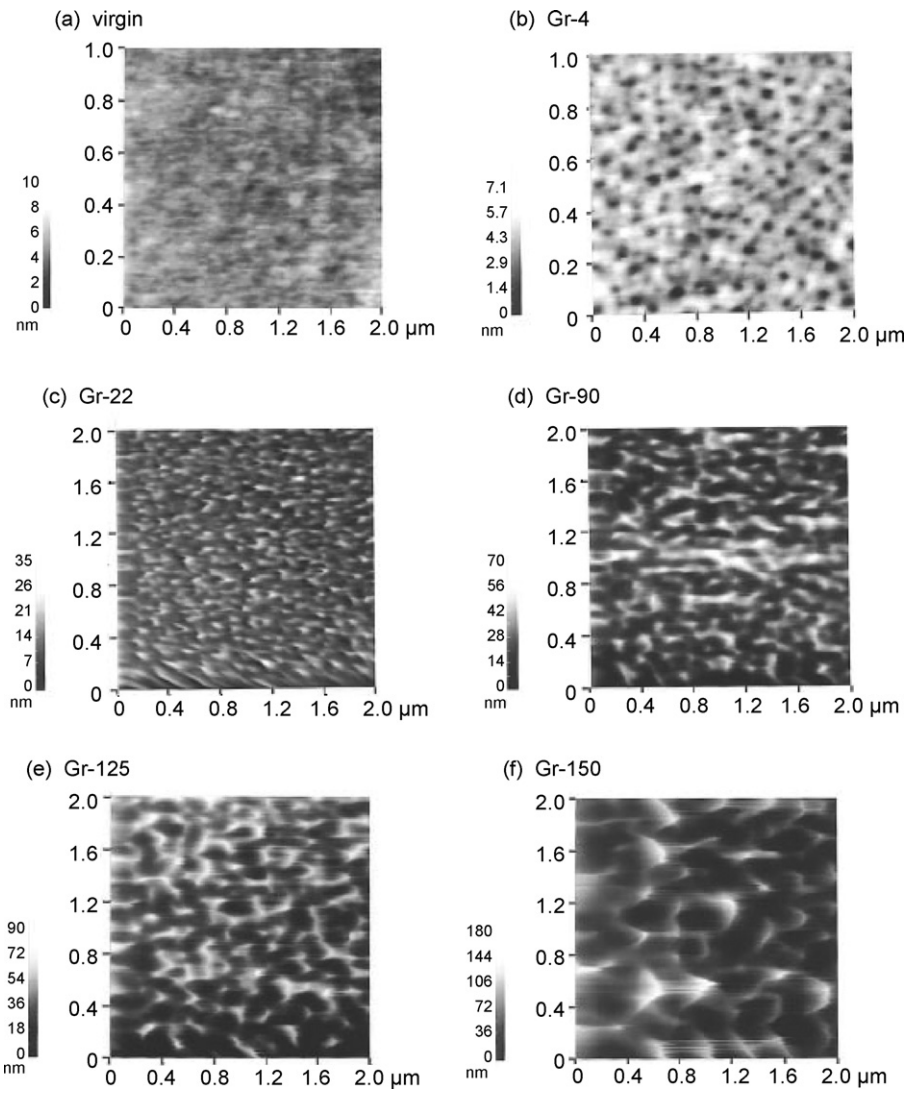

Fig. 4. AFM images of film surfaces grafted with different lengths of polyDMAEMA chains (5 nN load, 2 μm/s scanning speed, and 2 μm × 2 μm scan area except for a and b (1 μm × 1 μm). Brighter areas indicate higher levels (Ref. [201]).

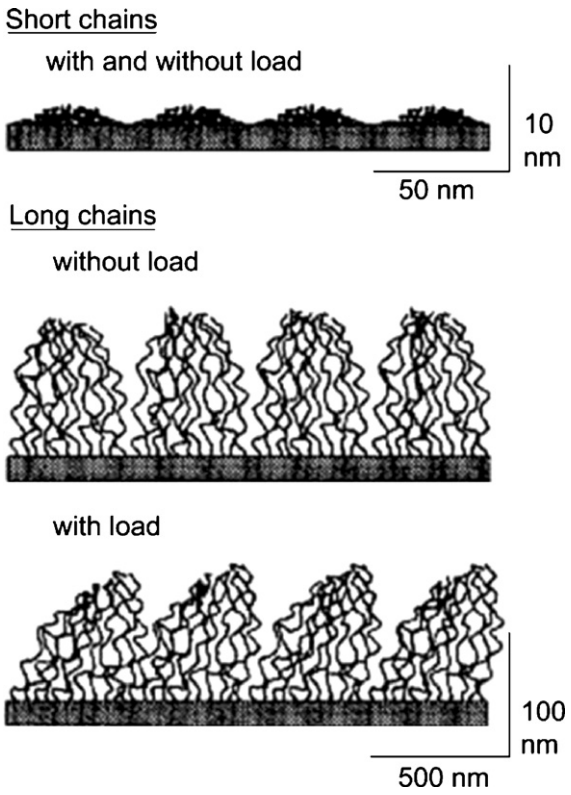

Fig. 5. Topographical models for short and long graft chains underwater (Ref. [201]).

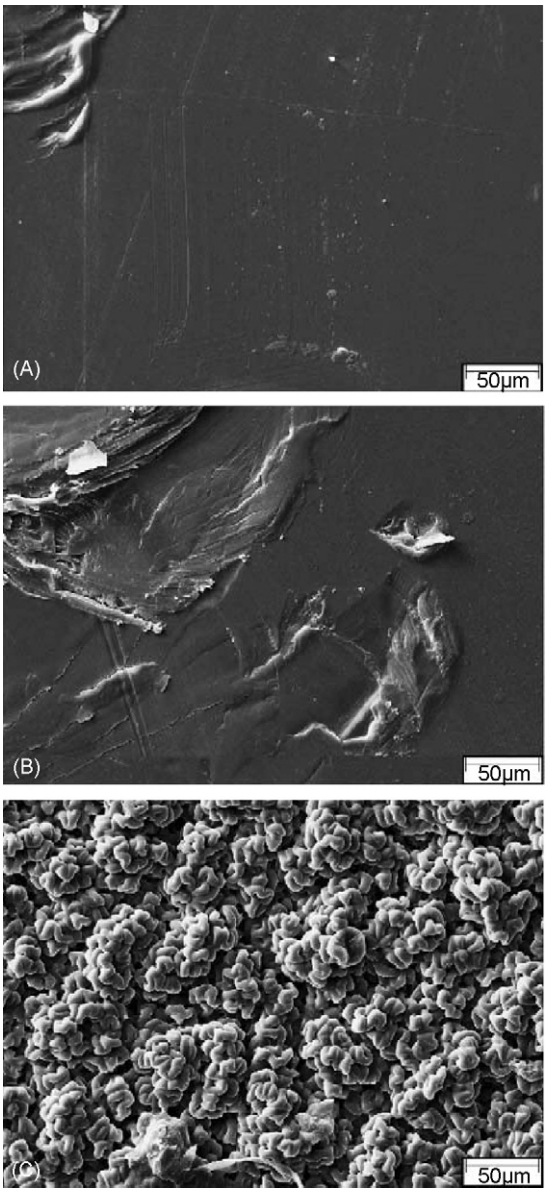

Fig. 6. SEM images of PET surfaces: (a) virgin, (b) oxidized by exposition to Hg lamp and (c) grafted through method 1 (magnification: 1000×) (Ref. [202]).

which were considered to result from the different affinity between the monomer and the substrate, the different reactivity of hydrogens in the substrate, and the UV transparency of the films [53]. As far as the reactivity of hydrogens is concerned, the influence from degree of crystallinity and regularity should be mentioned. For a substrate with high crystallinity, it is relatively difficult for the hydrogens to be abstracted, which is not favorable for the subsequent graft polymerization. This is the reason why less monomer was grafted on HDPE than on LDPE film under the same conditions [53]. Even for the same substrate, e.g., oriented PP prepared by drawing, the draw ratio exerted large influence on the grafting [197] (oriented PP was prepared by drawing; to determine the draw ratio, two ink marks were made on the PP samples before drawing, and then measure the increase in the separation between the two marks after drawing. For more details, see Ref. [197]).

Surface modification via photografting polymerization has been demonstrated to be extensively effective; yet for those substrates with complex structures or irregular forms, the commonly used UV irradiation method is not efficient enough because some parts of the substrate were blocked from UV light. Recently, Zhang et al. [198,199] reported a method purposely designed for the surface modification of substrates with complex and irregular forms, and the relevant principle is as follows. The photochemical reaction is separated into three events: absorbing UV light in one place, then transporting light energy to another place, and reacting there; namely, the conventional photochemical reaction is separated by space and time. The above mechanism is schematically illustrated in Scheme 15, and the experimental setup is shown in Fig. 3. In a typical experiment (Scheme 13, Fig. 3), the vapor containing initiator BP and monomer AA was exposed to UV radiation in a place where BP was excited, and then the excited BP diffused to another place that could not be irradiated by UV light directly, and induced grafting on the substrate there (dark reaction in Scheme 13). This strategy opened a new way to realize surface modification of those substrates and devices with irregular forms or complex structures such as

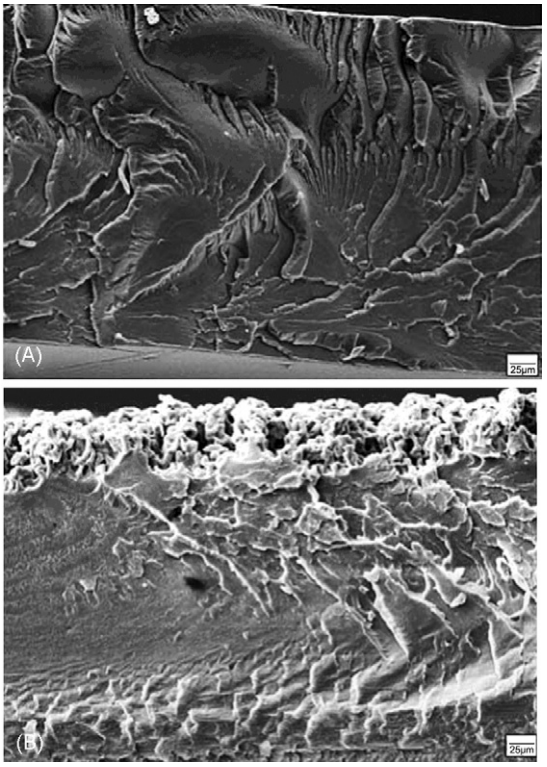

Fig. 7. SEM images of fractured PET films: (a) virgin and (b) grafted through method 1 on previously oxidized films by exposition to Hg lamp (magnification: 500×) (Ref. [202]).

the inner surfaces of polymeric containers and the porous materials.

3. Topography of the grafted surface

3.1. Granular structures

The grafting polymerization can be characterized with gravimetric analysis and ATR-IR [57,77,137] and X-ray photoelectron spectroscopy [84,85,87]. Usually water contact angle is measured to examine the surface hydrophilicity of the grafted substrates [85,91,134,174]. Attenuated total reflection infrared (ATR-IR) spectroscopy is used to explore the depth and the distribution of the grafted polymer chains in the substrate [54,56,73,165]. X-ray diffraction is another effective characterization method [72]. To explore the topography of the grafted substrates, the grafted surfaces can be imaged with atomic force microscopy (AFM) [84,92,161] and scanning electron microscopy (SEM) [92,164,165]. In a study by Wang and Brown [200], glycidyl methacrylate (GMA) was photografted onto HDPE film and the microstructure of the grafted chains was investigated using AFM. The surface of the grafted films exhibited granular structure, and the height of the granules increased linearly with their diameters. Moreover, each granule was assumed to be a single graft chain bearing a highly branched microstructure. The solvents greatly affected the density of the grafted chains and their degree of branching. Using AFM, Uchida and Ikada [201] examined the topography

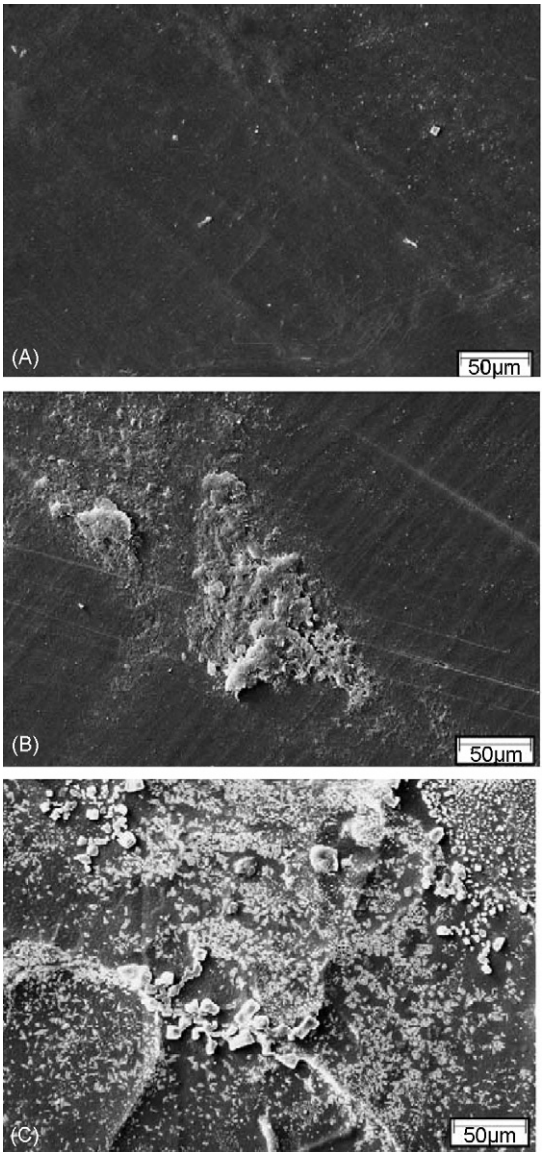

Fig. 8. SEM images of PS surfaces: (a) virgin, (b) oxidized by exposition to aqueous sodium persulfate, at 70 °C, and (c) grafted through method 1 (magnification: 1000×) (Ref. [202]).

of water-soluble polymer chains photografted onto PET film (Fig. 4). The graft polymer chains with a certain length stretched out in water to form a brush-like structure and the authors [201] also presented models for it (Fig. 5).

Muniz and coworkers [202] photografted poly(*N*-isopropylacrylamide) (PNIPAAm) onto PET and PS surfaces. According to their observations with SEM and AFM, a rising of roughness was observed for the grafted surfaces, and the grafted surfaces showed a hydrophobic and hydrophilic transformation while changing the temperature (Figs. 6–10). With AFM and optical microscopy (OM) techniques, Strumia et al. [203] investigated the topography of the modified films and found that the original featureless

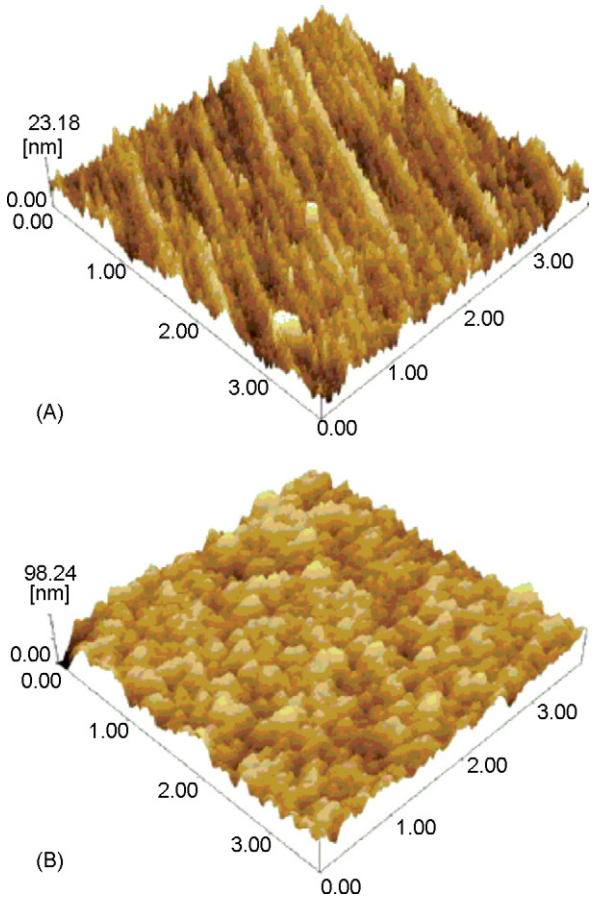

Fig. 9. AFM images of PET surfaces: (a) oxidized by exposition to Hg lamp and (b) grafted through method 1 (Ref. [202]).

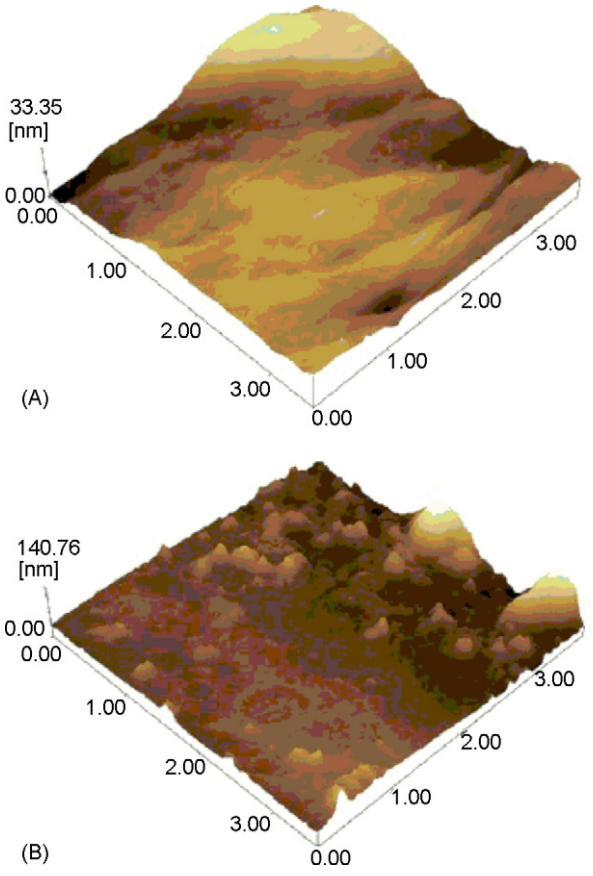

Fig. 10. AFM images of PS surfaces: (a) oxidized by exposition to aqueous sodium persulfate, at 70 °C and (b) grafted through method 1 (Ref. [202]).

topography of the raw film was substituted with growing aggregates after grafting. Moreover, the longer the treatment was, the higher the surface roughness rose.

Moon and coworkers [204] investigated the morphology of the membranes photografted with poly(acrylic acid) with SEM. The modified membranes prepared with different UV-irradiation times showed a denser structure and the pores in the membrane were gradually filled with the grafted chains of PAA. The pores could hardly be observed in the dense structure of the grafted membrane for the sample treated for 20 min. These phenomena can be clearly viewed in Fig. 11.

Wang and Yang [205] opened up a new strategy to achieve surface photografting polymerization and three-dimensional construction on the surface, i.e., firstly coated methyl methacrylate/1,2-divinylbenzene (MMA/DVB) microemulsion on casting polypropylene (CPP) films and then conducted photografting with BP as photoinitiator. AFM images demonstrated that the grafted layer was built up by nanoparticles ca. 30–50 nm in diameter. These particles were linked together and further covalently tethered onto the CPP surface. The possible mechanism for the formation of the above topography was schematically illustrated in Scheme 16.

With the same strategy introduced above, monolayer of nanoparticles on a substrate was produced facilely [206], as presented in Figs. 12 and 13. When *N*-vinyl pyrrolidone/*N*,*N*′-methylene bisacrylamide (NVP/MBAA) inverse microemulsion was used instead of the MMA/DVB emulsion mentioned above, superhydrophilic surfaces were attained [207]. Construction of discrete large spherical functional particles was achieved on biaxially oriented polypropylene (BOPP) film surface [208] (Fig. 14) and the assumed mechanism is shown in Scheme 17. Moreover, supramolecular polymer particles can also be prepared in a similar way but in the absence of the substrate [209]. These particles with or without substrates are expected to find a number of potential applications in a wide range of industries. Sui et al. [210] reported a surface-initiated ring-opening polymerization of ε-caprolactone from the surface of PP film containing an initiator layer composed of –OSn(Oct) groups, based on a technique developed by Yang et al. [211,212]. SEM images revealed that the graft polymer chains grew into regular spheroidal particles, which could be changed into other different morphologies by treatment with different solvents. Based on these findings, novel functional materials, particularly environment-responsive materials can be developed.

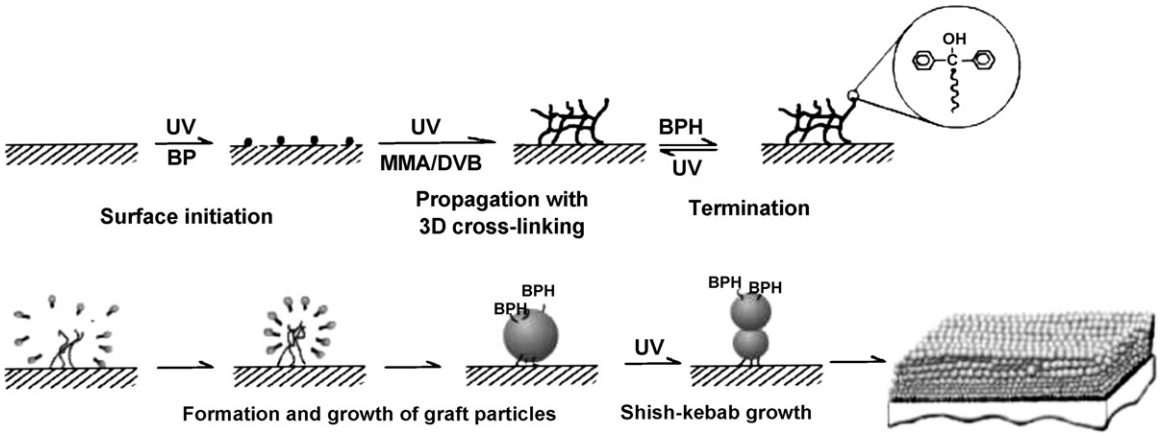

Scheme 16. Chemical formation of the graft chains and the growing mechanism of the graft particles (Ref. [205]).

3.2. Crosslinked structures

With multifunctional monomers, crosslinked graft layer on polymer substrates can be realized. In the work of Wang et al. [213], trimethylopropane triacrylate (TMPTA) was used as the monomer, and its surface photografting polymerization on LDPE film was conducted in THF/water mixed solvent. Via SEM and AFM techniques, the grafted surface was found to be planar when the photografting was carried out in pure THF. When some water was added in the solution, the formation of "craters" on the surface was observed, which was explained in terms of the phase separation process accompanying the graft polymerization of the monomer TMPTA. The corresponding SEM images are shown in Fig. 15 and the plausible mechanism is presented in Scheme 18.

In the report of Kubota and Koyama [214], multifunctional monomers were added in the graft polymerization of methacrylic acid. These monomers facilitated the grafting, with different magnitudes in the enhancement by different multifunctional monomers. With a two-step method consisting of photosensitizer and/or plasma pretreatment and thereafter photopolymerization, an interpenetrating polymer network coating was created on a PET substrate, as reported by Healy and coworkers [215].

In the presence of BP and an alkyl thiol self-assembled-monolayer (SAM) coated on the surface of gold, photografting polymerization of the monomer *N*,*N*-methylene bisacrylamide (MBAA), simultaneous as a crosslinking agent, resulted in a highly crosslinked polymer layer. The topography of the grafted surface was investigated by scanning force microscopy (SFM) [216]. The results [216] suggested that this approach, i.e., the photoinitiated graft copolymerization onto SAM-modified gold with adsorbed BP, is very straightforward and promising for the synthesis of tailored functional grafted polymer layers on sensors and other surfaces.

3.3. Well-defined structures

Most of the branched, especially superbranched polymers, exhibit unique properties such as low viscosity, good solubility, multi-functionality, etc. This type of polymers has attracted much attention in the past decade [217,218]. Matsuda and coworkers [219,220] prepared branched graft polymer chains using iniferter-based quasi-living radical photografting polymerization; Fig. 16 shows the schematic representation of the stem and branch designs. By the same "iniferter" method [221], they prepared a surface containing five different water-soluble polymer regions with micron order precision, and also prepared three different gradient surfaces with unidirectionally changing thicknesses of a water-soluble grafting polymer layer. Vasilets et al. [222] pre-irradiated Teflon FEP film with UV light to generate peroxide groups on the substrate surface and then performed grafting polymerization of 4-(6-acryloyloxyhexyloxy)benzoic acid at 70–100 °C. The thus prepared graft polymers could form a liquid crystal polymer brush.

Zhong et al. [223] reported on a novel method for preparing electrically conductive polyprolylene-*graft*-polyacrylic acid/polyaniline (PP-*g*-PAA/PANI) composite films. Firstly, 1,4-phenylenediamine (PDA) was introduced on the surface of PP-*g*-PAA film, which was prepared beforehand by surface photografting. Then, chemical oxidative polymerization of aniline was carried out on PP-*g*-PAA/PDA film to prepare the electrically conductive composite films. The process presenting the above strategy is shown in Scheme 19.

Each step of the processes was monitored AFM, as presented in Fig. 17. Compared with the relative smooth surface of the pure PP film (Fig. 17a and b), spheres with an average diameter of ca. 45 nm were observed on the PP-*g*-PAA film surface (Fig. 17c and d). After grafting polymerization of aniline, the film surface was obviously covered with PANI particles with diameters of about 150 nm. Moreover, the roughness of the PP-*g*-PAA/PANI film surface was relatively higher than that of the PP-*g*-PAA film surface, probably resulting from the PANI chains grown on the grafted PAA particles. The conductivity was about 0.21 S/cm at room temperature for the composite film with thickness about 0.4 μm and grafting percentage about 1.5 wt.%. This achievement provides a new way to prepare conductive materials.

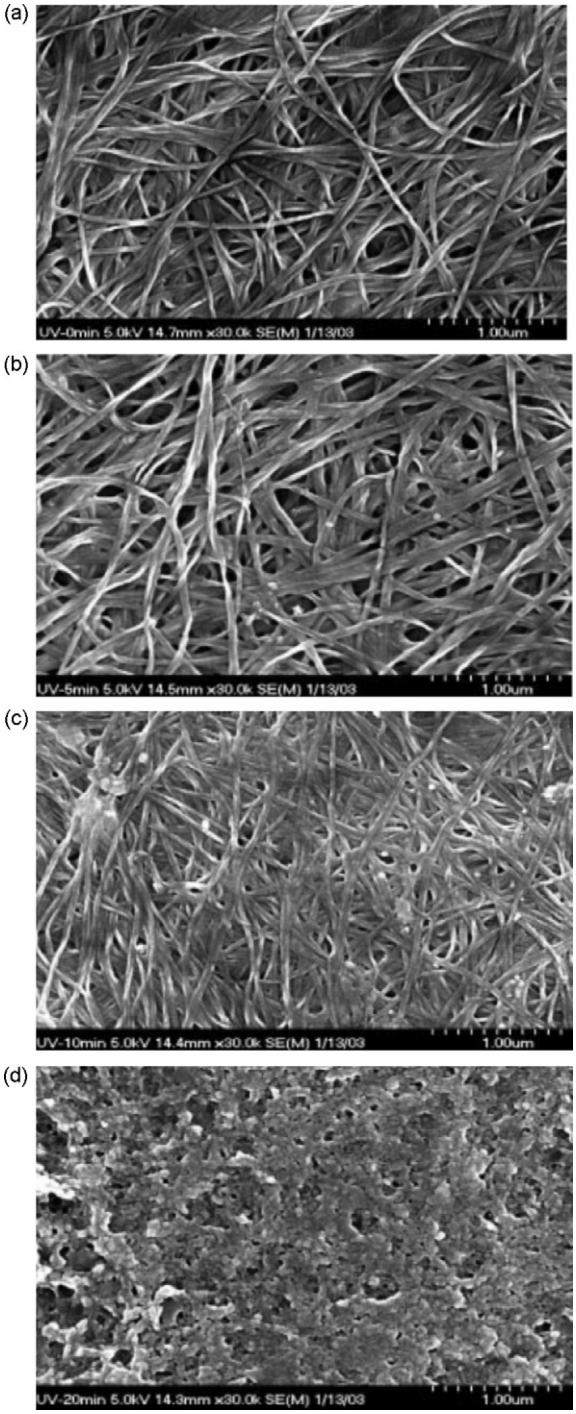

Fig. 11. Scanning electron micrographs of the surface of bacterial cellulose and AAc-modified BC membrane (a) bacterial cellulose, (b) AAc-modified BC (UV 5 min), (c) AAc-modified BC (UV 10 min), and (d) AAc-modified BC (UV 20 min) (Ref. [204]).

With the above strategy, Zhong et al. [224] prepared highly hydrophilic polyaniline nanowires and sub-micro/nanostructured dendrites on PP film surfaces. Field-emission scanning electron microscopy (FE-SEM) was employed to observe the surface morphology of the grafted films. The micrographs for PANI nanowires, PANI sub-micro/nanostructured dendrites immobilized on PP film surface are shown in Figs. 18 and 19. The grafting percentage of PAA has large influence on the morphology of the prepared PANI, and the resulting PP films exhibited different water contact angles. Based on this work, the same group also reported a novel method on synthesis of super-hydrophilic polypyrrole nanowire in high yield [225]. These results indicated that the approach developed in this work is potentially important for preparing highly hydrophilic PANI nanowires and sub-micro/nanostructured dendrites chemically implemented on various substrates, which may be useful for developing disposable chemical sensors or all-polymer field-effect transistors.

4. Performances and applications of the grafted surface

4.1. Wettability

For hydrophobic polymer substrates, one of the major aims of surface photografting polymerization is to improve the surface hydrophilicity of the substrate. For example, Gao and coworkers [226] and Hirt and coworkers [227] employed methacrylic acid and acrylic acid as the monomer, respectively, to perform surface photografting polymerization on poly(L-lactide) (PLA) substrate, targeting surface hydrophilicity modification. It should be noted that, in most cases, it is certainly expected to improve the surface hydrophilicity (e.g., by the introduction of hydroxyl group, by which to suppress the static electricity of the substrate [68]), but in some other special cases, surface hydrophobic property should be increased or/and moisture sorption should be reduced, as shown by the work of Kang and coworkers [228]. This can be achieved by photografting hydrophobic monomers rather than hydrophilic monomers onto the substrates [229].

4.2. Adhesion

Modification of the surface by introducing polar groups such as peroxide functionalities has been a main route to improve adhesion of polyolefins [230,231], and the synthesis of block copolymers consisting of a polyolefin-like part and a polar part is another alternative approach to improve the adhesion of polyolefins [232]. The idea of these two methods is to utilize the interaction between the polar groups and the target material to improve adhesion. Based on the same idea the surface adhesion of substrates can be improved effectively by surface photografting polymerization since the surface graft chains could be designed to have considerable polarity [233]. Kang et al. [234,235], Lecamp and coworkers [236], Lei et al. [237], Zhang et al. [238], and Castell et al. [239] made such attempts by photografting polymerization of acrylic acid and acrylates onto substrates, and found the surface adhesion and surface energy of the substrate were significantly improved. GMA [240] and acrylates [241] were also used as monomers to conduct photografting polymerization onto polyolefins to improve the autohesive properties of polyolefins.

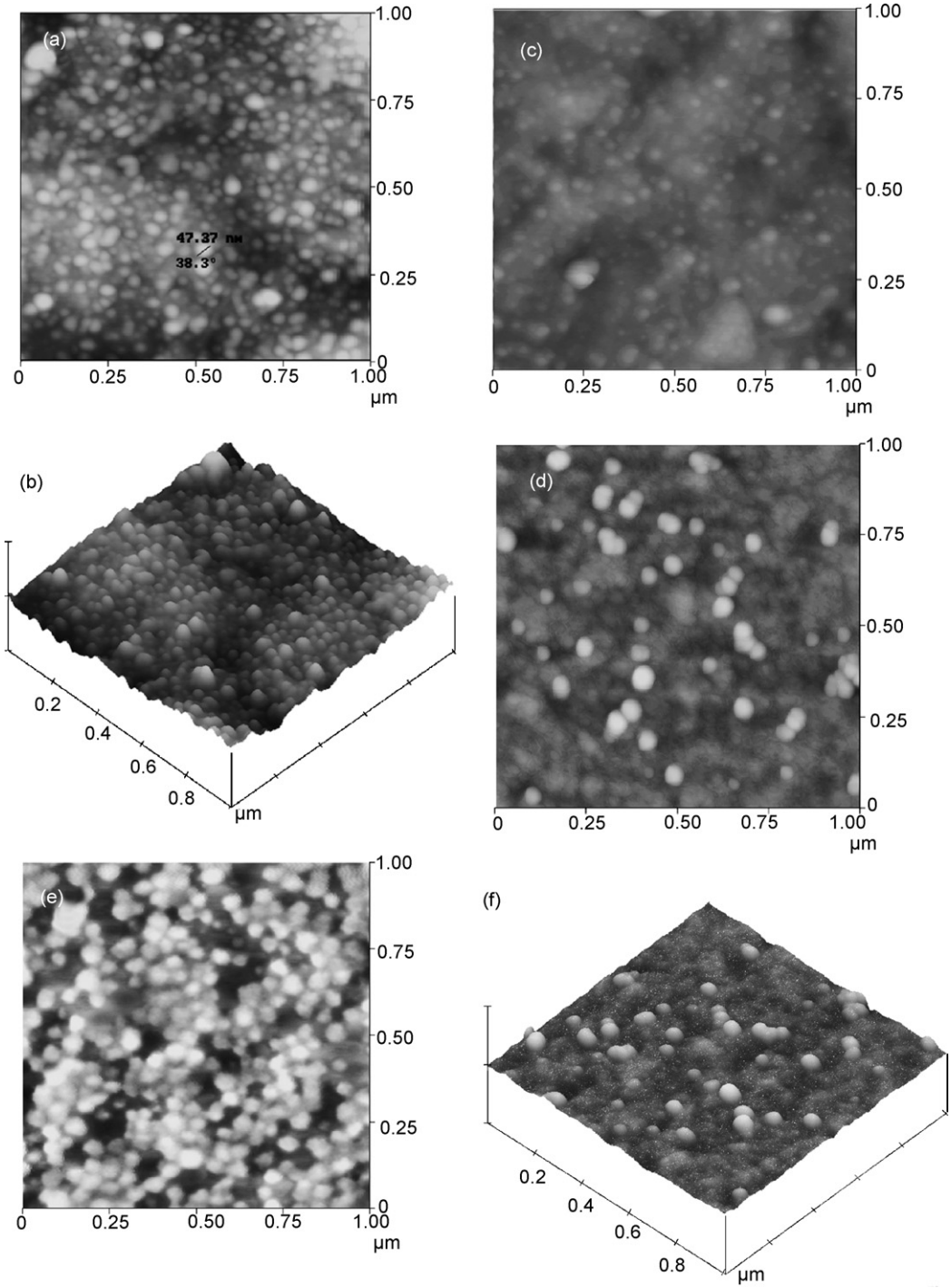

Fig. 12. AFM images of film topography after surface photografting microemulsion by the one-step method (MMA concentration 6 wt.% in a and b) and two-step method (MMA concentration 20 wt.% in c, d, and f; 30 wt.% in e): (a) height image of the film after 2 min UV irradiation; GY 0.679 wt.%; (b) three-dimensional (3D) effect of the height image in a; (c) height image of the film after 2 min UV irradiation; GY 0.070 wt.%; (d) height image of the film after 4 min UV irradiation; GY 0.095 wt.%; (e) height image of the film after 6 min UV irradiation; GY 0.188 wt.%; (f) 3D effect of the height image d (Ref. [206]).

4.3. Environment-response

Temperature-sensitive surfaces could be obtained when *N*-isopropylacrylamide (NIPAAm) was photografted onto a substrate. Li et al. [242] prepared temperature-sensitive surfaces by photografting polymerization of NIPAAm on PP films via two different methods: pre-dipping photografting (the PP films were first dipped into an acetone solution

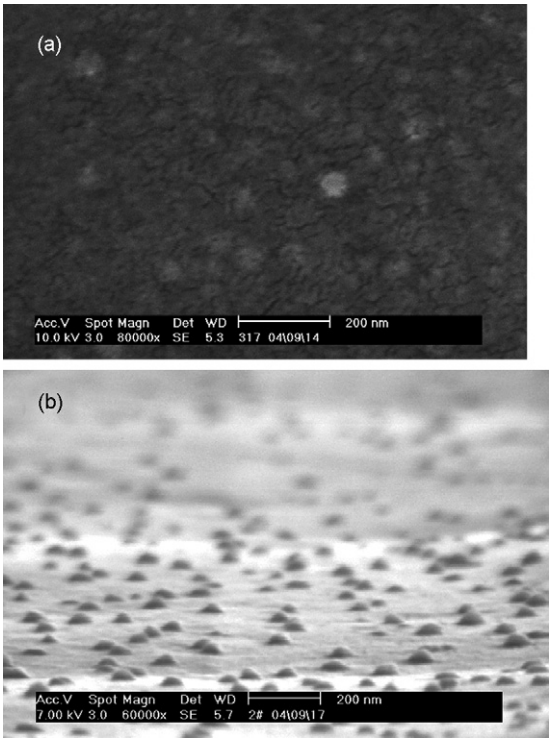

Fig. 13. ESEM images of surfaces topography in the two-step initiating surface photografting. MMA concentration 20 wt.%: (a) planform of the film corresponding to Fig. 2d and f; (b) side view of the film corresponding to Fig. 2d and f (Ref [206]).

of BP for a period, dried, and then put into an aqueous solution of NIPAAm and subjected to photoirradiation [242]) and dormant radical photografting (grafting polymerization of AA onto PP films was first performed and then the prepared PP films were subjected to grafting NIPAAm [242]). Nevertheless, the water absorbance of the grafted PP films prepared by the two methods was similar, and both of the films exhibited considerable sensitivity to temperature change. Using a silicone wafer as the substrate, Liang et al. [243] prepared temperature-sensitive surfaces by UV photografting reaction of NIPAAm in the presence of (*N*,*N*′-diethylamino)dithiocarbamoylpropyl (trimethoxy)silane as photosensitizer. A thin graft layer consisting of a single terminal PNIPAAm chain on the silicone wafer surface was produced. The mobile single PNIPAAm chains made the grafted surface possess a decreased lower critical solution temperature (LCST) and a narrower change range of transition temperature, when compared with the substrate grafted by PNIPAAm gel. In other words, the prepared grafted surface showed a faster response to a change in environmental temperature. Kubota and Shiobara [244] grafted PNIPAAm chains on cellulose by photografting polymerization, and the resulting grafted cellulose exhibited a remarkable temperature-responsive characteristic.

pH-responsive surfaces can be prepared through surface photografting polymerization with appropriate monomers. For example, Sebra et al. [245] reported the construction of pH-sensitive surface via the living photografting technique with poly(ethylene glycol)acrylate succinyl fluorescein as the macromonomer.

4.4. Lamination

Rånby and Yang developed an approach to achieve lamination of polymer films with a bulk surface photografting process [38–40,44,246,247]. In this method, a thin layer of acrylic monomer containing the photoinitiator (in most cases, BP) was sandwiched between two films and the setup was subjected to UV irradiation. Photolamination took place simultaneously accompanying the photografting polymerization of the monomer. Adhesion between the two films is thus markedly improved. By ozone-pretreatment of the substrate and then UV-induced grafting polymerization of monomer, Kang and coworkers [248] also realized photolamination. Yang and Rånby further proposed that the photolamination involves the formation of hyperbranched grafting chains and even a crosslinked network formed through the addition of multifunctional monomers [40].

Wang and Brown [249] investigated the adhesion mechanism of photolamination by photografting polymerization of acrylic acid between two HDPE films or sheets. They found that if methacrylic acid or hydroxyethyl methacrylate was used instead of acrylic acid, no adhesion was observed in HDPE films; when GMA or hydroxyethyl methacrylate was grafted together with acrylic acid, very good adhesion between HDPE sheets was obtained. Based on these results, the authors [249] assumed that a less branched graft chain structure could lead to much more chain entanglement, by which the adhesion between the two substrates could be increased.

4.5. Monolith and microfluidic devices

Monoliths, a form of rigid macroporous materials prepared by in situ polymerization within the confines of a cavity, are now used in a broad range of applications, e.g., immobilized enzyme reactors and fast media for the separation of synthetic or biopolymers, making uses of the large pores which allow liquid flow at low pressure [250,251]. Nevertheless, monoliths with very large pores usually possess limited surface area and thus display a limited number of functional groups on their surfaces. With some monoliths, applications are strictly limited because of the lack of surface functional groups. Therefore, some endeavors have been devoted to introducing functional groups onto the monolith surfaces to improve their surface properties. The research by Fréchet and coworkers [252,253] clearly demonstrated that photografting is applicable for realizing fast, efficient, and versatile surface functionalization of monoliths. The use of photomasks enables the precise control of specific functionalization in selected and predetermined areas of a single monolith. In addition, via photografting technique, two layers of polymer chains can be grafted onto the pore surface of a porous monolith: the interior layer was grafted with ionizable polymer chains, while the covering layer was composed of hydrophobic polymer chains [254]. Even a monolithic column with a lon-

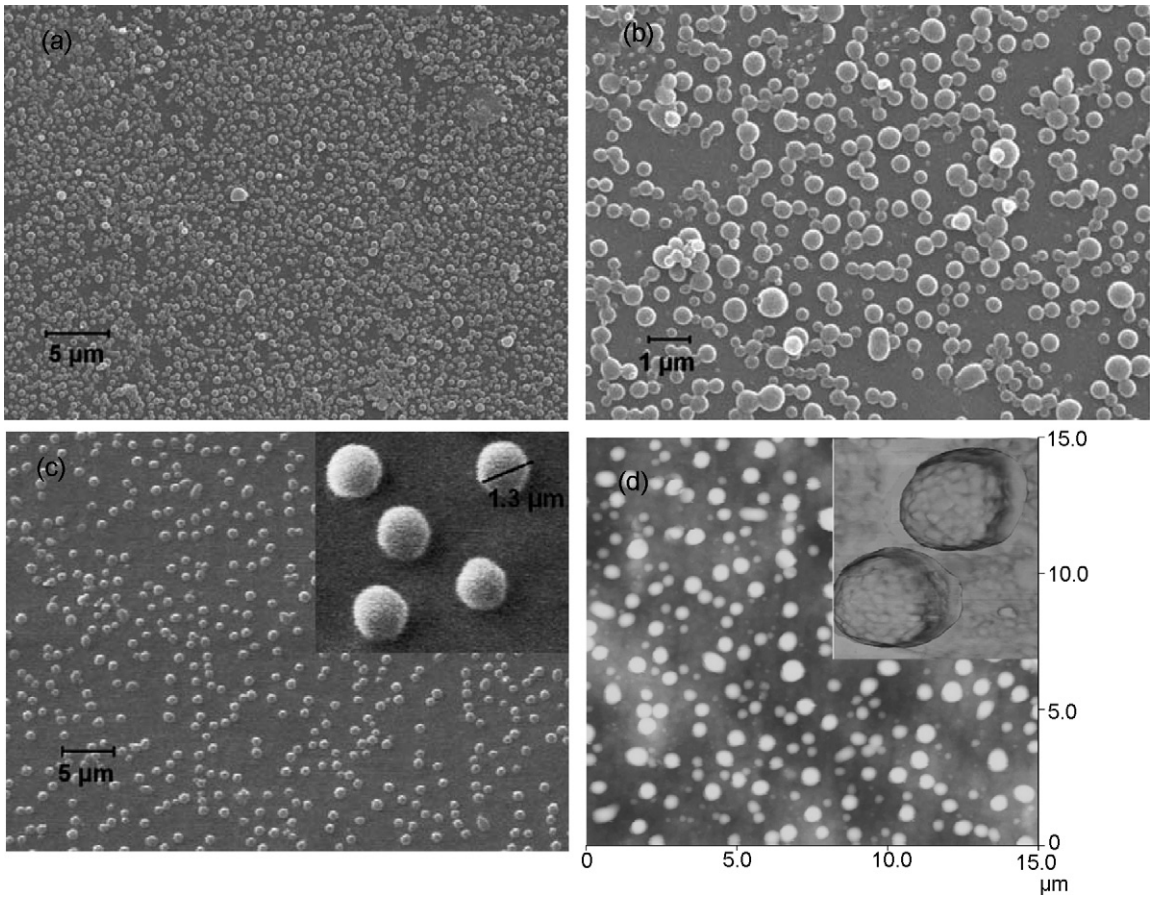

Fig. 14. Micrographs displaying the topography of BOPP films grafted with PMMA/PVP particles. The MMA concentration was 20 wt.%, the BP concentration 5×10^{-2} wt.%, the UV intensity 7 K μW/cm^2, and the irradiation time 10 min at room temperature. (a and b) SEM images where the NVP concentration was 5 wt.% and the particle diameter ~550 nm. (c) SEM image where the NVP concentration was 20 wt.% and the particle diameter ~1.3 μm; the inset displays a side view image. (d) AFM image where the NVP concentration was 5 wt.%; the inset displays the AFM phase image showing how the large particles were made up of nanoparticles (Ref. [208]).

gitudinal gradient of functionalities could be prepared via photografting method, as reported by Pucci et al. [253]. The same group also reported the fabrication of porous polymer monoliths covalently bonded on the walls of channels in plastic microdevices through photografting technique [255].

Microfluidic devices possess various potential applications in chemical sensors and the analysis of biological molecules in clinical diagnoses. Compared with the traditional sensing techniques, microfluidic devices have some obvious advantages, such as more efficient and responsive, partly due to the high surface-to-volume ratio of microfluidic geometries [256–260]. Introduction of surface-reactive sensing species onto microfluidic devices has also attracted large attention, and the commonly used method is surface modification by grafting [261–263]. Although many approaches for surface grafting have been developed, most of them are not applicable to microfluidic devices, since grafting should only be performed in some specified areas of the devices. Accordingly, the grafting initiated by UV light provides obvious advantages over the other grafting methods. In addition, the wide range of substrates and monomers suited to photografting polymerization also makes this approach attractive for the modification of microfluidic devices.

Allbritton and coworkers [264,265] reported the use of a one-step procedure to covalently link polymers to the surface of poly(dimethylsiloxane) (PDMS)-based microfluidic devices, in order to tailor the surface properties of the devices of interest. In this work [264,265], acrylic acid, acrylamide, dimethylacrylamide, 2-hydroxylethyl acrylate and poly(ethylene glycol)monomethoxyl acrylate were used as monomers. By grafting the polymers derived from these monomers, hydrophilic surfaces of PDMS were produced. Microchannels constructed from the grafted PDMS could be more easily filled with aqueous solutions, compared with the devices based on pristine PDMS. Allbritton and coworkers [266,267] developed a strategy for grafting mixed monomers onto PDMS microdevice using UV irradiation. The reason for using mixed monomers was to combine different chemical properties together, intending to obtain optimized electrophoretic separation of a set of analytes. The results demonstrated that by carefully selecting a mixture of monomers with appropriate properties, it is possible to tailor the surface of PDMS for a large number of different electrophoretic separations.

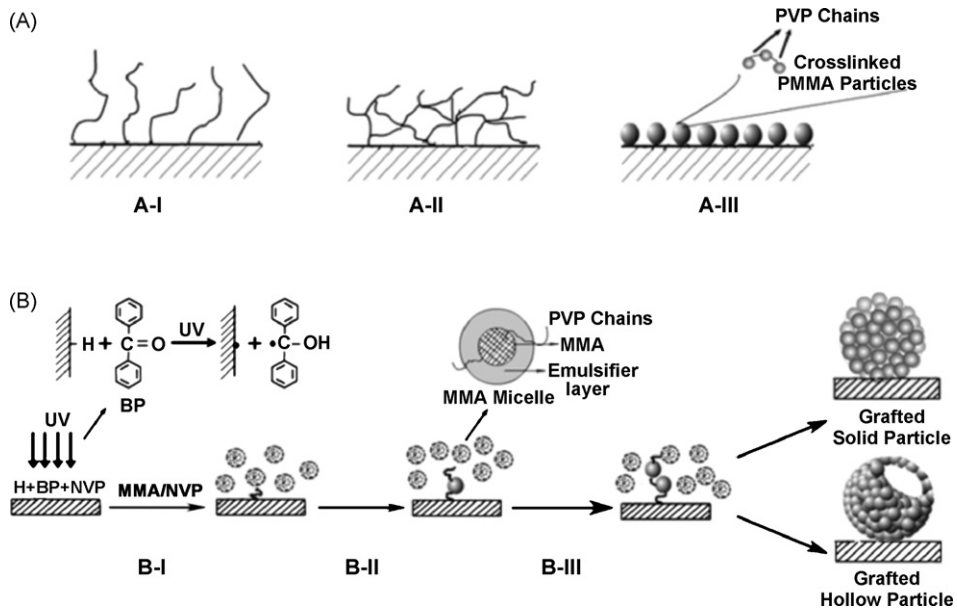

Scheme 17. (A) Illustration of three kinds of grafting topographies with (A-I) polymer brushes, (A-II) a thick layer of crosslinking polymer brushes, and (A-III) discrete spherical polymer particles; (B) chemical scheme for the fabrication of assembled microparticles by SPSA with the formation of (B-I) the precursors, (B-II) the primary particles, and (B-III) the assembled solid/hollow particles (Ref. [208]).

Fréchet and coworkers [268] prepared microfluidic devices with a dual function containing both a solid-phase extractor and an enzymatic microreactor via photografting. They also prepared protein-resistant surfaces for multifunctional microfluidic devices by surface photografting technique [269]. In another investigation, they achieved surface functionalization of thermoplastic polymers for the fabrication of microfluidic devices via photografting [270]. Ebara et al. [271] realized surface modification of microfluidic channels by photografting non-fouling "smart" polymers. In other studies, cyclic olefin copolymers (COC) were selected to build microfluidic devices using photografting methods by Pu et al. [272], Stachowiak et al. [273], and Li et al. [274]. The success in selective patterning of hydrophobic and hydrophilic areas inside microchannels of microfluidic device was reported by Besson et al. [275]. Via a combination of photochemical and alkaline hydrolysis etchings, Yang et al. [276] prepared micro/nanoscale wells and channels on organic polymer substrates, which provide platforms for microchips potentially useful for microarrays, heterogeneous immunoassays, biosensors, filtration, and/or microanalysis.

4.6. Modification/functionalization of membranes

Compared with other unit operations in (bio)chemical engineering, membrane technology possesses some advantages which are closely related to its selective transport principle. This principle allows the separations by membrane to work without the other additives, at low temperatures, and with low energy consumption [277]. The applications of membrane technology have been developed

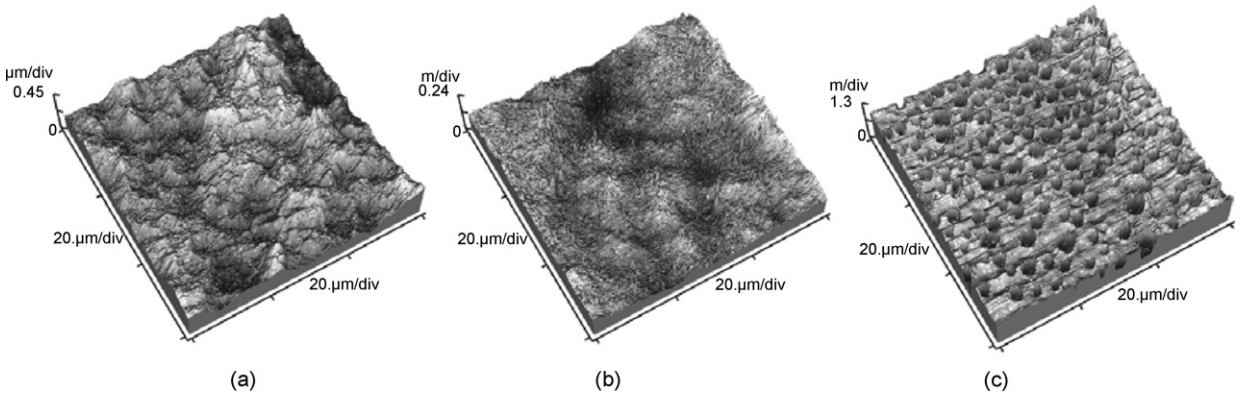

Fig. 15. 3D AFM images of the surfaces of the LDPE films prepared under different conditions. TMPTA: 10 wt.%, feed ratio of BP to TMPTA: 5 wt.%, UV irradiation time: 180 s, (a) blank LDPE film, (b) LDPE film grafted with TMPTA in THF, (c) LDPE film grafted with TMPTA in THF and H_2O, the mass percent of H_2O in the mixed solvent was 10 wt.% (Ref. [213]).

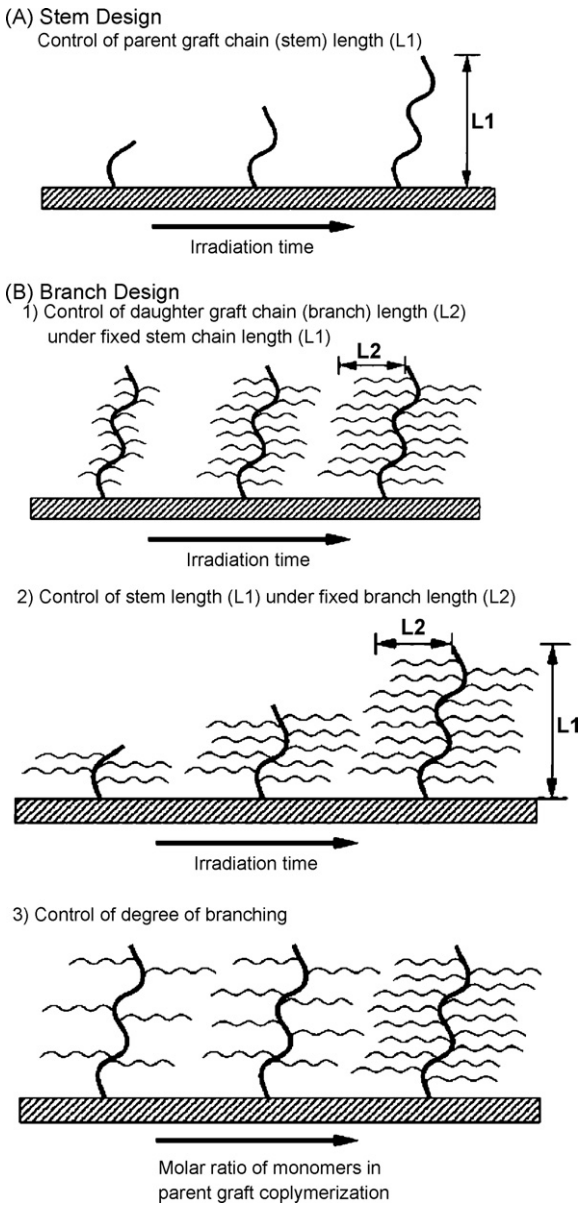

Fig. 16. Schematic representation of the stem and branch designs (Ref. [219]).

far beyond the range of simple separation. Membranes are the crucial component in polymer electrolyte fuel cells [278], separation devices based on affinity chromatography [279], various chemical- and bio-sensors [280,281], drug deliverable systems with controllable release [282,283], etc. However, a major part of the commercially available synthetic membranes are made of hydrophobic polymeric materials. Like hydrophobic polymer films, hydrophobic membranes are surface inert, thus resulting in high susceptibility to bio-fouling and decrease in flux. Surface photografting polymerization technique is a viable solution to overcome these disadvantages of hydrophobic membranes. Some specific uses of surface photografting in membrane are introduced below. It should be pointed out that with regard to membranes, it is difficult to limit the graft polymerization only to the surface layer; nevertheless, in most cases it is not necessary to overcome such a difficulty, since the simultaneous modification of both the surface and the walls of the pores is desirable.

4.6.1. Improving recognition and selective permeation

Yang et al. [284–286] developed a strategy to graft glycopolymer on membrane surface via photografting polymerization. Surface grafting polymerization of a monomer, e.g., 2-aminoethyl methacrylate hydrochloride (AEMA), 2-hydroxyethyl methacrylate (HEMA), or allyl glucoside (AG) onto the membrane was carried out under UV irradiation first, and then functionalization of the membrane surface with glycopolymers was performed to obtain membranes with glycosylated surfaces. The resulting membranes exhibited a considerably improved recognition of lectin [284].

A variety of polymeric membranes had been selected for CO_2 separation [287,288]. However, in practical applications, the means to develop gas separation membranes with not only high permeation rate and selectivity, but also fine chemical and thermal stability still remains a big problem. Kim et al. [289] realized selective permeation of CO_2 through pore-filled photografting process. The obtained membrane consisted of two polymeric materials: a porous substrate and filling polymers that filled the pores of the substrate. Asymmetric polyacrylonitrile (PAN) membrane was used as the substrate and methoxy poly(ethylene glycol) acrylate (MePEGA) as the filled grafting monomer. The thus prepared membrane showed high permselectivity of CO_2, which was attributed to the high solubility selectivity resulting from the high affinity of CO_2 to PEG segment. Via photografting method, Yang et al. [290] prepared styrene–butadiene–styrene triblock (SBS) copolymer membrane with O_2 permeability.

In the textile industry, membranes also have many practical applications [291–294]. Akbari et al. [295] used sodium *p*-styrene sulfonate and [2-(acryloyloxy)-ethyl]trimethyl ammonium chloride as monomer for the modification of a polysulfone ultrafiltration membrane. The grafted membranes were evaluated for the removal of six textile dyes and showed acceptable performances in terms of both flux and dye retention. The same group also reported the application of grafted membrane in treatment of anionic dye solutions [296]. Asano et al. [297] and Chen et al. [298] reported the preparation of proton-conducting membranes and fuel cell membranes using photografting, respectively.

4.6.2. Decreasing fouling

Membrane fouling during filtration is a big problem and results in significant loss of performance with respect to selectivity and permeation flux. Some attempts have been made to solve this problem [299–301]. The hydrophilization of membranes seems to be a promising approach to realize low fouling membrane [302,303]. Among a variety of alternatives to perform surface modification of membranes, photografting modification has

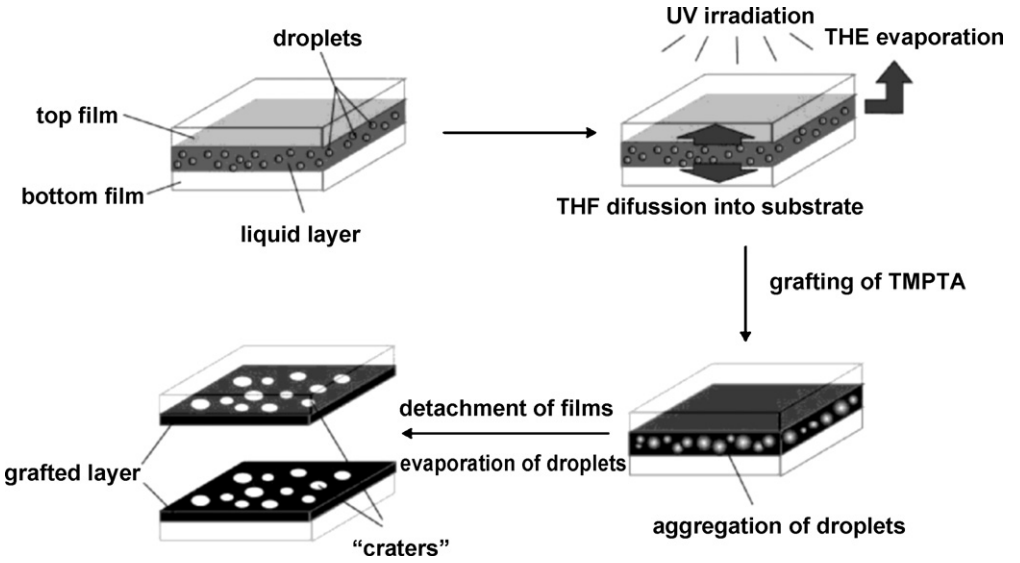

Scheme 18. Schematic representation of the possible mechanism for "craters" formation (Ref. [213]).

gathered much attention due to its distinct advantages. Belfort and coworkers [304–306] prepared low fouling membranes, i.e., membranes with high rejection to protein and natural organic matters. Ulbricht and coworkers [307] prepared low fouling membranes by photografting polymerization of poly(ethylene glycol) methacrylate (PEGMA) on polyethersulfone (PES) membrane. The modified membranes showed increased resistance to fouling and rejection with respect to a pristine membrane. In the work of Kang et al. [308], Hilal et al. [309], and Yang et al. [310], low fouling membranes were also reported, all of which were prepared via photografting method, demonstrating that the photografting method is applicable to this field.

4.6.3. Molecular imprinting technique

Molecular imprinting techniques (MIT: a technique to create template-shaped cavities in matrices with memory of the template molecules after removing the template) are effective for chiral separations, drug assays, and other applications and, therefore, have received much attention over the last decade [311,312]. The preparation of molecular imprinting polymers generally involves polymerizations in the presence of a crosslinking agent and a template molecule [313,314]. The combination of molecular imprinting and membrane modification techniques has allowed for the design of compact apparatuses which have demonstrated the potential for saving enormous amounts of energy in the processing and treating of great amounts of solution [315,316].

Photografting methods have been widely applied in molecular imprinted membranes. In the work of Wang et al. [317], a surface layer containing molecular imprint sites of theophylline (THO) was produced on a polyacrylonitrile (PAN) membrane using acrylic acid (AA) as monomer and *N*,*N*′-methylenebisacrylamide (MBAA) as crosslinker. After

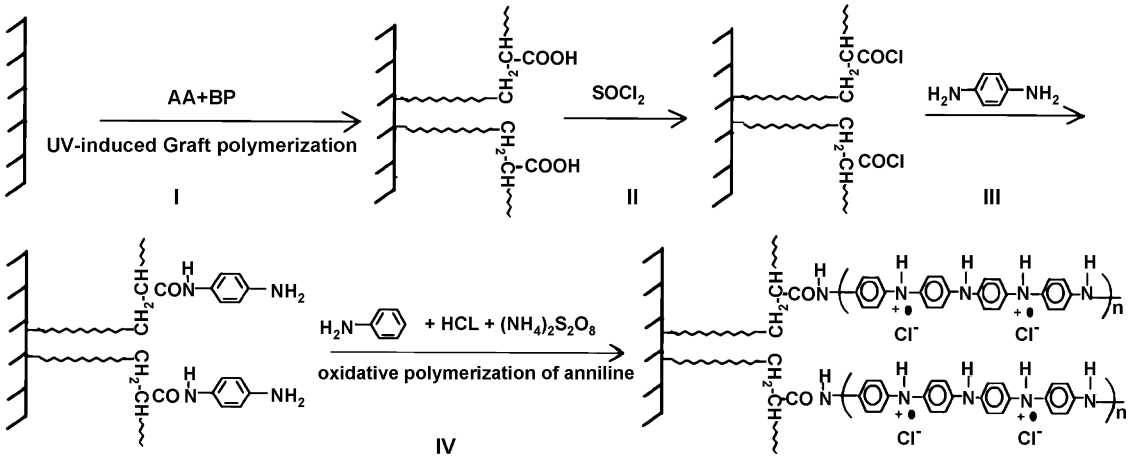

Scheme 19. Schematic diagram illustrating the processes for grafting polymerization of aniline on the surface of PP film. AA, acrylic acid; BP, benzophenone (Ref. [223]).

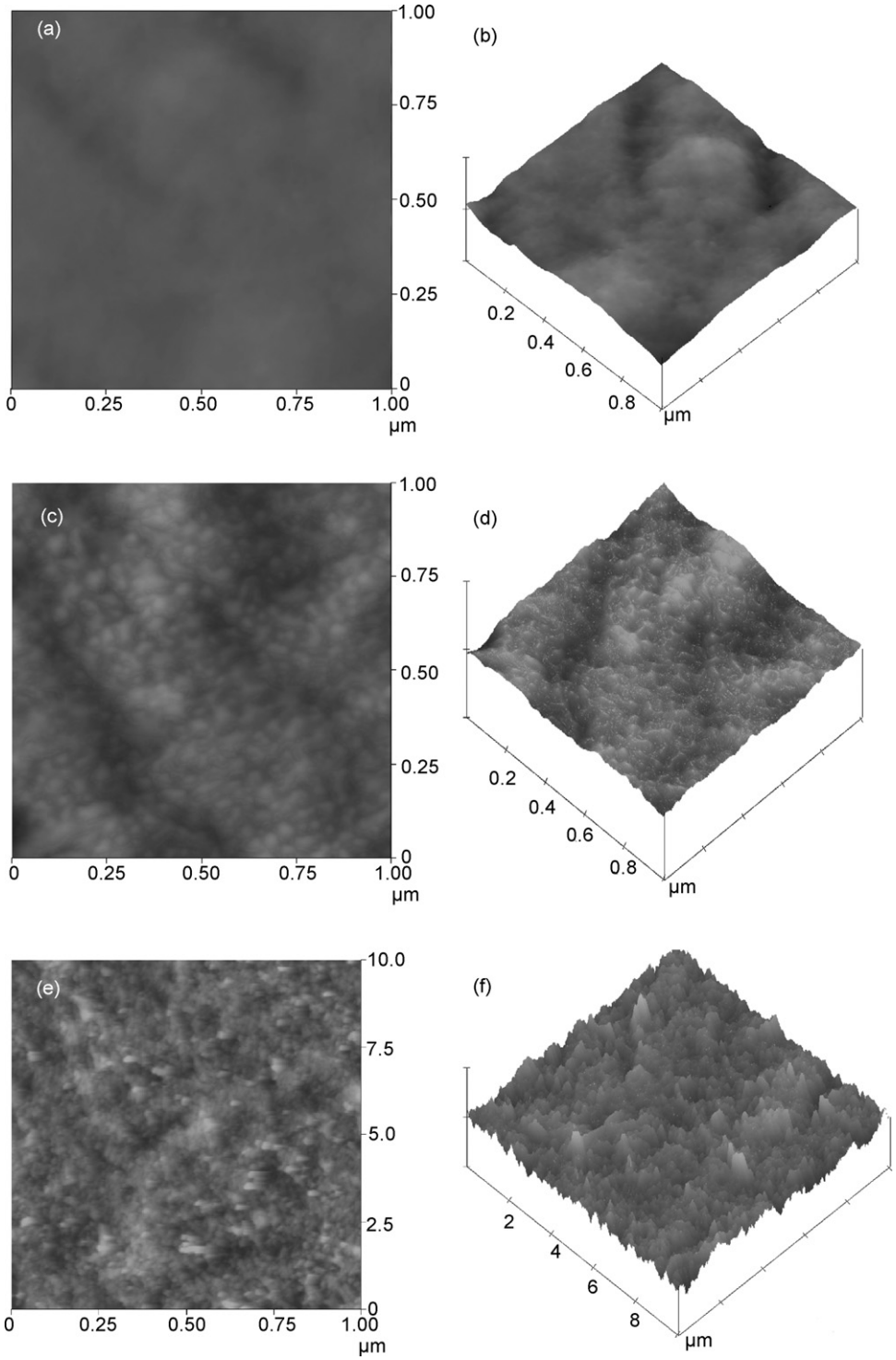

Fig. 17. AFM images for (a) and (b) PP film; (c) and (d) PP-g-PAA film, GP1, 1.10 wt.%; (e) and (f) PP-g-PAA/PANI film, GP4, 1.40 wt.% (Ref. [223]).

removal of the template molecules, the membrane showed recognition of THO with high efficiency.

Ulbricht et al. [318] prepared molecular imprinted polymer (MIP) membranes with desmetryn as the template. The produced membranes could be used in a fast preconcentration step and solid-phase extraction [319]. The MIP synthesis and the model for synthesis of a MIP desmetryn receptor are schematically shown in Scheme 20 and Fig. 20 [318].

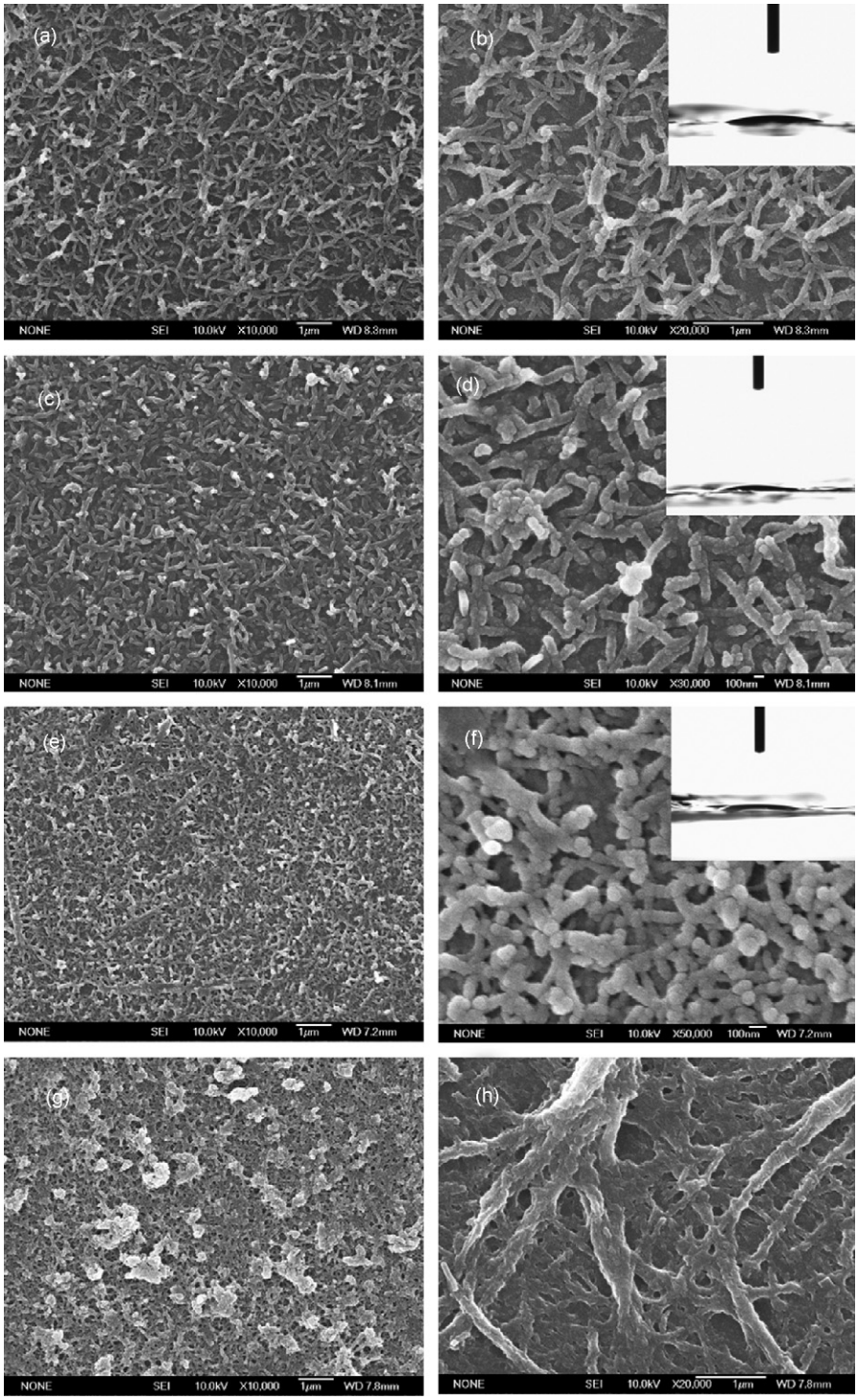

Fig. 18. FESEM images of PANI immobilized on the PP films' surfaces (the insets show the shapes of surface water droplets). The polymerization reaction under stirring was kept at 0–5 °C for 24 h. The concentration of aniline, PAA, and SDS were 0.09, 0.025, and 0.017 M, respectively. (a) Low magnification image and (b) high magnification image, PAAgrafting percentage, 0.8 wt.%; CA, 15°. (c) Low magnification image and (d) high magnification image, PAA grafting percentage, 1.1 wt.%; CA, 12°. (e) Low magnification image and (f) high magnification image, PAA grafting percentage, 1.5 wt.%; CA, 7°. (g) The concentration of aniline and PAA were 0.09 and 0.025 M, respectively, i.e., without SDS. (h) The concentration of aniline, PAA, and SDS were 0.09, 0.025, and 0.057 M, respectively, PAA grafting percentage, 1.1 wt.% (Ref. [224]).

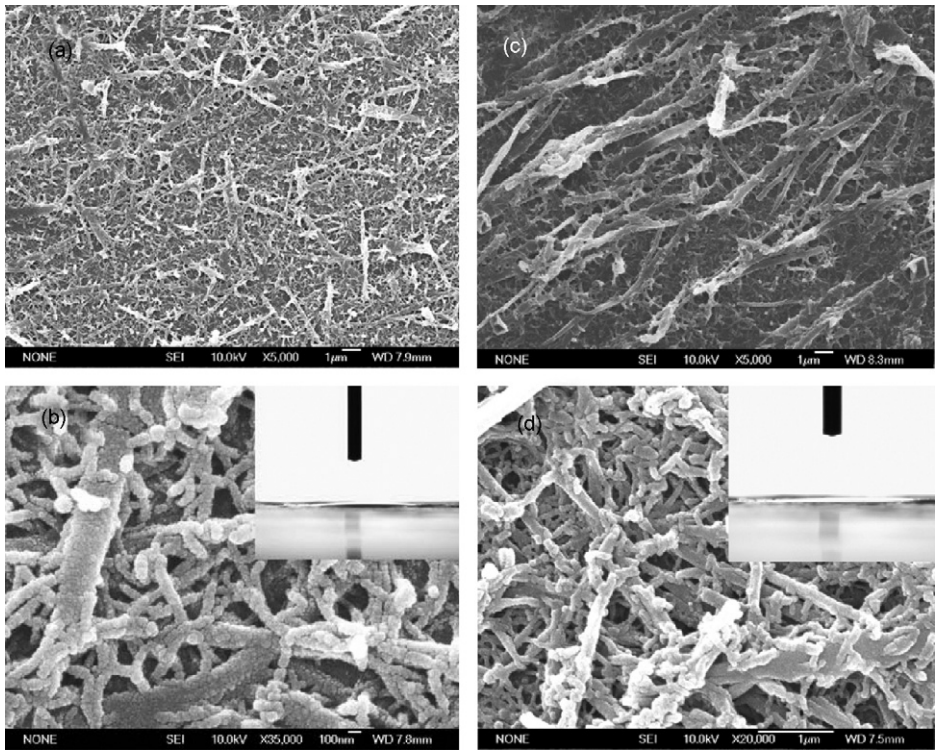

Fig. 19. FESEM images of PANI sub-micro/nanostructured dendrites immobilized on PP films' surfaces (the insets show the shape of water droplets). The reaction was stirred for 20 min (after APS was added into the mixture) and was allowed to stand for 24 h at 0–5 °C; the concentration of aniline, PAA, and SDS are 0.09, 0.025, and 0.017 M, respectively. (a) Low magnification image and (b) high magnification image, PAA grafting percentage, 1.1 wt.%; CA, 3°. (c) Low magnification image and (d) high magnification image, PAA grafting percentage, 1.5 wt.%; CA, 0° (Ref. [224]).

4.6.4. Stimuli-sensitive membrane

Stimuli-sensitive membranes, such as pH-sensitive [320,321], temperature-sensitive [322,323], and light-sensitive [324], have been produced through graft polymerization using some special monomers. Yang and Yang [325], Peng and Cheng [326], and Wu et al. [327], respectively, grafted NIPAAm and *N*,*N*′-diethylacrylamide (DEAAm) to prepare thermo-sensitive membranes. Lequieu et al. [328] also used photografting to prepare membranes with thermo-adjustable porosity and separation properties by surface immobilization of poly(*N*-vinylcaprolactam). Geismann and Ulbricht [329] reported the preparation of grafted membranes with "smart" polymer layers, i.e., pH-responsive layers based on poly(acrylic acid). Shim et al.

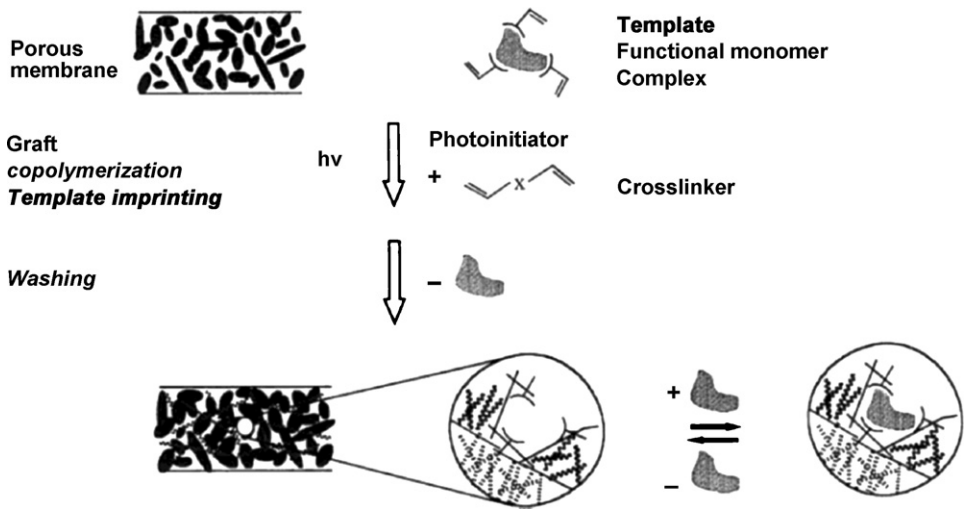

Scheme 20. MIP synthesis via surface photografting onto porous polymer membranes (Ref. [318]).

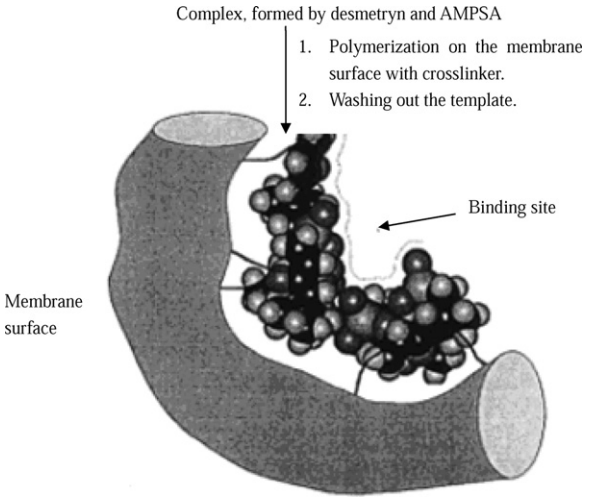

Fig. 20. Model for synthesis of a MIP desmetryn receptor via surface photografting of an AMPS polymer: (a) solution complex of desmetryn and AMPS, (b) surface grafted AMPS complex after desmetryn removal (Ref. [318]).

[330] reported membranes with pH-dependent permeability produced by UV irradiation technique.

4.6.5. Miscellaneous

There are a great number of other investigations regarding UV-induced grafting of membranes. The structure of the grafted chains played a significant role on the filtration performance of UV-modified poly(ether sulfone) (PES) membranes [331]. The preparation of nanofiltration membranes [168,332], modification of poly(ethylene terephthalate) (PET) nucleopore membranes [333] and pore-covering membranes as a full open/close valve [334], and synthesis of pore-filling polymeric monolith in microfiltration membranes [335] have been reported. Hilal et al. [336] modified a membrane surface with cationic polyelectrolyte, and examined the modified membranes with AFM. The membranes grafted with particularly designed polymer chains possessed the function of adsorption and desorption of metal ions, as presented by Hirata and coworkers [337,338]. When viologens (a family of 1,1′-disubstituted-4,4′-bipyridinium dications) were grafted on substrates, the redox properties of viologens provided an approach for the reduction of precious metal ions, as introduced by Kang and coworkers [339]. Some grafted substrates showed ion-conducting characteristics [340], and electrically conductive performance [341].

4.7. Biomedical applications

4.7.1. Anti-bacterial

Anti-bacterial materials have found a variety of applications ranging from biomedical products, packing materials, to filters of air-conditioning systems. So far the predominant approach to prepare anti-bacterial materials is to incorporate or adsorb bactericides into the existing matrices [342–346]. This widely used method usually requires a large amount of bactericide, which leads to high cost and possible damage of the bulk properties of the matrix as well. In addition, the added bactericides may be gradually released from the matrix and cause environment pollution. Therefore, the strategy through which anti-bacterial compounds are chemically bonded on the matrix is more desirable and is receiving much attention recently. Polymer-based bactericides have been created by grafting or coating anti-bacterial groups, such as heavy metal-based groups [347], quaternary ammonium salts [348,349], pyridinium salts [350], quaternary phosphonium salts [351], and so forth [352] on films or other forms.

Via surface photografting, Xing et al. [353] prepared anti-bacterial PP film grafted with polyvinylpyrrolidone–iodine complex, and the products showed an obvious anti-bacterial property with broad spectrum and high efficiency. Shi et al. [354] prepared PET film with antibacterial activity by surface photografting an asymmetric viologen, *N*-hexyl-*N*′-(4-vinylbenzyl)-4,4′-bipyridinium bromide chloride (HVV). The obtained film exhibited anti-bacterial activity, which was largely dependent on the concentration of pyridinium groups tethered on the film surface. Yang et al. [355] improved the hydrophilicity of nonwoven PET by photografting polymerization of water-soluble monomers. Thereafter, three biocides, $AgNO_3$ solution complexes, vinyl quarternary ammonium salt (VQAS), and chitosan, were combined, respectively, onto the grafted PET. The results proved that for biocidal properties, the Ag^+ ions provided the best effects.

4.7.2. Lubrication and anti-biofouling

Biomaterial surfaces require anti-biofouling properties, i.e., resisting protein adsorption and cell adhesion [356,357]. Otherwise, biomedical devices with tightly adsorbed proteins on them might lead to thrombus formation, inflammatory response, and bacterial adhesion when they are used inside human bodies. Furthermore, these responses could also raise crucial issues in the implantation of biomedical devices [358,359]. To minimize the above biological responses and tissue irritations, hydrophilic and lubricating surfaces of implanted biomedical devices are essential [360]. Most biological devices derived from polymer materials are hydrophobic, which necessitates surface modification to enhance surface biocompatibility [361].

Goda et al. [362] conducted photografting of poly(2-methacryloyloxyethyl phosphorylcholine) (MPC) from the poly(*p*-xyleylene) (parylene C) layer, and advanced lubrication and anti-biofouling properties were observed in the grafted surfaces. The as-obtained biocompatible films may have potential applications as not only implantable biomedical devices but also microfabricated devices used under biological conditions. For drug delivery devices [363], improving their surface biocompatibility by surface photografting modification is also one of the effective means to reduce their damage to vessel walls.

4.7.3. Biosensor

To prepare biosensors, surface-enlarging matrices, e.g., hydrogels are generally employed. These matrices should combine the property of low nonspecific binding with the ability to immobilize ligands. Therefore, matrices should be carefully chosen for advanced biosensors. One of the most widely used matrix is poly(ethylene glycol)

(PEG), which has been proved to be a suited polymer for protein-resistant matrix in biomaterial applications [364]. Larsson et al. [365] reported the use of PEG for biosensor applications. In their studies, PEG and its comonomer, 2-hydroxyethyl methacrylate (HEMA) were graft copolymerized onto cycloolefin polymer (COP)-coated substrate, followed by the subsequent carboxylation, activation/immobilization/deactivation treatment and protein–surface interaction. The results suggested that the treated PEG matrix was a good candidate for developing biochips and biosensors.

Viologens have intrigued great interest due to their significant reversibility and large change in the visible extinction coefficient following reduction [366]. A number of attempts using viologen family for practical purposes have been carried out, where viologens were combined with suitable polymers to create bioseparators and biosensors [367,368]. Liu et al. [369] also reported the surface functionalization of substrates via photografting viologens. The grafted films could potentially serve as active templates in biosensors. Besides, chemosensors could also be fabricated. In the report by Delaney et al. [370], ultrathin chemosensors were prepared by photografting molecularly imprinted polymer on the surface of alkanethiol-modified gold electrodes.

4.7.4. Immobilizing enzyme

Enzymes are important in modern science and technology. However, applications of not-immobilized enzymes are often limited due to their instability and separation difficulty. To circumvent these disadvantages, many endeavors have been made for enzyme immobilization [371,372]. Compared with physical immobilization routes, chemical approaches are obviously more advantageous [373,374], and therein UV-induced grafting serves as an effective way to introduce the functionalities required for enzyme immobilization. For instance, Yamada et al. [375] immobilized urease on expanded poly(tetrafluoroethylene) (ePTFE) films grafted with 2-hydroxyethyl methacrylate (HEMA) and 2-hydroxyethyl acrylate (HEA). Under the examined conditions, the results revealed that the immobilized urease could be used repeatedly without considerable decrease in reactivity. Cen et al. [376] immobilized glucose oxidase (GOD) on the surface of functionalized PP film using both physical and chemical methods, and the investigation showed that the covalent immobilization technique offered advantages over the physical entrapment technique. Another enzyme, trypsin [377], was also immobilized on polyaniline (PAN) and polypyrrole (PPY) film surface functionalized with photografted polymer chains. In general, immobilizing enzymes on substrates modified via photografting technique are expected to become an increasingly attractive field.

4.7.5. Cell attachment and culture

Bio-scaffolds play important roles in tissue engineering, because they are widely used for blood-contacting applications [378,379]. The hemocompatibility of these scaffolds is of significant importance. Nonetheless, most polymer surfaces are inert, which is unfavorable for cell adhesion and growth, and consequently require surface modifications [380–382]. Among the well-established methods for surface modification, photoinduced surface grafting was relatively more acceptable [383–388]. For example, Zhu et al. [389] improved the endothelial cell compatibility of porous polyurethane scaffolds using photografting; Ying et al. [390] immobilized galactose ligands onto modified PET films, which were used as substrates for hepatocyte culture. Thom et al. [391] and Janorkar et al. [392], respectively, investigated the cell–surface interactions and cell attachment on substrates after the treatment of photografting polymerization.

5. Further considerations

5.1. Direct characterization techniques

Some effective methods have been developed to characterize the graft polymerizations and the grafted surfaces, such as IR spectroscopy, UV–vis spectroscopy, AFM, SEM, etc. However, with respect to the length of the grafted chains and their distribution, the nature of the branched or superbranched graft polymer chains, the crosslinking structure and so forth mentioned in the above sections, how to characterize these parameters directly and even in-house and how to effectively control them to obtain uniformly modified surfaces still remain a challenging problem. This further poses another question in how to ensure the reproducibility of the grafting, which is crucial for the practical applications.

5.2. Degradation and rearrangement

Most polymer materials are somewhat sensitive to UV irradiation, and some of them even undergo degradation [393,394]. Surface photografting is undoubtedly a powerful technique for surface modification, but in some studies, degradation has been observed. For example, the surface water contact angle was reported to first decrease and then increase again, which was assumed to be aroused by the degradation of the substrate under UV irradiation [395]. In the work of Zhao et al. [149], a similar situation was also observed. In deed, most of the articles focusing on surface photografting paid little attention to this problem and even did not mention such a situation. Another point also deserves to be mentioned, i.e., the arrangement of the grafted chains after photografting. Just as presented in some articles concerning surface modification by plasma techniques [396,397], the rearrangement of the grafted functional groups led to the degraded properties of the substrates. Both the degradation of the substrate caused by UV light and the reduction of properties caused by the rearrangement of the grafted chains are not favorable from the viewpoint of practical applications.

5.3. Microenvironment effects

Compared with the free polymer chains in solution or bulk, the polymer chains covalently grafted on the substrate should behave differently to a certain degree. For example, the conformation of the graft chains should differ from free chains and the reactivity of the functional groups

thereon may change, possibly because of the existence of the substrate, the steric repulsion, and/or the entanglement of the grafted chains especially when the grafted polymer chains have a high density. For this reason, the performances of the grafted layers should be experimentally examined and compared with the corresponding free polymer chains. Especially for the biomedical applications, this must be taken into enough consideration. The inactivation occurred to the immobilized enzymes is one of the good examples, as reported by Chen and Chiu [373].

6. Conclusions

The discussion above demonstrates that polymer materials with expected surface properties can be obtained through grafting appropriate polymer chains onto the substrate. In this review, we have addressed the principal factors affecting UV-induced surface graft polymerization, especially the photoinitiators, the ways to realize controlled/living grafting, the newly emerging self-initiated grafting, as well as the grafting systems bearing CT complexes. In addition, special emphasis has been put upon the topography of the grafted surfaces. In addition, a number of applications have been described. It is worthwhile to point out that, the success in controlled/living grafting allows us to precisely control the grafting and even enables us to further put it into practical practices, such as the modification and preparation of microdevices. This frontier will gather much interest from both scientists and engineers due to its potential applications. Another point deserving mention is the self-initiated grafting polymerization of some special monomer systems, which might help us to design and develop novel photocuring and photografting systems without the addition of any photoinitiators. These two directions seem to be more valuable and promising in the future for both academic research and industrialization.

Acknowledgements

We gratefully thank “the Major Project of the National Science Foundation of China (no. 50433040), and “Major Project for Polymer Chemistry and Physics Subject Construction from Beijing Municipal Education Commission (BMEC)” (XK100100433, XK100100540) for financial support of this work.

References

[1] Ryntz RA. Coating adhesion to low surface free energy substrates. Prog Org Coat 1994;25:73–83.
[2] Noeske M, Degenhardt J, Strudthoff S, Lommatzsch U. Plasma jet treatment of five polymers at atmospheric pressure: surface modification and the relevance for adhesion. Int J Adhes Adhes 2004;24:171–7.
[3] Chambers LD, Stokes KR, Walsh FC, Wood RJK. Modern approaches to marine antifouling coatings. Surf Coat Technol 2006;201: 3642–52.
[4] Callow JA, Callow ME. Biofilms. In: Fusetani N, Clare AS, editors. Antifouling compounds. Progress in molecular and subcellular biology: marine molecular biotechnology, vol. 42. New York: Springer; 2006. p. 141–69.
[5] Bi H, Zhong W, Meng S, Kong J, Yang P, Liu B. Construction of a biomimetic surface on microfluidic chips for biofouling resistance. Anal Chem 2006;78:3399–405.
[6] Shimada S, Takahasi Y, Sugino Y, Hara S, Yamanoto K. Autonomic healing of a pinhole in polyethylene and photografted polyethylene-g-poly(hexyl methacrylate) films. J Polym Sci: Part B: Polym Phys 2004;42:1705–14.
[7] Li J, Sun Y, Zeng H, Xue W, Xiao Y, Yu Q. Preparation of photoluminescence films containing rare earth complexes by UV photograft polymerization. J Appl Polym Sci 2003;89:662–7.
[8] Zhao Y, Chen L, Zhang H, Zhao G. Novel fishnet fibers with antiadhesion of seaweeds obtained by UV-irradiation technique. J Appl Polym Sci 2007;103:1252–6.
[9] Yang P, Sun Y, Deng J, Liu W, Zhang L, Yang W. Synthesis and inhibition performance of a polymer-supported inhibitor. J Polym Sci: Part A: Polym Chem 2004;42:4074–83.
[10] Yamada K, Taki T, Sato K, Hirata M. Electrotransport of organic electrolytes through 2-(dimethylamino)ethyl methacrylate-grafted polyethylene films and their separation and concentration. J Appl Polym Sci 2003;89:2535–44.
[11] Ozdemir M, Yurteri CU, Sadikoglu H. Physical polymer surface modification methods and applications in food packaging polymers. Crit Rev Food Sci Nutr 1999;39:457–77.
[12] Jia Z, Du S, Tian G. Surface modification of acrylic fiber by grafting of casein. J Macromol Sci, Part A 2007;44:299–304.
[13] Suzuki M, Kishida A, Iwata H, Ikada Y. Graft copolymerization of acrylamide onto a polyethylene surface pretreated with a glow discharge. Macromolecules 1986;19:1804–8.
[14] Onishi M, Shimura K, Seita Y, Yamashita S, Takahashi A, Masuoka T. Preparation and properties of plasma-initiated graft copolymerized membranes for blood plasma separation. Int J Radiat Appl Instrum Part C 1992;39:569–76.
[15] Wavhal DS, Fisher ER. Hydrophilic modification of polyethersulfone membranes by low temperature plasma-induced graft polymerization. J Membr Sci 2002;209:255–69.
[16] Song YQ, Sheng J, Wei M, Yuan XB. Surface modification of polysulfone membranes by low-temperature plasma-graft poly(ethylene glycol) onto polysulfone membranes. J Appl Polym Sci 2000;78:979–85.
[17] Lei J, Liao X, Lin D. Studies on surface graft copolymerization of acrylic acid onto LDPE film through corona discharge. Chem J Internet 2000;2, 021006pc.
[18] Lei J, Li Q, He G, Lin X. Surface graft copolymerization of acrylic amide onto BOPP film through corona discharge. Acta Chim Sin 2000;58:598–600.
[19] Lei J, Shi M, Zhang J. Surface graft copolymerization of hydrogen silicon fluid onto fabric through corona discharge and water repellency of grafted fabric. Eur Polym J 2000;36:1277–81.
[20] Mok S, Worsfold DJ, Founda A, Matsuura T. Surface modification of polyethersulfone hollow-fiber membranes by gamma-ray irradiation. J Appl Polym Sci 1994;51:193–9.
[21] Furtado Filho A, Gomes AS. Copolymerization of styrene onto polyethersulfone films induced by gamma-ray irradiation. Polym Bull 2006;57:415–21.
[22] Bucio E, Arenas E, Burillo G. Radiation grafting of *N*-isopropylacrylamide onto polypropylene films by preirradiation method. Mol Cryst Liq Cryst 2006;447:203–13.
[23] Zhao B, Brittain WJ. Polymer brushes: surface-immobilized macromolecules. Prog Polym Sci 2000;25:677–710.
[24] Oster G, Shibata O. Graft copolymer of polyacrylamide and natural rubber produced by means of ultraviolet light. J Polym Sci 1957;26:233–4.
[25] Rao MH, Rao KN. Radiation induced grafting of mixed monomer onto polyester and polypropylene fibers. J Appl Polym Sci 1987;33:2707–14.
[26] Shkolnik S, Behar D. Radiation-induced grafting of sulfonates on polyethylene. J Appl Polym Sci 1982;27:2189–96.
[27] Haruvy Y, Rajbenbach LA. Grafting of acrylamide to Nylon-6 by the electron-beam preirradiation technique. II. Kinetic aspects and film permeability. J Appl Polym Sci 1982;27:2711–23.
[28] Ishigaki I, Sugo T, Senoo K. Graft polymerization of acrylic acid onto polyethylene film by preirradiation method. I. Effects of preirradiation dose, monomer concentration, reaction temperature, and film thickness. J Appl Polym Sci 1982;27:1033–41.
[29] Bhattacharyya SN, Maldas D. Radiation-induced graft copolymerization of mixtures of styrene and acrylamide onto cellulose acetate. I. Effects of solvents. J Polym Sci: Polym Chem Ed 1982;20:939–50.
[30] Kaji K. Grafting of polyacrylic acid onto PE filament and its distribution. J Appl Polym Sci 1983;28:3767–77.
[31] Okamoto J, Sugo T, Katakai A. Amidoxime-group-containg adsorbents for metal ions synthesized by radiation-induced grafting. J Appl Polym Sci 1985;30:2967–77.

[32] Edge S, Walker S, Feast WJ, Pacynko WF. Surface modification of polyethylene by photochemical grafting with 2-hydroxyethylmethacrylate. J Appl Polym Sci 1993;47:1075–82.
[33] Sarkar N, Bhattacharjee S, Sivaram S. Surface functionalization of poly(ethylene) with succinic anhydride: preparation, modification, and characterization. Langmuir 1997;13:4142–9.
[34] Allmer K, Hult A, Rånby B. Surface modification of polymers. I. Vapour phase photographing with acrylic acid. J Polym Sci 1988;A26:2099–111.
[35] Zhang PY, Rånby B. Surface modification by continuous grafting copolymerization. I. Photoinitiated graft copolymerization onto PE tape film surface. J Appl Polym Sci 1990;40:1647–61.
[36] Zhang PY, Rånby B. Surface modification by continuous grafting copolymerization. II. Photoinitiated graft copolymerization onto polypropylene film surface. J Appl Polym Sci 1991;43:621–36.
[37] Zhang PY, Rånby B. Surface modification by continuous grafting copolymerization. III. Photoinitiated graft copolymerization onto PET fiber surface. J Appl Polym Sci 1990;41:1459–67.
[38] Yang WT, Rånby B. Bulk surface photografting process and its applications. I. Reactions and kinetics. J Appl Polym Sci 1996;62:533–43.
[39] Yang WT, Rånby B. Bulk surface photografting process and its applications. II. Principal factors affecting surface photografting. J Appl Polym Sci 1996;62:545–55.
[40] Yang WT, Rånby B. Bulk surface photografting process and its applications. III. Photolamination of polymer films. J Appl Polym Sci 1997;63:1723–32.
[41] Yang WT, Rånby B. Radical living graft polymerization on the surface of polymeric material. Macromolecules 1996;29:3308–10.
[42] Rånby B. Photochemical modification of polymers-photocrosslinking, surface photografting, and lamination. Polym Eng Sci 1998;38:1229–43.
[43] Rånby B, Yang WT, Tretinnikov O. Surface photografting of polymer fibers, films and sheets. Nucl Instrum Meth Phys Res B 1999;151:301–5.
[44] Rånby B. Surface modification and lamination of polymers by photografting. Int J Adh Adhes Adhes 1999;19:337–43.
[45] Bhattacharya A, Misra BN. Grafting: a versatile means to modify polymers techniques, factors and applications. Prog Polym Sci 2004;29:767–814.
[46] Uyama Y, Kato K, Ikada Y. Surface modification of polymers by grafting. Adv Polym Sci 1998;137:1–39.
[47] Kato K, Uchida E, Kang E-T, Uyama Y, Ikada Y. Polymer surface with graft chains. Prog Polym Sci 2003;28:209–59.
[48] Goddard JM, Hotchkiss JH. Polymer surface modification for the attachment of bioactive compounds. Prog Polym Sci 2007;32:698–725.
[49] Ang CH, Garnett JL, Levotetal R. Photosensitized grafting of styrene, 4-vinyl pyridine and methyl methacrylate to polypropylene. J Polym Sci: Polym Lett Ed 1980;18:471–5.
[50] Dworjanyn PA, Garnett JL. Synergistic effect of urea with polyfunctional acrylates for enhancing the photografting of styrene to polypropylene. J Polym Sci: Part C: Polym Lett 1988;26:135–8.
[51] Jiang W, Awasum JN, Irgum K. Control of electroosmotic flow and wall interactions in capillary electrophoresis capillaries by photografted zwitterionic polymer surface layers. Anal Chem 2003;75:2768–74.
[52] Deng JP, Yang WT, Rånby B. Surface photografting polymerization of vinyl acetate (VAc), maleic anhydride (MAH), and their charge transfer complex. I. VAc(1). J Appl Polym Sci 2000;77:1513–21.
[53] Deng JP, Yang WT, Rånby B. Surface photografting polymerization of vinyl acetate (VAc), maleic anhydride (MAH), and their charge transfer complex. II. VAc(2). J Appl Polym Sci 2000;77:1522–31.
[54] Decker C, Zahouily K. Light-stabilization of polymeric materials by grafted UV-cured coatings. J Polym Sci: Part A: Polym Chem 1998;36:2571–80.
[55] Pan B, Viswanathan K, Hoyle CE, Moore RB. Photoinitiated grafting of maleic anhydride onto polypropylene. J Polym Sci: Part A: Polym Chem 2004;42:1953–62.
[56] Kondo T, Koyama M, Kubota H, Katakai R. Characteristics of acrylic acid and *N*-isopropylacrylamide binary monomers-grafted polyethylene film synthesized by photografting. J Appl Polym Sci 1998;67:2057–64.
[57] Ruckert D, Geuskens G. Surface modification of polymers-IV. Grafting of acrylamide via an unexpected mechanism using a water soluble photo-initiator. Eur Polym J 1996;32:201–8.
[58] Deng JP, Yang WT. Photo-grafting and cross-linking reaction of LDPE-VAC polymerization system (I). Effects of initiators. J Beijing Univ Chem Technol 2000;27:16–9.
[59] Geuskens G, Etoc A, Michele PD. Surface modification of polymers VII. Photochemical grafting of acrylamide and *N*-isopropylacrylamide onto polyethylene initiated by anthraquinone-2-sulfonate adsorbed at the surface of the polymer. Eur Polym J 2000;36:265–71.
[60] Cho J-D, Kim S-G, Hong J-W. Surface modification of polypropylene sheets by UV-radiation grafting polymerization. J Appl Polym Sci 2006;99:1446–61.
[61] Cho J-D, Kim E-O, Kim H-K, Hong J-W. An investigation of the surface properties and curing behavior of photocurable cationic films photosensitized by anthracene. Polym Test 2002;21:781–91.
[62] Nelson EW, Carter TP, Scranton AB. Fluorescence monitoring of cationic photopolymerizations: divinyl ether polymerizations photosensitized by anthracene derivatives. Macromolecules 1994;27:1013–9.
[63] Cho J-D, Kim H-K, Kim Y-S, Hong J-W. Dual curing of cationic UV-curable clear and pigmented coating systems photosensitized by thioxanthone and anthracene. Polym Test 2003;22:633–45.
[64] Cho J-D, Hong J-W. UV-initiated free radical and cationic photopolymerizations of acrylate/epoxide and acrylate/vinyl ether hybrid systems with and without photosensitizer. J Appl Polym Sci 2004;93:1473–83.
[65] Woo CK, Schiewe B, Wegner G. Multilayered assembly of cellulose derivatives as primer for surface modification by polymerization. Macromol Chem Phys 2006;207:148–59.
[66] Hu M-X, Yang Q, Xu Z-K. Enhancing the hydrophilicity of polypropylene microporous membranes by the grafting of 2-hydroxyethyl methacrylate via a synergistic effect of photoinitiators. J Membr Sci 2006;285:196–205.
[67] EI-Wakil AA. Synthesis, characterization, and evaluation of natural rubber-*graft*-*N*-(4-aminodiphynyl methane) acrylamide as an antioxidant. J Appl Polym Sci 2006;101:843–9.
[68] Zhou X, Liu P. Study on antistatic modification of polyurethane elastomer surfaces by grafting with vinyl acetate and antistatic agent. J Appl Polym Sci 2003;90:3617–24.
[69] Ojah R, Dolui SK. Graft copolymerization of vinyl monomers onto silk fibers initiated by a semiconductor-based photocatalyst. J Appl Polym Sci 2007;105:2164–75.
[70] Yang WT, Rånby B. Photoinitiation performance of some ketones in the LDPE-acrylic acid surface photografting system. Eur Polym J 1999;35:1557–68.
[71] Wang H, Brown HR. Aliphatic ketones as photoinitiators for photografting. Macromol Rapid Commun 2004;25:1257–62.
[72] Wang H, Brown HR, Li Z. Aliphatic ketones/water/alcohol as a new photoinitiating system for the photografting of methacrylic acid onto high-density polyethylene. Polymer 2007;48:939–48.
[73] Zhao L, Irwan GS, Kondo T, Kutota H. Acetone-initiated photografting of methacrylic acid on low-density polyethylene film in water solvent. Eur Polym J 2000;36:1591–5.
[74] Yanagishita H, Kitamoto D, Ikegami T, Negishi H, Endo A, Haraya K, et al. Preparation of photo-induced graft filling polymerized membranes for pervaporation using polyimide with benzophenone structure. J Membr Sci 2002;203:191–9.
[75] Qiu C, Nguyen QT, Ping Z. Surface modification of cardo polyetherketone ultrafiltration membrane by photo-grafted copolymers to obtain nanofiltration membranes. J Membr Sci 2007;295:88–94.
[76] Satoh M, Shirai K, Saitoh H, Yamauchi T, Tsubokawa N. Photografting of polymers onto nanosized silica surface initiated by eosin moieties immobilized onto the surface. J Polym Sci: Part A: Polym Chem 2005;43:600–6.
[77] Maji TK, Banerjee AN. Photograft copolymerization of methyl methacrylate on silk fiber using titanium (III) chloride-potassium persulphate redox initiator in a limited aqueous system. I. J Appl Polym Sci 1999;73:2187–93.
[78] Shukla SR, Athalye AR. Mechanical and thermal properties of glycidyl methacrylate grafted cotton cellulose. J Appl Polym Sci 1995;57:983–8.
[79] Lin OH, Kumar RN, Rozman HD, Noor MAM. Grafting of sodium carboxymethylcellulose (CMC) with glycidyl methacrylate and development of UV durable coatings from CMC-*g*-GMA induced by cationic photoinitiators. Carbohyd Polym 2005;59:57–69.
[80] Yang P, Deng JY, Yang WT. Surface photografting polymerization of methyl methacrylate in *N*,*N*-dimethylformamide on low density polyethylene film. Macromol Chem Phys 2004;205:1096–102.
[81] Yang WT, Ranby B. The role of far UV radiation in the photografting process. Polym Bull 1996;37:89–96.
[82] Xu SG, Sun YF, Du JM, Yang WT. Surface modification of LDPE by photografting acrylic acid. J Beijing Univ Chem Technol 2000;27:29–31.

[83] Pieracci J, Crivello JV, Belfort G. UV-assisted graft polymerization of *N*-vinyl-2-pyrrolidinone onto poly(ether sulfone) ultrafiltration membranes using selective UV wavelengths. Chem Mater 2002;14:256–65.
[84] Zhu Z, Kelley MJ. Grafting onto poly(ethylene terephthalate) driven by 172 nm UV light. Appl Surf Sci 2005;252:303–10.
[85] Ziani-Cherif H, Abe Y, Imachi K, Matsuda T. Visible-light-induced surface graft polymerization via camphorquinone impregnation technique. J Biomed Mater Res 2002;59:386–9.
[86] Uchina E, Uyama Y, Ikada Y. A novel method for graft polymerization onto poly(ethylene terephthalate) film surface by UV irradiation without degassing. J Appl Polym Sci 1990;41:677–87.
[87] Uchida E, Ikada Y. Introduction of quaternary amines onto a film surface by graft polymerization. J Appl Polym Sci 1996;61:1365–73.
[88] Harmer AA. Photomodification of surface using heterocyclic azides. Langmuir 1991;7:2010–2.
[89] Bohme P, Hicke H-G, Ulbricht M, Fuhrhop J-H. FT-IR spectroscopic investigations of photochemical grafting of amphiphiles onto polyacrylonitrile surfaces. J Appl Polym Sci 1995;55:1495–505.
[90] Thom V, Jankova K, Ulbricht M, Kops J, Jonsson G. Synthesis of photoreactive α-4-azidobenzoyl-ω-methoxy-poly(ethylene glycol)s and their end-on photo-grafting onto polysulfone ultrafiltration membranes. Macromol Chem Phys 1998;199:2723–9.
[91] Sugawara T, Matsuda T. Synthesis of phenylazido-derivatized substance and photochemical surface modification to immobilize functional groups. J Biomed Mater Res 1996;32:157–64.
[92] Renaudie L, Narvor CL, Lepleux E, Roger P. Functionalization of poly(ethylene terephthalate) fibers by photografting of a carbohydrate derivatized with a phenyl azide group. Biomacromolecules 2007;8:679–85.
[93] Knaus S, Nennadal A, Froschauer B. Surface and bulk modification of polyolefins by functional aryl nitrenes as highly reactive intermediates. Macromol Symp 2001;176:223–32.
[94] Ziani-Cherif H, Imachi K, Matsuda T. Preparation of aryldiazonium-, aryldiazo-, and arylazido-derivatized copolymers and their surface photografting. Macromolecules 1999;32:3438–47.
[95] Matsuda T, Saito N, Sugawara T. Ceric-ion-initiating surface graft polymerization with regional control and dimensional precision. Macromolecules 1996;29:7446–51.
[96] Chen G, Imanishi Y, Ito Y. Effect of protein and cell behavior on pattern-grafted thermoresponsive polymer. J Biomed Mater Res 1998;42:38–44.
[97] Deng JP, Sun YF, Du JM, Yang WT. Photo-grafting and cross-linking reaction of LDPE/acrylate polymerization systems. J Beijing Univ Chem Technol 2000;27:37–9.
[98] Janorkar AV, Metters AT, Hirt DE. Modification of poly(lactic acid) films: enhanced wettability from surface-confined photografting and increased degradation rate due to an artifact of the photografting process. Macromolecules 2004;37:9151–9.
[99] Lawson M, Bowman CN. Vancomycin derivative photopolymerized to titanium kills S. epidermidis. Clin Orthop Relat Res 2007;(461):96–105.
[100] Matyjaszewski K, Dong H, Jakubowski W, Pietrasik J, Kusumo A. Grafting from surfaces for "Everyone": ARGET ATRP in the presence of air. Langmuir 2007;23:4528–31.
[101] Matyjaszewski K, Miller PJ, Shukla N, Immaraporn B, Gelman A, Luokala BB, et al. Polymers at interfaces: using atom transfer radical polymerization in the controlled growth of homopolymers and block copolymers from silicon surfaces in the absence of untethered sacrificial initiator. Macromolecules 1999;32:8716–24.
[102] Lee SB, Koepsel RR, Morley SW, Matyjaszewski K, Sun Y, Russell AJ. Permanent, nonleaching antibacterial surfaces. 1. Synthesis by atom transfer radical polymerization. Biomacromolecules 2004;5:877–82.
[103] Ejaz M, Yamamoto S, Ohno K, Tsujii Y, Fukuda T. Controlled graft polymerization of methyl methacrylate on silicon substrate by the combined use of the Langmuir–Blodgett and atom transfer radical polymerization techniques. Macromolecules 1998;31:5934–6.
[104] Ma H, Davis RH, Bowman CN. A Novel sequential photoinduced living graft polymerization. Macromolecules 2000;33:331–5.
[105] Ma H, Davis RH, Bowman CN. Principal factors affecting sequential photoinduced graft polymerization. Polymer 2001;42:8333–8.
[106] Nakayama Y, Matsuda T. Surface macromolecular architectural designs using photo-graft copolymerization based on photochemistry of benzyl *N*,*N*-diethyldithiocarbamate. Macromolecules 1996;29:8622–30.
[107] Matsuda T, Ohya S. Photoiniferter-based thermoresponsive graft architecture with albumin covalently fixed at growing graft chain end. Langmuir 2005;21:9660–5.
[108] Nakayama Y, Matsuda T, Irie M. A novel surface photograft polymerization method for fabricated devices. Trans Am Soc Artif Intern Org J 1993;39:M545–9.
[109] Otsu T, Yoshida M. Role of initiator-transfer agent-terminator (iniferter) in radical polymerizations: polymer design by organic disulfides as iniferters. Makromol Chim: Rapid Commun 1982;3:127–32.
[110] Luo N, Hutchison JB, Anseth KS, Bowman CN. Synthesis of a novel methacrylic monomer iniferter and its application in surface photografting on crosslinked polymer substrate. J Polym Sci: Part A: Polym Chem 2002;40:1885–91.
[111] Nakayama Y, Anderson JM, Matsuda T. Laboratory-scale mass production of a multi-micropatterned grafted surface with different polymer regions. J Biomed Mater Res (Appl Biomater) 2000;53:584–91.
[112] Luo N, Metters AT, Hutchison JB, Bowman CN, Anseth KS. A methacrylated photoiniferter as a chemical basis for microlithography: micropatterning based on photografting polymerization. Macromolecules 2003;36:6739–45.
[113] Reddy SK, Sebra RP, Anseth KS, Bowman CN. Living radical photopolymerization induced grafting on thiol-ene based substrates. J Polym Sci: Part A: Polym Chem 2005;43:2134–44.
[114] Sebra RP, Masters KS, Bowman CN, Anseth KS. Surface grafted antibodies: controlled architecture permits enhanced antigen detection. Langmuir 2005;21:10907–11.
[115] Sebra RP, Anseth KS, Bowman CN. Integrated surface modification of fully polymeric microfluidic devices using living radical photopolymerization chemistry. J Polym Sci: Part A: Polym Chem 2006;44:1404–13.
[116] Lee HJ, Matsuda T. Surface photograft polymerization on segmented polyurethane using the iniferter technique. J Biomed Mater Res 1999;47:564–7.
[117] Guan J, Yang W. Photografting of PVC containing *N*,*N*-diethyldithiocarbamate groups with vinyl monomers. J Appl Polym Sci 2000;77:2569–74.
[118] Deng JP, Yang WT. Self-initiating performance of maleic anhydride on surface photografting polymerization. J Polym Sci: Part A: Polym Chem 2001;39:3246–9.
[119] Deng JP, Yang WT, Rånby B. Auto-initiating performance of styrene on surface photografting polymerization. Macromol Rapid Commun 2001;22:535–8.
[120] Deng JP, Yang WT, Rånby B. Surface photografting polymerization of styrene on LDPE film. J Macromol Sci-Pure Appl Chem 2002;A39:771–86.
[121] Wang H, Brown HR. Self-initiated photopolymerization and photografting of acrylic monomers. Macromol Rapid Commun 2004;25:1095–9.
[122] Jonsson S, Hultgren J, Sundell PE, Shimose M, Owens J, Vaughan K, et al. Photopolymerization initiated by N-substituted maleimides and electron donor olefin combinations. In: Proceedings of the RadTech Asia'. 1995. p. 283.
[123] Decker C, Morel F, Jonsson S, Clark SC, Hoyle CE. UV radiation curing photoinitiator-free formulations. In: Proceedings of the RadTech Europe'. 1997. p. 169.
[124] Garnett JL, Ng L-T, Viengkhou V. Role of CT complexes in grafting and curing reactions initiated by UV and ionizing radiation. Application of these processes including banknote production. In: Proceedings of the RadTech'. 1998. p. 627.
[125] Deng JP, Yang WT. Surface photografting polymerization of vinyl acetate, maleic anhydride, and their charge-transfer complex. V. Charge-transfer complex (1). J Appl Polym Sci 2005;95:903–9.
[126] Deng JP, Yang WT. Surface photografting polymerization of vinyl acetate, maleic anhydride, and their charge-transfer complex. VI. Charge-transfer complex (2). J Appl Polym Sci 2005;95:910–5.
[127] Deng JP, Yang WT. Surface photografting polymerization of vinyl acetate, maleic anhydride, and their charge-transfer complex. VII. Charge-transfer complex (3). J Appl Polym Sci 2006;99:2810–4.
[128] Deng JP, Yang WT. Surface photografting polymerization of vinyl acetate, maleic anhydride, and their charge-transfer complex. VIII. Charge-transfer complex (4). J Appl Polym Sci 2006;99:2710–20.
[129] Deng JP, Yang WT. Surface photografting polymerization of vinyl acetate, maleic anhydride, and their charge-transfer complex. IX. Charge-transfer complex (5). J Appl Polym Sci 2005;97:2230–7.
[130] Xing CM, Deng JP, Yang WT. Surface graft polymerization of binary monomers maleic anhydride/*n*-butyl vinyl ether on the polypropylene film via two-step method. Polym J 2003;35:613–21.
[131] Xing CM, Deng JP, Yang WT. Surface photografting polymerization of binary monomers maleic anhydride and *n*-butyl vinyl ether on

polypropylene film I. Effects of principal factors. Polym J 2002;34:801–8.
[132] Xing CM, Deng JP, Yang WT. Surface photografting polymerization of binary monomers maleic anhydride and *n*-butyl vinyl ether on polypropylene film II. Some mechanical aspects. Polym J 2002;34:809–16.
[133] Deng JP, Yang WT. Grafting copolymerization of styrene and maleic anhydride binary monomer systems induced by UV irradiation. Eur Polym J 2005;41:2685–92.
[134] Zhou Y, Bai Y, Wei J. Ultraviolet grafting of styrene and maleic anhydride on polyethylene-terephthalate film. J Appl Polym Sci 2006;102:285–8.
[135] Xing CM, Deng JP, Yang WT. Surface functionalization of polypropylene film via UV-induced photografting of *N*-vinylpyrrolidone/maleic anhydride binary monomers. Macromol Chem Phys 2005;206:1106–13.
[136] Garnett JL, Ng LT, Nguyen D, Swami S, Zilic EF. CT complexes in radiation polymerization processes including grafting, curing and hydrogel formation. Radiat Phys Chem 2002;63:459–63.
[137] Ng LT, Nguyen D, Adeloju SB. Photoinitiator-free UV grafting of styrene a weak donor, with various electron-poor vinyl monomers to polypropylene film. Polym Int 2005;54:202–8.
[138] Deng JP, Yang WT. Surface photografting polymerization of vinyl acetate, maleic anhydride, and their charge-transfer complex. IV. Maleic anhydride. J Appl Polym Sci 2003;87:2318–25.
[139] Deng JP, Yang WT. Surface photografting polymerization of vinyl acetate (VAc), maleic anhydride (MAH), and their charge-transfer complex (CTC). III. VAc (3). J Appl Polym Sci 2001;80:1426–33.
[140] Kang ET, Neoh KG, Tan KL, Senn BC, Pigram PJ, Liesegang J. Surface modification and functionalization of polytetrafluoroethylene films via graft copolymerization. Polym Adv Technol 1997;8:683–92.
[141] Loh FC, Lau CB, Tan KL, Kang ET. Surface modification of polyimide films by graft copolymerization. J Appl Polym Sci 1995;56:1707–13.
[142] Pun MY, Neoh KG, Kang ET, Loh FC, Tan KL. Protonation of polyaniline by surface-functionalized polymer substrates. J Appl Polym Sci 1995;56:355–64.
[143] Martínez JG, Benavides R, Guerrero C, Reyes BE. UB sensitization of polyethylenes for grafting of maleic anhydride. Polym Degrad Stabil 2004;86:129–34.
[144] Khan F, Ahmad SR, Kronfli E. UV-radiation-induced preirradiation grafting of methyl methacrylate onto lignocellulose fiber in an aqueous medium and characterization. J Appl Polym Sci 2004;91:1667–75.
[145] Khan F. UV-radiation-induced preirradiation graft copolymerization of methacrylic acid and acrylic acid onto jute fiber. Polym Int 2004;53:1581–4.
[146] Khan MA, Shehrzade S, Hassan MM. Effect of alkali and ultraviolet (UV) radiation pretreatment on physical and mechanical properties of 1,6-hexanediol diacrylate-grafted jute yarn by UV radiation. J Appl Polym Sci 2004;92:18–24.
[147] Chmela S, Teissedre G, Lacoste J. Photografting on ethylene/propylene/5-ethylidene-2-norbornene rubber initiated by photogenerated hydroperoxides. Macromolecules 1996;29:3055–9.
[148] Guan J, Gao C, Feng L, Shen J. Functionalizing of polyurethane surfaces by photografting with hydrophilic monomers. J Appl Polym Sci 2000;77:2505–12.
[149] Zhao G, Chen Y, Wang X. Surface modification of polyethylene film by arylamide graft and alcoholysis for improvement of antithrombogenicity. Appl Surf Sci 2007;253:4709–14.
[150] Chen Y, Liu P. Surface modification of polyethylene by plasma pretreatment and UV-induced graft polymerization for improvement of antithrombogenicity. J Appl Polym Sci 2004;93:2014–8.
[151] Wolf RA. Unique atmospheric plasma surface pretreatment approach for improving adhesion. J Vinyl Addit Technol 2007;13:87–90.
[152] Chen K-S, Ku Y-A, Lin H-R, Yan T-R, Sheu D-C, Chen T-M. Surface grafting polymerization of *N*-vinyl-2-pyrrolidone onto a poly(ethylene terephthalate) nonwoven by plasma pretreatment and its antibacterial activities. J Appl Polym Sci 2006;100:803–9.
[153] Chen K-S, Tsai J-C, Chou C-W, Yang M-R, Yang J-M. Effects of additives on the photo-induced grafting polymerization of *N*-isopropylacrylamide gel onto PET film and PP nonwoven fabric surface. Mater Sci Eng C 2002;20:203–8.
[154] Ng SW, Neoh KG, Wong YT, Sampanthar JT, Kang ET. Surface graft copolymerization of viologens on polymeric substrates. Langmuir 2001;17:1766–72.
[155] Zhang J, Cui CQ, Lim TB, Kang ET. Functionalization of self-assembled monolayers on gold by UV-induced graft polymerization. Macromol Chem Phys 2000;201:1653–61.
[156] Chen Y, Kang ET, Neoh KG, Tang KL. Surface functionalization of poly(tetrafluoroethylene) films via consecutive graft copolymerization with glycidyl and aniline. J Phys Chem B 2000;104:9171–8.
[157] Yu ZJ, Kang ET, Neoh KG. Electroless plating of copper on polyimide films modified by surface grafting of tertiary and quaternary amines polymers. Polymer 2002;43:4137–46.
[158] Zhang MC, Kang ET, Neoh KG, Cui CQ, Lim TB. Thermal imidization of poly(amic acid) precursors on glycidyl methacrylate (GMA) graft-polymerized aluminium and copper surfaces. Polymer 2001;42:453–62.
[159] Chun HJ, Cho SM, Lee YM, Lee HK, Suh TS. Graft copolymerization of mixtures of acrylic acid and acrylamide onto polypropylene film. J Appl Polym Sci 1999;72:251–6.
[160] Wang H, Brown HR. Ultraviolet grafting of methacrylic acid and acrylic acid on high-density polyethylene in different solvents and the wettability of grafted high-density polyethylene. 1. Grafting. J Polym Sci: Part A: Polym Chem 2004;42:253–62.
[161] Wang H, Brown HR. UV grafting of methacrylic acid and acrylic acid on high-density polyethylene in different solvents and the wettability of grafted high-density polyethylene. II. Wettability. J Polym Sci: Part A: Polym Chem 2004;42:263–70.
[162] Irwan GS, Kuroda S-I, Kubota H, Kondo T. Photografting of methacrylic acid on polyethylene film: effect of mixed solvents consisting of water and organic solvent. J Appl Polym Sci 2002;83:2454–61.
[163] Irwan GS, Kuroda S-I, Kubota H, Kondo T. Photografting of *N*-isopropylacrylamide on polyethylene film in mixed solvents composed of water and organic solvent. J Appl Polym Sci 2003;87:458–63.
[164] Irwan GS, Kuroda S-I, Kubota H, Kondo T. Examination of the role of oxygen in the photografting of methacrylic acid on a polyethylene film with a mixed solvent consisting of water and organic solvents. J Appl Polym Sci 2003;89:992–8.
[165] Irwan GS, Kuroda S-I, Kubota H, Kondo T. Effect of mixed solvent consisting of water and organic solvent on photografting of glycidyl methacrylate on polyethylene film. J Appl Polym Sci 2004;93:994–1000.
[166] Irwan GS, Aoyama Y, Kuroda S-I, Kubota H, Kondo T. Photografting of *N*-isopropylacrylamide and glycidyl methacrylate binary monomers on polyethylene film: effect of mixed solvent consisting of water and organic solvent. J Appl Polym Sci 2005;97:2469–75.
[167] Pieracci J, Wood DW, Crivello JV, Belfort G. UV-assisted graft polymerization of *N*-vinyl-2-pyrrolidinone onto poly(ether sulfone) ultrafiltration membranes: comparison of dip versus immersion modification techniques. Chem Mater 2000;12:2123–33.
[168] Béquet S, Remigy J-C, Rouch J-C, Espenan J-M, Clifton M, Aptel P. From ultrafiltration to nanofiltration hollow fiber membranes: a continuous UV-photografting process. Desalination 2002;144:9–14.
[169] Ulbricht M, Oechel A, Lehmann C, Tomaschewski G, Hicke H-G. Gas-phase photoinduced graft polymerization of acrylic acid onto polyacrylonitrile ultrafiltration membranes. J Appl Polym Sci 1995;55:1707–23.
[170] Lei J, Gao J, Zhou R, Zhang B, Wang J. Photografting of acrylic acid on high density polyethylene powder in vapour phase. Polym Int 2000;49:1492–5.
[171] Wirsén A, Sun H, Emilsson L, Albertsson AC. Solvent free vapor phase photografting of maleic anhydride onto poly(ethylene terephthalate) and surface coupling of fluorinated probes, PEG, and an RGD-peptide. Biomacromolecules 2005;6:2281–9.
[172] Wirsén A, Sun H, Albertsson AC. Solvent free vapor phase photografting of arylamide onto poly(methyl methacrylate). Polymer 2005;46:4554–61.
[173] Wirsén A, Sun H, Albertsson AC. Solvent-free vapor-phase photografting of acrylamide onto poly(ethylene terephthalate). Biomacromolecules 2005;6:2697–702.
[174] Martin TP, Sedransk KL, Chan K, Baxamusa SH, Gleason KK. Solventless surface photoinitiated polymerization: grafting chemical vapor deposition (gCVD). Macromolecules 2007;40:4586–91.
[175] Loo LS, Gleason KK. Hot filament chemical vapor deposition of polyoxymethylene as a sacrificial layer for fabricating air gaps. Electrochem Solid-State Lett 2001;4:G81–4.
[176] Lewis HGP, Caulfield JA, Gleason KK. Perfluorooctane sulfonyl fluoride as an initiator in hot-filament chemical vapor

deposition of fluorocarbon thin films. Langmuir 2001;17: 7652–5.
[177] Deng JP, Yang WT, Rånby B. Surface photograft polymerization of vinyl acetate on low density polyethylene film. Effects of solvent. Polym J 2000;32:834–7.
[178] Deng JP, Yang WT, Rånby B. Melt-photografting polymerization of maleic anhydride onto LDPE film. Eur Polym J 2002;38:1449–55.
[179] Zhang X, Kang ET, Neoh KG, Tang KL, Kim DY, Kim CY. Surface studies of pristine and surface-modified polypyrrole film. J Appl Polym Sci 1996;60:625–36.
[180] Ke Y, Wang Y, Ren L, Lu L, Wu G, Chen X, et al. Photografting polymerization of polyacrylamide on PHBV films (1). J Appl Polym Sci 2007;104:4088–95.
[181] Anancharungsuk W, Tanpantree S, Sruanganurak A, Tangboriboonrat P. Surface modification of natural rubber film by UV-induced graft copolymerization with methyl methacrylate. J Appl Polym Sci 2007;104:2270–6.
[182] Yu JJ, Ryu SH. Ultraviolet-initiated photografting of glycidyl methacrylate onto styrene–butadiene rubber. J Appl Polym Sci 1999;73:1733–9.
[183] Shanmugharaj AM, Kim JK, Ryu SH. Modification of rubber surface by UV surface grafting. Appl Surf Sci 2006;252:5714–22.
[184] Wang P, Tang KL, Ho CC, Khew MC, Kang ET. Surface modification of natural rubber latex films by graft copolymerisation. Eur Polym J 2000;36:1323–31.
[185] Wang J, Liang G, Zhao W, Lü S, Zhang Z. Studies on surface modification of UHMWPE fibers via UV initiated grafting. Appl Surf Sci 2006;253:668–73.
[186] Needles HL, Park M-J. The effect of *N*,*N*-dimethylformamide and polymer grafting on the morphology of polyester fibers in fabric substrate. J Appl Polym Sci 1996;59:1683–98.
[187] Hassan MM, Islam MR, Sawpan MA, Khan MA. Effect of silane monomer on the improvement of mechanical and degradable properties of photografted jute yarn with acrylamide. J Appl Polym Sci 2003;89:3530–8.
[188] Sawpan MA, Khan MA, Abedin MZ. Surface modification of jute yarn by photografting of low-glass transition temperature monomers. J Appl Polym Sci 2003;87:993–1000.
[189] Khan F, Ahmad SR. Graft copolymerization and characterization of 2-hydroxyethyl methacrylate onto jute fiber by photoirradiation. J Appl Polym Sci 2006;101:2898–910.
[190] Gangopadhyay R, Ghosh P. Uncatalyzed photografting of polyacrylamide from functionalized cellulose and lignocellulosic materials. J Appl Polym Sci 1999;74:1623–34.
[191] Kubota H, Shigehisa Y. Introduction of amidoxime groups into cellulose and its ability to adsorb metal ions. J Appl Polym Sci 1995;56:147–51.
[192] Khan F. Photoinduced graft-copolymer synthesis and characterization of methacrylic acid onto natural biodegradable lignocellulose fiber. Biomacromolecules 2004;5:1078–88.
[193] Kubota H, Ujita S. Reactivity of glycidyl-methacrylate-grafted cellulose prepared by means of photografting. J Appl Polym Sci 1995;56:25–31.
[194] Gangopadhyay R, Ghosh P. Uncatalysed photografting of poly(methyl methacrylate) from photofunctionalized sisal fiber. Eur Polym J 2000;36:1597–606.
[195] Shirai Y, Shirai K, Tsubokawa N. Effective grafting of polymers onto ultrafine silica surface: photopolymerization of vinyl monomers initiated by the system consisting of trichloroacetyl groups on the surface and $Mn_2(CO)_{10}$. J Polym Sci: Part A: Polym Chem 2001;39:2157–63.
[196] Panasyuk-Delaney T, Mirsky VM, Wolfbeis OS. Capacitive creatinine sensor based on a photografted molecularly imprinted polymer. Electroanalysis 2002;14:221–4.
[197] Amornsakchai T, Kubota H. Photoinitiated grafting of methyl methacrylate on highly oriented polyethylene: effect of draw ratio on grafting. J Appl Polym Sci 1998;70:465–70.
[198] Zhang ZD, Kong LB, Deng JP, Yang P, Yang WT. Photografting of unable-to-be-irradiated surfaces. I. Batch vapor-phase process by one-step method. J Appl Polym Sci 2006;101:2269–76.
[199] Zhang ZD, Kong LB, Deng JP, Luo HY, Yang WT. Photografting of unable-to-be-irradiated surfaces. I. Batch liquid-phase process by one-step method. J Appl Polym Sci 2007;103:118–24.
[200] Wang H, Brown HR. Atomic force microscopy study of the photografting of glycidyl methacrylate onto HDPE and the microstructure of the grafted chains. Polymer 2007;48: 477–87.
[201] Uchida E, Ikada Y. Topography of polymer chains grafted on a polymer surface underwater. Macromolecules 1997;30:5464–9.
[202] Curti PS, de Moura MR, Veiga W, Radovanovic E, Rubira AF, Muniz EC. Characterization of PNIPAAm photografted on PET and PS surfaces. Appl Surf Sci 2005;245:223–33.
[203] Costamagna V, Wunderlin D, Larrañaga M, Mondragon I, Strumia M. Surface functionalization of polyolefin films via the ultraviolet-induced photografting of acrylic acid: topographical characterization and ability for binding antifungal agents. J Appl Polym Sci 2006;102:2254–63.
[204] Choi Y-J, Ahn Y, Kang M-S, Jun H-K, Kim IS, Moon S-H. Preparation and characterization of acrylic acid-treated bacterial cellulose cation-exchange membrane. J Chem Technol Biotechnol 2004;79:79–84.
[205] Wang YX, Yang WT. MMA/DVB emulsion surface graft polymerization initiated by UV light. Langmuir 2004;20:6225–31.
[206] Wang YX, Zhong WB, Jiang N, Yang WT. Directly fabricating monolayer nanoparticles on a polymer surface by UV-induced MMA/DVB microemulsion graft polymerization. Macromol Rapid Commun 2005;26:87–92.
[207] Wang YX, Deng JP, Zhong WB, Kong LB, Yang WT. Facile surface superhydrophilic modification: NVP/MBA inverse microemulsion surface-grafting polymerization initiated by UV light. Macromol Rapid Commun 2005;26:1788–93.
[208] Wang YX, Bai YW, Zhong WB, Huang WQ, Yang WT. Direct construction of discrete large spherical functional particles onto organic material surfaces by photografting polymerization. Macromolecules 2007;40:756–9.
[209] Wang YX, Qiu ZB, Yang WT. One-pot fabrication of supramolecular polymer particles via situ polymerization stringed assembly of a two-monomer microemulsion. Macromol Rapid Commun 2006;27:284–8.
[210] Sui Y, Zhao JB, Gan SH, Zhao HC, Yang WT. Surface-initiated ring-opening polymerization of ε-caprolactone from the surface of PP film. J Appl Polym Sci 2007;105:877–84.
[211] Yang P, Deng JY, Yang WT. Confined photo-catalytic oxidation: a fast surface hydrophilic modification method for polymeric materials. Polymer 2003;44:7157–64.
[212] Zhao HC, Yang P, Deng JP, Liu LY, Zhu JW, Sui Y, et al. Fabrication of a molecular-level multilayer film on organic polymer surface via chemical bonding assembly. Langmuir 2007;23: 1810–4.
[213] Wang LF, Yu YB, Liu LY, Yang WT. Surface photografting polymerization of trimethylolpropane triacrylate onto LDPE substrate in tetrahydrofuran/water mixtures. J Appl Polym Sci 2007;106: 621–9.
[214] Kubota H, Koyama M. Photografting of methacrylic acid on low-density polyethylene film in presence of polyfunctional monomers. J Appl Polym Sci 1997;63:1635–41.
[215] Park S, Bearinger JP, Lautenschlager EP, Castner DG, Healy KE. Surface modification of poly(ethylene terephthalate) angioplasty balloons with a hydrophilic poly(acrylamide-co-ethylene glycol) interpenetrating polymer network coating. J Biomed Mater Res (Appl Biomater) 2000;53:568–76.
[216] Yang H, Lazos D, Ulbricht M. Thin, highly crosslinked polymer layer synthesized via photoinitiated graft copolymerization on a self-assembled-monolayer-coated gold surface. J Appl Polym Sci 2005;97:158–64.
[217] Jikei M, Kakimoto M. Hyperbranched polymers: a promising new class of materials. Prog Polym Sci 2001;26:1233–85.
[218] Hirao A, Hayashi M, Loykulnant S, Sugiyama K, Ryu SW, Haraguchi N, et al. Precise syntheses of chain-multi-functionalized polymers, star-branched polymers, star-linear block polymers, densely branched polymers, and dendritic branched polymers based on iterative approach using functionalized 1,1-diphenylethylene derivatives. Prog Polym Sci 2005;30:111–82.
[219] Lee HJ, Nakayama Y, Matsuda T. Spatio-resolved, macromolecular architectural surface: highly branched graft polymer via photochemically driven quasiliving polymerization technique. Macromolecules 1999;32:6989–95.
[220] Nakayama Y, Sudo M, Uchida K, Matsuda T. Spatio-resolved hyperbranched graft polymerized surfaces by iniferter-based photograft copolymerization. Langmuir 2002;18:2601–6.
[221] Higashi J, Nakayama Y, Marchant RE, Matsuda T. High-spatioresolved microarchitectural surface prepared by photograft copolymerization using dithiocarbamate surface preparation and cellular responses. Langmuir 1999;15:2080–8.
[222] Vasilets VN, Shandryuk GA, Savenkov GN, Shatalova AM, Bondarenko GN, Talroze RV, et al. Liquid crystal polymer brush with hydrogen bonds: structure and orientation behavior. Macromolecules 2004;37:3685–8.

[223] Zhong WB, Deng JP, Wang YX, Yang WT. Oxidative graft polymerization of aniline on the modified surface of polypropylene films. J Appl Polym Sci 2007;103:2442–50.
[224] Zhong WB, Chen XH, Liu SM, Wang YX, Yang WT. Synthesis of highly hydrophilic polyaniline nanowires and sub-micro/nanostructured dendrites on poly(propylene) film surfaces. Macromol Rapid Commun 2006;27:563–9.
[225] Zhong WB, Liu SM, Chen XH, Wang YX, Yang WT. High-yield synthesis of superhydrophilic polypyrrole nanowire networks. Macromolecules 2006;39:3224–30.
[226] Ma Z, Gao C, Yuan J, Ji J, Gong Y, Shen J. Surface modification of poly-L-lactide by photografting of hydrophilic polymers towards improving its hydrophilicity. J Appl Polym Sci 2002;85:2163–71.
[227] Janorkar AV, Proulx SE, Metters AT, Hirt DE. Surface-confined photopolymerization of single- and mixed-monomer systems to tailor the wettability of poly(L-lactide) film. J Polym Sci: Part A: Polym Chem 2006;44:6534–43.
[228] Zhao B, Neoh KG, Liu FT, Kang ET. Enhancement of electrical stability of polyaniline films in aqueous media by surface graft copolymerization with hydrophobic monomers. Langmuir 1999;15:8259–64.
[229] Zhang J, Khong KT, Kang ET. Surface passivation of Nylon-6,6 films by graft copolymerization for reduction of moisture sorption. J Appl Polym Sci 2000;78:1366–73.
[230] Zeiler T, Kellermann S, Münstedt H. Different surface treatments to improve the adhesion of polypropylene. J Adhes Sci Technol 2000;14:619–34.
[231] Tahara M, Cuong NK, Nakashima Y. Improvement in adhesion of polyethylene by glow-discharge plasma. Surf Coat Technol 2003;173/174:826–30.
[232] Hintze-Brüning H, Borgholte H. Coating of untreated polypropylene with halogen free aqueous materials. Prog Org Coat 2000;40:49–54.
[233] Wang HL. Improving the adhesion of polyethylene by UV grafting. J Adhes 2006;82:731–45.
[234] Kang ET, Shi JL, Neoh KG, Tang KL, Liaw DJ. Surface modification of polytetrafluoroethylene films via graft copolymerization for autoadhesion. J Polym Sci: Part A: Polym Chem 1998;36:3107–14.
[235] Kang ET, Neoh KG, Shi JL, Tan KL, Liaw DJ. Surface modification of polymers for adhesion enhancement. Polym Adv Technol 1999;10:20–9.
[236] Ei Kholdi O, Lecamp L, Lebaudy P, Bunel C, Alexandre S. Modification of adhesive properties of a polyethylene film by photografting. J Appl Polym Sci 2004;92:2803–11.
[237] Lei J, Gao J, Jiang L. Structure and adhesion properties of linear low-density polyethylene powders grafted with acrylic acid via ultraviolet light. J Appl Polym Sci 2006;100:2549–53.
[238] Zhang J, Kato K, Uyama Y, Ikada Y. Surface graft polymerization of glycidyl methacrylate onto polyethylene and the adhesion with epoxy resin. J Polym Sci: Part A: Polym Chem 1995;33:2629–38.
[239] Castell P, Wouters M, de With G, Fischer H, Huijs F. Surface modification of poly(propylene) by photoinitiators: improvement of adhesion and wettability. J Appl Polym Sci 2004;92:2341–50.
[240] Yamada K, Takeda S, Hirata M. Improvement of autohesive and adhesive properties of polyethylene plates by photografting with glycidyl methacrylate. J Appl Polym Sci 2007;103:493–500.
[241] Yamada K, Kimura J, Hirata M. Autohesive properties of polyolefins photografted with hydrophilic monomers. J Appl Polym Sci 2003;87:2244–52.
[242] Li B, Chen W, Liu X, Wang X, Zhou Q. Preparation of temperature-sensitive polymer films by surface photografting techniques. Polym Adv Technol 2002;13:239–41.
[243] Liang L, Rieke PC, Fryxell GE, Liu J, Engehard MH, Alford KL. Temperature-sensitive surfaces prepared by UV photografting reaction of photosensitizer and *N*-isopropylacrylamide. J Phys Chem B 2000;104:11667–73.
[244] Kubota H, Shiobara N. Photografting of *N*-isopropylacrylamide on cellulose and temperature-responsive character of the resulting grafted cellulose. React Funct Polym 1998;37:219–24.
[245] Sebra RP, Kasko AM, Anseth KS, Nowman CN. Synthesis and photografting of highly pH-responsive polymer chains. Sens Actuators B 2006;119:127–34.
[246] Rånby B. Photoinitiated modification of polymers: photocrosslinking, surface photografting, and photolamination. Mater Res Innov 1998;2:64–71.
[247] Rånby B, Yang WT, Tretinnikov ON, Tokarev V, Xu YH. Lamination of polymer films by bulk surface photografting process and properties. Chin J Polym Sci 2001;19:123–7.
[248] Wang T, Kang ET, Neoh KG. Surface modification of low-density polyethylene films by UV-induced graft copolymerization and its relevance to photolamination. Langmuir 1998;14:921–7.
[249] Wang H, Brown HR. Lamination of high-density polyethylene by bulk photografting and the mechanism of adhesion. J Appl Polym Sci 2005;97:1097–106.
[250] Svec F, Fréchet JMJ. New designs of macroporous polymers and supports: from separation to biocatalysis. Science 1996;273:205–11.
[251] Scec F, Fréchet JMJ. Molded rigid monolithic porous polymers: an inexpensive, efficient, and versatile alternative to beads for the design of materials for numerous applications. End Eng Chem Res 1999;38:34–48.
[252] Rohr T, Hilder EF, Donovan JJ, Svec F, Fréchet JMJ. Photografting and the control of surface chemistry in three-dimensional porous polymer monoliths. Macromolecules 2003;36:1677–84.
[253] Pucci V, Raggi MA, Svec F, Fréchet JMJ. Monolithic columns with a gradient of functionalities prepared via photoinitiated grafting for separations using capillary electrochromatography. J Sep Sci 2004;27:779–88.
[254] Hilder EF, Svec F, Fréchet JMJ. Shielded stationary phases based on porous polymer monoliths for the capillary electrochromatography of highly basic biomolecules. Anal Chem 2004;76:3887–92.
[255] Stachowiak TB, Rohr T, Hilder EF, Peterson DS, Yi M, Svec F, et al. Fabrication of porous polymer monoliths covalently attached to the walls of channels in plastic microdevices. Electrophoresis 2003;24:3689–93.
[256] Rondelez Y, Tresset G, Tabata KV, Arata H, Fujita H, Takeuchi S, et al. Microfabricated arrays of femtoliter chambers allow single molecule enzymology. Nat Biotechnol 2005;23:361–5.
[257] Lion N, Rohner TC, Dayon L, Arnaud IL, Damoc E, Youhnovski N, et al. Microfluidic systems in proteomics. Electrophoresis 2003;24:3533–62.
[258] Sia SK, Whitesides GM. Microfluidic devices fabricated in poly(dimethylsiloxane) for biological studies. Electrophoresis 2003;24:3563–76.
[259] Walker GM, Zeringue HC, Beebe DJ. Microenvironment design considerations for cellular scale studies. Lab Chip 2004;4:91–7.
[260] Mela P, Onclin S, Goedbloed MH, Levi S, Garcia-Parajo MF, van Hulst NF, et al. Monolayer-functionalized microfluidics devices for optical sensing of acidity. Lab Chip 2005;5:163–70.
[261] Delamarche E, Bernard A, Schmid H, Michel B, Biebuyck H. Patterned delivery of immunoglobulins to surfaces using microfluidic networks. Science 1997;276:779–81.
[262] Zhao B, Moore JS, Beebe DJ. Principles of surface-directed liquid flow in microfluidic channels. Anal Chem 2002;74:4259–68.
[263] Yakovleva J, Davidsson R, Bengtsson M, Laurell T. Microfluidic enzyme immunosensors with immobilized protein A and G using chemiluminescence detection emneus. J Biosens Bioelectron 2003;19:21–34.
[264] Hu S, Ren X, Bachman M, Sims CE, Li GP, Allbritton NL. Surface modification of poly(dimethylsiloxane) microfluidic devices by ultraviolet polymer grafting. Anal Chem 2002;74:4117–23.
[265] Hu S, Ren X, Bachman M, Sims CE, Li GP, Allbritton NL. Surface-directed, graft polymerization within microfluidic channels. Anal Chem 2004;76:1865–70.
[266] Hu S, Ren X, Bachman M, Sims CE, Li GP, Allbritton NL. Tailoring the surface properties of poly(dimethylsiloxane) microfluidic devices. Langmuir 2004;20:5569–74.
[267] Hu S, Ren X, Bachman M, Sims CE, Li GP, Allbritton NL. Cross-linked coatings for electrophoretic separations in poly(dimethylsiloxane) microchannels. Electrophoresis 2003;24:3679–88.
[268] Peterson DS, Rohr T, Svec F, Fréchet JMJ. Dual-function microanalytical device by in situ photolithographic grafting of porous polymer monolith: integrating solid-phase extraction and enzymatic digestion for peptide mass mapping. Anal Chem 2003;75:5328–35.
[269] Stachowiak TB, Svec F, Fréchet JMJ. Patternable protein resistant surfaces for multifunctional microfluidic devices via surface hydrophilization of porous polymer monoliths using photografting. Chem Mater 2006;18:5950–7.
[270] Rohr T, Ogletree DF, Svec F, Fréchet JMJ. Surface functionalization of thermoplastic polymers for the fabrication of microfluidic devices by photoinitiated grafting. Adv Funct Mater 2003;13:264–70.
[271] Ebara M, Hoffman JM, Stayton PS, Hoffman AS. Surface modification of microfluidic channels by UV-mediated graft polymerization of non-fouling and 'smart' polymers. Radiat Phys Chem 2007;76:1409–13.
[272] Pu Q, Oyesanya O, Thompson B, Liu S, Alvarez JC. On-chip micropatterning of plastic (cyclic olefin copolymer, COC) microfluidic channels for the fabrication of biomolecule microarrays using photographing methods. Langmuir 2007;23:1577–83.
[273] Stachowiak TB, Mair DA, Holden TG, Lee LJ, Svec F, Fréchet JMJ. Hydrophilic surface modification of cyclic olefin copolymer

microfluidic chips using sequential photografting. J Sep Sci 2007; 30:1088–93.
[274] Li C, Yang Y, Craighead HG, Lee KH. Isoelectric focusing in cyclic olefin copolymer microfluidic channels coated by polyacrylamide using a UV photografting method. Electrophoresis 2005;26:1800–6.
[275] Besson E, Gue A-M, Sudor J, Korri-Youssoufi H, Jaffrezic N, Tardy J. A novel procedure for patterning hydrophobic and hydrophilic SAMs for microfluidic devices by using UV photolithography. Langmuir 2006;22:8346–52.
[276] Yang P, Zhang X, Xie J, Chen J, Yang WT. Micro/nanoscale well and channel fabrication on organic polymer substrates via a combination of photochemical and alkaline hydrolysis etchings. Biomacromolecules 2006;7:2770–5.
[277] Ulbricht M. Advanced functional polymer membranes. Polymer 2006;47:2217–62.
[278] Hickner MA, Ghassemi H, Kim YS, Einsla BR, McGrath JE. Alternative polymer systems for proton exchange membranes (PEM). Chem Rev 2004;104:4587–612.
[279] Klein E. Affinity membranes: a 10-years review. J Membr Sci 2000;179:1–27.
[280] Adhikari B, Majumdar S. Polymers in sensor applications. Prog Polym Sci 2004;29:699–766.
[281] Bakker E, Bühlmann Ph, Pretsch E. Polymer membrane ion-selective electrodes—what are the limits? Electroanalysis 1999;11:915–33.
[282] Okimoto K, Ohike A, Ibuki R, Aoki O, Ohnishi N, Rajewski RA, et al. Factors affecting membrane-controlled drug release for an osmotic pump tablet (OPT) utilizing $(SBE)_{7m}$-β-CD as both a solubilizer and osmotic agent. J Control Rel 1999;60:311–9.
[283] Davaran S, Rashidi MR, Khandaghi R, Hashemi M. Development of a novel prolonged-release nicotine transdermal patch. Pharm Res 2005;51:233–7.
[284] Yang Q, Hu M-X, Dai Z-W, Tian J, Xu Z-K. Fabrication of glycosylated surface on polymer membrane by UV-induced graft polymerization for lectin recognition. Langmuir 2006;22:9345–9.
[285] Yang Q, Xi Z-K, Hu M-X, Li J-J, Wu J. Novel sequence for generating glycopolymer tethered on a membrane surface. Langmuir 2005;21:10717–23.
[286] Yang Q, Tian J, Hu M-X, Xu Z-K. Construction of a comb-like glycosylated membrane surface by a combination of UV-induced graft polymerization and surface-initiated ATRP. Langmuir 2007;23:6684–90.
[287] Saha S, Chakma A. Selective CO_2 separation from CO_2/C_2H_6 mixture by immobilized diethanolamine/PEO membranes. J Membr Sci 1995;98:157–71.
[288] Quinn R, Laciak D. Polyelectrolyte membranes for acid gas separations. J Membr Sci 1997;131:49–60.
[289] Kim JH, Ha SY, Nam SY, Rhim JW, Baek KH, Lee YM. Selective permeation of CO_2 through pore-filled polyacrylonitrile membrane with poly(ethylene glycol). J Membr Sci 2001;186:97–107.
[290] Yang J-M, Chian CPC, Hsu K-Y. Oxygen permeation in SBS-*g*-DMAEMA copolymer membrane prepared by UV photografting without degassing. J Membr Sci 1999;153:175–82.
[291] Porter JJ. Recovery of polyvinyl alcohol and hot water from the textile wastewater using thermally stable membranes. J Membr Sci 1998;151:45–53.
[292] Sanchuan Y, Congjie G, Hexiang S, Meihong L. Nanofiltration used for desalination and concentration in dye production. Desalination 2001;140:97–100.
[293] Van der Bruggen B, Daems B, Wilms D, Vandecasteele C. Mechanisms retention and flux decline for the nanofiltration of dye baths from the textile industry. Sep Purif Technol 2001;22/23:519–28.
[294] Van Der Bruggen B, Cornelis G, Vandecasteele C, Devreese I. Fouling of nanofiltration and ultrafiltration membranes applied for wastewater regeneration in the textile industry. Desalination 2005;175:111–9.
[295] Akbari A, Desclaux S, Rouch JC, Aptel P, Remigy JC. New UV-photografted nanofiltration membranes for the treatment of colored textile dye effluents. J Membr Sci 2006;286:342–50.
[296] Akbari A, Desclaux S, Rouch JC, Remigy JC. Application of nanofiltration hollow fibre membranes, developed by photografting, to treatment of anionic dye solutions. J Membr Sci 2007;297: 243–52.
[297] Asano M, Chen J, Maekawa Y, Sakamura T, Kubota H, Yoshida M. Novel UV-induced photografting process for preparing poly(tetrafluoroethylene)-based proton-conducting membranes. J Polym Sci: Part A: Polym Chem 2007;45:2624–37.
[298] Chen J, Asano M, Maekawa Y, Sakamura T, Kubota H, Yoshida M. Preparation of ETFE-based fuel cell membranes using UV-induced photografting and electron beam-induced crosslinking techniques. J Membr Sci 2006;283:373–9.
[299] Balakrishnan M, Dua M, Bhagat JJ. Effect of operation parameters on sugarcane juice ultrafiltration: results of a field experience. Sep Purif Technol 2000;19:209–20.
[300] Bhattacharya PK, Agarwal S, De S, Gopal UVSR. Ultrafiltration of sugarcane juice for recovery of sugar: analysis of flux and retention. Sep Purif Technol 2001;21:247–59.
[301] Balakrishnan M, Dua M, Khairnar PN. Significance of membrane type and feed stream in the ultrafiltration of sugarcane juice. Sep Sci Technol 2001;36:619–37.
[302] Nystrom M, Jarvinen P. Modification of polysulfone ultrafiltration membrane with UV irradiation and hydrophilicity increasing agent. J Membr Sci 1991;60:275–96.
[303] Sivik B, Wahlgren M, Miezis Y. A rheological screening method for membrane modification membrane polymer. Desalination 1990;77:181–93.
[304] Taniguchi M, Kilduff JE, Belfort G. Low fouling synthetic membranes by UV-assisted graft polymerization: monomer selection to mitigate fouling by natural organic matter. J Membr Sci 2003; 222:59–70.
[305] Kilduff JE, Mattaraj S, Pieracci JP, Belfort G. Photochemical modification of poly(ether sulfone) and sulfonated poly(sulfone) nanofiltration membranes for control of fouling by natural organic matter. Desalination 2000;132:133–42.
[306] Taniguchi M, Belfort G. Low protein fouling synthetic membranes by UV-assisted surface grafting modification: varying monomer type. J Membr Sci 2004;231:147–57.
[307] Susanto H, Balakrishnan M, Ulbricht M. Via surface functionalization by photograft copolymerization to low-fouling polyethersulfone-based ultrafiltration membranes. J Membr Sci 2007;288:157–67.
[308] Kang JS, Lee SJ, Huh H, Shim JK, Lee YM. Preparation of chlorinated poly(vinyl chloride)-*g*-poly(*N*-vinyl-2-pyrrolidinone) membranes and their water permeation properties. J Appl Polym Sci 2003;88:3188–95.
[309] Hilal N, Al-Khatib L, Atkin BP, Kochkodan V, Potapchenko N. Photochemical modification of membrane surfaces for (bio)fouling reduction: a nano-scale study using AFM. Desalination 2003;158:65–72.
[310] Yang JM, Wang MC, Hsu YG, Chang CH. The properties of SBS-VP copolymer membrane prepared by UV photografting without degassing. J Membr Sci 1997;128:133–40.
[311] Mosbach K. Molecular imprinting. Trends Biochem Sci 1994;19: 9–14.
[312] Wulff G. Biorecognition in molecularity imprinted polymers: concept, chemistry and applications. In: Ngo T, editor. Molecular interactions in bioseparations. New York: Plenum Press; 1993. p. 363–81.
[313] Sellergren B, Shea KJ. Chiral ion-exchange chromatography correlation between solute retention and a theoretical ion-exchange model using imprinted polymers. J Chromatogr A 1993;654:17–28.
[314] Vlatakis G, Andersson LI, Muller R, Mosbach K. Drug assay using antibody mimics made by molecular imprinting. Nature 1993;361:645–7.
[315] Kobayashi T, Wang HY, Fujii N. Molecular imprinting of theophylline in acrylonitrile-acrylic acid copolymer membranes. Chem Lett 1995;24:927–8.
[316] Wang HY, Kobayashi T, Fujii N. Preparation of molecular imprint membranes by the phase inversion precipitation technique. Langmuir 1996;12:4850–6.
[317] Wang HY, Kobayashi T, Fujii N. Surface molecular imprinting on photosensitive dithiocarbamoyl polyacrylonitrile membranes using photograft polymerization. J Chem Tech Biotechnol 1997;70:355–62.
[318] Piletsky SA, Matuschewski H, Schedler U, Wilpert A, Piletska EV, Thiele TA, et al. Surface functionalization of porous polypropylene membranes with molecularly imprinted polymers by photograft copolymerization in water. Macromolecules 2000;33: 3092–8.
[319] Sergeyeva TA, Matuschewski H, Piletsky SA, Bendig J, Schedler U, Ulbricht M. Molecularly imprinted polymer membranes for substance-selective solid-phase extraction from water by surface photo-grafting polymerisation. J Chromatogr A 2001;907:89–99.
[320] Mika AM, Childs RF, Dickson JM, McCarry BE, Gagnon DR. A new class of polyelectrolyte-filled microfiltration membranes with environmentally controlled porosity. J Membr Sci 1995;108:37–56.

[321] Ulbricht M. Photograft-polymer-modified microporous membranes with environment-sensitive permeabilities. React Funct Polym 1996;31:165–77.
[322] Park YS, Ito Y, Imanishi Y. Permeation control through porous membranes immobilized with thermosensitive polymer. Langmuir 1998;14:910–4.
[323] Choi YJ, Yamaguchi T, Nakao SI. A novel separation system using porous thermosensitive membranes. Ind Eng Chem Res 2000;39:2491–5.
[324] Chung DJ, Ito Y, Imanishi Y. Preparation of porous membranes grafted with poly(spiropyran-containing methacrylate) and photocontrol of permeability. J Appl Polym Sci 1994;51:2027–33.
[325] Yang B, Yang WT. Thermo-sensitive switching membranes regulated by pore-covering polymer brushes. J Membr Sci 2003;218: 247–55.
[326] Peng T, Cheng Y-L. Temperature-responsive permeability of porous PNIPAAm-*g*-PE membranes. J Appl Polym Sci 1998;70:2133–42.
[327] Wu G, Li Y, Han M, Liu X. Novel thermo-sensitive membranes prepared by rapid bulk photo-grafting polymerization of *N*,*N*-diethylacrylamide onto the microfiltration membranes Nylon. J Membr Sci 2006;283:13–20.
[328] Lequieu W, Shtanko NI, Du Prez FE. Track etched membranes with thermo-adjustable porosity and separation properties by surface immobilization of poly(*N*-vinylcaprolactam). J Membr Sci 2005;256:64–71.
[329] Geismann C, Ulbricht M. Photoreactive functionalization of poly(ethylene terephthalate) track-etched pore surfaces with "smart" polymer system. Macromol Chem Phys 2005;206: 268–81.
[330] Shim JK, Lee YB, Lee YM. pH-dependent permeation through polysulfone ultrafiltration membranes prepared by ultraviolet polymerization technique. J Appl Polym Sci 1999;74:75–82.
[331] Kaeselev B, Kingshott P, Jonsson G. Influence of the surface structure on the filtration performance of UV-modified PES membranes. Desalination 2002;146:265–71.
[332] Qiu C, Xu F, Nguyen QT, Ping Z. Nanofiltration membrane prepared from cardo polyetherketone ultrafiltration membrane by UV-induced grafting method. J Membr Sci 2005;255:107–15.
[333] Yang B, Yang WT. Photografting modification of PET nucleopore membranes. J Macromol Sci Part A-Pure Appl Chem 2003;A40: 309–20.
[334] Yang B, Yang WT. Novel pore-covering membrane as a full open/close valve. J Membr Sci 2005;258:133–9.
[335] Salam A, Ulbricht M. Effect of surface modification on the synthesis of pore-filling polymeric monoliths in microfiltration membranes made from poly(propylene) and poly(ethylene terephthalate). Macromol Mater Eng 2007;292:310–8.
[336] Hilal N, Al-Khatib L, Al-Zoubi H, Nigmatullin R. Atomic force microscopy study of membranes modified by surface grafting of cationic polyelectrolyte. Desalination 2005;184:45–55.
[337] Yamada K, Nagano R, Hirata M. Adsorption and desorption properties of the chelating membranes prepared from the PE films. J Appl Polym Sci 2006;99:1895–902.
[338] Yamada K, Saitoh Y, Haga Y, Matsuda K, Hirata M. Adsorption and desorption properties of grafted polyethylene films modified with polyethylenimine chains. J Appl Polym Sci 2006;102:5965–76.
[339] Wang WC, Neoh KG, Kang ET, Lim SL, Yuan D. Metal ion reduction and resultant deposition on viologen-functionalized LDPE films and viologen-containing microporous membranes. J Colloid Interface Sci 2004;279:391–8.
[340] Yeon K-H, Song J-H, Kim J-B, Moon S-H. Preparation and characterization of UV-grafted ion-exchange textiles in continuous electrodeionization. J Chem Technol Biotechnol 2004;79:1395–404.
[341] Zhong WB, Yang YS, Yang WT. Oxidative graft polymerization of aniline on the surface of poly(propylene)-graft-polyacrylic acid films. Thin Solid Films 2005;479:24–30.
[342] Klueh U, Wagner V, Kelly S, Johnson A, Bryers JD. Efficacy of silver-coated fabric to prevent colonization and subsequent device-based biofilm formation. J Biomed Mater Res Part B: Appl Biomater 2000;53B:621–31.
[343] Hipler UC, Elsner P, Fluhr JW. Antifungal and antibacterial properties of a silver-loaded cellulosic fiber. J Biomed Mater Res Part B: Appl Biomater 2006;77B:156–63.
[344] Shearer AEH, Paik JS, Hoover DG, Haynie SL, Kelley MJ. Potential of an antibacterial ultraviolet-irradiated Nylon film. Biotechnol Bioeng 2000;67:141–6.
[345] Choi JY, Kim KH, Choy KC, Oh KT, Kim KN. Photocatalytic antibacterial effect of TiO_2 film formed on Ti and TiAg exposed to *lactobacillus acidophilus*. J Biomed Mater Res Part B: Appl Biomater 2007;80B:353–9.
[346] Braunecker WA, Matyjaszewski K. Controlled/living radical polymerization: Features, developments, and perspectives. Prog Polym Sci 2007;32:93–146.
[347] Shanmugasundaram N, Sundaraseelan J, Uma S, Selvaraj D, Babu M. Design and delivery of silver sulfadiazine from alginate microspheres-impregnated collagen scaffold. J Biomed Mater Res Part B: Appl Biomater 2006;77B:378–88.
[348] Hazziza-Laskar J, Helary G, Sauvet G. Biocidal polymers active by contact. IV. Polyurethanes based on polysiloxanes with pendant primary alcohols and quaternary ammonium groups. J Appl Polym Sci 1995;58:77–84.
[349] Qin C, Xiao Q, Li H, Fang M, Liu Y, Chen X, et al. Calorimetric studies of the action of chitosan-*N*-2-hydroxypropyl trimethyl ammonium chloride on the growth of microorganisms. Int J Biol Macromol 2004;34:121–6.
[350] Tiller JC, Lee SB, Lewis K, Klibanov AM. Polymer surfaces derivatized with poly(vinyl-*N*-hexylpyridinium) kill airborne and waterborn bacteria. Biotechnol Bioeng 2002;79:465–71.
[351] Nonaka T, Noda E, Kurihara S. Graft copolymerization of vinyl monomers bearing positive charges or episulfide groups onto loofah fibers and their antibacterial activity. J Appl Polym Sci 2000;77:1077–86.
[352] Jayakumar R, Nwe N, Tokura S, Tamura H. Sulfated chitin and chitosan as novel biomaterials. Int J Biol Macromol 2007;40:175–81.
[353] Xing CM, Deng JP, Yang WT. Synthesis of antibacterial polypropylene film with surface immobilized polyvinylpyrrolidone–iodine complex. J Appl Polym Sci 2005;97:2026–31.
[354] Shi Z, Neoh KG, Kang ET. Antibacterial activity of polymeric substrate with surface grafted viologen moieties. Biomaterials 2005;26:501–8.
[355] Yang MR, Chen KS, Tsai JC, Tseng CC, Lin SF. The antibacterial activities of hydrophilic-modified nonwoven PET. Mater Sci Eng C 2002;20:167–73.
[356] Yeh PYJ, Kizhakkedathu JN, Madden JD, Chiao M. Electric field and vibration-assisted nanomolecule desorption and antibiofouling for biosensor application. Colloids Surf B: Biointerfaces 2007;59:67–73.
[357] Zhang F, Kang ET, Neoh KG, Wang P, Tan KL. Surface modification of stainless steel by grafting of poly(ethylene glycol) for reduction in protein adsorption. Biomaterials 2001;22:1541–8.
[358] Courtney JM, Lamba NMK, Sundaram S, Forbes CD. Biomaterials for blood-contacting applications. Biomaterials 1994;15:737–44.
[359] Ratner BD. The blood compatibility catastrophe. J Biomed Mater Res 1993;27:283–7.
[360] Ikada Y. Surface modification of polymers for medical applications. Biomaterials 1994;15:725–36.
[361] Lazos D, Franzka S, Ulbricht M. Size-selective protein adsorption to polystyrene surfaces by self-assembly grafted poly(ethylene glycols) with varied chain lengths. Langmuir 2005;21: 8774–84.
[362] Goda T, Konno T, Takai M, Ishihara K. Photoinduced phospholipid polymer grafting on parylene film: advanced lubrication and antibiofouling properties. Colloids Surf B: Biointerfaces 2007;54:67–73.
[363] Richey T, Iwata H, Oowaki H, Uchida E, Matsuda S, Ikada Y. Surface modification of polyethylene balloon catheters for local drug delivery. Biomaterials 2000;21:1057–65.
[364] Gonen-Wadmany M, Oss-Ronen L, Seliktar D. Protein–polymer conjugates for forming photopolymerizable biomimetic hydrogels for tissue engineering. Biomaterials 2007;28:3876–86.
[365] Larsson A, Ekblad T, Andersson O, Liedberg B. Photografted poly(ethylene glycol) matrix for affinity interaction studies. Biomacromolecules 2007;8:287–95.
[366] Bird CL, Kuhn AT. Electrochemistry of the viologens. Chem Soc Rev 1981;10:49–82.
[367] Silva SD, Cosnier S, Almeida MG, Moura JGJ. An efficient poly(pyrrole-viologen)-nitrite reductase biosensor for the mediated detection of nitrite. Electrochem Commun 2004;6:404–8.
[368] Yamaguchi H, Harada A. Amplification of detection signals for methyl viologen by using supramolecular formation of antibody with viologen dimmer in surface Plasmon resonance sensor. Chem Lett 2002;31:382–3.
[369] Liu X, Neoh KG, Zhao LP, Kang ET. Surface functionalization of glass and polymeric substrates via graft copolymerization of viologen in an aqueous medium. Langmuir 2002;18:2914–21.
[370] Delaney TL, Zimin D, Rahm M, Weiss D, Wolfbeis OS, Mirsky VM. Capacitive detection in ultrathin chemosensors prepared by

molecularly imprinted grafting photopolymerization. Anal Chem 2007;79:3220–5.
[371] Akgol S, Yacinkaya Y, Bayramoglu G, Denizli A, Arica MY. Reversible immobilization of urease onto procion brown MX-5BR-Ni(II) attached polyamide hollow-fiber membranes. Process Biochem 2002;38:675–83.
[372] Furuki S. Immobilization. In: Aehle W, editor. Enzymes in industry. Weinheim: Wiley-VCH; 2004 [Section 3.3].
[373] Chen JP, Chiu SH. A poly(*N*-isopropylacrylamide-*co*-*N*-acryloxysuccinimide-*co*-2-hydroxyethyl methacrylate) composite hydrogel membrane for urease immobilization to enhance urea hydrolysis rate by temperature swing. Enzyme Microb Technol 2000;26:359–67.
[374] Ayhan F, Ayhan H, Piskin E, Tanyolac A. Optimization of urease immobilization onto non-porous HEMA incorporated poly(EGDMA) microbeads and estimation of kinetic parameters. Bioresour Technol 2002;81:131–40.
[375] Yamada K, Iizawa Y, Yamada J, Hirata M. Rentention of activity of urease immobilized on grafted polymer films. J Appl Polym Sci 2006;102:4886–96.
[376] Cen L, Neoh KG, Kang ET. Surface functionalization of polypyrrole film with glucose oxidase and viologen. Biosens Bioelectron 2003;18:363–74.
[377] Loh FC, Tang KL, Kang ET, Kato K, Uyama Y, Ikada Y. XPS characterization of surface functionalized electroactive polymers. Surf Interf Anal 1996;24:597–604.
[378] Bernacca GM, Straub I, Wheatley DJ. Mechanical and morphological study of biostable polyurethane heart valve leaflets explanted from sheep. J Biomed Mater Res 2002;61:138–45.
[379] Fini M, Torricelli P, Giavaresi G, Rotini R, Castagna A, Giardino R. In vitro study comparing two collageneous membranes in view of their clinical application for rotator cuff tendon regeneration. J Orthop Res 2007;25:98–107.
[380] Biederman H, Slavínska D. Plasma polymer films and their future prospects. Surf Coat Technol 2000;125:371–6.
[381] Ko YG, Kim YH, Park KD, Lee HJ, Lee WK, Park HD, et al. Immobilization of poly(ethylene glycol) or its sulfonate onto polymer surfaces by ozone oxidation. Biomaterials 2001;22:2115–23.
[382] Karlsson JO, Gatenholm P. Preparation and characterization of cellulose-supported HEMA hydrogels. Polymer 1997;38:4727–31.
[383] Guan JJ, Gao CY, Shen JC. Preparation of functional poly(ether-urethane) for immobilization of human living cells. I. Surface graft polymerization of poly(ether-urethane) with 2-(dimethylamino)ethyl methacrylate and quaternization of grafted membrane. Eur Polym J 2000;36:2707–13.
[384] Guan JJ, Gao CY, Feng LX, Shen JC. Surface photo grafting of polyurethane with 2-hydroxyethyl acrylate for promotion of human endothelial cell attachment and growth. J Biomater Sci Polym Ed 2000;11:523–36.
[385] Guan JJ, Gao CY, Feng LX, Shen JC. Surface modification of polyurethane for promotion of cell adhesion and growth. I. surface photo-grafting with *N*,*N*-dimethylaminoethyl methacrylate and cytocompatibility of the modified surface. J Mater Sci Mater Med 2001;12:447–52.
[386] van der Heiden AP, Goebbels D, Pijpers AP, Koole LH. A photochemical method for the surface modification of poly(etherurethanes) with phosphorylcholine-containing compounds to improve hemocompatibility. J Biomed Mater Res 1997;37:282–90.
[387] Liu J-H, Jen H-L, Chung Y-C. Surface modification of polyethylene membranes using phosphorylcholine derivatives and their platelet compatibility. J Appl Polym Sci 1999;74:2947–54.
[388] Yamamoto M, Kato K, Ikada Y. Ultrastructure of the interface between cultured osteoblasts and surface-modified polymer substrates. J Biomed Mater Res 1997;37:29–36.
[389] Zhu YB, Gao CY, Guan JJ, Shen JC. Engineering porous polyurethane scaffolds by photografting polymerization of methacrylic acid for improved endothelial cell compatibility. J Biomed Mater Res 2003;67A:1367–73.
[390] Ying L, Yin C, Zhuo RX, Leong KW, Mao HQ, Kang ET, et al. Immobilization of galactose ligands on acrylic acid graft-copolymerized poly(ethylene terephthalate) film and its application to hepatocyte culture. Biomacromolecules 2003;4:157–65.
[391] Thom VH, Altankov G, Groth Th, Jankova K, Jonsson G, Ulbricht M. Optimizing cell–surface interactions by photografting of poly(ethylene glycol). Langmuir 2000;16:2756–65.
[392] Janorkar AV, Fritz Jr EW, Burg KJL, Metters AT, Hirt DE. Grafting amine-terminated branched architectures from poly(L-lactide) film surfaces for improved cell attachment. J Biomed Mater Res Part B: Appl Biomater 2007;81B:142–52.
[393] Rabek JF. Polymer degradation: mechanisms and experimental methods. London, UK: Chapman & Hall; 1995.
[394] Fox RB. Degradation of high polymers. Prog Polym Sci 1967;1:45–89.
[395] Zhu Y, Gao C, Shen J. Surface modification of polycaprolactone with poly(methacrylic acid) and gelatin covalent immobilization for promotin its cytocompatibility. Biomaterials 2002;23:4889–95.
[396] Chan C-M, Ko T-M, Hiraoka H. Polymer surface modification by plasmas and photos. Surf Sci Rep 1996;24:1–54.
[397] Terlingen JGA, Gerritsen HFC, Hoffman AS, Feijen J. Introduction of functional groups on poethylene surfaces by a carbon dioxide plasma treatment. J Appl Polym Sci 1995;57:969–82.

Progress in Polymer Science 34 (2009) 194–209

Contents lists available at ScienceDirect

Progress in Polymer Science

journal homepage: www.elsevier.com/locate/ppolysci

Trends in Polymer Science

Photobase generators: Recent progress and application trend in polymer systems

Kanji Suyama*, Masamitsu Shirai

Department of Applied Chemistry, Osaka Prefecture University, 1-1 Gakuen-Cho, Naka-Ku, Sakai, Osaka 599-8531, Japan

ARTICLE INFO

Article history:
Received 1 March 2008
Received in revised form 12 August 2008
Accepted 12 August 2008
Available online 14 November 2008

Keywords:
Photobase generator
Organic base
Precursor
Photoremovable protecting group
Photoinitiator
Photo-crosslinking
Photolatent catalyst

ABSTRACT

Recent progress in photochemical generation of organic bases and its applications to polymer science and technologies are reviewed. Although photobase generators (PBGs) have been desired as a novel photolatent catalyst, fewer examples are known compared to photoradical and photoacid generators. In this decade, several PBGs such as carbamates, *O*-acyloximes, and ammonium salts have been improved in thermal stability, solubility, multi-functionality, and photo-sensitivity. In addition, new molecular designs including amineimides, α-aminoketones, some amidine precursors, and aromatic ureas have been proposed as novel PBGs. New applications of these PBGs have been developed in photo-induced polymerization, depolymerization, crosslinking, and de-crosslinking as well as photo-imaging.

1. Introduction

The photochemical generation of active species such as free-radicals, acids, and bases is an attractive and important process in relation to the development of technologies in coating and imaging as well as polymer synthesis. Photo-induced chemical reaction can be initiated by irradiation, and generally thermal treatment is not required. Therefore, photo-induced reaction is applied to a variety of industrial fields. In the field of polymer chemistry, photochemically generated active species can be used in polymer synthesis, polymer degradation, and changes in physical properties of polymers. These features are useful in industrial applications such as two- and three-dimensional imaging, coating, and surface modification of polymers.

The systems of photochemical generation of free-radicals and acids have been studied in detail and widely used in polymerization and polymer reactions. However, the system using free-radicals includes the inactivation process by oxygen in air. On the other hand, the use of acids also causes some problems such as corrosion of metal substrates. Bases are free from these disadvantages and versatile catalysts for various reactions. Nevertheless, there are fewer examples of photochemically base-generating systems compared to photo-radical and photoacid generators.

In this article, recent development in the preparation and photochemistry of photobase generators (PBGs) and their applications are reviewed. Since some reviews regarding PBGs [1–3] have been published, the development in this decade is mainly described.

2. Photobase generators

2.1. Recent development of photobase generators

2.1.1. Carbamates

Photolabile carbamates are one of the protected amines and are widely used as photochemical precursors of

* Corresponding author.
E-mail address: suyama@chem.osakafu-u.ac.jp (K. Suyama).

0079-6700/$ – see front matter © 2008 Elsevier Ltd. All rights reserved.
doi:10.1016/j.progpolymsci.2008.08.005

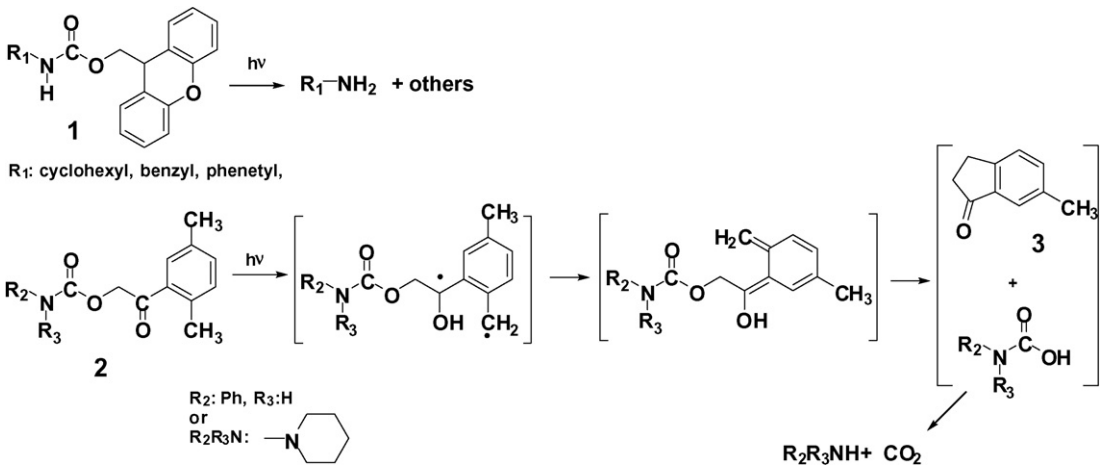

Fig. 1. Photo-generation of amines from carbamates.

primary and secondary amines. Many kinds of protecting groups have been proposed, especially, for the liberation of amino acids in biochemical applications. Photo-cleavable moieties such as *m*-nitrophenyl, 3,5-dimethoxybenzyl, 1-methyl-1-(3,5-dimethoxyphenyl)ethyl, α-methylnitropiperonyl, *o*-nitrobenzyl, 3,4-dimethoxy-6-nitrobenzyl, phenyl(*o*-nitrophenyl)methyl, 2-(2-nitrophenyl)ethyl, 6-nirtoveratryl, 4-methoxyphenacyl, and 3′,5′-dimethoxybenzoin carbamates are listed in a monograph [4].

New protecting groups for carbamates in Fig. 1 were proposed recently. **1** was a carbamate protected by 9-xanthenylmethyl group that was useful in peptide synthesis because of its stability against trifluoroacetic acid-treatment and catalytic hydrogenolysis [5]. 2,5-Dimethylphenacyl group in **2** was photochemically deprotected via *E*-isomer of photoenol [6]. After cyclized elimination of indanone **3**, a carbamic acid was produced which finally turned into CO_2 and an amine. Although the quantum yield of photo-decomposition of **2** was relatively low (<0.1), chemical yield of corresponding amine was as high as 85%.

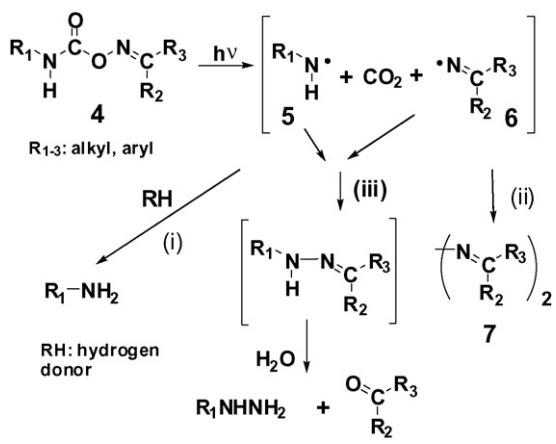

Fig. 2. Photochemical reactions of *O*-carbamoyloximes.

O-Carbamoyloximes **4** in Fig. 2 are carbamates protected by imino moiety and have also been proposed as novel PBGs [7–24]. Flash photolysis studies revealed that iminyl radical **6** was confirmed as an intermediate. From product analysis, an amine and an azine **7** were detected as products [7,11]. These results suggest that N–O bond cleavage in the excited **4** and subsequent decarboxylation proceeded, and resulting aminyl radical **5** abstracted hydrogen from surroundings to generate an amine as shown in path (i) in Fig. 2. **7** can be obtained by dimerization of **6** via path (ii). However, there is a possibility of path (iii) as observed for the formation of phenylhydrazine when R_1 was phenyl [12].

The amines generated from *O*-carbamoyloximes were applied to the photocrosslinking and imaging systems as will be described in detail in Section 3.

O-Carbamoyloxime **8** having N–H bond is a thermally less stable compared to *N*,*N*-dialkyl *O*-carbamoyloximes (**9** and **10**), because **8** tends to decompose into an isocyanate and an oxime at relatively low temperature. For example, the weight loss in thermogravimetric analysis (TGA) of **8** started around 120 °C as shown in Fig. 3 [23]. However, by introducing an alkyl-substituent at N–H position, TGA curves for **9** and **10** shifted to higher temperatures.

The introduction of rigid imide moieties such as phthalimide and naphthalimide was also effective for the increase in thermal decomposition temperature (T_d) as observed in the shift of TGA curves for **12** and **13** compared to **9** and **10**. Photoreactivity of carbamates **11**–**13** having imide moieties was lower than that of **8**–**10**, respectively, showing trade-off between photoreactivity and thermal stability. Product analysis revealed that corresponding amine was not generated by the photolysis of **10**, and the formation of other basic molecule from the carbamates was suggested.

2.1.2. *O*-Acyloximes

O-Acyloximes **14** are known to generate primary amines on irradiation as shown in Fig. 4. However, the influence of the molecular structure and required conditions for cleavages in excited states were still unclear. Thus, reaction mechanism and structure/property relationship were examined in detail. Laser spectroscopic studies revealed

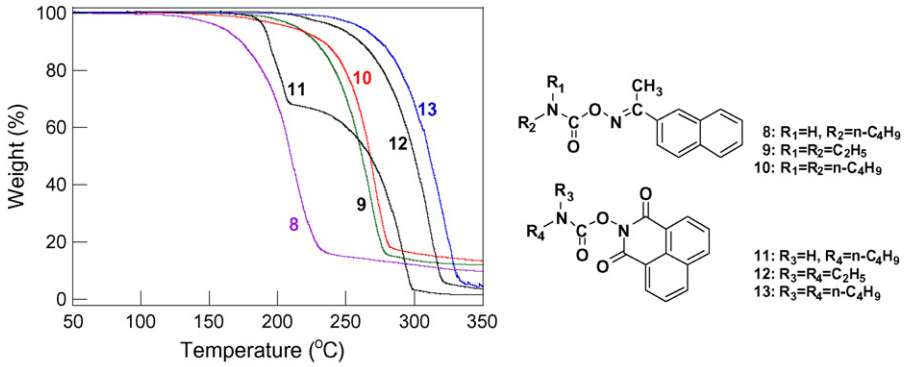

Fig. 3. TGA profiles of carbamate PBGs with heating rate at 10 K/min under N_2.

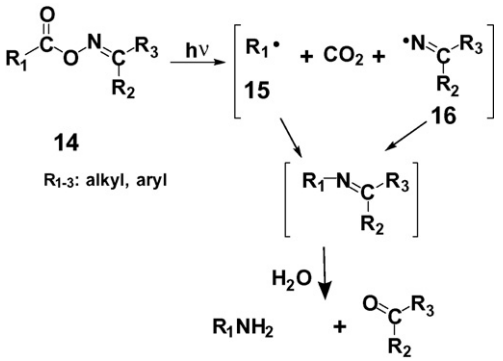

Fig. 4. Photochemical reactions of *O*-acyloximes.

that iminyl radials **16** were observed as long-lived transient at 300 nm in sensitized cleavage in most of the investigated *O*-acyloximes [25]. When R_1 and R_2 were phenyl and R_3 was methyl, another transient due to benzyl radical **15** was observed at 320 nm.

Multifunctional PBGs such as difunctional **18** [26] and trifunctional *O*-acyloxime **19** [27] in Fig. 5 were prepared in order to enhance the ability compared to monofunctional **17** as a crosslinker of polymers bearing epoxy groups. Furthermore, ABA type triblock copolymer **20** composed of 2-acetonaphthone *O*-acryloyloxime (AANO) and methyl acrylate (MA) was prepared by reversible addition-fragmentation transfer (RAFT) polymerization technique [28]. The rate of photolysis of *O*-acryloyloxime units in **17**–**20** were almost identical.

2.1.3. Ammonium salts

Some ammonium salts are known to release free amines on irradiation. From quaternary ammonium salts (QASs), tertiary amines can be obtained on irradiation. Neckers and coworkers studied the generation of tertiary amines from QASs with borate anions, whose chemical structures are shown in Fig. 6 [29–34]. Fig. 7 shows the proposed photoreaction mechanism for **21**, where single electron transfer (SET) from borate anion to cation proceeds initially to generate an intermediate **22**, then homolytic cleavage of C–N bond of **22** occurs in the next step, and finally second SET from **23** to **24** proceeds to produce a radical and an amine [32]. Generally there were no side reactions, and the generation of amines was nearly quantitative as confirmed by product analysis. The quantum efficiency of photolysis of QASs depended on the electron donating capability of anions and steric effects of cations [30]. For example, the quantum efficiency for QAS with butyltriphenylborate anion was higher than that with tetraphenylborate anion because the former anion was more easily oxidized than the latter, and the presence of bulky substituents on the quaternary N atom raised the efficiency in photolysis due to the release of strain energy.

QASs with anions other than borate anions have also been investigated [35–42] (Fig. 8). T_d of QASs with 1-

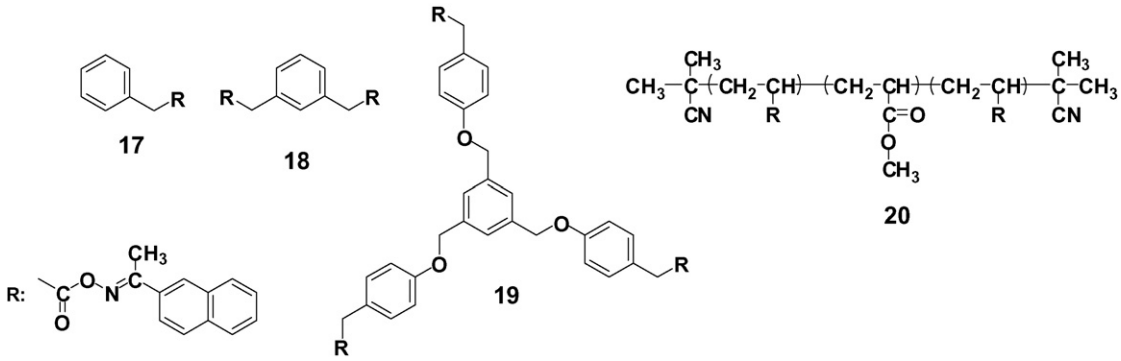

Fig. 5. Multifunctional *O*-acyloximes.

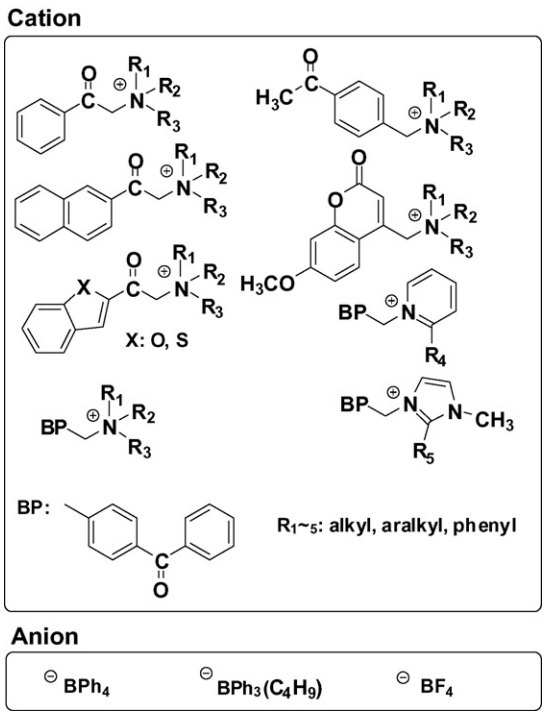

Fig. 6. QASs with borate anions as PBGs.

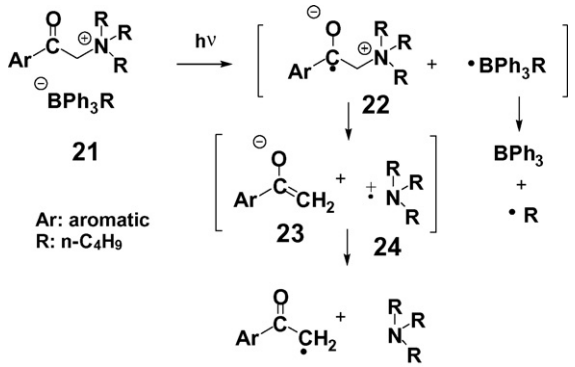

Fig. 7. Photochemical reactions of QASs with borate anions.

phenacyl-1-azania-4-azabicyclo[2.2.2]octane cation was in the order **25a** > **25c** > **25b** > **25d** > **25e** > **25f** > **25g**. Generally, there is trade-off relation between photoreactivity and thermal stability, and photoreactivity of QAS with dithiocarbamate anion **25g** was the highest, although **25g** was unstable in polymer matrix and organic solutions. Solubility of QASs in Fig. 8 in organic solvents was good, except **25a**. *tert*-Butyl substituent improved the solubility of **25a** as was observed for **25b**. Stronger organic bases such 4-(*N*,*N*-dimethylamino)pyridine (DMAP) [40] and 1,8-diazabicyclo[5.4.0]undec-7-ene (DBU) [42] were also generated from **25h** and **25i**, respectively, on irradiation.

QASs with thiocyanate anion showed moderate thermal stability and photoreactivity. However, as shown in Fig. 9, photoproduct from **25c** was still photochemically active, and finally turned into **26** that formed a complex **27** with generated amine [38–40].

2.2. New classes of PBGs

In the last decade, new classes of PBG have been proposed. Amineimides are well known to decompose thermally and generate tertiary amines. Recently, they were found to be photochemically active and released basic compounds as shown in Fig. 10 [43–46]. Thermal stability of **28** increased with electron withdrawing nature of the substituents on phenyl ring. Photoreactivity of nitro-substituted amineimide was the highest among the investigated amineimides, and the formation of **29** was observed. Although corresponding amine **30** could not be

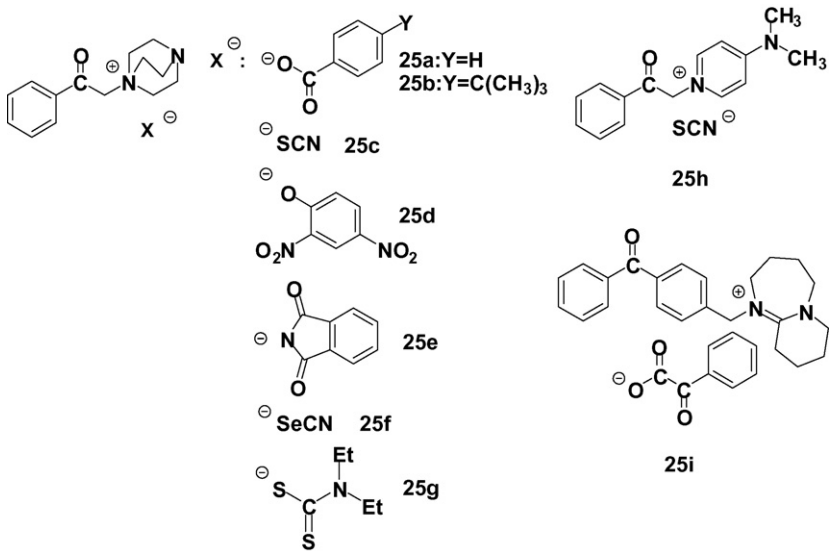

Fig. 8. QASs prepared as photobase generators.

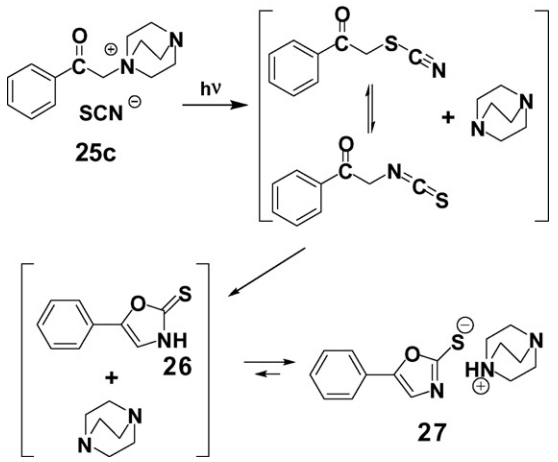

Fig. 9. Photochemical formation of ammonium/thiolate complex from **25c**.

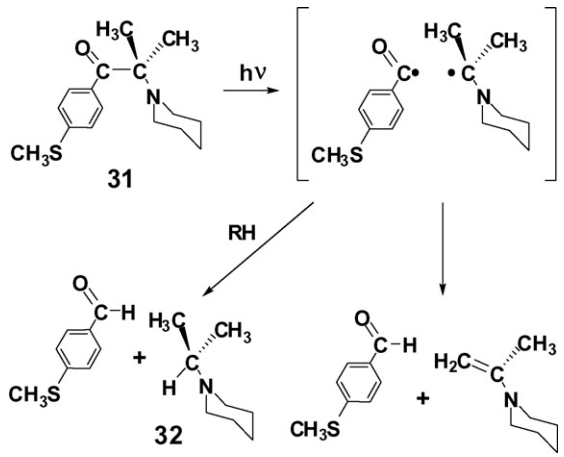

Fig. 11. Photochemical reaction of α-aminoketone.

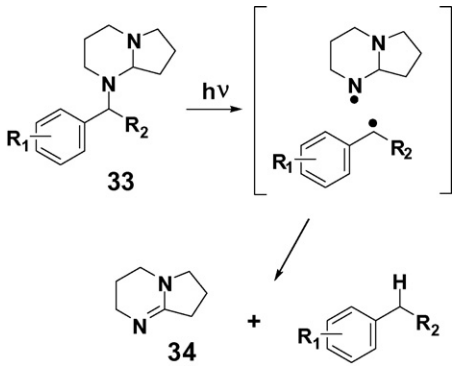

Fig. 12. Photochemical reaction of benzyl substituted amidine.

detected, the formation of basic compound was confirmed by pH change of the reactant. The photoreaction of the amineimides could be sensitized with typical triplet sensitizers whose triplet energy levels (E_Ts) were higher than 289 kJ/mol [46].

α-Aminoketones are known to undergo α-cleavage to generate free-radicals on irradiation and have been used as a photoradical initiator for the polymerization of acrylic monomers. However, when the amino group is sterically hindered and irradiation was carried out in the absence of acrylic monomers, tertiary amines were released on irradiation via hydrogen abstraction or disproportionation as shown in Fig. 11 [47]. The pK_b values of aqueous organic solutions of **31** and **32** were 5.5 and 4.9, respectively, showing no significant changes during irradiation. However, generated amine **32** had much higher activity and nucleophilicity due to the removal of steric shielding of the amino group by dimethyl groups in **31**, showing a new category of PBGs.

Dietliker and co-workers proposed reduced form of amidines as a new PBG whose C=N double bonds were alkylated with allyl and benzyl groups [48,49]. Direct or sensitized photoreaction proceeded as shown in Fig. 12, where excited **33** decomposed to radicals, followed by hydrogen abstraction of the resulting benzylic radical. Although **33** is a tertiary amine and relatively strong base, the basicity of the resulting amidine **34** is much higher than that of **33**. The pH jump (or ΔpK_b jump) was estimated to be 4.5 units, showing a significant difference in the basicity. Resulting amidines can be used as a catalyst for base-catalyzed Michael type addition of multifunctional acrylates and acetoacetates.

Photocleavage of aromatic urea **35** has been reported as shown in Fig. 13 [50]. In this reaction water was necessary, and the conversion of **35** to aniline and 2-aminopyridine depended on the concentration of water. This photochemical reaction was found during the investigation of the photo-degradation behavior of poly(1,4-phenylene-2,6-pyridylurea) for the matrix of organic light-emitting diodes

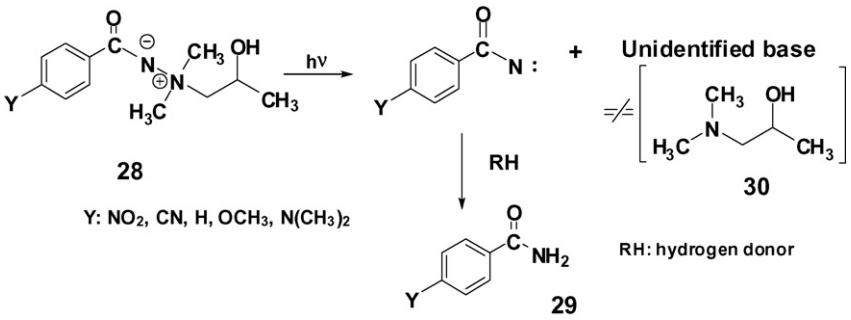

Fig. 10. Photochemical reactions of amineimides.

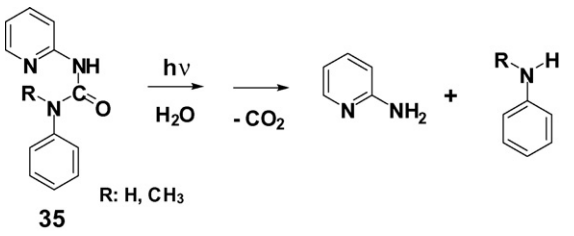

Fig. 13. Photochemical reactions of aromatic ureas in the presence of water.

(OLEDs), where the formation of 2,6-diaminopyridine and *p*-phenylenediamine was confirmed in the product mixture.

Because of the usefulness and importance in organic synthesis and biochemical applications, the development of photolabile protecting groups has been continued [51,52]. Fig. 14 shows new protecting groups of amino groups that have not appeared above. *o*-Aminocinnamamides **36** were proposed as a photoprecursor of amines, especially in releasing of peptides [53]. *N*-(2-Acetoxyethyl) group **37** [54] and coumarine derivatives **38** [55] provide secondary amines from tertiary amines on irradiation. Although these protecting groups generate free amino groups, these are not attractive PBGs from the viewpoint of generation of more active species, because they are in some degree basic even before irradiation.

2.3. Classification of PBGs by original structure

PBGs appeared above are classified from their original structure and summarized in Table 1.

Solubility of PBGs depends on its chemical structure. Generally, non-ionic PBGs such as carbamates, *O*-acyloximes, and nifedipines are soluble in organic solvents and show good compatibility with polymer matrices,

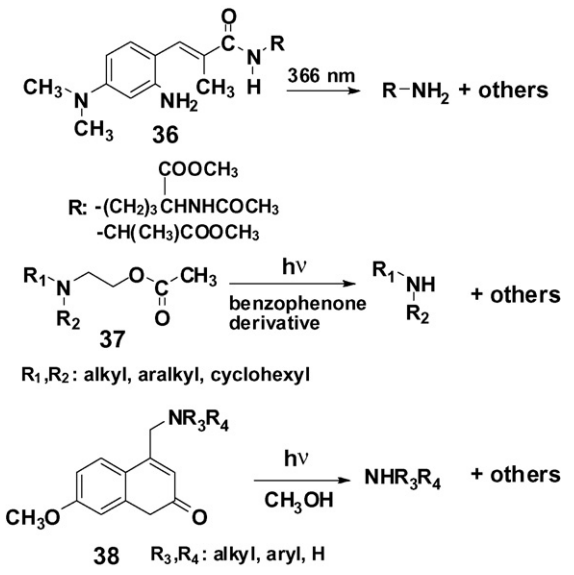

Fig. 14. Photoremovable protecting groups for amines.

while ionic ones such as ammonium salts, transition metal complexes, and amineimides have poor solubility in organic solvents. However, suitable substituents may improve the solubility of the ionic PBGs.

Thermal stability is one of the important properties in industrial applications. Sulfonamides are very stable, although their photoreactivity are not high, and in most cases, hydrogen donors are necessary in the system. Carbamates with N–H moiety and amineimides are relatively thermally less stable. The thermal stability of ammonium salts depends on its structure. Generally there is a trade-off between photoreactivity and thermal stability.

Transition metal compounds such as cobalt complexes and group 8 metallocenes have high potentiality as PBG. Many compounds absorb longer wavelength of light and thus have a wide process window. Instead, the use of metal may be a problem in some applications that must avoid the contamination of metals.

3. Application trends utilizing photo-induced base-generation

3.1. Sensitization of PBGs to longer wavelength of light

The use of near-ultraviolet or visible light is one of the recent trends in the fields of photo-curing, photopolymerization, and photo-crosslinking. This region of light gives little damages in biological systems, and the photoreactions of photoinitiators may proceed easily even though the formulation involves pigments or aromatic compounds that absorb shorter wavelength of light. Furthermore, strong emission from convenient light sources such as medium- and high-pressure mercury lamps at 366 nm (i-line) and 435 nm (g-line) can be utilized effectively. Recently, light emitting diodes and lasers of this region can be available as light sources with high intensity, low-energy consumption, and long life. Therefore, the sensitization system is still important in addition to the extension of sensitive wavelength region of the photosensitive groups.

Fouassier et al. studied the sensitization mechanism of *O*-acyloximes and *O*-carbamoyloximes [25,56]. From quenching study and Agmon–Levine–Balzani model [57,58], it was concluded that E_Ts of the oxime esters were lower than those obtained from phosphorescence study on acetophenone, benzophenone, and 2-acetonaphthone oximes. Such lower E_T was not observed for rigid oxime esters composed of fluorenone oxime. These results were explained by the flexibility of the molecules, where relaxation of the triplet state afforded lower E_T due to non-vertical character.

Sensitizers for near UV and visible region of light were explored, and ketobiscoumarins and thioxanthones were examined as sensitizers for visible light sensitive systems [59,60]. Fig. 15 shows UV–vis region of spectra of these sensitizers. Quantum yields of photolysis of pendant oxime ester moieties on irradiation at 405 nm (Φ_{405}) are summarized in Table 2. For all copolymers, Φ_{405} values decreased in the order **39** > **40** ≫ **41**. Solubility of these polymers in methanol on irradiation changed in general in the same order as that of Φ_{405}. These results can be explained by triplet energy transfer from sensitizers to PBGs. Fig. 16

Table 1
Photobase generators classified by functional unit structure.

Class	General structure[a]	Generated base	Property
Carbamates	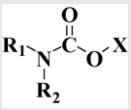	Primary and secondary amines	Most versatile
O-Acyloximes	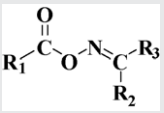	Primary amines	Water is required, thermally stable
Ammonium salts	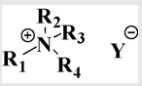	Secondary and tertiary amines, amidines	Lower solubility in organic solvents
Sulfonamides	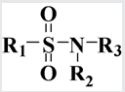	Primary and secondary amines	Thermally stable, reductant is needed
Formamides	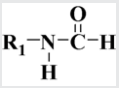	Primary aryl amines	Lower solubility in organic solvents
Nifedipines	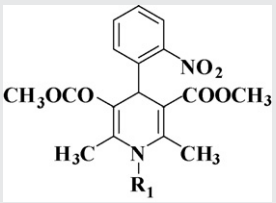	Hydroxy anion (R_1: CH_3), pyridine derivative (R_1: H)	Sensitive to longer wavelength of light
Transition metal complexes[b]		NH_3, thiocyanate anion acetoacetate anion	Lower solubility in organic solvents, metal contained, sensitive to longer wavelength of light
Metallocenes[c]	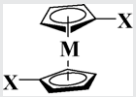	Cyclopentadienyl anion	Metal contained, sensitive to longer wavelength of light
Amineimide	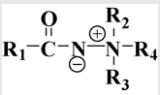	Unidentified base	Thermally unstable
α-Aminoketones	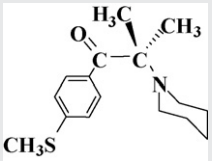	Tertiary amine	Release of steric shielding
Reduced form of amidines[d]	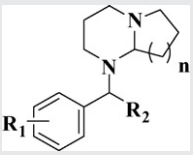	Amidines	pK_b jump

[a] R_1–R_4: H, alkyl, aryl, X: substituent, Y^-: anion.
[b] M: Co, Cr, Pt. L_1, L_2: organic and inorganic ligand.
[c] M: Fe, Ru.
[d] *n*: 1, 3.

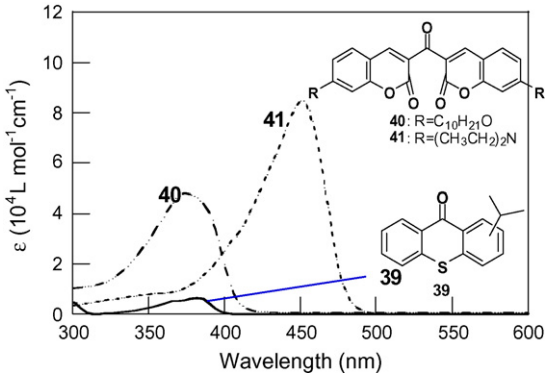

Fig. 15. UV–vis absorption spectra of sensitizers in THF.

Table 2
Quantum yields of sensitized photolysis (Φ_{405}) of base-generating groups in polymers[a].

Copolymer[b]	Φ_{405}		
	39	**40**	**41**
42a	0.50	0.29	0.03
42b	0.90	0.50	0.18
43a	0.84	0.48	0.08
43b	0.94	0.60	0.14

[a] [Base-generating group]:[sensitizer] = 10:1 (mol/mol).
[b] Structure of polymers is shown as follows:

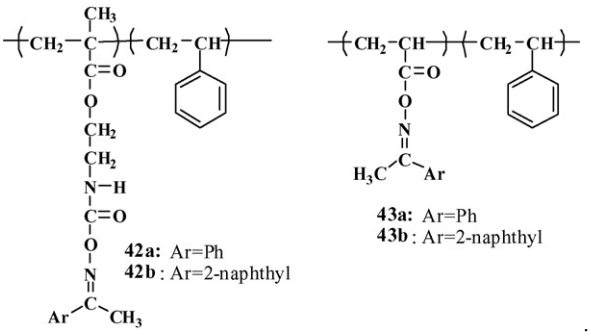

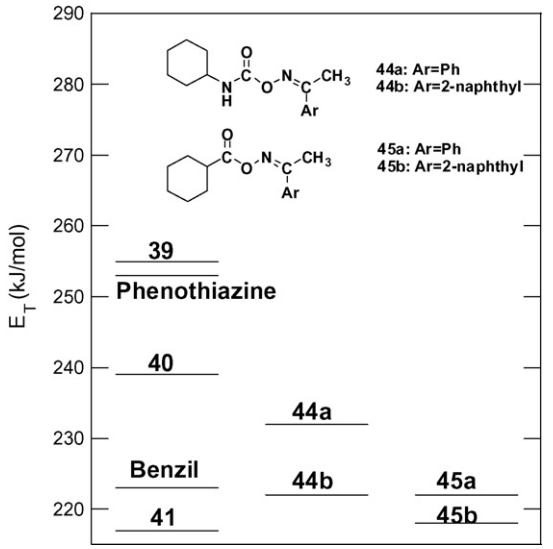

Fig. 16. E_Ts of sensitizers and PBGs.

shows the E_T values of the sensitizers and model PBGs (**44a**, **44b**, **45a**, and **45b**). E_Ts of effective sensitizers were higher than those of the model PBGs, and the photoreactivity corresponded to the greater difference between E_Ts of sensitizers and oxime esters, suggesting that triplet energy transfer from the sensitizers to the PBGs proceeded. The E_T values of PBGs having naphthyl groups were lower than those corresponding PBGs having phenyl groups.

In addition to E_T values, optical properties of sensitizers should be taken into account in the selection of near UV and visible light sensitive systems, because sensitizers having both adequate E_T value and an absorption band in near UV or visible light are limited. For example, benzil and phenothiazine that were not effective as a sensitizer of photolysis of oxime esters on irradiation at 405 nm. Although benzil absorbs 405 nm light, its E_T was as low as 223 kJ/mol. Phenothiazine has no absorption at 405 nm in spite that its E_T was 253 kJ/mol.

The incorporation of sensitizing groups in the side-chain of polymers is advantageous for effective sensitization due to homogeneous distribution in polymeric systems. For example, polymers bearing both sensitizing groups and *O*-acyloximes or *O*-carbamoyloximes were highly photosensitive [21,61,62].

3.2. Highly photo-sensitive base-generating systems

As has already been established for photoacid generating systems, highly sensitive photochemical generation of bases is strongly desired. Ichimura and Arimitsu have proposed a novel base-proliferation system as a highly photosensitive system [63–72]. 9-Fluorenylmethyl carbamate **46** in Fig. 17 underwent thermally base-catalyzed fragmentation to generate an amine **47**. The resulting amine could act as a catalyst for the decomposition of parent molecule, indicating an autocatalytic behavior. Therefore, only small amounts of the photo-generated amine were needed to attain a highly sensitive system.

Recently, another system for highly sensitive base-generation was proposed [73]. As shown in Fig. 18, protected compound **48** was deprotected by the photo-induced acid catalysis at lower temperature to form an intermediate **49** and 3,4-2*H*-dihydropyrane in the first step. **49** released an amine **47** and phthalide on heating in the second step. Here a small amount of PAG was used as a catalyst for the deprotection in chemically amplified manner in the first step. The catalytic amounts of the acid were finally neutralized by the amine generated.

3.3. Polymer synthesis and degradation by using PBGs

Only a few examples of PBG application are known in the fields of photo-induced anionic polymerization. Kutal and coworkers have been studying on the anionic polymerization of alkyl 2-cyanoacrylates (CAs) initiated by anionic species obtained on irradiation of group 8 metallocenes [74–81]. Non-substituted ferrocenes **50** and ruthenocenes **51** were photo-excited to induce the electron transfer from the metallocenes to the monomer CA. Resulting radical anion of CA initiated polymerization as shown in Fig. 19. A similar system was devised using benzoy-

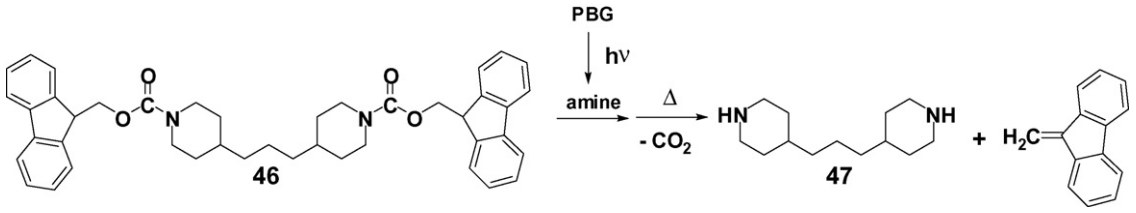

Fig. 17. Base-proliferation system.

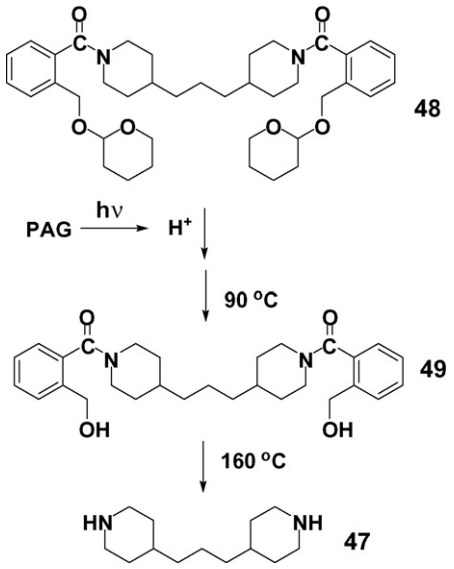

Fig. 18. Photo-triggered base-generation system using PAGs.

lated ferrocenes. Photo-induced intramolecular heterolytic cleavage of metal-ring bond is believed to be a primary process of the polymerization. Resulting cyclopentadienyl anion seems to attack CA to initiate the polymerization. Addition of benzoyl groups to one or both cyclopentadienyl rings of ferrocenes causes the shift of the absorption region at longer wavelength up to almost 500 nm.

QASs with borate anions generate tertiary amines as described in Section 2.1.3. Because the photochemical reaction proceeds via radical pathways, the QASs have been also used as an initiator of photo-induced radical polymerization [82–84]. The same compound was able to enhance the rate of UV-curing of commercial epoxy resins and multifunctional acrylates, respectively.

Photo-generated amines were also used for the preparation of polyimides. Photosensitive polyimide (PSPI) is attractive as thermally stable materials with short patterning processes. A positive-type system using naphthoquinonediazides and a negative-type one based on free-radical polymerization of acrylate units introduced in side-chains have been proposed as PSPI [85]. Because amine is a good catalyst for imidization of poly(amic acid)s **52**, PBGs are expected as a photo-sensitive component of novel type of PSPI as shown in Fig. 20a. In fact, **52** containing a PBG showed a good contrast curve on irradiation at 365 nm followed by post-exposure bake at 160 °C for 5 min. Fortunately, the imidization proceeded completely as low as 200 °C due to the catalytic ability of the generated amine [86]. This technology was applied to obtain polyimide patterns with low dielectric constant [87,88], optical waveguides with lower loss [89], and semi-alicyclic polyimide [90]. In addition to *o*-nitrobenzyl-based carbamates, *O*-carbamoyloxime was also used recently [24].

Poly(*p*-phenylenevinylene) (PPV) derivatives are one of the promising materials as a matrix of organic light emitting diodes (OLEDs). Because PPVs are insoluble in most solvents, many attempts have been proposed for film formation and patterning of the PPVs. One example is the utilization of acids from PAGs as a catalyst of dehydrohalogenation of halo-precursor PPVs. Amines from PBGs are also expected to induce the dehydrohalogenation. In this regard, *o*-nitrobenzyl-type carbamate has been applied to the dehydrohalogenation of **53** as shown in Fig. 20b [91]. On irradiation followed by soft bake at 100 °C for 1 min, films of **53** containing PBG showed UV, fluorescence, and IR spectra similar to that of fully conjugated PPV films which could be obtained on baking at 250 °C for 6 h in vacuum. These results show that photo-generated diphenylamine caused the dehydrohalogenation successfully. Because the irradiated area of **53** films containing PBG became insoluble in cyclohexanone, fine patterning could be achieved

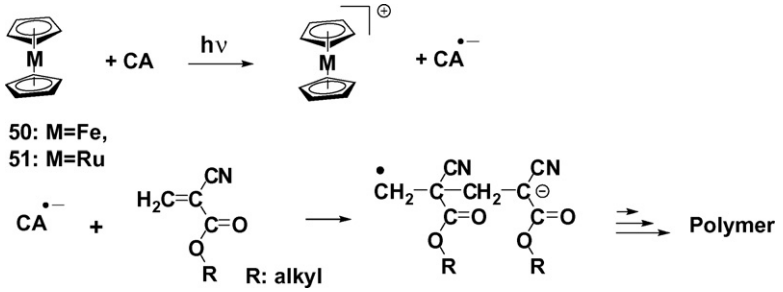

Fig. 19. Photo-induced anionic polymerization of CA initiated by group 8 metallocenes.

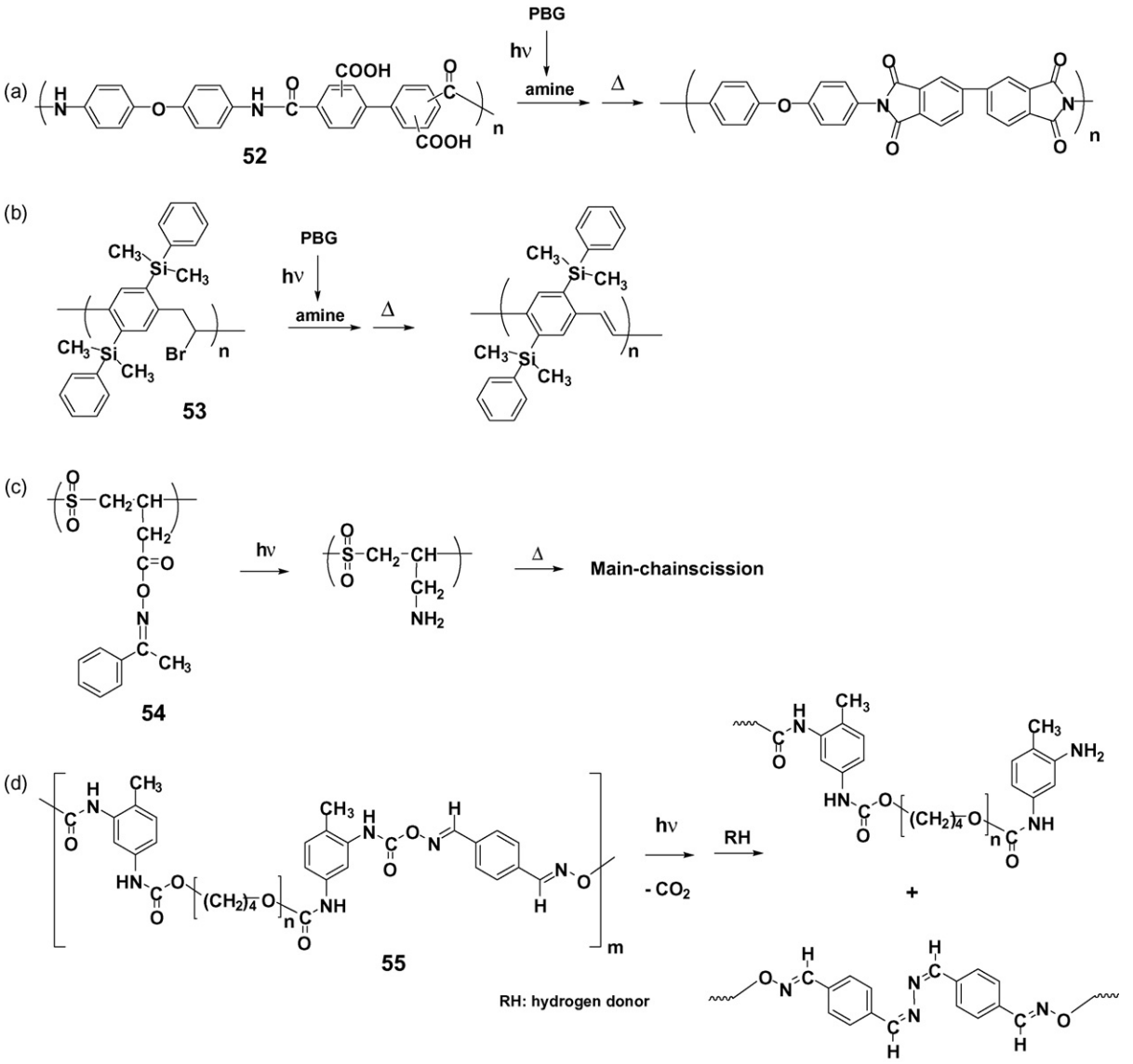

Fig. 20. Polymer modification by using PBGs.

after development. Photochemically converted PPV films showed a lower turn-on voltage and a higher maximum brightness value than thermally converted ones. The possibility of the role of hole-transporting material of generated diphenylamine was proposed to explain the excellent EL characteristics.

Photochemically generated amines can be used as a catalyst for polymer degradation. Polyolefinsulfones contain sulfonyl groups in main chain. Due to the electron withdrawing character of the sulfonyl groups, the neighboring methylene hydrogen is acidic and abstractable even by weak bases. An alternative copolymer **54** composed of sulfone and vinyl monomers bearing *O*-acyloxime moiety can be degraded as shown in Fig. 20c [92]. The number average molecular weight of **54** decreased from 83,000 to 31,000 after irradiation, and the polymer films became soluble in 0.012N HCl solution.

Degradation of the polymer **55** composed of *O*-carbamoyloxime moiety in the main chain has also been proposed as shown in Fig. 20d [20]. On irradiation, the main chain in **55** was cleaved, and the viscosity of the polymer solutions decreased. Because resulting chain ends of the polymers were amino groups, films of PGMA blended with a small amount of **55** became insoluble on irradiation followed by heating.

3.4. Solubility control of polymers by using PBGs

Generally, solubility of polymers bearing photobase-generating groups in polar solvents increases on irradiation due to the generation of polar basic groups. This character has been applied to negative- and positive-tone imaging systems as well as polymers bearing photoacid-generating groups.

A negative-type imaging using PBGs and a copolymer of styrene and acrylic acid was reported [93,94]. In this system, the photochemically generated amine worked as a base catalyst for decarboxylation of the pendant carboxylic acid groups in the copolymers on heating. The irradiated area turned hydrophobic, giving a negative-tone image after development with aqueous tetramethylammonium hydroxide solution.

Negative-tone patterning can also be achieved by photocrosslinking with PBGs as crosslinkers. Recently, photocrosslinking of polycarbodiimide [95,96], and poly(vinyl phenol) (PVP) in combination with epoxy compounds [97,98] was reported. Silyl hydride groups in hydrogen silsesquioxane can be transformed in Si–O–Si bonds in the presence of base and water [99,100]. PBGs used here were *o*-nitrobenzyloxycarbamate and *N*-methylnifedipine that generate a secondary amine and hydroxy anion, respectively. The photoreactivity of the latter was higher than that of the former due to stronger light absorption around 250 nm in addition to the broad band at 300–400 nm. In order to get a high sensitivity of the Si–O–Si linkage formation, post-exposure bake treatment at 80–180 °C was needed.

The crosslinking reactions of polymers bearing photobase-generating groups were also proposed with pendant epoxy groups [19].

Quinones have an absorbance band at longer wavelength and have been used both as a sensitizer and a crosslinker of a polymer bearing *O*-acyloxime moiety [101,102]. For example, films of **43a** containing *p*-benzoquinone were crosslinked on irradiation at 405 nm followed by heating due to the addition reaction of conjugated double bond in *p*-benzoquinone with photochemically generated amino groups [102].

O-Carbamoyloximes are easily decomposed into isocyanates and oximes on heating as described in Section 2.1.1. Therefore, *O*-carbamoyloxime moiety introduced in the side-chains of polymers can be transformed into amino groups photochemically and into isocyanato groups thermally. Since amino and isocyanato groups can react to form stable urea linkages, polymers bearing *O*-carbamoyloxime moiety work as a photo-thermal crosslinking systems [9,13,16]. Enhanced crosslinking behavior for oligomers bearing the *O*-carbamoyloxime moiety was observed on heating after irradiation at 254 nm, even though only irradiation or heating did not induce the insolubilization [15].

A terpolymer **56** composed of acetophenone *O*-methacryloyloxyethylcarbamoyloxime (AMCO), 2-butanone *O*-methacryloyloxyethylcarbamoyloxime (BMCO), and methyl methacrylate was prepared, and the photo-thermal behavior was studied. Only *O*-carbamoyloxime moiety in AMCO was photolyzed on irradiation at 366 nm. In this system, the amino moieties generated by the photolysis of AMCO form urea linkages by the reaction with isocyanato groups generated by the thermolysis as shown in Fig. 21 [21].

Multi-functional *O*-acyloximes were applied to the photo-crosslinking of poly(glycidyl methacrylate) (PGMA). When the molar ratio of *O*-acyloxime moieties to epoxy groups was equal, PGMA films containing **18** required lower irradiation energy, and final insoluble fraction was higher than those containing **17**, indicating the advantage of difunctional PBG than monofunctional one as a crosslinker. Trifunctional *O*-acyloxime **19** also showed a higher ability as a crosslinker of multi-functional epoxy compounds. Blended films of PGMA with AANO-MA-AANO triblock copolymer **20** showed a higher degree of insolubilization on irradiation followed by heating than those with corresponding random copolymers.

Although crosslinked polymers have excellent thermal and mechanical properties, their recycling is difficult because of insoluble and infusible characters. Recently, controlled de-crosslinking of photo-crosslinked polymers has been studied [103]. Fig. 22 shows photo-crosslinking with the de-crosslinkable property by using a PBG. Films of an oligomer bearing epoxy groups **57** containing a PBG became insoluble in THF on irradiation and heating at 100–160 °C. The insolubilization was due to the network formation by the addition reaction of epoxy groups and photochemically generated amine. The crosslinked films became soluble in methanol on heating at 180–200 °C [104,105].

3.5. PBG containing polymers for patterning applications

Irradiation of a selected area of polymer films bearing photobase-generating groups allows the patterning of some functional materials including dyes, biomolecules, and nanoparticles.

Dyes are often selected as a functional material. Chae and coworkers demonstrated the diazotization of pendant amino groups generated photochemically [17]. *O*-Carbamoyloxime moiety in **58** in Fig. 23 was transformed into amino group on irradiation and then diazonium salt moiety. Coupling reaction of the diazonium salt moiety with resorcinol and naphthol AS gave yellow and red colored patterns, respectively.

Fluorescence dyes are also used as the other functional material to give fluorescent images. Irradiated polymer **59** bearing 3,4-dimethoxy-6-nitrobenzyloxycarbonyl (NVOC)-protected amino groups was functionalized with fluorescein isothiocyanate [106]. A similar fluorescent patterning using fluorescamine was reported [22].

The patterning ability of polymers bearing photobase-generating groups was applied to the selective immobilization of antigens and antibodies using polyacrylamide gels bearing *o*-nitrobenzyl carbamate moieties **60** [107]. After irradiation, generated amino groups were reacted with 2,4,6-trinitrobenzenesulfonic acid to produce orange trinitrophenyl derivatives. Due to the affinity of tetramethylrhodamine-labeled anti-dinitrophenyl rabbit immunoglobulin (α-DNP-TRITC-IgG) to the trinitrophenyl moiety, irradiated area showed fluorescent patterns. Furthermore, ^{125}I-labbeled α-DNP-TRITC-IgG was also patterned successfully.

The patterning of proteins was accomplished by using a copolymer **61** bearing photochemically base-generating groups [108]. It was confirmed that a protein, AlexaFluor 546 labeled chicken immunoglobulin (IgG), was adsorbed only on non-irradiated area of **61** films. This was due to the nature of the protein which tends to be adsorbed on hydrophobic surfaces. On the other hand, laser ablation by pulsed N_2 laser at 337 nm produced the scission of poly-

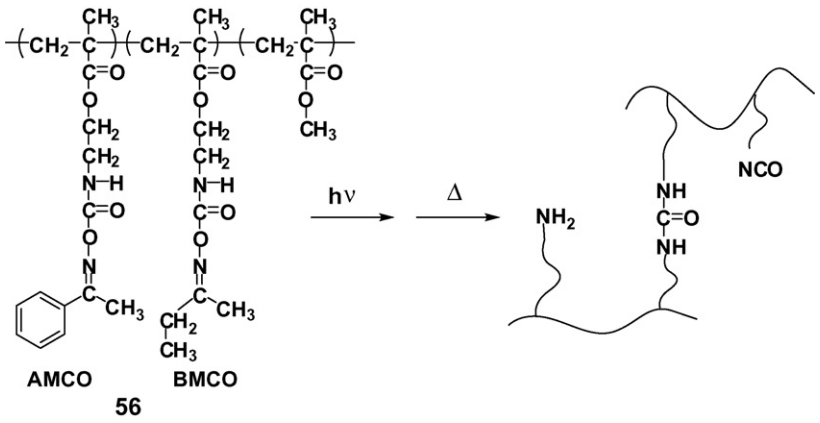

Fig. 21. Highly sensitive crosslinking system utilizing photo- and thermal-reaction of *O*-carbamoyloxime moieties.

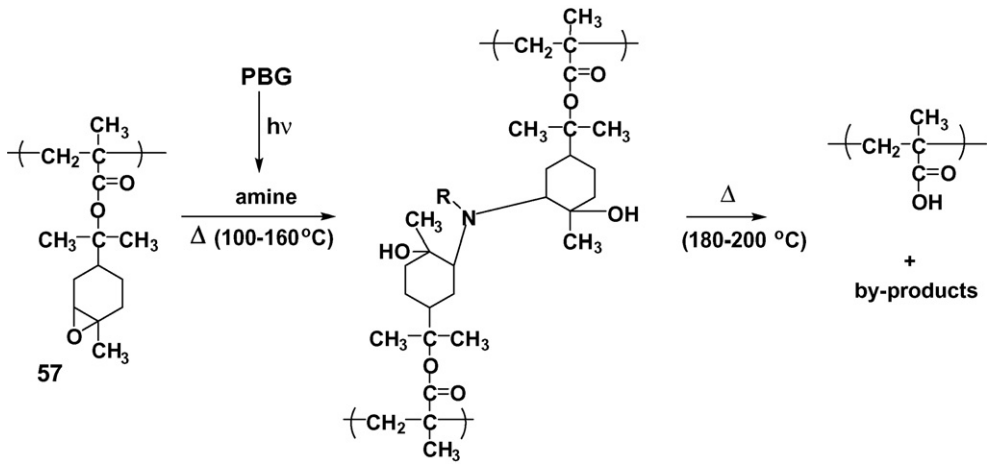

Fig. 22. Crosslinking and de-crosslinking system by using PBG and thermal decomposition units.

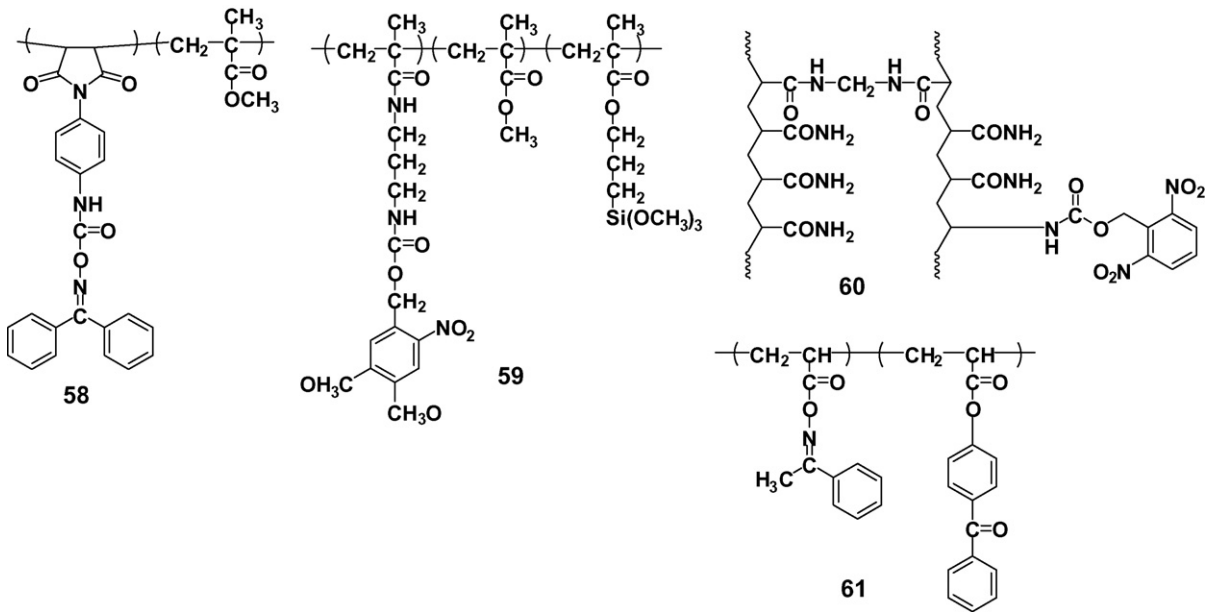

Fig. 23. Polymers bearing photobase-generating groups used for patterning.

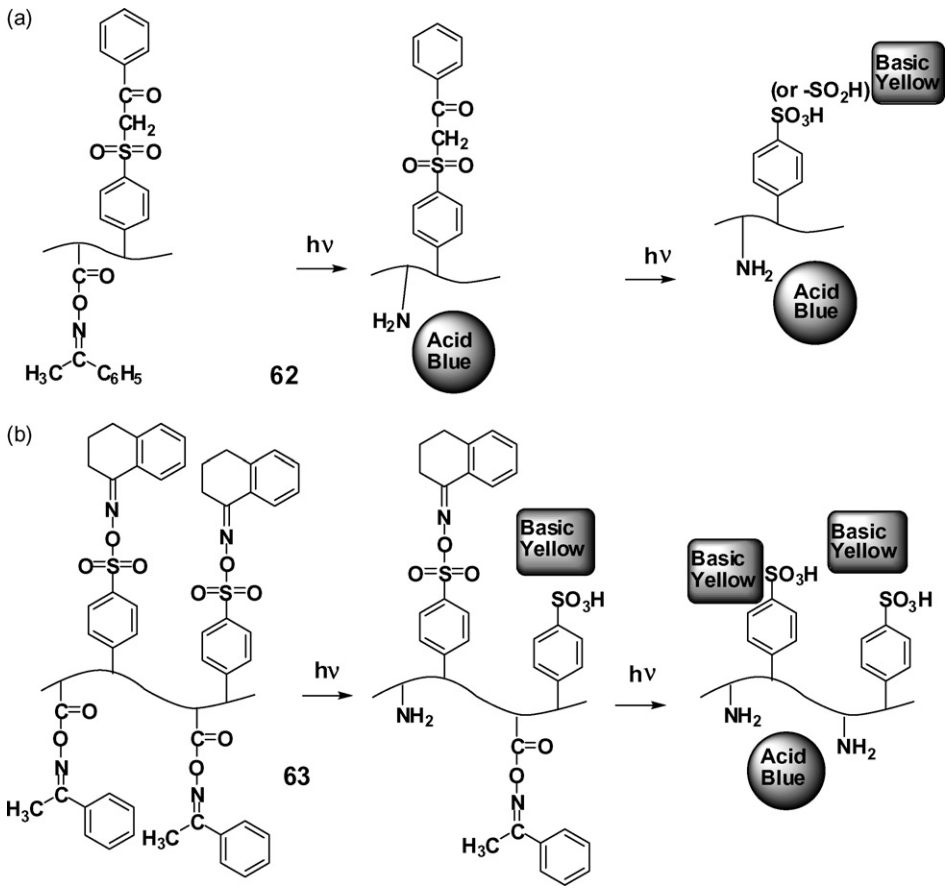

Fig. 24. Dyeing of polymers bearing photochemically acid- and base-generating groups.

mer backbone and side-chains and finally rough surface of the films. When the surface modified polymer films were treated with bovine serum albumin (BSA) solution, the BSA was adsorbed onto the ablated area, producing a positive-tone protein feature. The patterned protein was further utilized for selective recognition of anti-chicken IgG by selective antibody–antigen recognition.

PBGs are also used in the formation of nanoparticle assemble on substrates [109]. A glass slide treated with 3-aminopropyldimethylethoxysilane was modified by nitroveratryloxycarbonylglycine to give NVOC-terminated sample surface. Patterned exposure of UV light afforded the selective deprotection of the NVOC groups to generate amino groups. The glass slide was dipped in a solution containing gold nanoparticles capped with 12-aminododecane. The gold nanoparticles could be bound to the irradiated area by ligand exchange reactions.

3.6. Combination with PAGs

Several examples of simultaneous use of PBGs and PAGs have been reported. Polymers bearing both *O*-acyloxime and iminosulfonate moieties in side-chains were used as photoresists for a surface imaging [110,111]. Here, a flood exposure at 254 nm generated sulfonic acid units at whole surface of the sample film. Then, a patterned exposure at 146 or 193 nm was conducted to generate amino groups. When the sample was exposed to alkoxysilane vapor, polysiloxane was formed at the patterned exposure areas. Resulting polysiloxane layer showed a good plasma etching resistance, giving a negative-tone pattern.

The dissolution behavior of polymeric systems containing both photoacid- and photobase-generating groups was investigated [112]. The dissolution of the copolymer of acetophenone *O*-acryloyloxime (AAPO) and MMA was enhanced by the addition of low molecular weight PAGs on irradiation. A similar enhancement behavior was observed for the copolymer bearing *o*-nitrobenzyl-protected carboxyl groups in the presence of additive PBGs, probably due to the formation of ionic pairs that improved the solubility of the film matrix.

The dyeing of polymers **62** and **63** showed characteristic dyeing behaviors as shown in Fig. 24 [113]. A polymer bearing only photobase-generating groups was dyed with an acid dye after irradiation even though the dye bath contained both an acid and basic dyes. In the same condition, a polymer bearing only photoacid-generating groups was dyed with a basic dye. However, **62** became dyeable with the acid dye after a short period of irradiation and with the basic dye after a longer irradiation time due to the formation of amino groups prior to acid generation. When **63** was irradiated, both sulfonic acid group and

amino group were generated simultaneously. Due to the formation of strong acid groups, basic dye was adsorbed preferentially. Imaging of color patterns using these polymer films was successfully performed in a single staining process.

4. Conclusions and perspectives

Recent progress of PBGs and their new applications are demonstrated. Some studies regarding PBGs are focused on the improvement in thermal stability, solubility in organic solvents, multi-functionality, and photosensitivity. These improvements made the PBGs more stable and easier to handle. In addition to the improvement in classical PBGs, new classes of PBGs have been reported such as amineimides, α-aminoketones, aromatic ureas, and novel amidine precursors. These include new concepts of PBGs that are based on the control of steric shielding and photo-triggered pK_b jump. However, these advances are not satisfactory as a catalyst in many applications, and further development in molecular design and new concept of base-generation is desired.

The application field of PBGs has been expanding in this decade. The advances in photo-induced polymerization, depolymerization, crosslinking and decrosslinking by using PBGs opened a window for new fields of polymer synthesis and degradation. The application of PBGs to imaging of proteins and other biologically important molecules has been advanced and will be extended in the future because of the importance of photo-induced generation of amino and analogous nitrogen-containing basic groups. Although PBGs have not been used in modern lithographic technologies, there may be a possibility as a photo-sensitive component as used in electron beam lithography [114].

Considering the unique characteristics and potentiality in many applications, the development of PBG will be continued. Recently, several reviews and books on photobase generators and their applications have been published [115–122].

References

[1] Frechet JMJ. The photogeneration of acid and base within polymer coatings: approaches to polymer curing and imaging. Pure Appl Chem 1992;64:1239–48.
[2] Shirai M, Tsunooka M. Photoacid and photobase generators: chemistry and applications to polymeric materials. Prog Polym Sci 1996;21:1–45.
[3] Shirai M, Tsunooka M. Photoacid and photobase generators: prospects and their use in the development of polymeric photosensitive systems. Bull Chem Soc Jpn 1998;71:2483–507.
[4] Wuts PGM, Greene TW. Green's protective groups in organic chemistry. 4th ed. Hoboken, NJ: John Wiley & Sons Inc.; 2007.
[5] Du H, Boyd MK. The 9-xanthenylmethyl group: a novel photocleavable protecting group for amines. Tetrahedron Lett 2001;42:6645–7.
[6] Kammari L, Plistil L, Wirz J, Klan P. 2,5-Dimethylphenacyl carbamate: a photoremovable protecting group for amines and amino acids. Photochem Photobiol Sci 2007;6:50–6.
[7] Bucher G, Scaiano JC, Sinta R, Barclay G, Cameron JF. Laser flash photolysis of carbamates derived from 9-fluorenone oxime. J Am Chem Soc 1995;117:3848–55.
[8] Chae KH. Thermal curing reaction of poly(glycidyl methacrylate) using photogenerated amines from oxime-urethane derivatives. Macromol Rapid Commun 1998;19:1–4.
[9] Roesher GA, De Ruiter B. Use of oxime-protected isocyanate groups in the UV curing of resins at low temperature, and UV-curable resins that contain such oxime-protected isocyanate groups and the use of thereof in UV-curable coating compositions. de Bruijn Leendert, C., Netherland: PCT Int Appl. Wo; 1998, 63 pp.
[10] Chae KH, Jang DJ. A new photobase generator containing oxime-urethane group and its application. Macromol Symp 1999;142:173–83.
[11] Hwang H, Jang DJ, Chae KH. Photolysis reaction mechanism of dibenzophenoneoxime hexamethylenediurethane, a new type of photobase generator. J Photochem Photobiol A: Chem 1999; 126:37–42.
[12] Tsunooka M, Tachi H, Asakino K, Suyama K. Synthesis of photobase generators and their use for design of polymeric photosensitive systems. J Photosci 1999;6:145–51.
[13] Tinnesmans A, Roescher A. Low-temperature powder coatings: a new UV-curing reaction at moderate temperatures. Prog Org Coat 2000;40:191–4.
[14] Chae KH, Gwark JC, Chang T. Image recording material based on the polymeric photobase generator containing oxime-urethane groups. Macromol Rapid Commun 2000;21:1007–12.
[15] Suyama K, Iriyama H, Shirai M, Tsunooka M. Curing systems using photolysis of carbamoyloxyimino groups and thermally regenerated isocyanate groups. J Photopolym Sci Technol 2001;14: 155–8.
[16] Singha NK, Hunnekens T, Eversdijk J, Chlon C, Vercauteren F, De Ruiter B. Photoinitiated thermal crosslinking of epoxides using oxime-blocked 2-isocyanato-ethyl-methacrylate. Paint Coat Ind 2003;19:48–55.
[17] Chae KH, Jang HJ. Photochemical modification of polymer surface by the pendant photobase generator containing oxime-urethane groups and its application to an image-recording material. J Polym Sci: Polym Chem 2002;40:1200–7.
[18] Chae KH, Sung KH. A Polymeric photobase generator containing oxime-urethane groups: crosslinking reaction and application to negative photoresist. J Polym Sci: Polym Chem 2004;42:975–84.
[19] Chae KH, Park JH. A one-component negative photoresist based on an epoxy terpolymer containing oxime-urethane groups as a photobase generator. Macromol Res 2004;12:352–8.
[20] Buruiana E, Olaru M, Simionescu BC. Photobase-generating new polyurethanes with oxime-urethane groups in the main chain. J Appl Polym Sci 2004;94:2324–32.
[21] Suyama K, Iriyama H, Tsunooka M, Shirai M. Crosslinking of oligomers utilizing sensitized photoreaction at 366 nm and thermal decomposition of pendant carbamoyloxyimino groups. J Photopolym Sci Technol 2004;17:707–12.
[22] Choi WS, Noh YY, Chae KH. Prefluorescent-dye-induced chemically reversible fluorescent imaging based on a polymeric photobase generator. Adv Mater 2005;17:833–7.
[23] Suyama K, Nakao S, Shirai M. Thermally stable carbamates as novel photobase generator. J Photopolym Sci Technol 2005;18:141–8.
[24] Jang YM, Seo JY, Chae KH, Yi MH. Positive-type photosensitive polyimide based on a photobase generator containing oxime-urethane groups as a photosensitive compound. Macromol Res 2006;14:300–5.
[25] Lalevée J, Allonas X, Fouassier JP, Tachi H, Izumitani A, Shirai M, et al. Investigation of the photochemical properties of an important class of photobase generators: the *O*-acyloximes. J Photochem Photobiol A: Chem 2002;151:27–37.
[26] Ohba T, Nakai D, Suyama K, Shirai M. Photo-crosslinking of poly(glycidyl methacrylate) using di-functional photobase generators. J Photopolym Sci Technol 2004;17:11–4.
[27] Okamura H, Terakawa T, Suyama K, Shirai M. Reworkable photocrosslinking system using multifunctional epoxides and photobase generators. J Photopolym Sci Technol 2006;19:85–8.
[28] Suyama K, Nakai D, Ohba T, Shirai M. Polymeric photobase generator with a new architecture: comparison of random and block copolymers prepared by RAFT polymerization technique. J Photopolym Sci Technol 2005;18:707–10.
[29] Sarker AM, Kaneko Y, Nikolaitchik AV, Neckers DC. Photoinduced electron-transfer reactions: highly efficient cleavage of C–N bonds and photogeneration of tertiary amines. J Phys Chem A 1998;102:5375–82.
[30] Sarker AM, Lungu A, Mejiritski A, Kaneko Y, Neckers DC. Tetraorganylborate salts as convenient precursors for photogeneration of tertiary amines. J Chem Soc, Perkin Trans 1998;2:2315–21.
[31] Kaneko Y, Sarker AM, Neckers DC. Mechanic studies of photobase generation from ammonium tetraorganyl borate salts. Chem Mater 1999;11:170–6.

[32] Sarker AM, Kaneko Y, Neckers DC. Electron transfer followed by double fragmentation reactions: mechanism of photogeneration of tertiary amines and radicals from tetraorganyl borates. J Photochem Photobiol A: Chem 1999;121:83–90.
[33] Zhang W, Feng K, Wu X, Martin D, Neckers DC. Photochemical properties of 4-benzoylbenzylammonium borates. J Org Chem 1999;64:458–63.
[34] Sarker AM, Kaneko Y, Neckers DC. Synthesis of tetraorganylborate salts: photogeneration of tertiary amines. Chem Mater 2001;13:3949–53.
[35] Tachi H, Shirai M, Tsunooka M. Photolysis of quaternary ammonium dithiocarbamates and their use as photobase generators. J Photopolym Sci Technol 2000;13:153–6.
[36] Tsunooka M, Tachi H, Yamamoto T, Akitomo K, Shirai M. Stability of quaternary ammonium salts in various solvents and their use as photobase generators. J Photopolym Sci Technol 2001;14:153–4.
[37] Tachi H, Yamamoto T, Shirai M, Tsunooka M. Photochemical reactions of quaternary ammonium dithiocarbamates as photobase generators and their use in the photoinitiated thermal crosslinking of poly(glycidyl methacrylate). J Polym Sci A: Polym Chem 2001;39:1329–41.
[38] Tsunooka M, Yamamoto T, Kurokawa Y, Suyama K, Shirai M. Photocuring systems using quaternary ammonium thiocyanates. J Photopolym Sci Technol 2002;15:47–50.
[39] Suyama K, Fuke K, Shirai M, Tsunooka M. Photo- and thermochemical behavior of quaternary ammonium thiocyanates and their use as crosslinkers. J Photopolym Sci Technol 2003;16:83–6.
[40] Suyama K, Fuke K, Yamamoto T, Kurokawa Y, Tsunooka M, Shirai M. Photochemical formation of ammonium/thiolate complexes from quaternary ammonium thiocyanates and its use in crosslinking of polymers. J Photochem Photobiol A: Chem 2006;179:87–94.
[41] Suyama K, Fuke K, Shirai M. Effect of anions on photoreactivity and stability of quaternary ammonium salts as photobase generators. J Photopolym Sci Technol 2004;17:15–8.
[42] Suyama K, Araki H, Shirai M. Quaternary ammonium salt as DBU-generating photobase generator. J Photopolym Sci Technol 2006;19:81–4.
[43] Katogi S, Yusa M. Photo-induced thermal curing of epoxy/thiol system with amineimide derivatives as a new photobase generator. J Photopolym Sci Technol 2001;14:151–2.
[44] Katogi S, Yusa M. Structural effects of nitro-substituted amineimide derivatives on the photobase generation in an epoxide/thiol curing system. J Photopolym Sci Technol 2002;15:35–40.
[45] Katogi S, Yusa M. Photobase generation from amineimide derivatives and their use for curing an epoxide/thiol system. J Polym Sci A: Polym Chem 2002;40:4045–52.
[46] Katogi S, Yusa M, Shirai M, Tsunooka M. Base generation by the photolysis of an aminimide with triplet-sensitizers and its use for an epoxide/thiol curing system. Chem Lett 2003;32:418–9.
[47] Kura H, Oka H, Birbaum JL, Kikuchi T. Study on photobase generation from α-aminoketones: photocrosslinking of epoxides with carboxylic acids. J Photopolym Sci Technol 2000;13:145–52.
[48] Turner SC, Baudin G. Photoactivatable nitrogen-containing bases on α-amino alkenes. Switzerland: PCT Int Appl. Wo: (Ciba Specialty Chemicals Holding Inc.); 1998, 51 pp.
[49] Baudin G, Dietliker K, Jung T. Photoactivatable nitrogen bases. Switzerland: PCT Int Appl. Wo: (Ciba Specialty Chemicals Holding Inc.); 2003, 62 pp.
[50] Mwaura J, Yang B, Li R, Morton M, Papadimitrakopoulos F. Photocleavage of pyridiyl-based aromatic polyurea. Macromolecules 2003;36:9775–83.
[51] Bochet CG. Photolabile protecting groups and linkers. J Chem Soc, Perkin Trans 2002;1(2):125–42.
[52] Falvey DE, Sundararajan C. Photoremovable protecting groups based on electron transfer chemistry. Photochem Photobiol Sci 2004;3:831–8.
[53] Li H, Yang J, Porter NA. Preparation and photochemistry of *o*-aminocinnamates. J Photochem Photobiol A: Chem 2005;169:289–97.
[54] Cossy J, Rakotoarisoa H. The *N*-(2-acetoxyethyl) group as a new photolabile protecting group. Tetrahedron Lett 2000;41:2097–9.
[55] Schoenleber RO, Giese B. Photochemical release of amines by C, N-bond cleavage. Synlett 2003:501–4.
[56] Allonas X, Lalevée J, Fouassier JP, Tachi H, Shirai M, Tsunooka M. Triplet state of *O*-acyloximes studied by time-resolved absorption spectroscopy. Chem Lett 2000:1090–1.
[57] Levine RD. Free energy of activation: definition, properties, and dependent variables with special reference to "linear" free energy relations. J Phys Chem 1979;83:159–70.
[58] Balzani V, Bolletta F, Scandola F. Vertical and "nonvertical" energy transfer processes: a general classical treatment. J Am Chem Soc 1980;102:2152–63.
[59] Suyama K, Ohba T, Shirai M, Tsunooka M. Visible light crosslinking of polymeric photobase generators using ketobiscoumarins. J Photopolym Sci Technol 2002;15:43–6.
[60] Ohba T, Suyama K, Shirai M. Visible light-induced formation of pendant basic groups by using triplet sensitizers. React Funct Polym 2006;66:1189–97.
[61] Tsunooka M, Matsuoka T, Miyamoto Y, Suyama K. Photo- and thermo-chemical behavior of polymeric photobase generators bearing pendant sensitizing groups. J Photopolym Sci Technol 1998;11:123–4.
[62] Suyama K, Ito A, Shirai M, Tsunooka M. Effective utilization of 366 nm-light in photo-generation of pendant amino groups using pendant thioxanthone groups. J Photopolym Sci Technol 2000;13:747–50.
[63] Arimitsu K, Miyamoto M, Ichimura K. Applications of a nonlinear organic reaction of carbamates to proliferate aliphatic amines. Angew Chem Int Ed 2000;39:3425–8.
[64] Arimitsu K, Ichimura K. Nonlinear organic reaction of 9-fluorenylmethyl carbamates as base amplifiers to proliferate aliphatic amines and their application to a novel photopolymer system. J Mater Chem 2004;14:336–43.
[65] Ichimura K. Nonlinear organic reactions to proliferate acidic and basic molecules and their applications. Chem Record 2002;2:46–55.
[66] Ichimura K, Igarashi A, Arimitsu K, Seki T. Polymers with base-amplifying side chains. Synthesis and properties. J Photopolym Sci Technol 2004;17:433–4.
[67] Arimitsu K, Kobayashi H, Gunji T, Abe Y, Ichimura K. Positive-working photoimaging materials based on base-amplifying silicone resins having fluorenyl groups. J Photopolym Sci Technol 2005;18:171–2.
[68] Arimitsu K, Inoue S, Gunji T, Abe Y, Ichimura K. Positive-working photoimaging materials based on base-amplifying silicone resins having phenylsulfonyl groups. J Photopolym Sci Technol 2005;18:173–4.
[69] Isoda K, Arimitsu K, Gunji T, Abe Y, Ichimura K. Highly sensitive UV-curing materials containing base-amplifying tetrasiloxane. J Photopolym Sci Technol 2005;18:225–6.
[70] Arimitsu K, Ito Y, Gunji T, Abe Y, Ichimura K. Application of novel base amplifiers with 3-nitropentan-2-yl group to UV-curing materials. J Photopolym Sci Technol 2005;18:227–8.
[71] Igarashi A, Arimitsu K, Aoki K, Ichimura K. Water-developable base-amplifying copolymers. J Photopolym Sci Technol 2005;18:419–20.
[72] Inoue S, Arimitsu K, Gunji T, Abe Y, Ichimura K. Positive-working photoimaging materials based on base-amplifying silicon resins with photobase-generating groups. J Photopolym Sci Technol 2006;19:73–4.
[73] Ohba T, Kitamoto K, Nakai D, Suyama K, Shirai M. Generation of amines by using photo-triggered thermal deprotection. J Photopolym Sci Technol 2007;20:299–302.
[74] Yamaguchi Y, Palmer BJ, Kutal C, Wakamatsu T, Yang DB. Ferrocenes as anionic photoinitiators. Macromolecules 1998;31:5155–7.
[75] Yamaguchi Y, Kutal C. Efficient photodissociation of anions from benzoyl-functionalized ferrocene complexes. Inorg Chem 1999;38:4861–7.
[76] Yamaguchi Y, Kutal C. Benzoyl-substituted ferrocenes: an attractive new class of anionic photoinitiators. Macromolecules 2000;33:1152–6.
[77] Sanderson CT, Palmer BJ, Morgan A, Murphy M, Dluhy RA, Mize T, et al. Classical metallocenes as photoinitiators for the anionic polymerization of an alkyl 2-cyanoacrylate. Macromolecules 2002;35:9648–52.
[78] Brinkmann NR, Schaefer III HF, Sanderson CT, Kutal C. Can the radical anion of alkyl-2-cyanoacrylates initiate anionic polymerization of these instant adhesive monomers? J Phys Chem 2002;106:847–53.
[79] Ding W, Sanderson CT, Conover RC, Johnson MK, Amster J, Kutal C. Characterization of the low-energy electronic excited states of benzoyl-substituted ferrocenes. Inorg Chem 2003;42:1532–7.
[80] Sanderson CT, Quinlan JA, Conover RC, Johnson MK, Murphy M, Dluhy RA, et al. Characterization of the low-energy electronic excited states of benzoyl-substituted ruthenocenes. Inorg Chem 2005;44:3283–9.
[81] Yamaguchi Y, Ding W, Sanderson CT, Borden ML, Morgan A, Kutal C. Electronic structure, spectroscopy, and photochemistry of group 8 metallocenes. Coord Chem Rev 2007;251:515–24.
[82] Yu X, Chen J, Yang J, Zeng Z, Chen Y. Preparation of a series of photoinitiators and their use in the thermal curing of epox-

ide and radical polymerization of acrylate. Polymer 2005;46: 5736–45.
[83] Zhong R, Yang J, Zeng Z, Chen Y. Behavior of quaternary ammonium salt photobase generators on initiating free radical photopolymerization. Polym Int 2006;55:650–6.
[84] Yu X, Chen J, Yang J, Zeng Z, Chen Y. Synthesis and photoinitiation properties of a novel quaternary ammonium tetraphenylborate salt. J Appl Polym Sci 2006;100:399–405.
[85] Hasegawa M, Horie K. Photophysics, photochemistry, and optical properties of polyimides. Prog Polym Sci 2001;26:259–335.
[86] Fukukawa K, Shibasaki Y, Ueda M. Direct patterning of poly(amic acid) and low-temperature imidization using a photo-base generator. Polym Adv Technol 2006;17:131–6.
[87] Mochizuki A, Kurata N, Fukuoka T. Development of photosensitive polyimide with low dielectric constant. J Photopolym Sci Technol 2001;14:17–22.
[88] Mochizuki A, Fukuoka T, Kanada M, Kinjou N, Yamamoto T. Development of photosensitive porous polyimide with low dielectric constant. J Photopolym Sci Technol 2002;15:159–66.
[89] Mochizuki A, Mune K, Naitou R, Fukuoka T, Tagawa K. New photosensitive polyimide materials and their application to low-loss optical waveguides. J Photopolym Sci Technol 2003;16:243–6.
[90] Mizoguti K, Shibasaki Y, Ueda M. Development of negative-type photosensitive semi-alicyclic polyimide using a photobase generator. J Photopolym Sci Technol 2007;20:181–6.
[91] Lee SK, Jung BJ, Ahn T, Song I, Shim HK. Photolithographic micropatterning of an electroluminescent polymer using photobase generator. Macromolecules 2003;36:9252–6.
[92] Yaguchi H, Sasaki T, Matsuda M. Photosolubilization of polyolefinsulfone containing side-chain oxime ester groups. Chem Lett 2006;35:760–1.
[93] Song S, Takahara S, Yamaoka T. Photogenerated base catalyzed decarboxylation in polymers with an aliphatic or an aromatic carboxyl group. J Photopolym Sci Technol 1998;11:171–2.
[94] Song S, Yokoyama S, Takahara S, Yamaoka T. Novel dual-mode photoresist based on decarboxylation by photogenerated base compound. Polym Adv Technol 1998;9:326–33.
[95] Mochizuki A, Takeshi K, Haba O, Kato S, Ueda M. Synthesis of photosensitive polycarbodiimide. J Photopolym Sci Technol 1998;11:225–30.
[96] Mochizuki A, Sakamoto M, Yoshioka M, Fukuoka T, Takeshi K, Ueda M. Novel photosensitive polymer based on polycarbodiimide and photoamine generator. J Polym Sci A: Polym Chem 2000;38:329–36.
[97] Okamura H, Harada C, Morishita S, Shirai M, Tsunooka M, Fujiki T, et al. Photocrosslinking system based on poly(vinyl phenol) and fluorene derivatives with epoxy unit using photoacid and photobase generators. J Photopolym Sci Technol 2001;14:159–62.
[98] Okamura H, Watanabe Y, Tsunooka M, Shirai M, Fujiki T, Kawasaki S, et al. I-line sensitive photoacid and photobase generators and their use for photocrosslinking system based on poly(vinylphenol) and diepoxy fluorene derivatives. J Photopolym Sci Technol 2002;15:145–52.
[99] Harkness BR, Takeuchi K, Tachikawa M. Demonstration of a directly photopatternable spin-on-glass based on hydrogen silsesquioxane and photobase generators. Macromolecules 1998;31:4798–805.
[100] Harkness BR, Takeuchi K, Tachikawa M. Photopatternable thin films from silyl hydride containing silicone resins and photobase generators. Polym Adv Technol 1999;10:669–77.
[101] Tachi H, Jun P, Tsunooka M. Photo-initiated thermal crosslinking of polymeric photobase generators by the use of vapor deposition of *p*-benzoquinone. J Photopolym Sci Technol 1998;11:121–2.
[102] Suyama K, Natsui D, Ohba T, Shirai M, Tsunooka M. Generation of pendant amino groups on irradiation of visible light in the presence of benzoquinonylsulfanyl derivatives. J Photopolym Sci Technol 2001;14:745–8.
[103] Shirai M. Reworkable UV curing materials. Prog Org Coat 2007;58:158–65.
[104] Ohba T, Shimizu T, Suyama K, Shirai M. Photocrosslinking and redissolution properties of oligomers bearing photoamine generating groups and epoxy groups. J Photopolym Sci Technol 2005;18:221–4.
[105] Ohba T, Nakai D, Suyama K, Shirai M. Photocrosslinking and thermal degradation of epoxy-containing polymers using photobase generators. Chem Lett 2005;34:818–9.
[106] Braun F, Eng L, Trogisch S, Voit B. Novel labile protected amine terpolymers for the preparation of patterned functionalized surfaces: synthesis and characterization. Macromol Chem Phys 2003;204:1486–96.
[107] Sanford MS, Charles PT, Commisso SM, Roberts JC, Conrad DW. Photoactivatable cross-linked polyacrylamide for the site-selective immobilization of antigens and antibodies. Chem Mater 1998;10:1510–20.
[108] Wright J, Ivanova E, Pham D, Filipponi L, Viezzoli A, Suyama K, et al. Positive and negative tone protein patterning on a photobase generating polymer. Langmuir 2003;19:446–52.
[109] Vossmeyer T, DeIonno E, Heath JR. Light-directed assembly of nanoparticles. Angew Chem Int Ed Engl 1997;36:1080–3.
[110] Shirai M, Endo M, Tsunooka M, Endo M. Positive surface modification resist system. J Photopolym Sci Technol 1999;12:669–72.
[111] Shirai M, Nakaseko H, Tsunooka M. Surface modification resists using photoacid and photobase generating polymers. J Photopolym Sci Technol 2000;13:531–4.
[112] Suyama K, Yamaguchi S, Shirai M, Tsunooka M. Enhanced dissolution of copolymers bearing photobase- or photoacid-generating groups in polar solvents by photochemical formation of ionic pairs. J Polym Sci A: Polym Chem 2001;39:1708–15.
[113] Suyama K, Yamaguchi S, Shirai M, Tsunooka M. Image formation by dyeing of copolymers bearing photogenerated acid and base groups with dye bath containing acid and basic dyes. J Polym Sci A: Polym Chem 2000;38:3043–51.
[114] Jeyakumar A, Henderson CL. Enhancing the electron beam sensitivity of hydrogen silsesquioxane (HSQ). Proc SPIE 2004;5376: 490–501.
[115] Kutal C. Generation of bases and anions from inorganic and organometallic photoinitiators. Coord Chem Rev 2001;211: 353–68.
[116] Dietliker K, Birbaum JL, Hüsler R, Baudin G, Wolf JP. Photolatent catalysts. Chimia 2002;56:197–202.
[117] Shirai M, Suyama K, Okamura H, Tsunooka M. Development of novel photosensitive polymer systems using photoacid and photobase generators. J Photopolym Sci Technol 2002;15:715–30.
[118] Dietliker K, Jung T, Benkhoff J, Kura H, Matsumoto A, Oka H, et al. New developments in photoinitiators. Macromol Symp 2004;217:77–97.
[119] Dietliker K, Misteli K, Jung T, Contich P, Benkhoff J, Sitzmann E. Novel Chemistry for UV coatings. Eur Coat J 2005:20–4.
[120] Suyama K, Tsunooka M, Shirai M. Photo-generation of organic bases in polymers using 366 nm- or longer wavelength of light. In: Fouassier JP, editor. Photochemistry and UV curing: new trends 2006. Kerala, India: Research Signpost; 2006. p. 219–28.
[121] Tsunooka M, Suyama K, Okamura H, Shirai M. Development of photoacid and photobase generators as the key materials for design of novel photopolymers. J Photopolym Sci Technol 2006;19: 65–71.
[122] Dietliker K, Husler R, Birbaum JL, Ilg S, Villeneuve S, Studer K, et al. Advancements in photoinitiators-opening up new application for radiation curing. Prog Org Coat 2007;58:146–57.